High Throughput Technologies for Formulation and Screening of Liquid Crystals

By

Tobias Richard Cull

Thesis for the degree of Doctor of Philosophy

The University of Edinburgh

College of Science and Engineering

School of Chemistry

March 2007

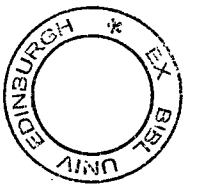

University of Edinburgh; College of Science and Engineering

ABSTRACT

HIGH THROUGHPUT TECHNOLOGIES FOR FORMULATION AND SCREENING OF LIQUID CRYSTALS

By Tobias Cull

Thermotropic calamitic liquid crystals (LC) have found many important commercial applications. Satisfying the stringent demands for physical characteristics means that complex mixtures of liquid crystals must be efficiently formulated and characterised to give the desired properties. To date this process has been achieved using a purely classical approach which involves the slow and laborious creation (and characterisation) of arbitrary compositions. For emerging applications requiring properties that are more demanding, classical techniques are unable to reveal the full extent of the formulation landscape efficiently, inherently limiting the discovery process.

There is thus a massive potential in the field of liquid crystals for the development of techniques, already adopted in other areas of materials science, for the efficient and comprehensive exploration of the formulation landscape. Two main areas were identified for study in this PhD thesis, high-throughput (HT) formulation and parallel high-throughput screening of novel LC formulations. The development of apparatus for the parallel characterisation of liquid crystal phase transitions suitable for the initial screening of LC libraries is described. The technique developed was demonstrated to be reproducible and consistent with data obtained by differential scanning calorimetry (DSC), and was used to analyse LCs for melting points, smectic and nematic mesophase transitions. The 100-fold increase in throughput obtained over classical techniques consequently qualified the requirement for high-throughput formulation techniques

Two approaches to formulation; robotic liquid handling and inkjet printing were used to formulate mixtures of liquid crystals, creating a large library of discrete, known mixtures. Screening using the high-throughput technique for the determination of phase transitions identified eutectic phases that were directly correlated with samples prepared by conventional processes. Both techniques were successful in creating reproducible formulations in a high-throughput manner, inkjet printing (IJP) having a number of clear advantages for use in an HT workflow. This was the first example of IJP for generation of formulation-based libraries.

Inkjet printing was also studied as a tool for the high-throughput deposition of thin film libraries. In parallel with robotic formulation, libraries of chiral nematic reactive mesogens were created, allowing an investigation into the dependence of chiral dopant concentration and enantiomeric excess on the wavelength of selective reflection. Comparison with theoretical results reveals the IJP method to be a useful tool in the creation of film based libraries.

DECLARATION OF AUTHORSHIP

The research described in this thesis was carried out by the author under the supervision of Prof. Mark Bradley at the University of Southampton between October 2002 and January 2005 and at the University of Edinburgh between January 2005 and March 2006. No part of this thesis has been previously submitted at this or any other university for a degree or a professional qualification. Parts of this work have been published in the scientific literature.

Publications:

- Cull, T., Goulding, M., Bradley, M., *Review of Scientific Instruments*, **2005**, *76*, 062216

- Cull, T.; Goulding, M.; Bradley, M., *Adv. Mater.*, **2007**, *19*, 2355

Signed:.....

Date: 02.04.2008

ACKNOWLEDGEMENTS

I would like to thank firstly my supervisor, Professor Mark Bradley for his guidance, patience, and enthusiasm throughout my research, and for providing me with many opportunities. I would also like to thank my supervisor at Merck Chemicals, Dr. Mark Goulding for his excellent advice, supervision, support, and useful discussion.

Thanks go to Merck Chemicals and the EPSRC for the provision of funding through a CASE studentship, without which this work would not have been possible. Additionally I would like to thank the staff at Merck's Chilworth Technical Centre for useful discussions, efficient supply of materials and for the training and use of analytical equipment on site.

I would like to thank the Bradley group (both past and present) for their support, friendship, knowledge and guidance during time in both Edinburgh and Southampton. In particular, I would like to thank Juan Jo, Rosario and Alba for being such excellent hosts on my visits back to Edinburgh.

I would like to thank my family Angela, Michael, Edward and Adam for their continued support in all areas throughout my education, and also finally, I would like thank my Fiancée Emma, for her understanding, support and endless motivation throughout my research and during my move to Edinburgh. Thanks also to Emma's family (Linda, Colin, Matt and Will) for their support and concern.

CONTENTS

ABBREVIATIONS

AC	Alternating current
Cr	Crystalline solid phase
Ch	Cholesteric liquid crystal phase
CMYK	Cyan – Magenta – Yellow - Key colour model
cp	Clearing point
CSL	le Chatalier-Schroeder-van Laar
DSC	Differential scanning calorimetry
DSM	Dynamic scattering mode
DTA	Differential thermal analysis
DCM	Dichloromethane
$\Delta\varepsilon$	Dielectric anisotropy.
Δn	Birefringence.
$\Delta\lambda$	Bandwidth of absorption band
ee	Enatiomeric excess
fps	Frames per second
HPLC	High performance liquid chromatography
HT	High throughput
HTP	Helical twisting power
I	Isotropic liquid phase.
IPP	Image pro-plus
IJP	Inkjet printing
IJ	Inkjet
IPS	In-plane switching
IR	Infrared region of electromagnetic spectrum.
ITO	Indium tin oxide
λ_{max}	Wavelength of maximum absorption / nm
LC	Liquid Crystal
LCD	Liquid Crystal Display
LH	Left-handed sense of circularly polarised light
MVA	Multi-domain vertically aligned
mp	Melting point
N	Nematic liquid crystal phase
N*	Chiral nematic liquid crystal phase

n	Director of liquid crystal phase
NMR	Nuclear magnetic resonance spectroscopy
NW	Normally white mode
NB	Normally black mode
N_2	Nitrogen
PET	Polyethylene terephthalate
PVA	Poly(vinyl)alcohol
PGMEA	Propylene glycol monomethyl ether acetate
PC	Personal Computer
RH	Right-handed sense of circularly polarised light
RM	Reactive mesogen
RMS	Reactive mesogen solution
R	Gas Constant
SVL	Schroeder-van-Laar
SOHO	Small office - home office
Sm	Smectic liquid crystal phase
STN-LCD	Supertwisted nematic liquid crystal display
TFT-LCD	Thin film transistor – liquid crystal display
TN-LCD	Twisted nematic liquid crystal display
T_{N-I}	Nematic - Isotropic transition temperature
T_{Cr-N}	Crystal - Nematic transition temperature (melting point)
TAC	Triacetyl cellulose
UV	Ultra-violet region of the electromagnetic spectrum
UV-Vis	Ultraviolet to visible region of the electromagnetic spectrum
VBA	Visual basic application
VB	Visual Basic (Microsoft)
v/v %	Volume / volume percent
w/w %	Weight / weight percent

Chapter 1 - Introduction

1.1 General Introduction

Liquid crystals can be found in almost all aspects of modern life. Mobile phones, personal organisers, laptop computers and a host of other mobile devices would not be viable without liquid crystal technologies, which provide a thin, light, low power and energy efficient means of visualising information through liquid crystal displays (LCD). Modern active matrix thin film transistor liquid crystal displays (TFT-LCD) offer many benefits over traditional cathode ray tube devices,[1-3] such as improved ergonomics, low weight, low space requirement and reduced power consumption. Consequently, LCDs have almost replaced the demand for cathode ray tube devices in personal computing.

The first displays, although pioneering, did not satisfy the strong consumer expectation and industrial demand for more complex devices capable of high-information display.[4] Over the years, through extensive academic and industrial research, a synergistic relationship between technology and application was observed, and as major issues such as display addressing methods, poor brightness, poor contrast, long response-time, and poor viewing angle were resolved new applications were envisaged.

The characteristics of liquid crystals (LC) required for application in displays are numerous. Due to the high specification and often competing demands, a single liquid crystal cannot be created to satisfy every requirement for a display application.[1,5] To produce a material which has the required properties necessitates the formulation of mixtures, with components combined in such a way that the overall bulk property of the mixture meets the characteristics required for the device. In a typical modern display there may be in excess of 20, and often up to 40 different components in amounts as little as 0.1 w/w %.[6-9] The properties of the LC mixture crucial for satisfactory display operation include,[10] a nematic mesophase with a high clearing point and broad range which extends over the temperature at which the device is to be used, high optical anisotropy, low rotational viscosity, optimised dielectric anisotropy and elastic constants of high or low magnitude depending on the intended display construction. These and other properties, including their measurement, are discussed in section 1.3.

Although single liquid crystals cannot be used in isolation, they still represent an important part of LC research and optimisation. To achieve changes in the properties of a LC molecule,

variations in the molecular structure are required, usually achieved *via* the synthesis of a homologous series, which through subsequent characterisation could be used to establish structure-property relationships. There exist a great many reviews published over the years which give an excellent and comprehensive overview of the effect of structural modification on LC properties.[11-14] The process of producing a new mixture for liquid crystal displays is therefore a multistep process in which materials that possess one or more of the required properties are selected, and then formulated. Many unique mixtures can be produced by modification of component ratios, which can highlight compositional trends, and identify composition-property relationships.

To satisfy the industry-driven demand for accelerated development of materials, methodologies originally developed for combinatorial high-throughput synthesis and screening of pharmaceuticals can be adopted. Although this type of research has been common place in synthetic chemistry and biochemistry for many years, only in the past decade[15] has high-throughput experimentation been widely applied to alternative fields of materials chemistry such as catalysis,[15-23] inorganic materials[24-27] and polymer research[28-30] for the discovery of new functional materials. This technology drastically reduces the time required to probe all possible chemical compositions and identify trends in structure-property relationships.[24] Despite the commercial interest, the adoption of parallel and high-throughput (HT) chemistry for the synthesis of liquid crystals[31] has been slow, with many research groups continuing to produce large datasets using standard organic chemistry techniques by synthesising individual homologues and then analysing each material for properties of interest. The first example of parallel methodologies being applied to the liquid crystal area was in synthesis, where there has been a vast amount of research on the adaptation of standard chemistry techniques to combinatorial or parallel methods.[32-37] Liquid crystals are well suited to a parallel synthesis method as libraries can be created through modification of one section of the molecule (head group, tail group or lateral substituent) whilst retaining the common central core unit[38-40] to form a series of structurally diverse compounds. In this way, the effect of the modification on the properties can be identified. However, liquid crystal synthesis also provides a challenge as materials must be synthesised with purity of greater than 99 %, requiring extensive purification,[41] and on a much larger scale (approx 0.5 g required for basic characterisation) than typical medchem combinatorial synthesis, which tends to produce μmol quantities of each compound.[42] Examples of the types of techniques used include parallel synthesis, one pot solution based synthesis and solid supported

synthesis.[32-37] There has also been a feasibility study by Styring[31] on the use of micro reactor technology for liquid crystal synthesis. These initial studies have shown that it is possible to create diverse liquid crystal libraries in high purity using these techniques showing the potential for future synthesis.

In the area of reactive mesogens (Chapter 4) and liquid crystal mixtures (Chapter 3) for display application, there is little precedent for a high-throughput approach. Current methods of creating a range of compositionally diverse compounds use prior experiments as a guide to identify compositional areas of interest. In the more recent past, the advancement of computing has allowed for complex theories and molecular modelling to be used, allowing LC properties to be predicted[43,44] without the need for time-consuming and costly synthesis. Although the prediction of the optical birefringence and dielectric anisotropy has reached a stage such that the result is often in good agreement with measured values,[45,46] computer simulations of bulk properties such as viscosity, melting and clearing points, LC phases and elastic constants are still at an early stage.[47] This is due to their dependence on numerous interdependent parameters and therefore, for final optimisation, experimental formulation is required as the simulation method is not robust enough to reveal the subtleties of liquid crystal behaviour. In all cases, the screening of liquid crystal formulations or novel libraries is carried out using a "single compound – single analysis" approach, with techniques such as differential scanning calorimetry (DSC) and polarising microscopy most often being employed as an initial screen. Although these techniques are well established and accurate and can be used to distinguish a wide range of liquid crystalline phases, they are time-consuming and can only be performed on one compound at a time. For smaller libraries these drawbacks are relatively insignificant, however once larger datasets are produced using HT parallel methods, the analysis time becomes the limiting factor, the process only being as fast as its slowest step. The lack of methods allowing HT or parallel analysis of samples not only severely restricts a rapid discovery process by limiting the practical formulation speed of new liquid crystalline materials, which is the major route to optimising new LC mixtures, but is also a major obstacle to the development and success of high-throughput chemistry techniques in this area.

1.2 Liquid Crystals; The Early Days

The field of liquid crystal science began in 1888 with the discovery of the liquid crystalline behaviour of cholesteryl benzoate by Reinitzer.[48] Research over the following years established the basic principles of liquid crystalline behaviour, including the work of Friedel[49] in 1922, identifying a number of different liquid crystalline "polymorphs", which occurred between the crystalline solid (Cr) and isotropic liquid (I) phase. These were named the nematic (N), smectic (S) and cholesteric (Ch) mesophases,

1.2.1 Liquid Crystal Mesophases

Liquid crystals exhibit properties both of an isotropic liquid (fluid flow characteristics, a degree of positional order) and a crystalline solid (long-range orientational order), and exist in an intermediate state between the two. Not all substances exhibit LC behaviour, those that do are referred to as mesogenic materials and can be categorised as lyotropic, thermotropic or amphotropic.

Lyotropic materials[50] are the most common of liquid crystals, occurring naturally in biological systems. Lyotropic liquid crystal phases occur only in mixtures, where an amphiphilic molecule comprising a polar and non-polar region is dissolved into a suitable solvent. The interaction of the solvent and solute together results in the aggregation of micelles, vesicles and bilayers, clusters of molecules in which the polar or non-polar regions pack in close proximity. At low concentrations, there is no ordering of the micelles and vesicles themselves. At higher concentration, the structure changes so that the micelles and vesicles self-organise into a multitude of liquid crystal phases.[51] The formation of such liquid crystal phases is therefore concentration dependent. Examples of lyotropic mesophases are soaps and detergents[50,52] and biological cell membranes.[53]

Thermotropic materials are those with one or more intermediate mesophases, the so-called fourth state of matter lying between the solid and liquid phases. These materials exhibit a temperature-dependent phase formation, such as the cholesterol derivative observed by Reinitzer.[48] Molecules which exhibit thermotropic mesophases are generally rod or lath shaped (the axis along the plane of the molecule is longer than the axis across the plane of the molecule), and rigid. There also a number of other molecules, deviating from the classical shapes, which have been found to exhibit mesogenic and anisotropic behaviour.[54-57] These include discotic materials.[58,59]

Amphotropic materials are those which exhibit both a concentration and thermally dependent phase.[60] Examples of amphotropic materials include some surfactants, which are able to self-assemble into lyotropic mesophases or self-organise to form thermotropic phases.

Thermotropic liquid crystals can exhibit two types of phases, either enantiotropic in which the phase occurs above the material's melting point, or monotropic where the phase exists below the melting point, and therefore can only be revealed on super-cooling. The phases arise depending on the degree of orientation and positional order of the calamitic molecules in the bulk. To help in the description of the orientational order a unit vector or director n is defined, which describes the average, common direction in which the long molecular axis of each molecule orientates. It should be noted that in the orientation of molecules both n and – n are equal and the position of the permanent dipole has no bearing on the director.[61]

1.2.1.1 Nematic Phase

The nematic phase (N) possesses long range orientational order (the long molecular axis of the rod shaped molecules align preferentially parallel to one other),[61,62] but lacks any positional order. The origin of the name is from the Greek *nematos* meaning 'thread' due to the thread-like textures observed in the bulk material. This phase is the least ordered[63,64] of the liquid crystal mesophases, and is usually observed by cooling from the isotropic phase or by heating from the crystal or smectic phases. Due to rotational symmetry around the director, nematics are uniaxial. To understand the relationship between the director and the long axis of the molecule an order parameter S has been defined,[65] in which θ represents the angle between the long molecular axis and the average director orientation. Equation 1.1 is applied either to a single molecule over time, or an average of many molecules at the same time.[66]

$$S = \langle P2(\cos\theta) \rangle = (3\cos^2\theta - 1)/2 \qquad \textit{Equation 1.1}$$

In the nematic phase, the fluctuation of molecules about their average positions gives rise to a value of S between 0.3 and 0.75 and therefore the system is reasonably disordered on approaching the isotropic phase. For comparison, a value of 1.0 represents perfect order (solid) and zero equates to no order. The order parameter is determined by experiment, using methods such as diamagnetism or birefringence where S can be derived from measurements

of macroscopic properties, or by NMR in which the order parameter is directly proportional to the frequency splitting of the NMR line.[67] In the bulk nematic phase the director changes continuously and undergoes microscopic fluctuations in its orientation, which gives materials a turbid appearance due to scattering of light. The structure and relationship to the other liquid crystal phases is illustrated in Figure 1.1.

1.2.1.2 Smectic Phases

Smectic phases possess orientational order and a degree of positional order. This manifests itself as a layered arrangement in which the molecules form stacked, regularly spaced two-dimensional liquid layers.[61] Various smectic phases exist, and these are classified depending on the orientation of the director within layers with respect to the adjacent layers. Friedel[49] in his original classification named only one smectic phase, which we now know as the smectic A (SmA) phase.

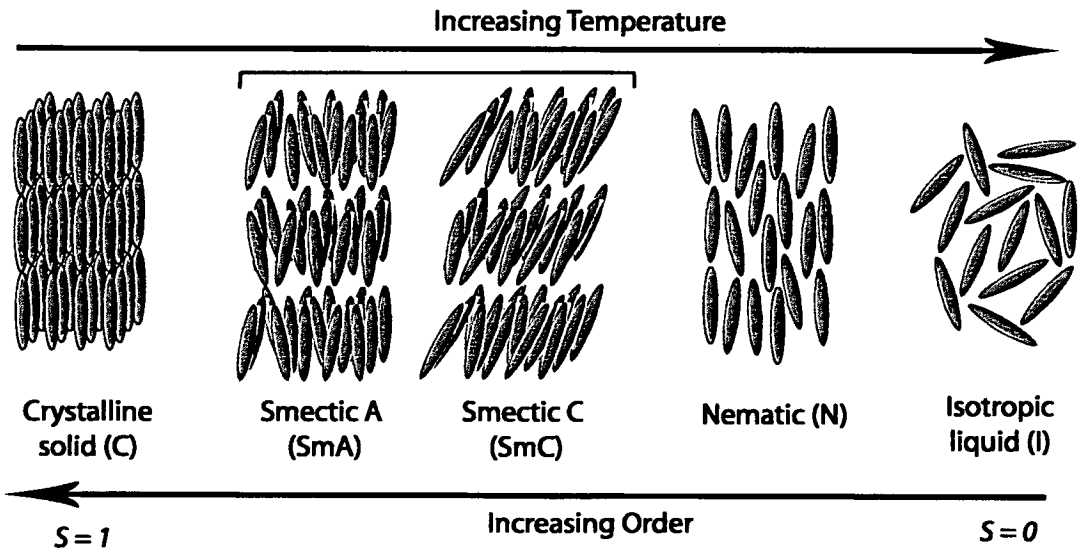

Figure 1.1: The phases that can be formed by heating a liquid crystal sample from the crystalline solid. The order of the system decreases as the temperature is increased. The smectic phases do not always occur in every substance.

In much later work other types of smectic structures were observed and classified,[68-71] and a comprehensive treatment of smectic liquid crystals can be found in the book by Gray and Goodby.[72] The two most commonly occurring phases, in their order of appearance from the

crystalline melt, are smectic A (SmA) and smectic C (SmC). In the SmA phase, a layered structure is formed in which the director of the constituent molecules lies perpendicular to the layer.[73] Within these layers there is no long range order, each layer in effect being considered as a 2D liquid.[61] In the SmC phase a layered structure is also formed. However this is a tilted phase in which the long molecular axis is tilted with respect to the layer normal.[73] Chiral smectic layers can also be formed, such as the chiral smectic C phase (SmC*), in which a helical pitch is formed due to an incremental rotation of the tilt direction when moving between adjacent layers. Other higher order smectic phases, which are observed less frequently, have structures in which the mesogens form 2D lattices within the layers.[73,74] Many materials do not exhibit a smectic phase instead forming a nematic directly from the melt. Smectic phases are often observed as waxy solids, which exhibit mainly solid characteristics in that they do not flow and retain their shape. The origin of the name smectic is from the Greek word for "soap" due to their waxy and 'soap-like' consistency.

1.2.1.3 Chiral Nematic (Cholesteric) Phase

In the chiral nematic phase, nematic order is disrupted by the presence of a molecule lacking a plane of symmetry. This results in an environment in which the molecular packing causes a slight and gradual rotation of the director in adjacent molecules, perpendicular to the molecular axis. Locally, the molecular order is considered identical to that of a nematic but macroscopically the director describes a uniform helix,[75] creating a phase with form chirality (Figure 1.2). The stereogenic centre which induces the chiral nematic phase[76] can be incorporated using either an intrinsically chiral liquid crystal, or through inclusion of a chiral dopant into the nematic host.[77-79] Chiral dopants are molecules either with, or without liquid crystalline properties,[80] which possess stereochemistry due to the presence of one or more chiral centres[77] (a sp3-hybridised, tetrahedrally bonded centre possessing four different substituents). Alternatively, chirality can be created by asymmetry, restricting the rotation around a specific bond by steric hindrance, therefore creating two rotameric forms of a molecule which exist as enatiomers with opposite absolute configuration.[81] In many cases, the solubility of chiral components in the nematic host can be poor and so the chiral component requires modification through derivatisation with groups similar to those found in the nematic liquid crystal host.[82]

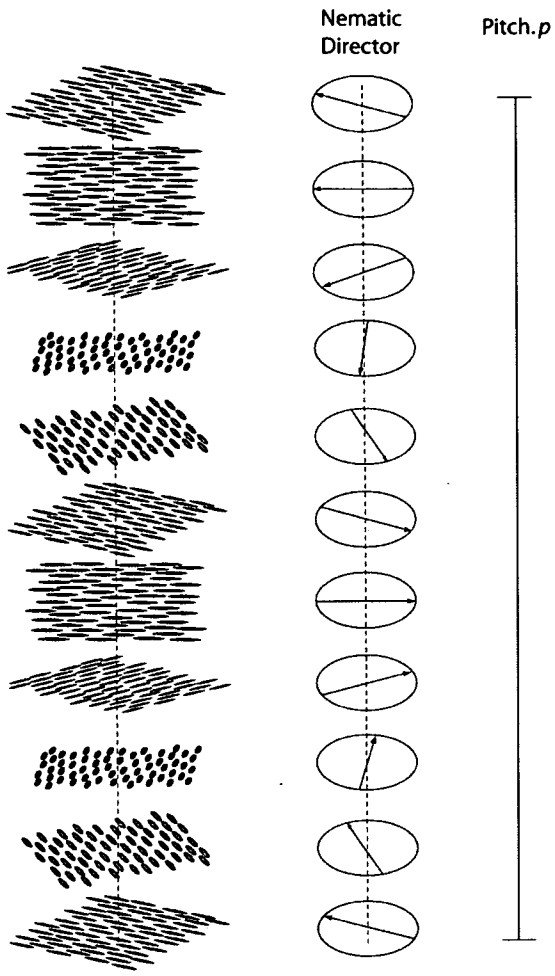

Figure 1.2: A cross section of a cholesteric liquid crystal sample showing the continuous rotation of the liquid crystal director, which is seen to adopt a helical orientation. It should be noted that the cholesteric phase is not a layered structure.

In a doped chiral nematic, the pitch, p (μm^{-1}), of the helix described by the nematic director (defined by the distance along the optical axis for the director to twist 360°) is calculated from the inverse of the concentration of added dopant, c (expressed between zero and one as either mol fraction or w/w %), multiplied by the helical twisting power (HTP), β μm^{-1} (Equation 1.2)

$$p = (c.\beta)^{-1} \qquad \textit{Equation 1.2}$$

HTP is derived experimentally *via* measurement of the helical pitch of the chiral phase using an optical technique, such as a Grandjean-Cano wedge cell. In this technique, disclination lines are obtained from analysis of an aligned chiral nematic liquid crystal, which can be

used to calculate the helical pitch length and the HTP.[83,84] The higher the HTP, the more efficient a dopant is in inducing a twist with tighter helical pitch at a defined concentration.[85,86]

A chiral nematic pitch can be described as being 'handed' depending on the direction of the helix, and its interaction with circularly polarised light, discussed in section 1.2.2. A right-handed helix spirals clockwise and a left-handed helix spirals anticlockwise. The handedness is inherited from the chiral dopant or the chiral mesogen. Gray and Mcdonnell[87] defined rules in which the absolute configuration of a molecule's chiral centre (*R* or *S*) and the number of atoms between the point of asymmetry (odd or even), can be used to determine whether the chiral molecule, and hence the doped chiral nematic phase, exhibits a *dextro* (right handed) or *laero* (left handed) sense of helical rotation. Chiral additives are utilised in the twisted nematic display (TN)[88] where a small amount of chiral dopant added to the nematic liquid crystal ensures that only a helix of one sense is formed between the front and back surfaces of the cell (Section 1.4).

1.2.2 Interaction of Light with Chiral Nematics

Chiral nematic networks exhibit unique properties in that they are able to reflect circularly polarised light of one handedness over a range of wavelength, while light of the opposite handedness is transmitted fully.[77] The handedness of light transmitted in a chiral nematic network corresponds to the handedness of the chiral nematic helix (Figure 1.3).[89] This is illustrated in Figure 1.4 by two films, created using a chiral dopant with right-handed selective reflection and visualised under two circularly polarising filters of opposite handedness. The film under the left-hand polarised appears colourless due to the full transmission of light with left-handed polarisation. In contrast, under the right-handed polariser, visible wavelengths of right-handed circularly polarised light are reflected, and so the film is seen to exhibit colour. This phenomenon occurs not only in the visible region but also in the IR and UV and was observed by Reinitzer[48] in his studies of chiral cholesterol benzoate in 1888.

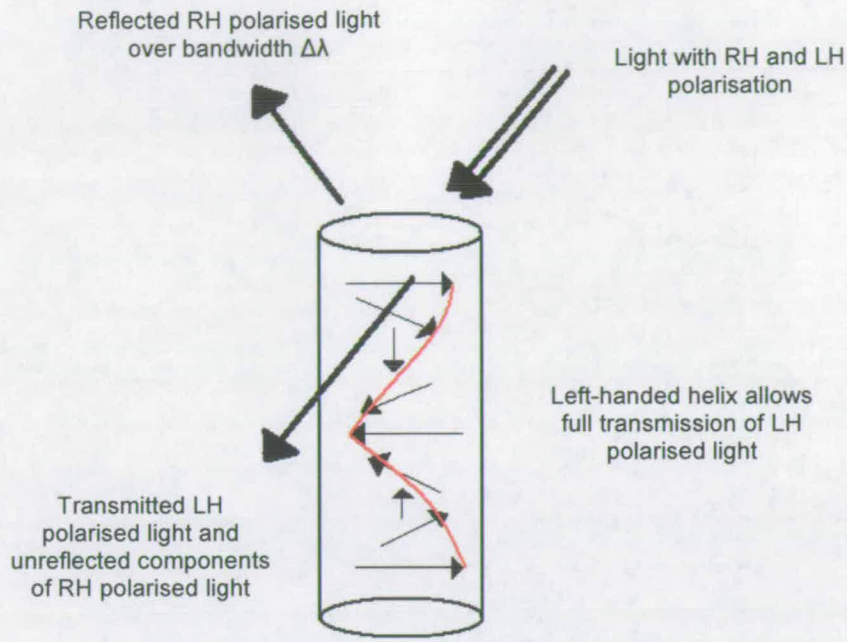

Figure 1.3: The cause of selective reflection of light of one handedness in a chiral nematic liquid crystal phase

Figure 1.4: A red and green chiral reactive mesogen film illuminated from below with white, unpolarised light and visualised through two circular polarisers of opposite handedness.

The relationship between incident and reflected light at angle α, and the central wavelength of the selectively reflective band, λ_{max}, has been described mathematically using the Bragg law of reflection;[90-93] $n_o + n_e$ are the ordinary and extraordinary refractive index of the chiral nematic.

$$\lambda_{max}(\alpha) = \lambda_o.cos[sin^{-1}(2 \sin \alpha)/n_o + n_e)] \qquad \textit{Equation 1.3}$$

The bandwidth, $\Delta\lambda$, of light reflected at λ_{max} is related to the change in average birefringence, Δn, of the liquid crystal with respect to the director.

$$\Delta\lambda = 2\lambda_o[(no-ne)/(no+ne)] = \lambda o[\Delta n/n] \qquad \textit{Equation 1.4}$$

The wavelength, λ_o, is the value of $\lambda_{max}(\alpha)$ when $\alpha = 0$ (normal incidence) and hence angular dependence on the reflected wavelength can be eliminated so that λ_o is related in equation 1.5 to the materials averaged refractive index, $\tilde{n}$, and the pitch, p. Equation 1.5 is only valid when incident light propagates parallel to the helical pitch.

$$\lambda_o = \tilde{n}p \qquad \textit{Equation 1.5}$$

Surface alignment can be used to ensure that the helical pitch forms in a well-defined monodomain, and hence optimum selective reflection is achieved. The coating of a chiral nematic onto a substrate such as polymer film, unidirectionally rubbed to induce parallel alignment, causes the mesogens in contact with the surface to lie flat against the surface (the director parallel to the direction of rubbing). As the mesogens stack, the asymmetry of the chiral phase results in a helical twist, exhibited through the director orientation, which spirals away from the anchored surface. In this arrangement, light incident normal to the film is parallel to the helix.

1.2.2.1 Modification of Properties

By manipulation of either the pitch or the refractive index of the nematic host allows the value of λ_{max} to be modified. For visible selective reflection, the pitch should be approximately the wavelength of visible light (0.7-0.4 μm). Substitution of the nematic host or chiral nematic mesogen for a material with higher Δn will produce a broader reflection bandwidth at a modified value of λ_{max}, according to equations 1.3 and 1.4. For a cholesteric monomer the refractive index can be modified by structural manipulation or by producing a blend of a cholesteric and non-cholesteric reactive monomers, in which case the birefringence becomes dependent on the concentration of the non-chiral additive.[94]

Alternatively, λ_{max} can be manipulated by use of chiral dopants with different HTP or by changing the concentration of dopant. In this case as the pitch of the chiral helix increases, so does the value of λ_{max} (equation 1.2). In general it is desirable to use dopants with as high a

HTP as possible so that the concentration added to the nematic liquid crystal can be kept low; in part due to solubility limitations,[86] but mainly as higher concentrations of dopants (>10 %) can begin to negatively influence the properties (birefringence, refractive index, mesophase transitions) of the nematic liquid crystal formulation.[95] For these reasons Equation 1.2 has been shown to hold only at low concentration.[96-98]

Another method of modifying λ_{max} is by exploiting the dependence of both pitch, p, and the ordinary and extraordinary indices of refraction, n_o and n_e, on temperature.[61,99,100] It is this dependence that has lead to a number of thermochromic applications for chiral nematic liquid crystals[101,102] in areas such as medical screening, thermal mapping, non-destructive materials testing, aerodynamic research, radiation detection, surface thermometers, battery testers and colour effect jewelry.[102,103]

1.2.3 Polymerisable Liquid Crystals (Reactive Mesogens)

Reactive mesogens (RM) are analogous to low molecular mass LC molecules, exhibiting thermotropic mesomorphic behaviour, but additionally containing two reactive sites in the structure (Figure 1.5). The addition of a functional groups, such as acrylates[104,105] to the LC end group enables photo-polymerisation of the monomer units to form a highly cross-linked, high molecular weight, polymer network (Figure 1.6).[105-107] Alternatively epoxide[108,109] or vinyl ether[110-112] functionality can be included, and cross-linked through UV sensitive cationic initiation processes.

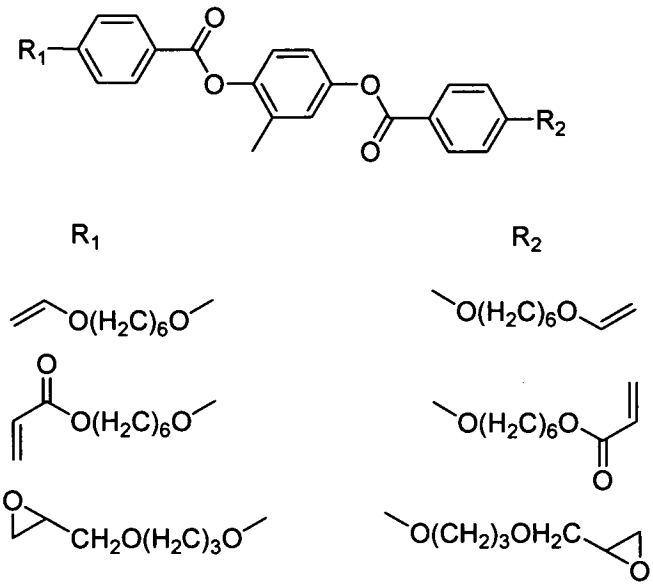

Figure 1.5: Typical Direactive nematic compounds used in polymerisable RM films

The in-situ photopolymerisation of the orientated monomeric units 'freezes' the structure[99,113] resulting in preservation of anisotropic optical properties from the fluid LC phase to the intractable polymer. By coating thin films using methods such as bar coating or spin coating (Chapter 4), monomeric RMs in their nematic state can be polymerised into thermally and mechanically robust coatings.[114-116] The properties of the coating can then be exploited over a large temperature range,[85] where the monomeric material would exhibit a mesophase transition out of the nematic phase. Photo-polymerisation has been shown to be effective not only for nematic phases,[117] but also for locking other mesophases[112,118] such as smectics and chiral nematics[119-123] into stable polymeric structures.

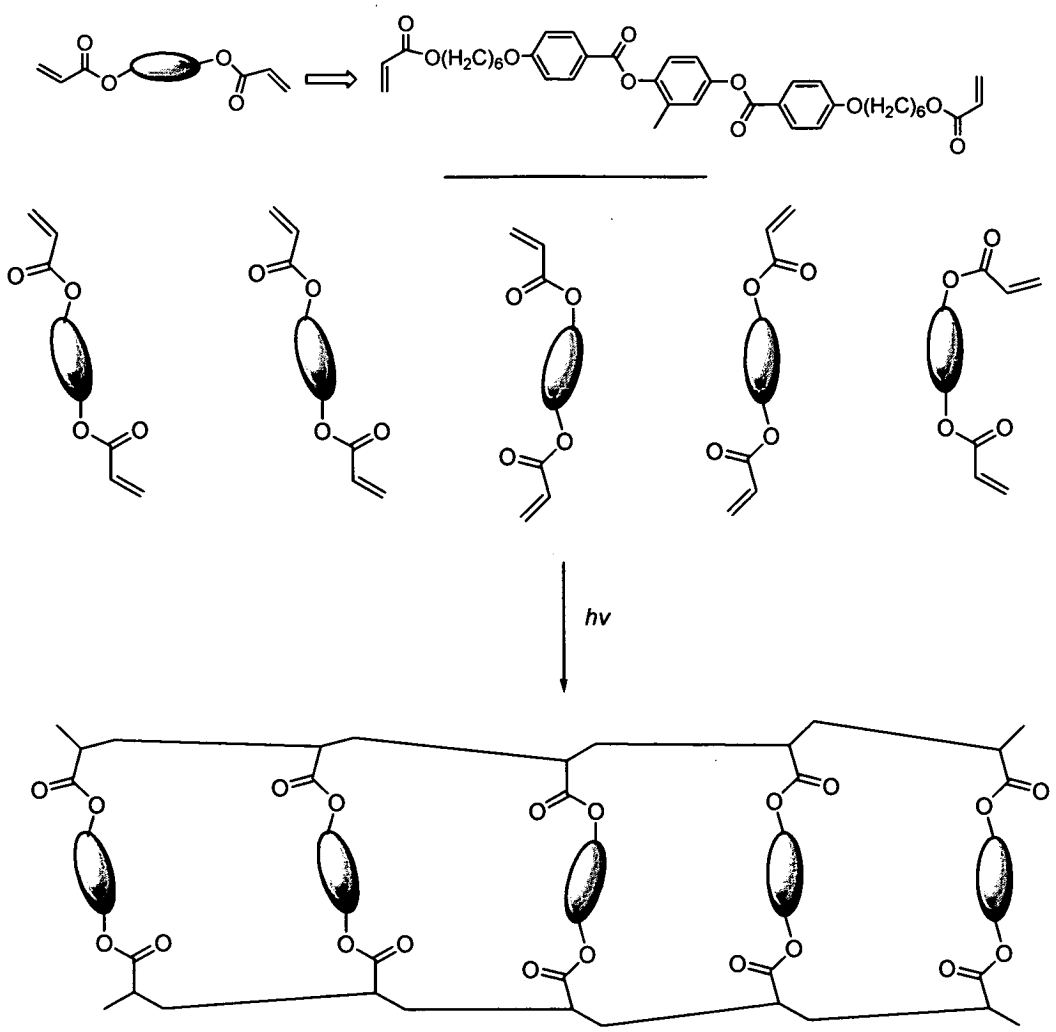

Figure 1.6: A simplified representation of the chemical structure of diacrylate mesogens before and after photo initiated cross-linking

1.2.3.1 Alignment of Reactive Mesogens for Optical Filters

To produce optically anisotropic films necessitates the alignment and orientation of liquid crystal mesogens in such a way that the material's optical anisotropy can be exploited. The short-range effect of aligning effects of the surface can be propagated through the sample to produce a mono-domain, which is then retained through polymerisation. Common alignments are illustrated in Figure 1.7.

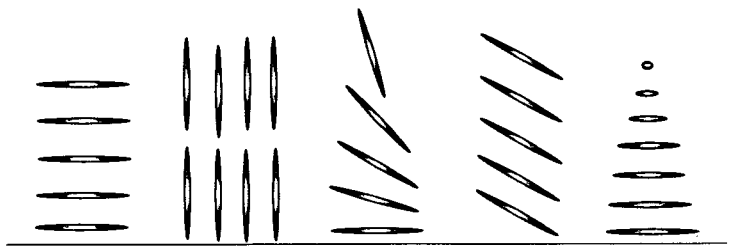

Figure 1.7: Some liquid crystal alignments which can be induced. From the left; parallel (homogeneous), perpendicular (homeotropic), splayed, tilted and twisted.

Different techniques can be employed to achieve control of the surface alignment. One common alignment layer is spin-coated polyimide, directionally rubbed to promote homogeneous alignment through interaction between the liquid crystal mesogens and the polymer.[85] Homeotropic alignment can be induced by treatment with lecithin or propyltrichlorosilane[85] to create a low energy surface. To produce a splayed alignment requires a homogeneous bottom interface and a homeotropic top interface, such that the mesogens splay between the two.[85] Overall alignment techniques in which two surfaces are present are well known,[124-126] having been the subject of much research for STN[37] and TN[88] LCD devices, however less is known about thin film systems in which only one interface is present[85] (the second interface is the LC – air surface). Studies into free standing films have revealed that the polarity of LC core groups[127] and terminal groups[128] are factors in determining the alignment at the air interface. Due to the weak strength of the interactions at this surface,[85] in the design of anisotropic polymer optical films the choice of alignment at the solid interface together with the choice of LC mixtures and mesogen substituents are the contributing factors.[129]

Chiral nematic reactive mesogens, introduced in section 1.2.3, are also able to be photo-polymerised into a thin film in the same way as nematic or smectic phases (Figure 1.8). Chiral nematic mesophases can be produced by a number of methods (section 1.2.1.3). Reactive mesogens can have intrinsic chirality and exhibit enantiotropic chiral nematic and other chiral LC mesophases. Alternatively, nematic reactive mesogens can be doped with chiral additives to induce a chiral nematic phase. The additives can themselves contain polymerisable groups, but do not possess their own LC phases.[80]

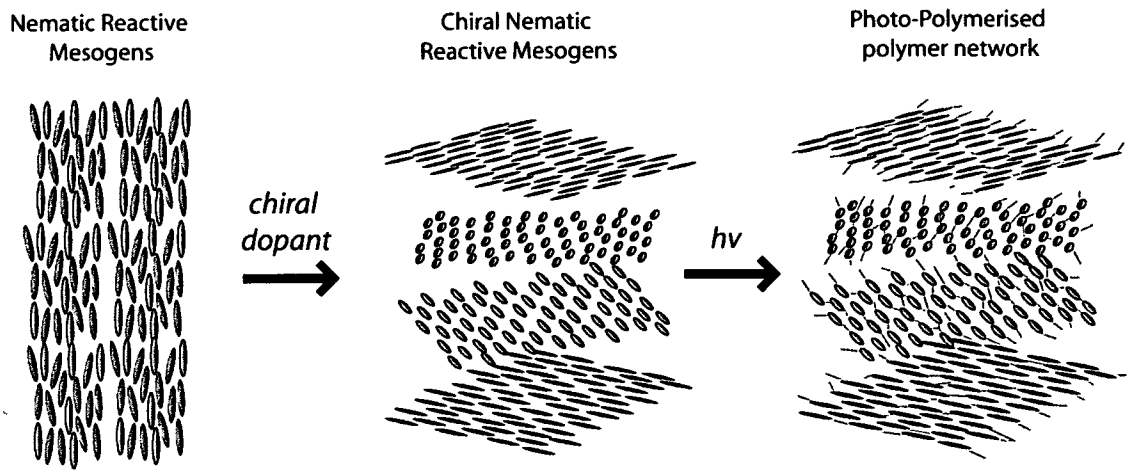

Figure 1.8: Formation of a chiral mesophase from the nematic by addition of a chiral dopant followed by photo-initiated cross-linking, in which the chiral structure is retained.

There are many advantages to creating optical films using reactive mesogens over traditional stretched polymer techniques.[85] These include lower cost, greater ease of manufacture, low film thickness (an order of magnitude thinner than other technologies) and ease of customisation. These benefits have led to many important commercial applications of this technology.[130-132] Films exhibiting properties such as half and quarter wave retardation[133,134] have been used to optimise the path of polarised light through displays, increasing viewing angles, off-axis brightness and contrast. The use of such compensation films is highly cost effective, the film being simply added to the display face.[135]

1.2.4 Development of Liquid Crystal Applications

Prior to the 1960s interest in liquid crystals was seen as an academic curiosity with little practical use,[136] however this was all to change. In 1963 Williams *et al*[137] observed an effect in a nematic LC sample that on application of a electric field the transparent, non scattering liquid crystal would begin to form visible patterns or 'domains'. Removal of the field caused the domains to vanish and the LC return to the original state. Heilmeier[138] discovered that at an increased voltage the domains observed by Williams were destroyed and in their place a turbulent and strongly light scattering state developed. This state was used to create the dynamic scattering mode (DSM) display, the first device to control the propagation of light electrically using a liquid crystal[102,139,140] which was used in the 1970's for digital watches

and calculators. This pioneering work rekindled the research interest in liquid crystals and within a few years, assisted by the invention of the twisted nematic field effect cell in 1971 by Schadt *et al*[88] and Fergason[141] and through the discovery of room temperature nematic cyanobiphenyl liquid crystals in 1973 by Gray *et al,*[142] the vision of Williams *et al* became fully realised. Through combined advances in solid-state electronics, the first commercial TN liquid crystal display was produced which superseded inferior DSM displays for low information display applications.[143] In the years that followed an extraordinary amount of research was carried out into the physical, chemical and technological aspects of liquid crystals and their application to display devices, resulting in exponential commercial growth of the liquid crystal industry.[144]

Liquid crystals, in addition to their use inside the display as an optical switch, have also found a market in the production of LCD compensators.[135] These devices are typically, but not exclusively, created by thin film coating of solvent-based reactive mesogen (RM) liquid crystal mixtures, which contain dual cross-linkable functionality, formulated to exhibit a mesophase at room temperature. Using substrate treatment, the microscopic structure of the film can be modified and macroscopic films can be made to exhibit optical properties. Using an *in-situ* photo-polymerisation process[99,113] the films can be cross linked preserving the structure and creating a resilient, temperature independent film. These films can be used to reflect specific wavelengths of light,[145] rotate the plane of polarised light[146] or filter unwanted polarisations[94] and have been widely used in the manipulation of the optical path through LCDs, for the improvement of brightness,[147] off axis contrast[146,148] and colouration.[149-151] Reactive mesogens will be discussed in more detail in section 1.2.3 and chapter 4.

1.3 Liquid Crystal Properties and Characterisation

Liquid crystals exhibit a number of unique anisotropic properties and hence a great many physical characteristics can be measured. For consideration in this thesis, it is pertinent to include an overview of screening methods employed in the traditional characterisation of liquid crystals, and to develop an understanding of the analytical techniques. The major properties that are exhibited by LC materials are summarised in the following sections. It is

necessary to determine many of these properties to assess a materials potential use in commercial LC display devices (see section 1.4).

1.3.1 Optical Phase Identification

Individual LC materials may exhibit one or more of the liquid crystal mesophases described in section 1.2, over a variable temperature range. The technique of optical polarising microscopy is used to assist structural classification of each of these phases through identification of the textures exhibited in samples prepared between glass slides, and observed between crossed linear polarisers[73] (Figure 1.9). In a crossed polariser configuration, the sample is placed between two linear polarisers, which are aligned with their axis of polarisation at 90° to each other so that light transmitted through the first polariser is extinguished by the second.

In the nematic phase, textures such as threads and brushes referred to as the 'Schlieren'[152] texture, can be seen in the LC sample (Figure 1.9). These occur due to defects in the nematic liquid crystal where the director, which is not continuous throughout the sample and hence forms micro domains of similar alignment, meets a second micro domain with an alternative orientation. At this position, a point or line defect is formed where the LC alignment is poorly defined.[153] Where the LC director is exactly parallel or perpendicular to the axis of polarisation the sample appears optically extinct (black) at this point, as the linearly polarised light propagating through the sample experiences only one refractive index and passes without change.[154] At all other director orientations the light experiences both ordinary and extraordinary refractive indices, so light propagates at different speeds creating bright or coloured areas due to optical interference. Samples are heated from the melt using a controlled hot stage, observing the textures formed and the temperature at which they change through a microscope. To enhance the textures and allow differentiation and identification of mesophases the glass slides can be pre-treated[155] to promote the alignment of liquid crystal mesogens on the surface.

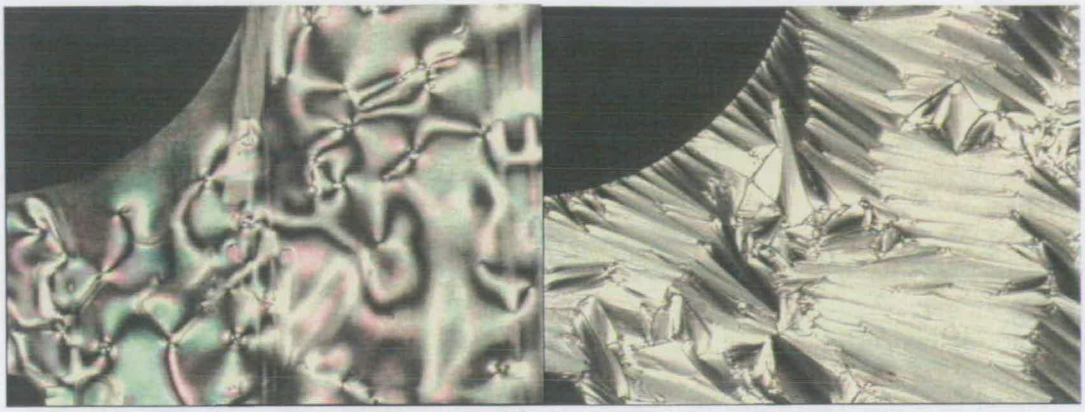

Figure 1.9: The Textures exhibited by liquid crystal K27 when coated onto an untreated glass substrate (homogeneous alignment) and observed under crossed polarisers. The Schlieren textures of the nematic (N) phase and the focal conic textures in the smectic A (SmA) phase can be seen due to birefringence.

Homogeneous alignment can be achieved by coating the surface of the glass slides with polyimide (*via* spin coating), followed by uni-directional rubbing of the polyimide using a micro fibre textile such as velvet which is able to re-align the polymer chains of the polyimide in the direction of rubbing. A liquid crystal in contact with this interface will tend to align parallel to the polymer surface due to interactions with the face of the phenyl ring. In this arrangement the mesogens, and hence the director, lie in the plane of the surface (Figure 1.10). If homeotropic alignment is invoked (Figure 1.10) using a PVA or lecithin aligning layer on the glass, the mesogens stand perpendicular to the substrate surface due to the favourable interaction with the polar end of the liquid crystal. In this alignment, the liquid crystal between two glass slides will exhibit a black texture that flashes on perturbation of the alignment layers, due to the director orientation becoming disturbed from the perpendicular. This occurs due to the two components of incident light propagating through the cell experiencing identical refractive indices down the molecular axis, *i.e.* the material is considered uniaxial[156] and no birefringence is observed. Untreated glass can exhibit either homeotropic or homogeneous alignment depending on the liquid crystal film thickness.

Smectic phases exhibit different textures depending on their structure (SmA, SmB, SmC) and the surface alignment. Typical textures include the focal conic of the smectic A and smectic C in homogeneous alignment, and the Schlieren texture of the smectic C texture in the homeotropic alignment (Figure 1.9). A thorough overview of the technique and the different textures can be found in Dierking`s book.[157] The optical appearance of textures is

due to birefringence, the cause of which will be explained later in this section. The technique of optical microscopy is highly sensitive and gives a great deal of information about the liquid crystal phases. However, microscopy is also a very time-consuming and laborious process, which requires a trained eye to identify the many complex textures formed.

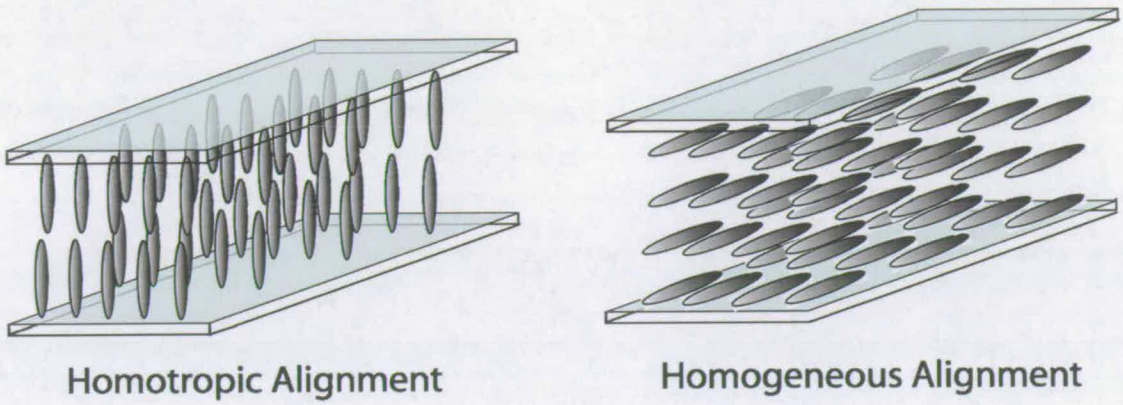

Figure 1.10: The two alignments used to observe LC textures.

1.3.2 Calorimetric Measurements

In addition to the different types of phase formed in a liquid crystal material, the temperatures at which these phases form are important in the characterisation of LC materials. The measurement of two transitions, the crystalline solid to liquid crystal, and the liquid crystal to isotropic liquid defines the stability of the liquid crystal phase, within which smectic transitions may also exist. Measurement of transition temperatures has been carried out by a great many methods[158] including optical microscopy (microscope hot stage), optical transmission measurement (Mettler oven), differential thermal analysis (DTA) and differential scanning calorimetry (DSC). Of these the most widely used are optical transmission, microscopy and differential scanning calorimetry.[159]

The method of optical measurement involves monitoring the variation in transmitted light intensity through a sample (using a photodiode), as a function of temperature. In a mesogenic material, the formation of crystalline, smectic, nematic and isotropic phases can be determined due to the different light scattering ability of these phases.

The technique of polarising microscopy has already been described and can be used to identify the transition temperatures by the change in optical textures caused by birefringence in the liquid crystal phase.

Differential scanning calorimetry (DSC) is a highly sensitive technique which in some cases can identify transitions not detected by other methods and therefore is the most commonly used.[160] The sample is loaded into a furnace and heated, at the same rate as a second reference furnace containing a reference sample. During a phase transition, more energy is required by the sample as its structure changes and hence more power needs to be provided by the sample furnace to maintain its temperature at an identical value to the reference. This increase in energy flow is monitored and can be used to show the temperatures at which transitions occur. Although this technique is highly sensitive and the most reliable experimental tool in the identification of phase transitions,[160] it has a disadvantage over polarising microscopy as it gives no data on the structure of the mesophase. DSC does however provide information on the enthalpy, which can be used to identify the type of transition involved. A melting transition is a major structural rearrangment, involving an enthalpy change of 30-50 kJ/mol.. In contrast, an LC to LC or LC to isotropic transition involves a much more subtle change and therefore shows an enthalpy of 0.3-6 kJ/mol depending on the mesophase. As a result, DSC and polarising microscopy have become important complementary techniques.

1.3.3 Optical Anisotropy

Optical anisotropy (birefringence) is a fundamental property of liquid crystals, a result of the material possessing different refractive indices parallel and perpendicular to the director. This occurs due to a combination of anisotropic polarisability, molecular structure[161] and macroscopic orientational order.[156,162]

In a uniaxial birefringent material such as a liquid crystal, incident light will be split into two components, the ordinary ray propagates parallel to the molecular axis experiencing the ordinary refractive index $n_{\perp}$ and the extraordinary ray propagates perpendicular to the molecular axis experiencing the extraordinary refractive index $n_{\parallel}$ (Figure 1.11).

The difference in the two refractive indices is due to the polarisability of the molecule, a result of the tendency of the charge distribution (the presence of delocalised non-bonding or π electrons over the molecule) to be affected by application of an external field. Anisotropic polarisability occurs in calamitic liquid crystals because of their shape and structure, resulting in the polarisability being higher in one direction than in the other. Thus, light polarised parallel or perpendicular to the director propagates through the liquid crystal with

no change its polarisation, whereas light polarised at an angle between parallel and perpendicular will have one component of its polarisation retarded. This optical retardation results in linear polarised light emerging elliptically polarised due to the phase difference between the components. The magnitude of the phase difference is dependent on the thickness of the sample, the wavelength of incident light and the temperature.

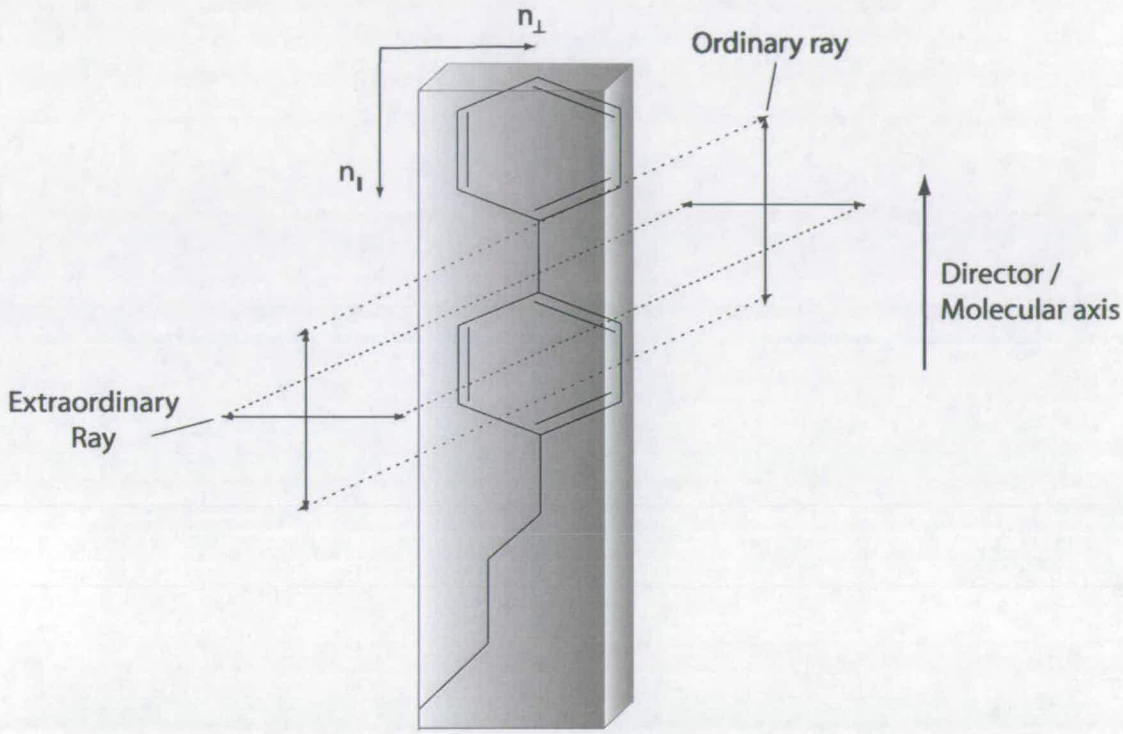

Figure 1.11: The interaction of ordinary and extraordinary components of light with the anisotropic liquid crystal. The refractive index across the molecule is different from that along the molecular axis.

The birefringence of the LC material is defined by the difference between the extraordinary and ordinary refractive index (equation 1.6). Birefringence can therefore take either a positive or a negative value. For calamitic nematics, where the long axis posses a large molecular polarisability, $n_{\parallel} > n_{\perp}$ and hence Δn is positive. In the case of materials such as discotics, in which the short axis has a larger polarisability than the long axis, $n_{\perp} > n_{\parallel}$ and hence Δn is negative.

$$\Delta n = (n_{\parallel} - n_{\perp})^{163} \qquad \textit{Equation 1.6}$$

In an optically isotropic medium, light will travel through the material at the same velocity whatever its orientation with respect to the field. In this case the anisotropy Δn is zero. Measurement of refractive indices and Δn can be achieved either by observation of the deviation of a ray through a sample using an Abbe double prism refractometer, by an interference method such as a wedge cell in which the separation of interference fringes are used to derive the birefringence,[164] or using a rotating analyser by monitoring and comparing the phase angle of rotated light to that of a reference beam.[165,166]

1.3.4 Dielectric Anisotropy

The dielectric anisotropy is the difference in the relative dielectric permittivity (ε) of the material measured when a field is applied parallel ($\varepsilon_{\parallel}$) and perpendicular ($\varepsilon_{\perp}$) to the LC director in an aligned sample. (Equation 1.7)

$$\Delta\varepsilon = (\varepsilon_{\parallel} - \varepsilon_{\perp}). \qquad \textit{Equation 1.7}$$

The dielectric permittivity is measured using capacitance, where C is the capacitance of a filled capacitor and C_o the capacitance of a empty capacitor[167] (Equation 1.8). The dielectric anisotropy occurs due to the charge distribution along the molecular axis responding differently to the applied field than the charge distribution across the molecular axis.

$$\varepsilon = C/C_o \qquad \textit{Equation 1.8}$$

To measure the dielectric anisotropy requires alignment of the liquid crystal director. This can be achieved using two separate parallel plate capacitors with the electrodes coated in an alignment layer so that in one a homogeneous and the other a homeotropic orientation to the electrode surface is induced. The capacitance of the filled and empty capacitors can then be measured to obtain values of $\varepsilon_{\parallel}$ and $\varepsilon_{\perp}$. An alternative method using a single cell involves the alignment of the liquid crystal director using an external magnetic field. The capacitor electrode coated with a homogeneous aligning layer induces a parallel orientation, so in the absence of a field $\varepsilon_{\parallel}$ can be gained. By application of a field across the cell, the molecules orientate so that the director is perpendicular to the electrode, enabling $\varepsilon_{\perp}$ to be obtained. In both cases, capacitance is measured by low frequency AC excitation which prevents director orientation with the applied electric field occuring due to rapid phase inversion. $\Delta\varepsilon$ is

temperature and field dependent and its value and sign play an important role in the applications of LCs. A larger value of $\Delta\varepsilon$ indicates that the LC can orientate to a low voltage applied field.

1.3.5 Diamagnetic Susceptibility Anisotropy

An organic LC exhibits diamagnetism, and therefore can be aligned by an external magnetic field,[168] in a similar way to an electric field. The diamagnetic susceptibility anisotropy ($\Delta\chi$) is defined by the diamagnetic susceptibility components parallel ($\chi_{\parallel}$) and perpendicular ($\chi_{\perp}$) to the director

$$\Delta\chi = (\chi_{\parallel} - \chi_{\perp}). \qquad \textit{Equation 1.9}$$

$\Delta\chi$ is able to take both positive and negative values and so external control of the alignment of the LC director is possible by application of a magnetic field.

Measurement of diamagnetic properties must be carried out using highly sensitive and complex equipment such as a Faraday-balance for measurement of a force exerted on a sample in an inhomogeneous magnetic field, or a superconducting quantum interference device (SQUID) method[169] in which the applied field can be varied during measurements. Alternatively NMR[170] or magneto-electro-optical methods[171] can be used.

1.3.6 Elastic Constants

When LCs are influenced by an external field their molecular dipoles interact to orientate along the external field lines. However when the field is removed the molecules return to their original orientation by influence of an elastic torque. The torque is broken down into splay, twist and bend forces, associated to the elastic constants k_1, k_2 and k_3 which describe how resilient the LC is to director distortion.[172] Elastic constants are directly related to the structure of the LC molecules; generally the core structure and linking group contribute the most.[173] Measurement of elastic constants can be achieved using any method in which a perturbation of the director orientation produces a measurable response,[174] and therefore a great many techniques are reported in the literature.[175,176]

The most commonly used technique is measuring the response of a thin sample of nematic to an external magnetic or electric field *via* measurement of capacitance or birefringence.[177]

Each measurement is very time-consuming, as equilibrium must be reached before collecting data. An alternative method is an optical technique in which light, elliptically polarised by the LC cell, is analysed during the application of a magnetic or electric field. The resulting transmitted intensity is then related to k_1, k_2 and k_3 and values derived theoretically.[178]

1.3.7 Viscosity

A nematic LC exhibits complex anisotropy in its viscosity, described for a nematic liquid crystal using five viscosity coefficients[162] grouped into 4 shear viscosity coefficients, η_1, η_2, η_3, $\eta_{1,2}$ and a rotational viscosity γ_1. The magnitude of these viscosities becomes important when considering the rate at which energy can be dissipated as the LC director returns to its equilibrium state after an external perturbation. Measurement of these viscosity coefficients is through a first principles method either by measuring direct properties, or by indirect measurements considering the associated physical measurements, which are related to the viscosity coefficients, and then deriving them through theoretical models requiring the knowledge of other quantities. More information on these properties and their measurements can be found in the literature[159] including methods of measurement.[179,180] They will not be dealt with here due to their complexity. In addition to these methods, bulk viscosity can be measured by the use of a commercial rheometer.

1.4 Liquid Crystal Displays

The principle behind an optical display is that of an electrically controlled light gate. The use of liquid crystals as the medium for such a device[137] is possible because the orientation of a thermotropic calamitic liquid crystalline material, due to its large dielectric anisotropy,[181] can be manipulated by an external field. The first device to be developed using this principle was the dynamic scattering mode display.[137,138,182] These displays found few uses due to their relatively high power consumption, limited lifespan and poor contrast. In 1971 Fergason[141] and Schadt *et al*[88] developed the twisted nematic (TN) display with much improved properties, offering low power consumption, high contrast ratio, high brightness and long term stability. This display was the first to enter mass production, remaining in production to date due to its low cost.

The successors of the TN display, many of which are used for the manufacture of today's advanced LCDs,[88] include super twisted nematic (STN),[37,183] in-plane switching (IPS)[184-186] vertically aligned,[187-190] guest-host dichroic,[191] laser addressed smectic A,[192] ferroelectric smectic C*[193] and polymer dispersed liquid crystalline.[194] These displays all rely on different principles of light modulation. There are useful reviews on the various types of LCD`s in books by Bahadur[195] and Castellano.[190]

1.4.1 Twisted Nematic Mode of Operation

The twisted nematic (TN) cell consists of two glass plates, which are coated on one face with a transparent electrode (usually indium tin oxide (ITO)). Onto the electrode side of the substrate a polyimide film is deposited, used both for parallel alignment of the liquid crystal[85] through uni-directional rubbing, and for providing a non-conductive barrier over the electrode. The two substrates are placed on top of each other in a sandwich arrangement, separated by a spacer to maintain a constant cell gap. The rubbing of the polyimide film on the top and bottom glass plates is arranged to be perpendicular. The cell is then filled with LC material before being hermetically sealed. (Figure 1.12)

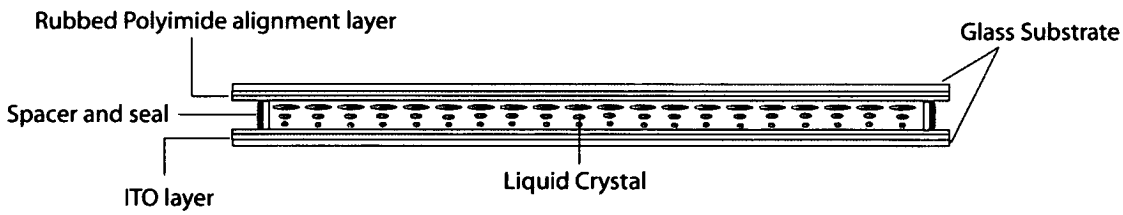

Figure 1.12: The construction of a liquid crystal display optical cell.

The perpendicular arrangement of the two rubbed surfaces induces a twist in the director across the cell, promoted by the addition of a small amount of chiral dopant to ensure that the twist is not confined to domains[196] (Figure 1.13). The pitch, p, must be much larger than the wavelength of light, λ, to fulfil the Maugin limit expressed in equation 1.10.[197]

$$\lambda << (n_e - n_o)\, p \qquad \textit{Equation 1.10}$$

If this condition is fulfilled and the incident light is perpendicular to the LC axis, then the TN cell acts as a wave-guide without destroying linear polarisation. Thus, in the inactivated ('off') state in which no current is applied across the cell, linear polarised light entering the cell has its plane of polarisation rotated and is able to exit through the second, perpendicularly aligned polariser on the opposite side of the cell. This results in the cell appearing translucent. Light travelling through the wave-guide has its polarisation rotated by angle $2\pi.d/p$ with respect to its original direction;[197] to ensure that the polarisation is rotated through 90 °C and optimum transmission through the second polariser is achieved, the cell gap d is optimised (typically in the order of 10μm).

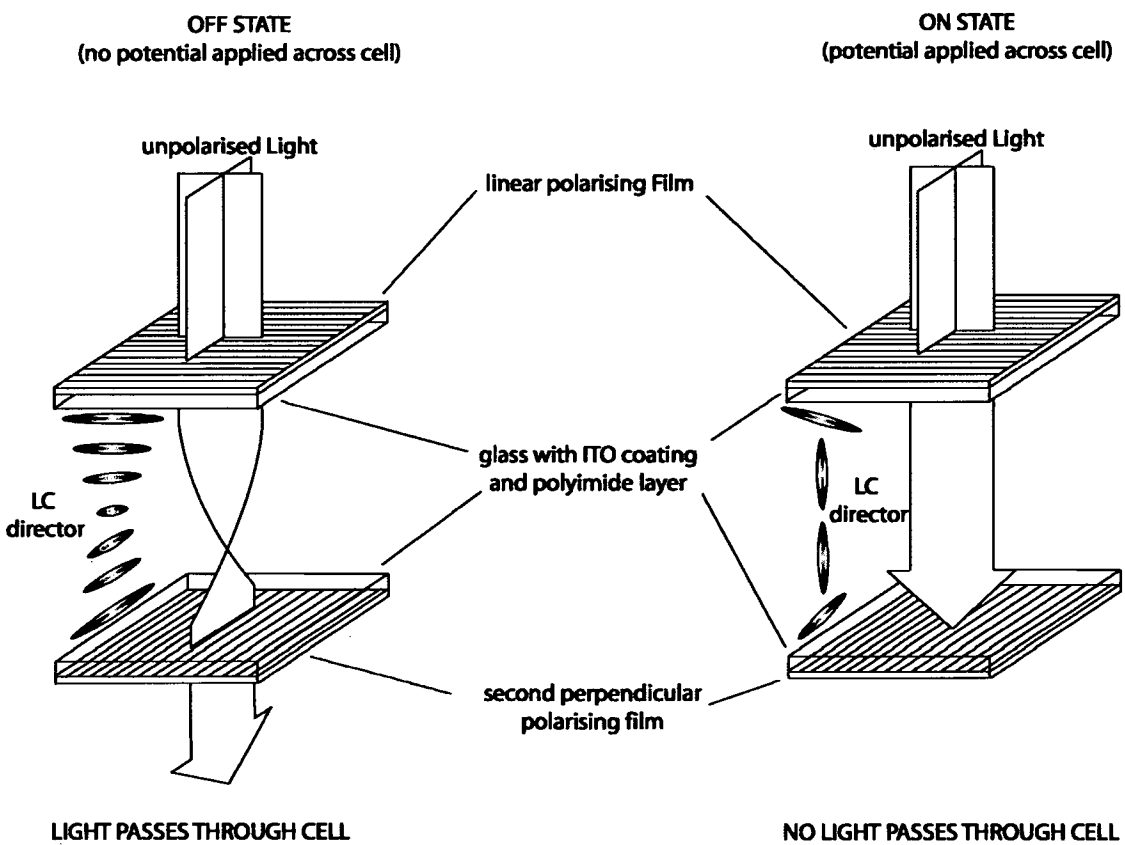

Figure 1.13: The operation of a twisted nematic liquid crystal cell in the on and off states.

In the 'on' state, when a potential V is applied across the cell the dielectrically anisotropic liquid crystals align with the field, destroying the twisted director orientation and the waveguiding properties of the cell. This orientation no longer rotates the plane of linear

polarised light and so the light passing through the cell is blocked by the second polariser, making the cell appear black. If the polarisers are aligned with their plane of polarisation perpendicular, transmission will only occur in the 'off' state (normally white (NW) mode), whereas in polarisers aligned with their plane of polarisation parallel across the cell transmittance will only occur in the 'on' state (normally black (NB) mode). Removal of the voltage causes the LC to return to its original alignment through elastic forces, which reorientate the director to the lowest energy equilibrium state.[6]

1.5 Combinatorial and High Throughput Methods

Over the past two decades the concept of combinatorial chemistry has revolutionised the pharmaceutical industry, becoming a key technology in the development of new lead structures and structure optimisation.[198] This growth has enabled the creation and screening of thousands of compounds on a very short timescale providing higher success rates, shorter lead development times, reduction in research costs and a quicker time-to-market for new materials.[15] The combinatorial process involves the design and synthesis of structurally or compositionally diverse, high-density libraries, followed by rapid screening of a relevant physical or chemical property to identify families of compounds with desirable characteristics. Once identified these 'hits' can then be produced on a larger scale to enable more detailed characterization.[15]

To date, virtually all LC synthesis and formulation has been performed using traditional methods. As a consequence, full exploration of the experimental landscape is restricted due to limitations of time and practicality. Shortening the time taken to probe the bulk properties of chemical compositions for trends would be desirable.[24] Through analysis of the current literature on HT methods in liquid crystal chemistry, there is clear potential for further development in the areas of synthesis, formulation and characterisation. The first area to adopt combinatorial and parallel methodologies in liquid crystal material research was synthesis, where over the last few years there have been a number of publications[32-37] illustrating how the classical route for the synthesis of liquid crystals can be adapted. Deeg et al[32] showed the parallel combinatorial synthesis of a library (225 members) of *p*-quaterphenyl based liquid crystals in high yield, introducing diversity into to a central core by a combination of parallel and one-pot reactions so that structure property relationships could be explored by automated DSC analysis. An alternative solid supported[199]

combinatorial synthesis of a tropinoid LC library was demonstrated by Hashimoto et al,[33] in which a 40 member library was produced with sufficient purity to determine mesomorphic properties. Other solid phase techniques include the work of Hioki,[34] who developed a 28 member azomethine linked liquid crystal library using a traceless linker[200] to detach the final product from the resin,[201] and Mori[35] who prepared a 100 member library of two and three ring benzenoid amides on solid support. Other examples of LC synthesis include the methods of Goulding[36] who demonstrated the one pot parallel synthesis of multiple 4-alkyl-4`cyanobiphenyls followed by preparative HPLC purification, and Kang[37] who prepared a 40 member library by the coupling of resorcinol derivatives, 4-formylbenzoic acids and 4-alkoxyanalines to form bent shaped mesogens. Styring[31] has also explored the possibility of using micro reactor technologies in the synthesis of LC libraries. Although many of these libraries have been basic, due to their small size, they illustrate that this procedure is feasible and through up-scaling much larger libraries can be produced.

The other technique used in the production of new materials is that of mixture formulation. Formulation is an important area of research, allowing the design of mixtures with properties that are not possible to achieve using a single liquid crystal. The process of formulation is relatively straightforward, mixing a number of components together and testing the properties of the resulting material. Through an iterative method, the composition can be changed so that properties with the desired magnitudes are obtained. It appears bizarre that this process of formulation is usually carried out manually, and by a gravimetric process despite the huge advances in liquid handling robots over the past decade. One reason for this can be attributed to the lack of a suitable high-throughput screening method, and the nature of LC materials that exhibit solid, LC and liquid phases at room temperature, making accurate dispensing difficult.

The lack of availability of techniques for HT liquid crystal characterisation is a fundamental drawback in HT liquid crystal research. In pharmaceutical research, methods of combinatorial chemical synthesis have evolved together with rapid analysis, HT screening. advancements in automation, computation and high capacity informatics.[15] Unfortunately, in the area of liquid crystals new HT techniques are required for the development of screening methods, whilst at the same time HT screening methods are required to make the development of HT techniques worthwhile.

In synthesis, although good progress has been made in establishing combinatorial methods, the characterisation in every case is by either optical polarising microscopy, DSC or a

combination of the two. These time-consuming, 'one at a time' techniques offer acceptable throughput for smaller libraries, allowing detailed results to be obtained speeded by the advances in DSC auto sampling. The problem occurs when the rate of synthesis is increased ten-fold using combinatorial methods (combinatorial synthesis, parallel synthesis or robotic formulation), but the screening rate cannot be increased by a similar factor, therefore creating a bottleneck. The time taken to analyse a large dataset in full can increase dramatically, detracting from the value of increased synthetic efficiency. These reasons can go some way to explain why HT techniques have been only recently adopted, as they only became feasible when high-throughput analysis (lower cost, auto-sampling DSC) was made available. The same reasons can also explain why HT mixture formulation techniques have not yet been developed, despite the availability of advanced robotics. The diverse screening techniques required for materials libraries involve a different approach from that of pharmaceutical libraries. Each new application requires a specific technique, which often has to be developed in parallel with the combinatorial methodology.

The development of high-throughput methods is unlikely to have an influence on the current mature and well-established manufacturing processes for liquid crystal display devices. However, the continued production of optimised materials is of crucial importance in the search for new applications and for technological improvements, which are required to sustain the economic growth of the liquid crystal market. Of particular importance is the possibility of using materials in non-display applications, here a great many materials have application potential but are yet to be established as commercially viable. Only through the development of high-throughput methods, which enable previously unexplored avenues to be investigated, will novel and improved materials be discovered with speed and efficiency. By establishing the same synergistic relationship between technology and application which drove the development of LCD technology, novel applications can be envisaged.

1.6 Aims of The Work

The objectives of the work discussed and described in this thesis are to apply high-throughput techniques to liquid crystals *via*:

- *The development of new high-throughput screening techniques for liquid crystals*

by evaluation of current analytical methods and the development of new or modified high-throughput techniques for the characterisation of liquid crystal properties, especially those important for initial screening and relevant to their application in liquid crystal display devices.

- *Use of current and cutting edge technologies to create formulation arrays*

to investigate the available technologies for producing formulation libraries, selecting suitable methods for the creation of liquid crystal mixtures ensuring that the sensitive mesophase behaviour is preserved.

- *Use of high-throughput screens to analyse formulation arrays*

using the methods of high-throughput formulation and high-throughput screening to create a large liquid crystal library and identify areas in which desired optimum properties can be observed.

- *Assessment of high-throughput screening and formulation technologies in other areas of liquid crystal research*

investigating the transfer of formulation and screening techniques to other areas of liquid crystal technology – specifically focusing on the area of formulation and screening of reactive mesogen films.

1.7 References

(1) D. Pauluth and K. Tarumi, *J. Mater. Chem.*, **2004**, *14*, 1219.
(2) G. Meier, E. Sackmann and J. G. Grabmaier, *Applications of liquid crystals*, Berlin: Springer-Verlag, **1975**.
(3) S. Kobayashi, H. Hori and Y. Tanaka In *Handbook of liquid crystal research*, P. J. Collings and J. S. Patel (Eds.), New York ; Oxford: Oxford University Press, **1997**. p 415.
(4) M. Hird In *Physical properties of liquid crystals : Nematics*, D. Dunmur, A. Fukuda and G. R. Luckhurst (Eds.), London: Institute of Electrical Engineers, **2001**. p 10.
(5) M. Francis, D. Ionescu, M. Goulding, K. Adlem, B. Rieger, H. Hirschmann, V. Reiffenrath and A. Kojima, *Mol. Cryst. Liq. Cryst.*, **2004**, *411*, 1113.
(6) G. W. Gray and S. M. Kelly, *J. Mater. Chem.*, **1999**, *9*, 2037.
(7) A. K. Singh, R. Manohar, J. P. Shukla and A. M. Biradar, *Acta Phys. Pol., A*, **2006**, *110*, 485.
(8) J. D. Margerum, C. I. Van Ast, G. D. Myer and W. H. Smith, Jr., *Mol. Cryst. Liq. Cryst.*, **1991**, *198*, 29.
(9) J. Constant, E. P. Raynes, G. W. Gray, D. Lacey and D. G. McDonnell, GB Patent, GB2061311, **1981**.
(10) H. Hirschmann and V. Reiffenrath In *Handbook of liquid crystals: Low molecular weight liquid crystals i*, D. Demus, J. W. Goodby, G. W. Gray, H. W. Spiess and V. Vill (Eds.), Weinheim ; Chichester: Wiley-VCH, **1998**, Vol. 2A. p 221.
(11) G. H. Brown and W. G. Shaw, *Chem. Rev.*, **1957**, *57*, 1049.
(12) G. W. Gray, *Mol. Cryst. Liq. Cryst.*, **1969**, *7*, 127.
(13) G. W. Gray, *Molecular structure and the properties of liquid crystals*, London: Academic Press, **1962**.
(14) M. Hird In *Physical properties of liquid crystals : Nematics*, D. Dunmur, A. Fukuda and G. R. Luckhurst (Eds.), London: Institute of Electrical Engineers, **2001**. p 3
(15) B. Jandeleit, D. J. Schaefer, T. S. Powers, H. W. Turner and W. H. Weinberg, *Angew. Chem., Int. Ed. Engl.*, **1999**, *38*, 2495.
(16) S. M. Senkan, *Nature*, **1998**, *394*, 350.
(17) S. J. Taylor and J. P. Morken, *Science*, **1998**, *280*, 267.
(18) T. R. Boussie, C. Coutard, H. Turner, V. Murphy and T. S. Powers, *Angew. Chem., Int. Ed. Engl.*, **1998**, *37*, 3272.
(19) T. Bein, *Angew. Chem., Int. Ed. Engl.*, **1999**, *38*, 323.
(20) W. F. Maier, *Angew. Chem., Int. Ed. Engl.*, **1999**, *38*, 1216.
(21) M. T. Reetz, *Angew. Chem., Int. Ed. Engl.*, **2001**, *40*, 284.
(22) P. P. Pescarmona, J. C. van der Waal, I. E. Maxwell and T. Maschmeyer, *Catal. Lett.*, **1999**, *63*, 1.
(23) F. Schuth, O. Busch, C. Hoffmann, T. Johann, C. Kiener, D. Demuth, J. Klein, S. Schunk, W. Strehlau and T. Zech, *Top. Catal.*, **2002**, *21*, 55.
(24) X. D. Xiang, X. D. Sun, G. Briceno, Y. L. Lou, K. A. Wang, H. Y. Chang, W. G. Wallacefreedman, S. W. Chen and P. G. Schultz, *Science*, **1995**, *268*, 1738.
(25) E. Danielson, J. H. Golden, E. W. McFarland, C. M. Reaves, W. H. Weinberg and X. D. Wu, *Nature*, **1997**, *389*, 944.
(26) J. S. Wang, Y. Yoo, C. Gao, I. Takeuchi, X. D. Sun, H. Y. Chang, X. D. Xiang and P. G. Schultz, *Science*, **1998**, *279*, 1712.
(27) K. Choi, D. Gardner, N. Hilbrandt and T. Bein, *Angew. Chem., Int. Ed. Engl.*, **1999**, *38*, 2891.
(28) M. A. R. Meier, R. Hoogenboom and U. S. Schubert, *Macromol. Rapid Commun.*, **2004**, *25*, 21.
(29) S. Schmatloch, M. A. R. Meier and U. S. Schubert, *Macromol. Rapid Commun.*, **2003**, *24*, 33.

(30) R. Hoogenboom, M. A. R. Meier and U. S. Schubert, *Macromol. Rapid Commun.*, **2003**, *24*, 16.
(31) P. Styring, *Mol. Cryst. Liq. Cryst.*, **2004**, *411*, 1059.
(32) O. Deeg, P. Kirsch, D. Pauluth and P. Bauerle, *Chem. Commun.*, **2002**, 2762.
(33) M. Hashimoto, A. Mori, H. Inoue, H. Nagamiya, T. Doi and T. Takahashi, *Tetrahedron Lett.*, **2003**, *44*, 1251.
(34) H. Hioki, M. Fukutaka, H. Takahashi, M. Kodama, K. Kubo, K. Ideta and A. Mori, *Tetrahedron Lett.*, **2004**, *45*, 7591.
(35) A. Mori, I. Akahoshi, M. Hashimoto, T. Doi and T. Takahashi, *Tetrahedron Lett.*, **2004**, *45*, 813.
(36) M. Goulding, K. Adlem and R. Tanner, *Mol. Cryst. Liq. Cryst.*, **2004**, *411*, 1043.
(37) S. Kang, J. Thisayukta, H. Takezoe, J. Watanabe, K. Ogino, T. Doi and T. Takahashi, *Liq. Cryst.*, **2004**, *31*, 1323.
(38) P. J. Collings and M. Hird, *Introduction to liquid crystals : Chemistry and physics*, London: Taylor & Francis, **1997**, p 47.
(39) M. Neubert In *Liquid crystals : Experimental study of physical properties and phase transitions*, S. Kumar (Eds.), Cambridge: Cambridge University Press, **2001**. p 393.
(40) T. Thiemann and V. Vill In *Handbook of liquid crystals: Fundamentals*, D. Demus, J. W. Goodby, G. W. Gray, H. W. Spiess and V. Vill (Ed.), Weinheim: Wiley-VCH, **1998**, Vol. 1. p 87.
(41) T. Thiemann and V. Vill In *Handbook of liquid crystals: Fundamentals*, D. Demus, J. W. Goodby, G. W. Gray, H. W. Spiess and V. Vill (Eds.), Weinheim: Wiley-VCH, **1998**, Vol. 1. p 107.
(42) N. K. Terrett, *Combinatorial chemistry*, Oxford: Oxford University Press, **1998**.
(43) R. A. Pelcovits In *Handbook of liquid crystal research*, P. J. Collings and J. S. Patel (Eds.), New York ; Oxford: Oxford University Press, **1997**. p 88.
(44) D. J. Cleaver In *Physical properties of liquid crystals : Nematics*, D. Dunmur, A. Fukuda and G. R. Luckhurst (Ed.), London: Institution of Electrical Engineers, **2001**. p 644.
(45) M. Bremer and K. Tarumi, *Adv. Mat.*, **1993**, *5*, 842.
(46) M. Klasen, M. Bremer, A. Gotz, A. Manabe, S. Naemura and K. Tarumi, *Jpn. J. Appl. Phys. 2*, **1998**, *37*, L945.
(47) S. Kuwajima and A. Manabe, *Chem. Phys. Lett.*, **2000**, *332*, 105.
(48) F. Reinitzer, *Monatsh. Chem.*, **1888**, *9*, 421
(49) G. Friedel, *Ann. Phys.*, **1922**, *18*, 273.
(50) P. J. Collings and M. Hird, *Introduction to liquid crystals : Chemistry and physics*, London: Taylor & Francis, **1997**, p 133.
(51) P. J. Collings and M. Hird, *Introduction to liquid crystals : Chemistry and physics*, London: Taylor & Francis, **1997**, p 12.
(52) C. Fairhurst, S. Fuller, J. Gray, M. C. Holmes and G. J. T. Tiddy In *Handbook of liquid crystals: Low molecular weight liquid crystals ii*, D. Demus, J. W. Goodby, G. W. Gray, H. W. Spiess and V. Vill (Eds.), Weinheim: Wiley-VCH, **1998**, Vol. 3. p 341.
(53) S. Hoffmann In *Handbook of liquid crystals: Low molecular weight liquid crystals ii*, D. Demus, J. W. Goodby, G. W. Gray, H. W. Spiess and V. Vill (Eds.), Weinheim: Wiley-VCH, **1998**, Vol. 3. p 393.
(54) H. Ringsdorf, B. Schlarb and J. Venzmer, *Angew. Chem., Int. Ed. Engl.*, **1988**, *27*, 113.
(55) H. Zimmermann, R. Poupko, Z. Luz and J. Billard, *Z. Naturforsch. A.*, **1985**, *40*, 149.
(56) J. Malthete, H. T. Nguyen and C. Destrade, *Liq. Cryst.*, **1993**, *13*, 171.
(57) J. Malthete and A. Collet, *New J. Chem*, **1985**, *9*, 151.
(58) S. Chandrasekhar, B. K. Sadashiva and K. A. Suresh, *Pramana*, **1977**, *9*, 471.
(59) J. Billard, J. C. Dubois, N. Huutinh and A. Zann, *New J. Chem*, **1978**, *2*, 535.

(60) D. Blunk, K. Praefcke and V. Vill In *Handbook of liquid crystals: Low molecular weight liquid crystals ii*, D. Demus, J. W. Goodby, G. W. Gray, H. W. Spiess and V. Vill (Eds.), Weinheim: Wiley-VCH, **1998**, Vol. 3. p 305.
(61) P. G. de Gennes and J. Prost, *The physics of liquid crystals*, Oxford: Clarendon Press, **1979**, p 12.
(62) M. Hird In *Physical properties of liquid crystals : Nematics*, D. A. Dunmur, A. Fukuda and G. R. Luckhurst (Eds.), London: Institute of Electrical Engineers, **2001**. p 3
(63) P. G. de Gennes and J. Prost, *The physics of liquid crystals*, 2nd ed. Oxford: Clarendon Press, **1993**, p 10.
(64) P. J. Collings and M. Hird, *Introduction to liquid crystals : Chemistry and physics*, London: Taylor & Francis, **1997**, p 181.
(65) W. Maier and A. Saupe, *Z. Naturforsch. A.*, **1959**, *14*, 882.
(66) P. J. Collings and M. Hird, *Introduction to liquid crystals : Chemistry and physics*, London: Taylor & Francis, **1997**, p 1.
(67) S. Kumar In *Liquid crystals : Experimental study of physical properties and phase transitions*, S. Kumar (Eds.), Cambridge: Cambridge University Press, **2001**. p 184.
(68) G. Englert and A. Saupe, *Mol. Cryst.*, **1966**, *1*, 503.
(69) J. Nehring and A. Saupe, *Mol. Cryst. Liq. Cryst.*, **1969**, *8*, 403.
(70) E. Sackman, *Fortsch. Chem. Forsch.*, **1969**, *12*, 349.
(71) A. Devries and D. L. Fishel, *Mol. Cryst. Liq. Cryst.*, **1972**, *16*, 311.
(72) G. W. Gray and J. W. Goodby, *Smectic liquid crystals : Textures and structures*, Glasgow: Leonard Hill, **1984**.
(73) I. Janossy (Ed.). *Optical effects in liquid crystals,* Dordrecht ; Boston: Kluwer Academic. **1991**, p 1.
(74) S. Singh, *Liquid crystal fundamentals*, New Jersey ; London: World Scientific, **2002**, p 9.
(75) C. W. Oseen, *Trans. Faraday. Soc.*, **1933**, *29*, 883.
(76) J. W. Goodby In *Handbook of liquid crystals: Fundamentals*, D. Demus, J. W. Goodby, G. W. Gray, H. W. Spiess and V. Vill (Eds.), Weinheim ; Chichester: Wiley-VCH, **1998**, Vol. 1. p 123.
(77) B. Bahadur In *Liquid crystals, applications and uses*, B. Bahadur (Ed.): World Scientific Publishing, **1990**, Vol. 3. p 301.
(78) D. K. Yang, L. C. Chien and Y. K. Fung In *Liquid crystals in complex geometries : Formed by polymer and porous networks*, G. P. Crawford and S. Zumer (Eds.), London: Taylor & Francis, **1996**. p 103.
(79) H.-G. Kuball and E. Dorr In *Physical properties of liquid crystals : Nematics*, D. A. Dunmur, A. Fukuda and G. R. Luckhurst (Eds.), London: Institute of Electrical Engineers, **2001**. p 333
(80) H. Finkelmann, *Makromol. Chem., Rapid Commun.*, **1982**, *3*, 859.
(81) M. Goulding, *Phd Thesis*, University of Southampton, **1995**, p 41.
(82) R. A. van Delden and B. L. Feringa, *Angew. Chem., Int. Ed. Engl.*, **2001**, *40*, 3198.
(83) M. Goulding, *Phd Thesis*, University of Southampton, **1995**, p 112.
(84) Z. Dogic and S. Fraden, *Langmuir*, **2000**, *16*, 7820.
(85) D. Coates, O. Parri, M. Verrall, K. Slaney and S. Marden, *Macromol. Symp.*, **2000**, *154*, 59.
(86) M. R. Wilson and D. J. Earl, *J. Mater. Chem.*, **2001**, *11*, 2672.
(87) G. W. Gray and D. G. Mcdonnell, *Mol. Cryst. Liq. Cryst.*, **1977**, *34*, 211.
(88) M. Schadt and W. Helfrich, *Appl. Phys. Lett.*, **1971**, *18*, 127.
(89) P. G. de Gennes and J. Prost, *The physics of liquid crystals*, 2nd ed. Oxford: Clarendon Press, **1993**, p 263.
(90) S. V. Belayev, M. Schadt, M. I. Barnik, J. Funfschilling, N. V. Malimoneko and K. Schmitt, *Jpn J Appl Phys 2*, **1990**, *29*, L634.
(91) M. Schadt and J. Funfschilling, *Jpn J Appl Phys 1*, **1990**, *29*, 1974.
(92) S. M. Kelly, M. Schadt and H. Seiberle, *Liq. Cryst.*, **1992**, *11*, 761.

(93) S. M. Kelly, *J. Mater. Chem.*, **1995**, *5*, 2047.
(94) D. J. Broer, J. Lub and G. N. Mol, *Nature*, **1995**, *378*, 467.
(95) T. R. Welter, WO Patent, WO2005061425, **2005**.
(96) T. Nakagiri, H. Kodama and Kobayash.Kk, *Phys. Rev. Lett.*, **1971**, *27*, 564.
(97) H. Hanson, A. J. Dekker and F. Vanderwoude, *Mol. Cryst. Liq. Cryst.*, **1977**, *42*, 1025.
(98) H. Stegemeyer, *Ber. Bunsen-Ges. Phys. Chem.*, **1974**, *78*, 860.
(99) P. J. Shannon, *Macromolecules*, **1984**, *17*, 1873.
(100) J. L. Fergason, *Mol. Cryst.*, **1966**, *1*, 293.
(101) M. Braun, A. Hahn, M. Engelmann, R. Fleischer, W. Frank, C. Kryschi, S. Haremza, K. Kűrschner and R. Parker, *Chem. Eur. J.*, **2005**, *11*, 3405.
(102) H. J. Coles In *Handbook of liquid crystals: Low molecular weight liquid crystals i*, D. Demus, J. W. Goodby, G. W. Gray, H. W. Spiess and V. Vill (Eds.), Weinheim ; Chichester: Wiley-VCH, **1998**, Vol. 2A. p 243.
(103) H. Gleeson In *Handbook of liquid crystals: Fundamentals*, D. Demus, J. W. Goodby, G. W. Gray, H.-W. Spiess and V. Vill (Eds.), Weinheim: Wiley-VCH, **1998**, Vol. 1. p 824.
(104) D. J. Broer, J. Boven, G. N. Mol and G. Challa, *Makromol. Chem.*, **1989**, *190*, 2255.
(105) D. J. Broer, G. N. Mol and G. Challa, *Makromol. Chem.*, **1991**, *192*, 59.
(106) D. J. Broer, *Mol. Cryst. Liq. Cryst.*, **1995**, *261*, 513.
(107) L. Lestel, G. Galli, M. Laus and E. Chiellini, *Polym. Bull.*, **1994**, *32*, 669.
(108) D. J. Broer, J. Lub and G. N. Mol, *Macromolecules*, **1993**, *26*, 1244.
(109) S. Jahromi, J. Lub and G. N. Mol, *Polymer*, **1994**, *35*, 622.
(110) H. Jonsson, H. Andersson, P. E. Sundell, U. W. Gedde and A. Hult, *Polym. Bull.*, **1991**, *25*, 641.
(111) H. Andersson, U. W. Gedde and A. Hult, *Polymer*, **1992**, *33*, 4014.
(112) R. A. M. Hikmet and R. Howard, *Phys. Rev. E*, **1993**, *48*, 2752.
(113) D. J. Broer, H. Finkelmann and K. Kondo, *Makromol. Chem.*, **1988**, *189*, 185.
(114) Y. Bouligand, P. E. Cladis, L. Liebert and L. Strzelecki, *Mol. Cryst. Liq. Cryst.*, **1974**, *25*, 233.
(115) S. B. Clough, A. Blumstein and E. C. Hsu, *Macromolecules*, **1976**, *9*, 123.
(116) L. Liebert, L. Strzelecki and D. Vacogne, *Bull. Soc. Chim. Fr, B*, **1975**, 2073.
(117) D. J. Broer In *Liquid crystals in complex geometries : Formed by polymer and porous networks*, G. P. Crawford and S. Zumer (Eds.), London: Taylor & Francis, **1996**. p 240.
(118) D. J. Broer In *Radiation curing in polymer science and technology*, J. P. Fouassier and J. F. Rabek (Eds.), London: Elsevier Applied Science, **1993**, Vol. 3. p 383.
(119) R. A. M. Hikmet and B. H. Zwerver, *Mol. Cryst. Liq. Cryst.*, **1991**, *200*, 197.
(120) R. A. M. Hikmet and B. H. Zwerver, *Liq. Cryst.*, **1992**, *12*, 319.
(121) R. A. M. Hikmet and B. H. Zwerver, *Liq. Cryst.*, **1993**, *13*, 561.
(122) D. K. Yang, J. L. West, L. C. Chien and J. W. Doane, *J. Appl. Phys.*, **1994**, *76*, 1331.
(123) L. Liebert and L. Strzelecki, *Bull. Soc. Chim. Fr.*, **1973**, 603.
(124) B. Jerome In *Handbook of liquid crystals: Fundamentals*, D. Demus, J. W. Goodby, G. W. Gray, H. W. Spiess and V. Vill (Eds.), Weinheim: Wiley-VCH, **1998**, Vol. 1. p 535.
(125) J. Cognard, *Mol. Cryst. Liq. Cryst.*, **1982**, 1.
(126) T. Uchida and H. Seki In *Liquid crystals, applications and uses*, B. Bahadur (Ed.): World Scientific Publishing, **1990**, Vol. 3. p 14.
(127) B. Jerome, J. Commandeur and W. H. DeJeu, *Liq. Cryst.*, **1997**, *22*, 685.
(128) J. Cognard, *J. Adhes.*, **1984**, *17*, 123.
(129) H.-S. Kitzerow In *Liquid crystals in complex geometries : Formed by polymer and porous networks*, G. P. Crawford and S. Zumer (Eds.), London: Taylor & Francis, **1996**. p 220.
(130) J. L. Fergason, *Sci. Am.*, **1964**, *211*, 76.

(131) J. L. Fergason, N. N. Goldberg and R. J. Nadalin, *Mol. Cryst.*, **1966**, *1*, 309.
(132) R. D. Ennulat and J. L. Fergason, *Mol. Cryst. Liq. Cryst.*, **1971**, *13*, 149.
(133) D. J. Broer and I. Heynderickx, *Macromolecules*, **1990**, *23*, 2474.
(134) I. Heynderickx and D. J. Broer, *Mol. Cryst. Liq. Cryst.*, **1991**, *202*, 113.
(135) A. Mori, *J. Display Technol.*, **2005**, *1*, 179.
(136) G. Barbero and G. Durand In *Liquid crystals in complex geometries : Formed by polymer and porous networks*, G. P. Crawford and S. Zumer (Eds.), London: Taylor & Francis, **1996**. p 21.
(137) R. Williams, *J. Chem. Phys.*, **1963**, *39*, 384.
(138) G. Heilmeier, L. A. Zoanoni and L. A. Barton, *Appl. Phys. Lett.*, **1968**, *13*, 46.
(139) E. F. Carr, *Mol. Cryst. Liq. Cryst.*, **1969**, *7*, 253.
(140) W. Helfrich, *J. Chem. Phys.*, **1969**, *51*, 4092.
(141) J. L. Fergason, US Patent, US3627408, **1971**.
(142) G. W. Gray, K. J. Harrison and J. A. Nash, *Electron. Lett.*, **1973**, *9*, 130.
(143) H. Kawamoto, *Proc. IEEE*, **2002**, *90*, 460.
(144) B. R. Chalamala, F. E. Libsch, R. H. Reuss and B. E. Gnade, *Proc. IEEE*, **2002**, *90*, 447.
(145) J. Lub, P. van de Witte, C. Doornkamp, J. P. A. Vogels and R. T. Wegh, *Adv. Mat.*, **2003**, *15*, 1420.
(146) H. Mori, *J. Disp. Tech.*, **2005**, *1*, 179.
(147) D. Coates, M. J. Goulding, S. Greenfield, J. M. Hanmer, S. A. Marden and O. L. Parri In *SID 96 Applications Digest* 1996; Vol. 67, p 67.
(148) G. C. Koch, B. K. Winker and W. J. Gunning III, US Patent, US5619352, **1997**.
(149) I. Fukuda In *Proc. 8th Intl. Disp. Res. Conf.* 1988, p 159.
(150) S. Matsumoto In *Proc. 8th Intl. Disp. Res. Conf.* 1988, p 182.
(151) H. Odai In *Proc. 8th Intl. Disp. Res. Conf.* 1988, p 195.
(152) D. Demus In *Liquid crystals, applications and uses*, B. Bahadur (Eds.): World Scientific Publishing, **1990**, Vol. 1. p 1.
(153) Y. Bouligand In *Handbook of liquid crystals: Fundamentals*, H. Kelker and R. Hatz (Ed.), Weinheim: Verlag Chemie, **1998**. p 406.
(154) P. J. Collings and M. Hird, *Introduction to liquid crystals : Chemistry and physics*, London: Taylor & Francis, **1997**, p 34.
(155) S. Morozumi In *Liquid crystals, applications and uses*, B. Bahadur (Ed.): World Scientific Publishing, **1990**, Vol. 1. p 171.
(156) P. J. Collings and M. Hird, *Introduction to liquid crystals : Chemistry and physics*, London: Taylor & Francis, **1997**, p 19.
(157) I. Dierking, *Textures of liquid crystals*, Weinheim: Wiley-VCH, **2003**.
(158) J. Thoen In *Handbook of liquid crystals: Fundamentals*, D. Demus, J. W. Goodby, G. W. Gray, H. W. Spiess and V. Vill (Eds.), Weinheim: Wiley-VCH, **1998**, Vol. 1. p 281
(159) S. Singh, *Liquid crystal fundamentals*, New Jersey ; London: World Scientific, **2002**, p 60
(160) M. Sorai In *Physical properties of liquid crystals : Nematics*, D. A. Dunmur, A. Fukuda and G. R. Luckhurst (Eds.), London: Institute of Electrical Engineers, **2001**. p 142.
(161) L. Pohl and U. Finkenzeller In *Liquid crystals, applications and uses*, B. Bahadur (Ed.): World Scientific Publishing, **1990**, Vol. 1. p 139.
(162) W. H. De Jeu, *Physical properties of liquid crystalline materials*: Gordon and Breach Science, **1980**.
(163) D. A. Dunmur In *Physical properties of liquid crystals : Nematics*, D. Dunmur, A. Fukuda and G. R. Luckhurst (Eds.), London: Institute of Electrical Engineers, **2001**. p 316.
(164) D. A. Dunmur, D. A. Hitchen and X. J. Hong, *Mol. Cryst. Liq. Cryst.*, **1986**, *140*, 303.
(165) K. C. Lim and J. T. Ho, *Mol. Cryst. Liq. Cryst.*, **1978**, *47*, 173.

(166) D. W. Bruce, D. A. Dunmur, P. M. Maitlis, M. M. Manterfield and R. Orr, *J. Mater. Chem.*, **1991**, *1*, 255.
(167) S. Urban In *Physical properties of liquid crystals : Nematics*, D. Dunmur, A. Fukuda and G. R. Luckhurst (Eds.), London: Institute of Electrical Engineers, **2001**. p 268.
(168) W. Haase In *Physical properties of liquid crystals : Nematics*, D. Dunmur, A. Fukuda and G. R. Luckhurst (Eds.), London: Institute of Electrical Engineers, **2001**. p 288.
(169) J. S. Philo and W. M. Fairbank, *Rev. Sci. Instrum.*, **1977**, *48*, 1529.
(170) P. I. Rose, *Mol. Cryst. Liq. Cryst.*, **1974**, *26*, 75.
(171) J. Kedzierski, Z. Raszewski, J. Rutkowska, T. Opara, J. Zielinski, J. Zmija and R. Dabrowski, *Mol. Cryst. Liq. Cryst.*, **1994**, *249*, 129.
(172) P. J. Collings and M. Hird, *Introduction to liquid crystals : Chemistry and physics*, London: Taylor & Francis, **1997**, p 32.
(173) S. Singh, *Liquid crystal fundamentals*, New Jersey ; London: World Scientific, **2002**, p 87
(174) D. A. Dunmur In *Physical properties of liquid crystals : Nematics*, D. A. Dunmur, A. Fukuda and G. R. Luckhurst (Eds.), London: Institute of Electrical Engineers, **2001**. p 216.
(175) W. H. De Jeu, *Physical properties of liquid crystalline materials*: Gordon and Breach Science, **1980**, p 76.
(176) D. A. Dunmur In *Handbook of liquid crystals: Fundamentals*, D. Demus, J. W. Goodby, G. W. Gray, H.-W. Spiess and V. Vill (Eds.), Weinheim: Wiley-VCH, **1998**, Vol. 1. p 266.
(177) H. Saito In *Physical properties of liquid crystals : Nematics*, D. Dunmur, A. Fukuda and G. R. Luckhurst (Eds.), London: Institute of Electrical Engineers, **2001**. p 583
(178) J. Moscicki In *Physical properties of liquid crystals : Nematics*, D. Dunmur, A. Fukuda and G. R. Luckhurst (Eds.), London: Institute of Electrical Engineers, **2001**. p 398
(179) J. Moscicki In *Physical properties of liquid crystals : Nematics*, D. Dunmur, A. Fukuda and G. R. Luckhurst (Eds.), London: Institute of Electrical Engineers, **2001**. p 387
(180) P. Photinos In *Liquid crystals : Experimental study of physical properties and phase transitions*, S. Kumar (Eds.), Cambridge: Cambridge University Press, **2001**. p 140.
(181) S. Naemura In *Physical properties of liquid crystals : Nematics*, D. Dunmur, A. Fukuda and G. R. Luckhurst (Eds.), London: Institution of Electrical Engineers, **2001**. p 524.
(182) B. Bahadur In *Liquid crystals, applications and uses*, B. Bahadur (Ed.): World Scientific Publishing, **1990**, Vol. 1. p 195.
(183) T. J. Scheffer, J. Nehring, M. Kaufmann, H. Amstutz, D. Heimgartner and P. Eglin, *SID Digest of Technical Papers*, **1985**, *XVI*, 120.
(184) R. Kiefer, B. Weber, F. Windscheid and G. Bauer In *Proc.12th Intl. Disp. Res. Conf.* 1992, p 547.
(185) M. Oh-E, M. Ohta, S. Aratani and K. Kondo In *Asia Display '95 Digest* 1995, p 577.
(186) M. Oh-E and K. Kondo, *Liq. Cryst.*, **1997**, *22*, 379.
(187) S. Yamauchi, M. Aizawa, J. F. Clerc, T. Uchida and J. Duchene, *SID Digest of Technical Papers*, **1989**, *XX*, 378.
(188) H. Hirai, Y. Kinoshita, K. Shohara, A. Murayama, H. Hatoh and S. Matsumoto In *Japan Display '89* 1989, p 184.
(189) Y. Koike, S. Kataoka, T. Sasaki, H. Chida, H. Tsuda, A. Takeda, K. Ohmuro, T. Sasabayashi and K. Okamoto In *International Display Workshops 97 Digest* 1997, p 159.
(190) J. A. Castellano, *Liquid gold : The story of liquid crystal displays and the creation of an industry*, Hackensack, N.J. ; London: World Scientific, **2005**.
(191) G. Heilmeier, J. A. Castellano and L. A. Zanoni, *Mol. Cryst. Liq. Cryst.*, **1969**, *8*, 293.
(192) N. A. Clark and S. T. Lagerwall, *Appl. Phys. Lett.*, **1980**, *36*, 899.

(193) D. Coates In *Liquid crystals, applications and uses*, B. Bahadur (Ed.): World Scientific Publishing, **1990**, Vol. 1. p 292.
(194) H. G. Craighead, J. Cheng and S. Hackwood, *Appl. Phys. Lett.*, **1982**, *40*, 22.
(195) B. Bahadur, *Liquid crystal displays*, New York: Gordon and Breach, **1984**.
(196) G. Solladie and R. G. Zimmermann, *Angew. Chem., Int. Ed. Engl.*, **1984**, *23*, 348.
(197) P. Photinos In *Liquid crystals : Experimental study of physical properties and phase transitions*, S. Kumar (Ed.), Cambridge: Cambridge University Press, **2001**. p 116.
(198) G. Jung, *Combinatorial chemistry : Synthesis, analysis, screening*, Weinheim: Wiley-VCH, **1999**, p 1.
(199) N. K. Terrett, *Combinatorial chemistry*, Oxford: Oxford University Press, **1998**, p 7.
(200) N. K. Terrett, *Combinatorial chemistry*, Oxford: Oxford University Press, **1998**, p 131.
(201) R. B. Merrifield, *J. Am. Chem. Soc.*, **1963**, *85*, 2149.

Chapter 2 - High Throughput Screening of Liquid Crystals

2.1 Introduction

The use of high-throughput parallel and combinatorial strategies in materials chemistry has enabled ever-increasing numbers of compounds and formulations to be prepared, at an ever-increasing rate. The issue arising is the lack of suitable high-throughput analytical techniques,[1] without which the time-saving benefits of combinatorial methods become insignificant as the process can only be as fast as its slowest step. In materials combinatorial chemistry, HT screening can take a variety of forms depending on the application with techniques usually requiring adaptation of conventional analytical tools or the development of novel methodologies.[2] The literature shows that a great many devices have been developed using the technique of optical screening as a tool, for example in the HT screening of ternary-metal-alloy libraries,[3] imaging of phosphor discover libraries by UV excited photoluminescence,[4,5] and screening of catalyst libraries by IR imaging.[6]

The aim of a screening technique is to allow characterisation in parallel, of one or more properties of the liquid crystal materials under study in this thesis. Such a technique can therefore drastically reduce the time taken for full analysis of a large library. Screening a large library and identifying materials, which have a property with values that fall outside the desired range, allows these to be discarded from further studies so that fewer materials are taken further for more time-consuming analysis.

In the study of new LC materials a number of properties can be screened, including those characteristics described in Chapter 1. To analyse many these properties requires the use of customised, specialist test-equipment to measure a response in the system to an external influence. A high degree of sensitivity is required to obtain such data, which is not easily achieved using high-throughput techniques. Existing techniques for measurment of properties such as diamagnetic anisotropy, elastic constants and viscosity coefficients are often too complex to be adapted for HT analysis and therefore were not considered.

The traditional technique of measuring dielectric anisotropy and birefringence, using a cell to confine and orientate the LC for measurement, was seen to have potential for HT modification. If matrixes of multiple analysis cells on reduced scale are produced, then the parallel measurement of properties becomes a possibility. The main problem with such an

approach is that any apparatus used in a single analysis (lasers, analysers, waveform generators) would also need to be duplicated in a parallel arrangement. This represents costs for which ultimately a number of individual instruments could be purchased, and still provide a similar high-throughput. Due to the complexity of such techniques and the extensive use of expensive electric measurement apparatus and laser optics, which were not readily available in chemistry based research laboratory, these techniques were not adapted for a HT screen.

The phase transitions of a liquid crystal material are a property that is perhaps the simplest to measure and therefore an ideal candidate for HT adaptation. The temperature at which the crystalline solid melts into a LC mesophase (melting point), and the temperature at which the LC mesophase melts into an isotropic liquid (clearing point) can be measured for any LC material, and defines the temperature range over which the liquid crystalline properties can be exploited. This is of importance in LC applications, such as display technologies, in which the liquid crystal mixture must possess a stable nematic mesophase throughout the device's operating temperature range (usually -40 °C to 100 °C).[7] In the literature, it is common for new mixtures and compounds be characterised first for LC phase transitions, using a combination of methods. DSC is used to determine the temperatures at which transitions occur (together with their associated enthalpies), followed by optical polarising microscopy to identify, and subsequently classify the type of phases that occur.

A HT screening technique for the determination of phase transitions provides a method for identifying positive hits, reducing the size of the library and cutting analysis time. The rapid identification of materials with desirable LC properties can drive the development of HT synthesis or formulation methodologies in the area of liquid crystals, for example using such methods for the creation of large mixture libraries which to date is unfeasible due to the limitations that traditional screening techniques impose.

The aim of the research was to develop methods by which phase transitions could be analysed in a parallel fashion, enabling the testing of larger numbers of materials in a much-reduced timeframe. After establishing a suitable technique, optimisation and assessment of experimental accuracy will establish its viability for the analysis of a large liquid crystal library.

2.2 High Throughput Measurement of Phase Transitions

A literature search for previous approaches to high-throughput screening of phase transitions revealed only one other significant application. The apparatus, patented by Bradley,[8] was developed for the measurement of melting points of multiple samples in the field of polymer science by exploiting the change in luminosity or reflectance (turning from opaque to translucent) of solids undergoing a phase change. Using a combination of optical imaging and image processing, a large number of samples could be analysed simultaneously for melting point. The concept of monitoring the change in the translucency of materials with increasing temperature is not new, and has been used extensively in the study of liquid crystals.[9-12] One example, the Mettler oven, is a device that can indicate phase transitions by monitoring the change in sample translucency as a function of increasing temperature. To the naked eye, LCs appear as turbid liquids as a result of light scattering caused by random director fluctuations in crystalline domains which form in the bulk material.[11] Scattering in the nematic phase is in the order of 10^6 times greater than that of the isotropic phases,[13] therefore allowing easy differentiation between the two. Due to the virtually insignificant dependence of scattering efficiency on temperature,[13] the transition between liquid crystal and isotropic liquid is sharp, and hence easily detected. It is also possible to differentiate the smectic phase from the nematic phase, due to the differences in the size and order of the crystalline domains. These domains affect the scattering in the bulk substance (focal conic textures in smectics are visually scattering textures).[14]

The apparatus developed by Bradley[8] could be used for the HT screening of LCs to allow the measurement of transitions in an almost identical way to that of the Mettler oven, but with the benefit of enabling multiple samples to be screened in the same time that a single sample could be analysed in using traditional techniques.

2.2.1 Evaluation of a Technique for Multiple Clearing Point Determination

The multiple melting point apparatus was used as described in the literature[8] to analyse four commercial liquid crystals[15] (Merck Chemicals Ltd.). Samples, which consisted of both single LCs and LC mixtures, were loaded directly onto the support plate of the heating device and monitored for change in intensity on heating using a webcam. After processing, the intensity results were plotted against temperature (Figure 2.1 and Table 2.1).

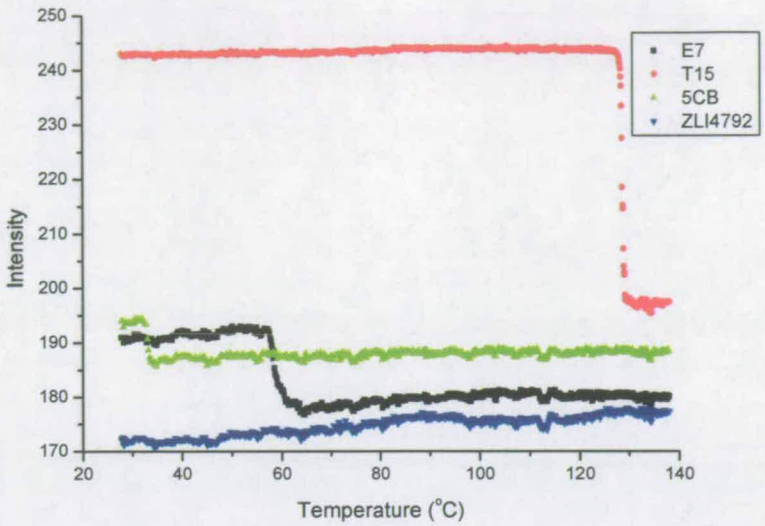

Figure 2.1: The phase transitions of four liquid crystals analysed using the multiple clearing point apparatus.

LC	Transition	Temperature / C	Literature value / C	Δn
5CB	T_{N-I}	33.1	35.1	≈0.15
E7	T_{N-I}	58.4	58.0	≈0.15
ZLI-4792	T_{N-I}	-	92.0	≈0.1
T15	T_{C-N}	128.6	131.0	≈0.3
	T_{N-I}	-	217.2	

Table 2.1: Comparison between clearing / (melting) transitions obtained using the multiple clearing point apparatus and the literature values

The only sample analysed possessing a melting point (T15), illustrated the strength of the apparatus the sample showing a very sharp transition from high to mid intensity as the opaque solid melted to a cloudy turbid LC phase. The transition from LC mesophase to isotropic liquid (clearing point) exhibited in 5CB, E7 and ZLI-4792 was not so defined. Weak transitions were observed in 5CB and E7, but for ZLI-4792 no transition could be detected. In the LC phase, ZLI-4792 is not as opaque as the other LC samples due to its lower birefringence (Table 2.1) and therefore the resolution of the apparatus was not sufficient to capture the subtle change in intensity on clearing. This mixture is representative

of the properties and types of substance to be examined using such an apparatus and therefore, this method will display some limitations.

2.3 Development of a Screening Technique Using Birefringence

The principle of monitoring a property that exhibits optically identifiable changes on passing a threshold value is well suited for a HT screening device. One such property that all LC materials possess by definition is optical anisotropy,[16] the causes of which have been previously described. If linearly polarised light enters a LC sample (The electric and magnetic field components of the light to oscillate in only one direction), it becomes split into ordinary and extraordinary components. Due to the formation of micro domains in the bulk material and microscopic director fluctuation, the two components experience different average refractive indices as they pass through the material, which imparts a phase difference between them. On recombination, linear polarisation is lost instead forming circularly polarised light (the polarization of the light rotating around the direction of propagation). Outside of the temperature for mesophase formation (above the clearing point) the optical anisotropy is reduced to zero and hence linearly polarised light passing through the material is affected by only one refractive index, regardless of the orientation, and so emerges from the medium unaffected. Using these principles enables visualisation of the anisotropic state using polarised light, to determine the temperature at which the samples undergo transitions to or from LC phases Figure 2.2 shows an experimental schematic for visualising birefringence. By placing a light source behind the first polariser and analysing transmitted light through the second polariser, phase changes could be identified optically by a change in intensity. The liquid crystalline state was identified as a white, high intensity spot. Samples not in a LC state show zero intensity, due to zero anisotropy, so are not detectable from the black background. The intensity of the spot depends on the degree of order in the LC. If a sample has a more ordered structure (larger value of *S*), or aligns strongly with the glass surface then the incident light will experience the refractive index perpendicular to the alignment / layer direction to a greater extent, and hence elliptical polarisation will be reduced resulting in a spot of lower intensity. This effect allows the determination of more ordered smectic mesophases from the nematic phase.

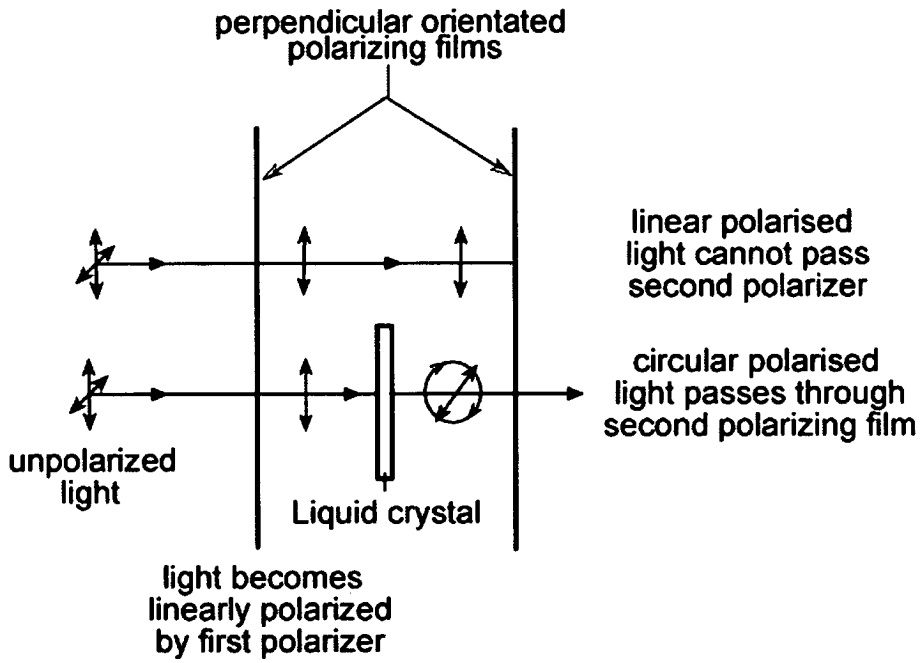

Figure 2.2: Two plane polarisers can be placed either side of a birefringent material, aligned so that their planes of polarisation lie at 90° to each other. Incident light becomes polarised upon entering the apparatus, and if not affected by the sample will be blocked by the second perpendicular polarizer. Light, which falls onto and travels through the sample, undergoes a change in the plane of polarization, emerging circularly polarised due to the anisotropy of the refractive indices in the medium. Optically the light is now able to exit through the second polarising film as it possesses a linear component not at 90° to the first polariser.

2.3.1 Requirements for a Device Based on Birefringence

The design of a HT screening device using birefringence was considered, taking into account a number of factors. The most challenging of these was the sample loading stage, which must allow a clear optical path through the sample in addition to sample heating abilities. To ensure a high resolution, the optical path from the light source to the analyser should be as direct as possible. To achieve this, a transparent heated stage onto which samples can be loaded, heated, and analysed was considered. A supplier search for this type of apparatus revealed that as the majority of applications of this equipment are in microscopy, the largest transparent heater that could be purchased was circular, with diameter of 2 cm to 3 cm and hence not suitable for our purpose. The production of larger substrates with the required heating range and homogeneity was unfeasible and so alternative methods were considered.

One idea to eliminate the requirement for transparency was to redesign the apparatus with a reflective heating surface and a modified optical path through the sample (Figure 2.3).

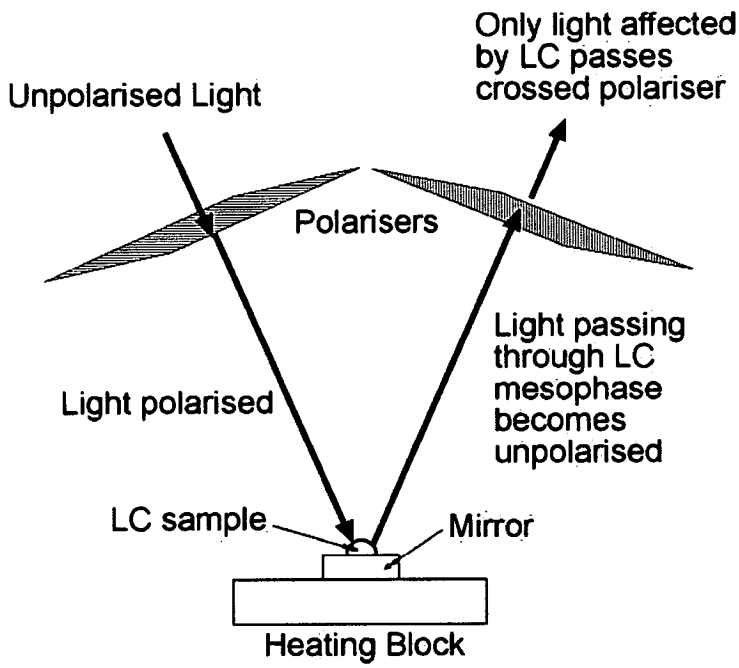

Figure 2.3: The design of an experiment for parallel characterisation of LCs using birefringence to detect phase transitions.

In this design, incident light was able to pass through the sample before being reflected for analysis. Thermal control of the reflective surface would enable the sample to be heated, and the effect of light transmission on the temperature could be recorded. For this design to be successful, the heating block needed to be fabricated from metal to provide good conductive abilities, and either polished to create a mirrored surface, or a piece of silvered glass placed on top of the metal surface. Although the intensity of reflected light in this experiment was reduced compared to the linear optical path, the apparatus was considerably easier to manufacture. To assess the design a prototype was constructed.

2.3.2 Construction of a Prototype HT Screening Apparatus

In constructing the prototype apparatus, the following basic components were required:

- A controlled heating block which is either reflective, or on to which a reflective substrate can be placed and samples loaded
- A method of polarisation such that the ingress of non polarised light is excluded
- A light source
- Camera for analysis
- Software tools and methods for subsequent data analysis

Many of these requirements such as the controlled heating block, camera and software tools for the extrapolation of image data were met by the polymer melting point apparatus, and since this equipment was available was reused and adapted for our needs.

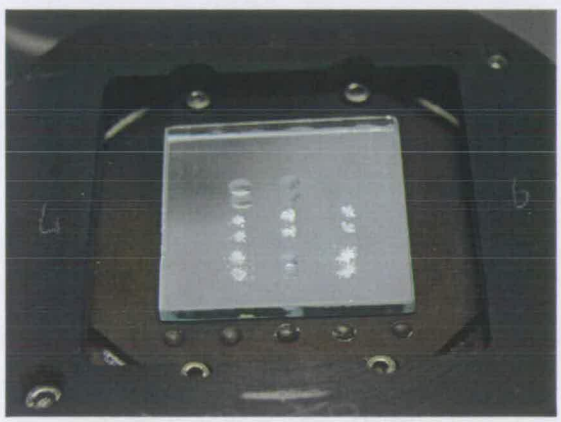

Figure 2.4: Solid and liquid LC samples spotted onto the glass mirror, placed onto the heating block to provide a reflective surface

The interior of the aluminium heating block contained two 24 V heating elements and a thermocouple interfaced to a Calcomms 3300 unit, providing thermostatic control. A PC interfaced to the calcomms unit was used to log data. To the top of the aluminium block was mounted a 100x100x35 mm steel plate, which due to the metal surfaces highly diffuse reflectivity, was not suitable for the loading of samples. To temporally overcome this limitation, a silvered glass mirror (1 cm depth x 3 cm diameter) was placed onto the sample stage. Samples for analysis were placed onto the mirror in either solid or liquid form. (Figure 2.4)

Attached to the top of the heating block was a removable enclosure and onto the two faces were mounted polarising filters as seen in Figure 2.5. The angle and height of these films were optimised, so that the reflection of the opposite film could be observed on the surface of the mirror inside the enclosure when viewed through a polarising film on one face of the apparatus. This arrangement ensures that the linear polarised light is incident on the mirror at the correct angle to ensure reflection onto, and out of, the second polarising film. By orientation of the two polarisers with their plane of polarization at 90° to each other, the reflected light was unable to pass the second polariser in the absence of a birefringent liquid crystal sample. In addition to holding the polarising films, the enclosure also prevents the ingress of non-polarised light into the apparatus therefore increasing the contrast and resolution between light and dark states. The initial prototype chamber fitted to the heating block is seen in Figure 2.6

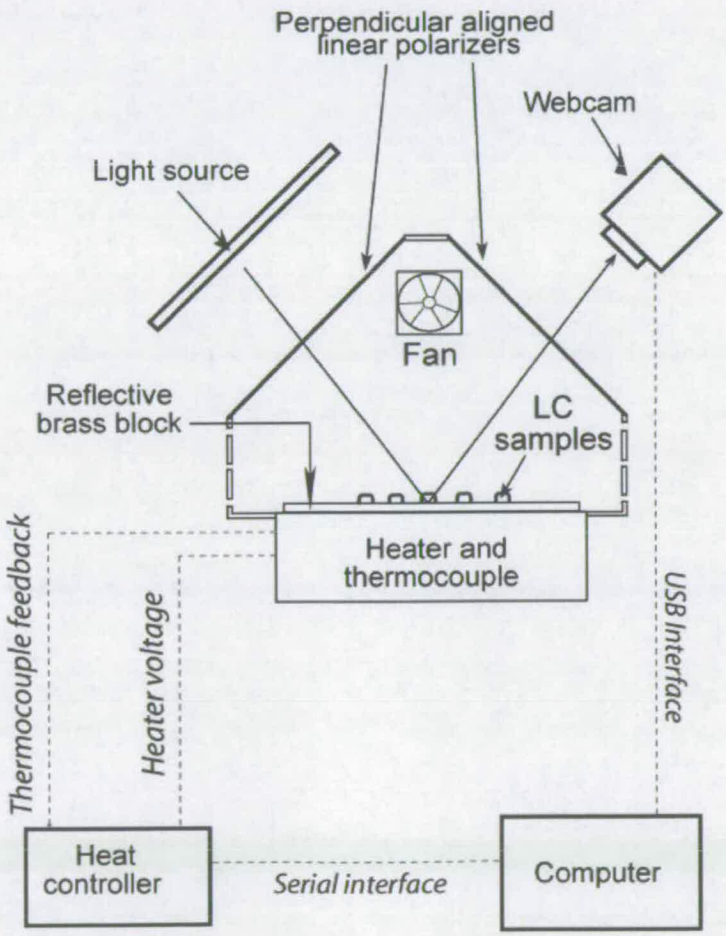

Figure 2.5: A schematic representation of the HT liquid crystal screening device.

Figure 2.6: An image showing the removable enclosure mounted onto the top of the heating block. The black square on the roof of the box is the polarising film above which a webcam is mounted. The lightbox can be seen positioned on the opposite face of the enclosure above the second polariser.

To monitor the intensity of the samples inside the chamber, a webcam interfaced to a PC was positioned above one of the polarising films mounted to the heating stage enclosure. An Ilford 80W light box was suspended above the other film. The camera was focused onto the heating stage mirror, such that in the absence of a liquid crystal sample the stage appeared black.

2.3.3 Data Collection

In the analysis procedure a linear temperature ramp was initiated, heating the samples loaded onto the analysis area, and relaying temperature data *via* the Calcomms controller to a PC where it was recorded once every three seconds. Using the same PC, the webcam was configured to record a video sequence of the samples on the analysis area at a rate of one frame per second (fps). The result of the analysis was a 1 fps video sequence, showing the intensity change of the samples and a spreadsheet relating sequence time (which directly correlates with the frame number) to the sample temperature (Figure 2.7). To obtain the intensity temperature relationship for each sample individually, required the data to be processed and analysed.

2.3.4 Data Analysis

To extract the intensity values from each sample in the video sequence the software Image Pro Plus (Media Cybernetics) was used, adopting an almost identical approach to that used by Bradley.[8] Due to the length of some of the video sequences (generally those in which a very slow heating rate or an extended range of heating was used) sequences were sub-sampled to ensure they did not exceed 500 frames in total. The sub-sampling function of IPP allowed this task to be performed quickly by removing unwanted frames as required and shrinking the footage. This sampling technique resulted in reduced measurement accuracy but also decreased the time and computer resources required for analysis. Sequences were usually sampled by a value of three or four maximum (sub sample 4 = four seconds between frames). This means that the temperature change between data points in the sequence was 0.33 °C or 0.25 °C, compared to 0.085 °C when sampled every second. Using the reduced sequence, the XY coordinates of each sample spot were manually identified and defined in the first frame, as a circle of diameter three pixels. The measurement function in IPP was then used to evaluate the white intensity of each area in each frame as an integer between 0 and 255, exporting the data for each sample in each frame of the sequence to a Microsoft Excel spreadsheet.

To correlate the value of temperature to the frame number, time and temperature data obtained from the Calcomms instrument was plotted to obtain a linear correlation. As time corresponded directly to the frame number (considering any sequence sub-sampling), the equation of the line could be used to calculate the temperature of each frame so that intensity vs. temperature for each sample could be plotted.

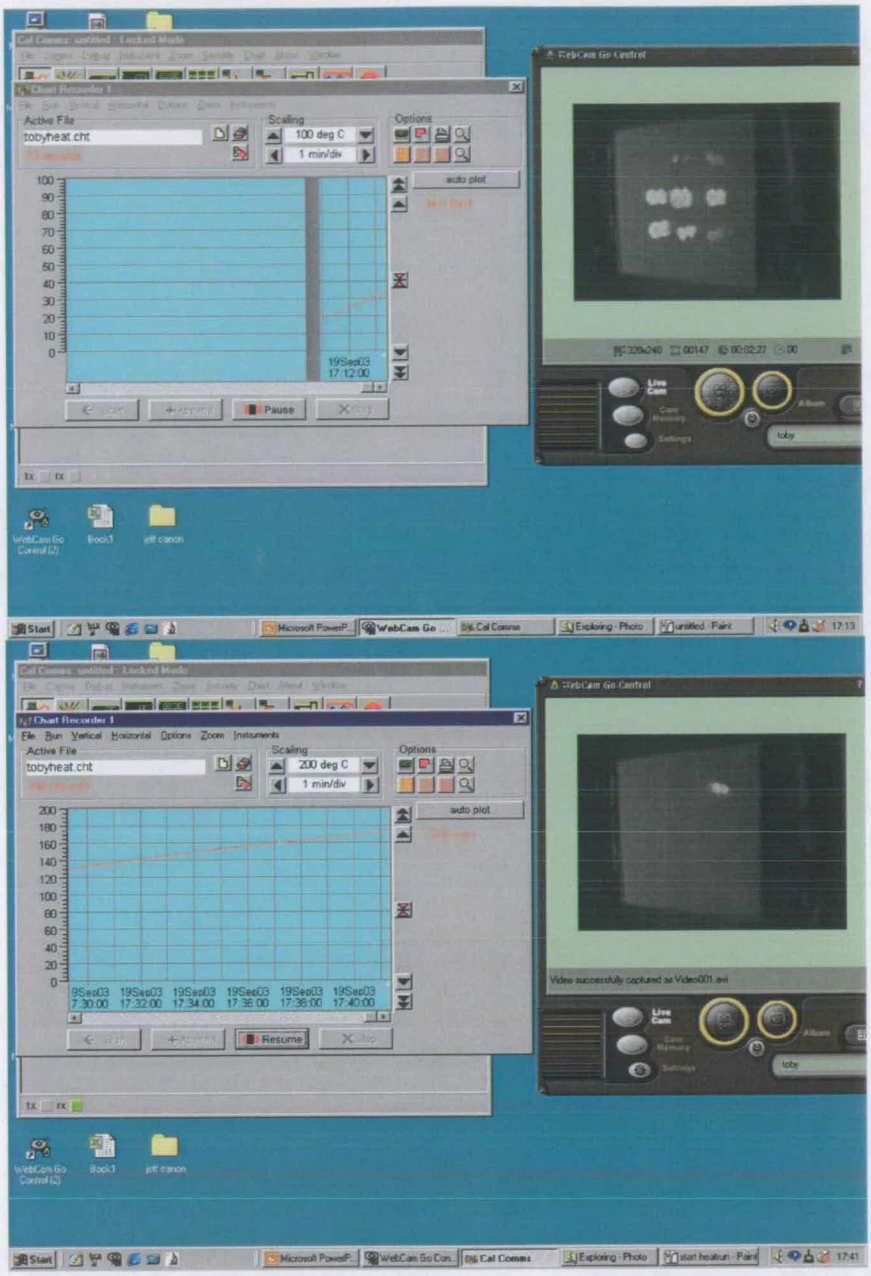

Figure 2.7: Screenshots of the Calcomms program for recording temperature and the webcam software for recording the video sequence. The top image shows the start of the analysis run and the bottom image the end of the analysis run. The white spots seen on the webcam in the left image, can be seen to have disappeared in the right image indicating that the LC sample has passed into the isotropic phase.

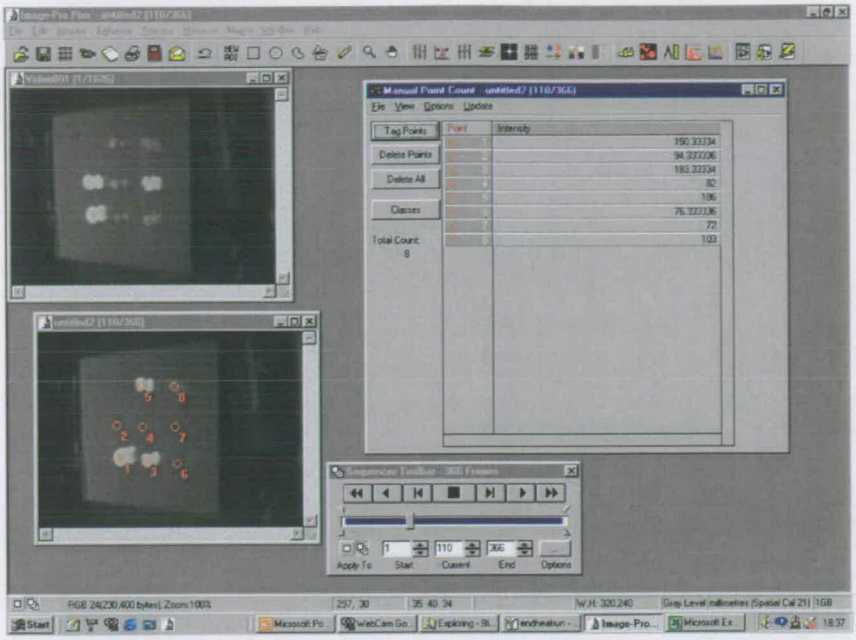

Figure 2.8: A screen shot showing the analysis procedure for a video sequence obtained using the HT screening apparatus. The position of the samples on the video sequence are marked (red circles) so that the intensity of each spot can be obtained as the temperature is increased.

2.3.5 Interpretation of Data

Figure 2.9 shows data for two selected compounds, with phase transitions observed as discontinuities in the intensity data signals. To extrapolate the transition from the data, a standard measurement point needed to be defined. The majority of data plots showed sharp transitions and in these cases, the temperature at the central point in the transition was recorded. However, in the case of some LC mixtures the transition was much broader making it unclear as to where the transition temperature should be read. Many of these transitions showed instability in the intensity prior to the transition, possibly due to pre-transitional effects in the sample where equilibrium between nematic and isotropic domains caused fluctuation in the intensity. Because of these observations, it was difficult to identify the exact location of the transition onset and hence for these types of transitions the temperature reading from the penultimate data point prior to stabilisation of intensity in the isotropic phase was used as a measure of temperature change.

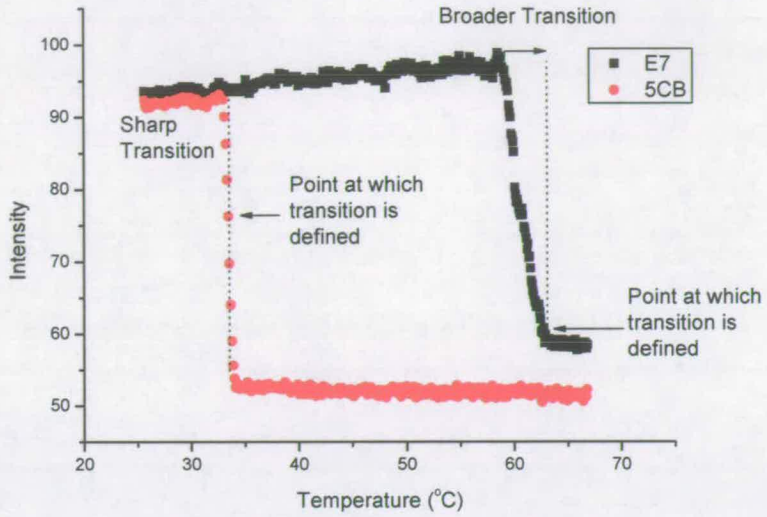

Figure 2.9: A representation of a sharp transition and a broad transition as measured using the HT screening apparatus. In the case of a sharp transition, the temperature is recorded as the mid-point of the transition. In a broader transition, the temperature is recorded at the end-point.

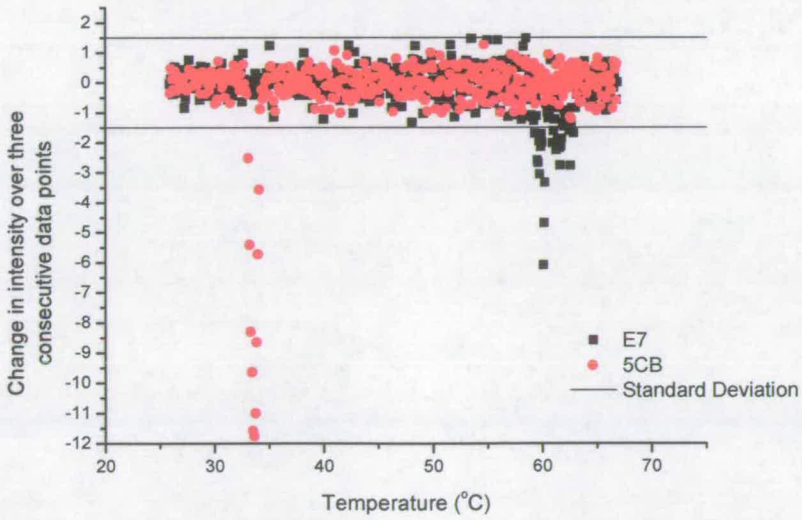

Figure 2.10: Averaging the data by subtracting the average of the previous three data-points from the current data point can be used to identify the location of transitions, where the rate at which intensity changes is highest.

The data could also be processed further to ease identification and eliminate noise caused by fluctuations in background light levels over the course of the experiment. This was achieved by evaluating the change in intensity between sequential data points, subtracting the average of the previous three points from the current value to produce a scatter plot identifying significant deviation from the normal common level (Figure 2.10). The transitions are clearly identifiable by the sharp breaks above or below the normal line. In the majority of experiments, the transitions could be clearly identified visually and therefore this technique was seldom required. The standard deviation of the date is shown in Figure 2.10 as two thin horizontal lines. The peaks corresponding to phase transitions lie significantly above or below these lines showing that the event was significant and not a result of experimental error.

2.4 Validation of Apparatus

To assess the capability of the new apparatus and allow subsequent optimisation, a selection of commercially available LCs were analysed so that comparison could be drawn between literature and HT experimental results. Analysing materials between polarises orientated with their plane of polarisation either parallel or perpendicular to each other, made it possible to analyse materials in one of two modes, either normally white (NW) or normally black (NB) (in the NB mode plane polarised light passing into the apparatus was blocked by the second, perpendicularly aligned polarizer so the background appeared dark. In the NW mode the polarizer's were aligned parallel, allowing all light to pass through the apparatus, except when affected by the optically anisotropic medium). Initial experiments using the apparatus were performed in both NW and NB modes to assess the optimal alignment mode. The data for three selected LC materials, showing the data obtained in both modes, is shown in Figure 2.11.

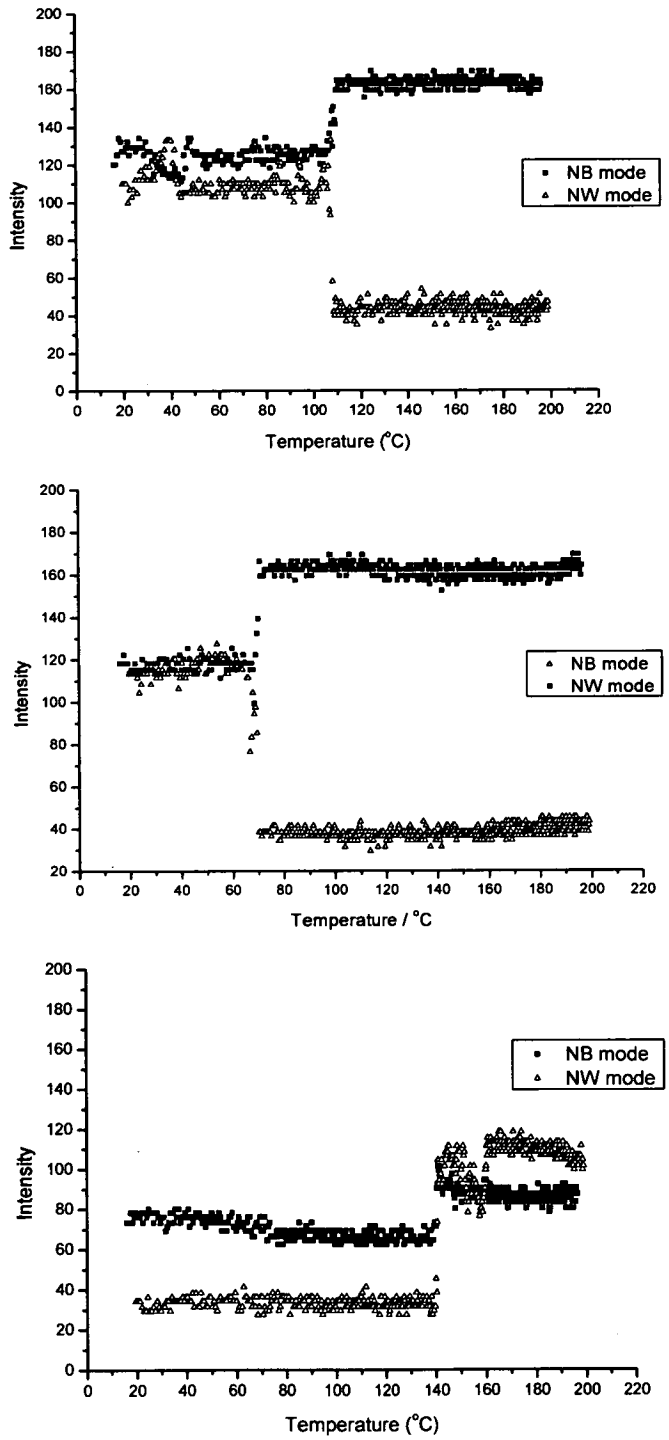

Figure 2.11: Plots showing both NW and NB analysis of three different LC samples. NW mode shows a drop in intensity as the N-I transition is passed, NB mode shows as increase in intensity. For the Cr-N transition the NW and NB results both show an increase in intensity.

Liquid Crystal	T_{N-I} / °C NB mode	T_{N-I} / °C NW mode	T_{N-I} / °C Literature	Deviation / °C NW	Deviation / °C NB
5CB	43	45.8	35.1	10.7	7.9
E7	66.7	71.1	58	13.1	8.7
ZLI-4792	108.1	109.4	92	17.4	16.1
T15	140.5 (melt)	141.5 (melt)	131	10.5	9.5

Table 2.2: A comparison of the clearing points of four liquid crystals measured in the NW and NB mode and analysis of their deviation from literature values.

The revised apparatus using the birefringence method was shown to be more successful at identification of mesophases than the HT polymer MP apparatus using the optical scattering method. In the graphs, each of the samples showed a pronounced discontinuity in intensity which identified the transition. In particular, the transition of the ZLI mixture was now enhanced. It was noticed that the temperature at which each transition occurs was consistently higher than literature, attributed to the thickness of the glass mirror on which the samples were spotted. Because of the poor thermal conductivity of glass (1.05 W/mK), the surface temperature of the glass (and the sample) did not accurately represent the temperature at the surface of the heating plate. This was a point for improvement; however, it is important to note that the deviation is relatively consistent and therefore can be considered a systematic error. To ensure that the large discrepancy observed in the experiment was indeed due to the thickness of the mirror it was replaced with a larger, thinner mirror and the analysis repeated. Table 2.3 shows this replacement was successful in reducing the deviation between the HT values and the literature values obtained, however further optimisation was still required to further reduce the divergence from literature.

Liquid Crystal	T_{N-I} / °C Old mirror	T_{N-I} / °C New mirror	T_{N-I} / °C Literature	Deviation / °C
5CB	43	36.3	35.1	1.2
E7	66.7	60.8	58	2.8
ZLI-4792	108.1	100	92	8
T15	140.5 (melt)	137.9 (melt)	131	7.9

Table 2.3: A comparison of the clearing and melting transitions of selected liquid crystals analysed by the HT screening apparatus. The effect of reducing the thickness of the mirror used for analysis is shown.

The two different modes of operation in Figure 2.11 showed similar results (with an opposite directional change in intensity) for the nematic to isotropic transition. However when observing the crystal to nematic mode, the NB mode has clear advantages (final plot of Figure 2.11). The NB and NW mode both showed an increase in intensity on the transition from solid to nematic. As the NW mode also showed the same direction of change from the nematic to isotropic phase, it was more preferable to work with the NW phase as any difference in light intensity during the analysis would show false transitions. The NB mode of operation was preferable giving stronger transitions and showing more detail in the plots due to better contrast.

2.5 Optimisation of the Optical Clearing Point Apparatus

The apparatus has been established as a viable method for the measurement of multiple liquid crystal phase transitions. However, the prototype apparatus still had an excessive systematic error especially at elevated temperatures caused by the thickness of the mirror on the sample stage. In addition, although the resolution was sufficient for visualisation of basic mixtures and singles, further enhancement was required. Three areas for improvement were outlined to enhance the efficiency, accuracy, and sensitivity of the analysis

- Decreasing the surrounding light to increase sensitivity.
- Increasing the incident light to increase resolution.
- Increasing the thermal accuracy.

2.5.1 Reducing Ingress of Surrounding Light

The prototype apparatus was constructed using cardboard which while easy to adapt and modify was not suitable for long-term use. The apparatus was redesigned (Ventacon, Winchester) using a plastic composite material, improving the design in the process (Figure 2.12 and Figure 2.13) This apparatus was highly efficient in eliminating the ingress of non-polarised light, which could reduce the sensitivity of the apparatus by decreasing the contrast between white LC spots and the dark background. The large windows on the roof of the box accepted replaceable squares of polarising film. On one side the polariser orientation was fixed, on the other 3^{o} of movement was allowed so that the optimum alignment and extinction could be gained. The dimensions of the films were increased from the previous

design, allowing for a greater visible analysis area inside of the box (the analysis area is only as large as the reflected image of the opposite polariser on the mirrored heating stage). To increase the resolution of the experiment further, the amount of unpolarised light entering the apparatus was reduced using a high-grade polarising film (99 % polarising efficiency) provided by Merck. To prevent the build-up of heat inside the enclosure, a fan was fitted to draw cool air into the apparatus through holes in the sides of the enclosure above the level of the sample heating stage. Due to the use of more efficient polarising film, the intensity and homogeneity of light emitted from the 80 W light box was not sufficient resulting in the outline of the bulb filaments being seen through the crossed polarisers. To prevent this effect a cold cathode backlight, as fitted to a TFT-LCD display device, was substituted for the light box.

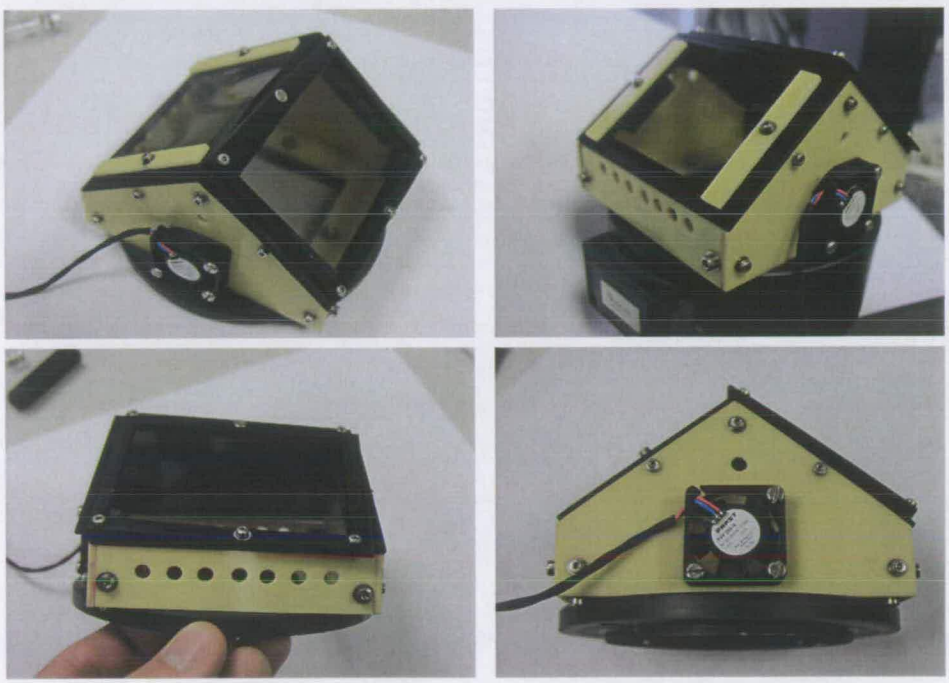

Figure 2.12: The professionally fabricated polarising enclosure that is fitted to the top of the heating block to prevent the ingress of non-polarised light. The design has been improved to include a cooling fan, vent holes and adjustable mounts to hold the polarising films.

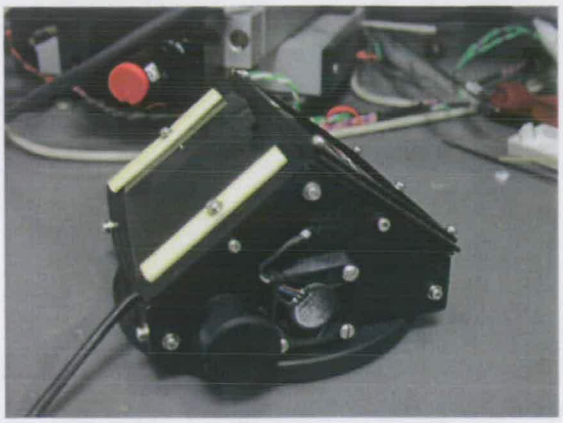

Figure 2.13: The Polarising enclosure after spray painting black to eliminate ingress of light through the composite walls.

Figure 2.14 and Figure 2.15 illustrate the differences in resolution when the intensity of the light source was increased, greatly increasing the white birefringent areas whilst decreasing the dark areas. This gave experimental results of greater clarity in which transitions could be clearly differentiated, and the overall intensity of the spots was increased which reduced noise. The improvements also aided in the identification of smectic phases of BCH-52F and K27 as shown in Figure 2.14.

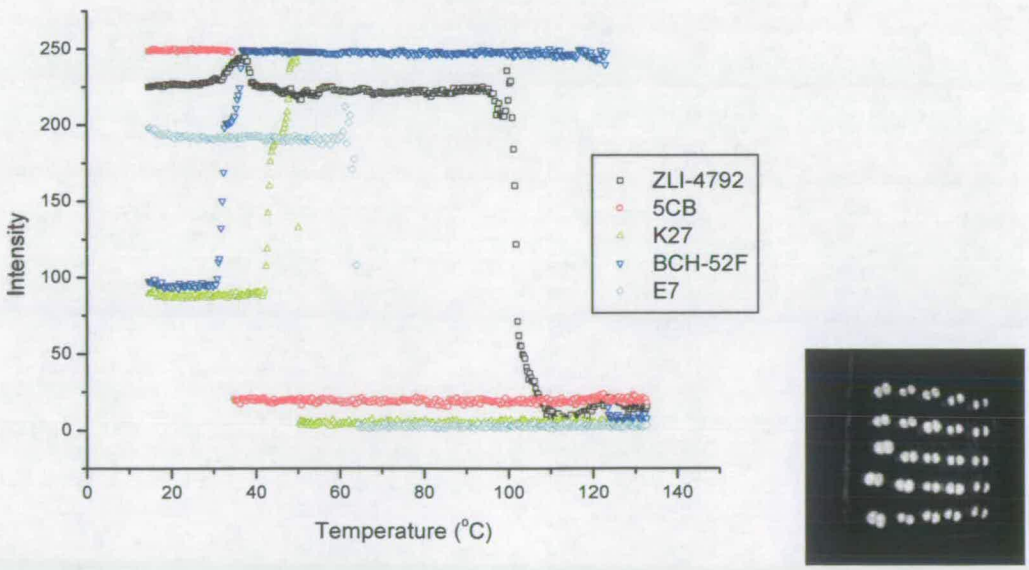

Figure 2.14: The transitions of five liquid crystals obtained using the HT screening apparatus after improvement and optimisation of the polarising enclosure and the use of an improved backlight. The 'thick' mirror visualised in the experiment is illustrated inset

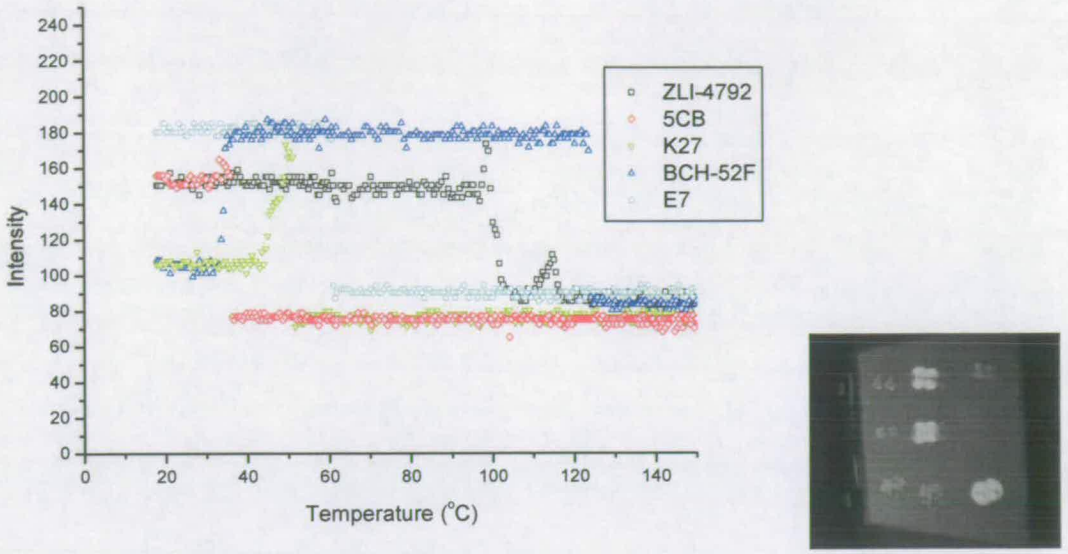

Figure 2.15: The transitions of five liquid crystals obtained using the HT screening apparatus before improvements to the backlight and polarising enclosure were made. The 'thick' mirror visualised in the experiment is illustrated inset

2.5.2 Thermal Accuracy

One of the major problems to be addressed in the prototype apparatus was the thermal accuracy of transitions. Using the current apparatus, transitions were observed at between 1 and 10 °C above the expected temperature. The discrepancy was caused due to the poor thermal conductivity of glass, which produced a lag between the surface in contact with the heating block and the surface in contact with the sample. To overcome this discrepancy a very thin, silvered-glass cover slip with minimal thermal lag could be placed on the stage onto which samples could be analysed. Another more elaborate option considered, was plating of the heating stage with a reflective metal on which the samples could be loaded. Due to the cost and handling issues of producing thin, silvered glass substrates the method of metal plating the top-plate was selected. To create a durable and resilient coating two materials (steel and chrome) were considered, which could be polished to provide a highly reflective and chemically resistant surface. This type of top plate could be substituted in place of the plate used on the existing apparatus. Initially, a stainless steel plate (16 W/mK) was trialled but observation of mesophases using the apparatus showed poor contrast, due to the surface not possessing sufficient reflectivity. To ensure a highly polished surface chrome

plating of a brass (109 W/mK) top-plate was used to provide a highly heat conductive, resilient and reflective surface for analysis (Figure 2.16).

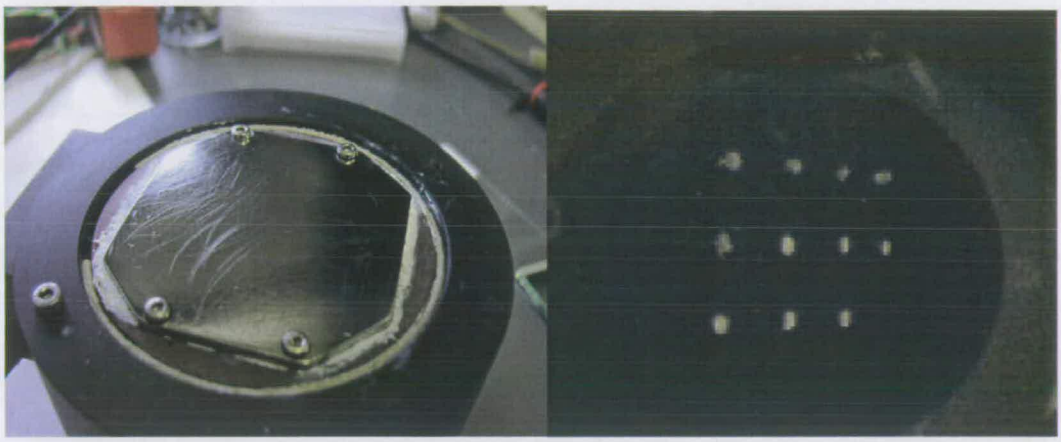

Figure 2.16: The heating stage shown with the chrome plated brass analysis plate attached (left) and loaded with solid and liquid LC samples, seen through the polarising enclosure(right).

The optimised surface gave significantly improved data, eliminating the heat lag and parallax seen when using the mirror. The data in Table 2.4 shows transitions occur at consistently lower temperatures when analysed on the chrome surface. The only disadvantage was a reduction in the level of transmitted light due to the decreased reflectivity of the chrome compared to the mirror.

Liquid crystal	Analysis Surface	Transition	Temperature/°C
E7	Chrome	T_{N-I}	58.2
	Glass	T_{N-I}	61.2
BCH-52F	Chrome	T_{C-N}	30.1
	Chrome	T_{N-I}	116.2
	Glass	T_{C-N}	33.5
	Glass	T_{N-I}	123.4
5CB	Chrome	T_{N-I}	34.1
	Glass	T_{N-I}	36.4

Table 2.4: A comparison of a selection of LC transitions analysed on either the glass mirror or the chrome analysis plate. The temperatures of the transitions measured using the glass mirrors are higher due to the poor thermal conductivity of glass.

2.5.3 Identification of Smectic Phases

As well as identifying the crystal to nematic and nematic to isotropic transitions of liquid crystals, the identification of smectic phases was important. The difference in birefringence between the nematic and smectic phases is more subtle than that between the solid and nematic, requiring a sensitive detection technique.

The nematic phase is seen as a step between the melting and nematic transitions. This step is observed (on a glass substrate) to lie at intensity between the crystal and nematic phases. When using a metal surface to analyse LCs, an anomaly is seen where the formation of smectic phases results in an intensity drop prior to the formation of the nematic phase and associated increase in intensity. Figure 2.17 illustrates the difference between glass, steel and chrome surfaces.

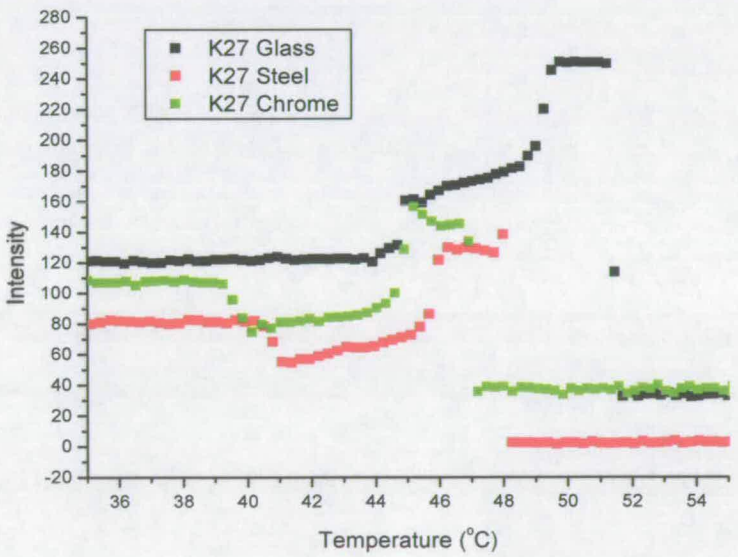

Figure 2.17: Observation of differences in the intensity of smectic transitions when analysed on glass, steel and chrome heating surfaces.

Further investigation revealed that after a heating cycle on a metal surface, this behaviour was reversed and behaviour identical to that on glass observed. (Figure 2.18) The transition between the solid and smectic can be seen to decrease in intensity during the first run and increase in intensity during the second run. A possible cause for this effect can be attributed to the different surface energies of the two materials. Upon melting to the nematic phase

different alignments are induced due to the ability of the LC to wet the glass surface efficiently, but not the metal. This is illustrated through the differences in scattering and intensity. After the formation of the nematic phase, the energy of the system becomes large enough to overcome the energy barrier of the surface such that wetting occurs, and behaviour characteristic of the glass surface are regained. The only transition to be influenced in this way is the smectic phase. This observation could be used to provide a quantification of the smectic phase, or can be removed by analysing using a heat-cool-heat cycle.

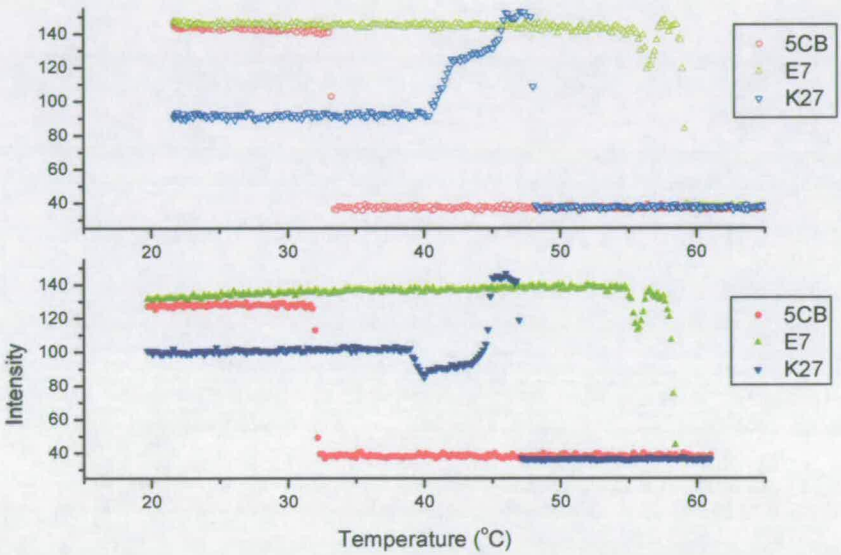

Figure 2.18: Three liquid crystals showing various different phase transitions analysed over three consecutive heat-cool runs on a chrome analysis surface. The initial heat cycle (top) shows a different trend in the intensity of the smectic phase of K27, to that seen in the third heat cycle (bottom). Other transitions wee not affected in subsequent runs.

2.6 Optimisation of the Analysis Method

2.6.1 Heating Rate and External Calibration

The Calcomms controller was calibrated to ensure the reported temperature was the true value of the heating plate. This was achieved using a digital thermometer with a flat shoe. The thermometer was attached to the middle of the heating plate using a thermal transfer

compound at the interface, and the Calcomms apparatus set to ramp to 150 °C. The temperature shown on the external thermometer was recorded at every 10 °C, as shown on the Calcomms apparatus. This data was then inputted into the controller's optimisation sequence, resulting in a calibrated heating ramp. The calibration routine is fully documented in the Calcomms user guide. Following calibration, the heating rate was optimised. Using a rate of 10 °C/min resulted in a short analysis time but, as the heating block was not capable of sustaining this rate, a non-linear heating curve was observed at higher temperatures. To identify the fastest achievable linear heating rate, a series of increasing rates (2.5 to 10 °C/min) were assessed. Identification of the first rate at which non-linearity was observed revealed the limit of the apparatus heating capability. Figure 2.19 shows the maximum sustainable heating rate to be 5 °C/min.

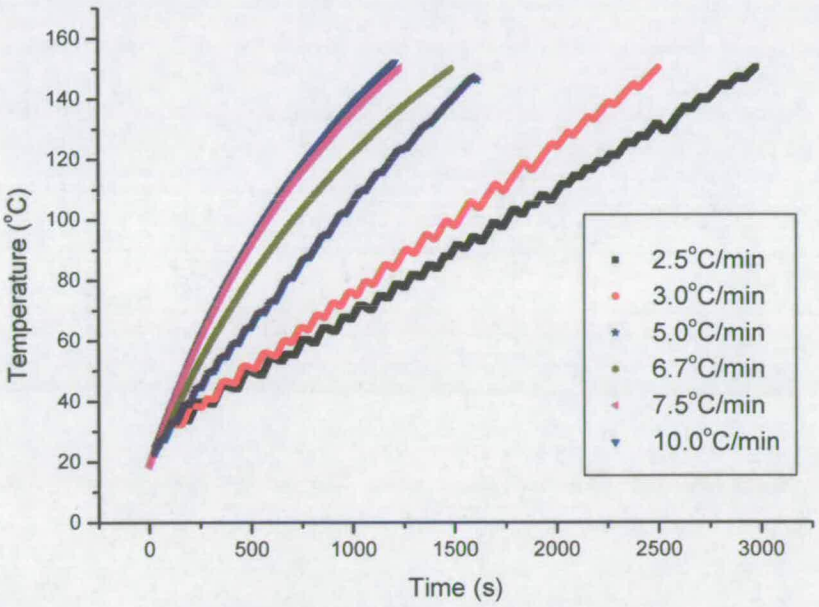

Figure 2.19: Data obtained by setting the heating rate of the Calcomms instrument to values between 2.5 and 10 °C/min. 5 °C/min is the maximum rate at which a linear relationship between temperature and time is maintained

One observation is that the heating ramp, although linear, exhibited a 'saw tooth' structure which was particularly visible at slower heating rates. Plotting the rate of change of temperature with respect to time (Figure 2.20) reveals that there are long periods at which the heat flow into the system is negative, showing the Calcomms controller is not applying

power. This is due to the controller operating on a feedback loop, which controls when the heater is switched on. The large fluctuations in the heating rate are caused by a long feedback time, preventing the heater from restarting immediately. This feedback time can be adjusted in the Calcomms controller and so an adjustment was made, considering a 5 °C /min heat rate was to be used. The optimised plot can be seen in Figure 2.20 where the rate appears much smoother and as a result remains almost linear throughout the heating sequence. The plot still contains a small degree of variance but this is negligible over the sampling period used to analyse the data

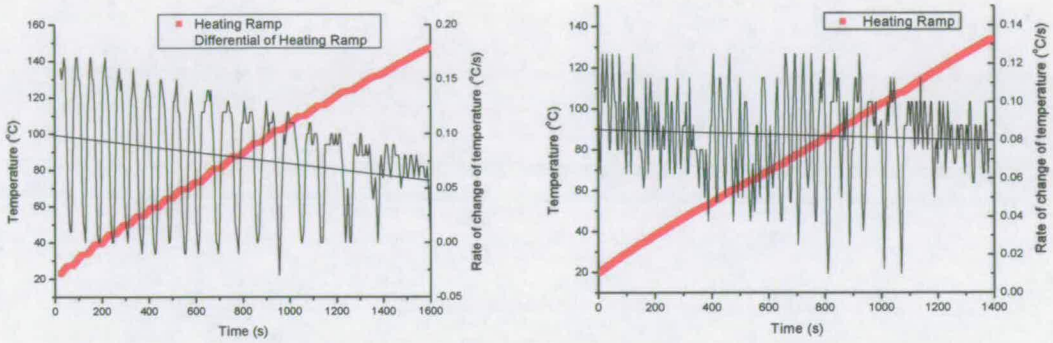

Figure 2.20: The heating ramp, differential of the heating ramp and a linear best fit to the differential for the 5 °C/min rate before (left) and after (right) optimisation. After optimisation, the time between events in the differential was dramatically reduced because of a shorter sampling time in the feedback loop.

Following optimisation, all subsequent experiments were run using the 5 °C/min heating rate. Although the difference in heating rate was shown to have a minimal effect on the recorded transition temperatures (Table 2.5) a reproducible rate enabled more consistent results and allow comparisons to be drawn with other techniques.

		HT Analysis		
Liquid Crystal	Transition	5°C/min	10°C/min	Literature
K27	T_{C-Sm}	39.3	39.5	42.0
	T_{Sm-N}	44.3	43.4	48.0
	T_{N-I}	46.4	44.6	50.0
BCH-32F	T_{C-N}	38.7	38.6	42.0
	T_{N-I}	113.3	113.4	117.3
T15	T_{C-N}	127.4	127.7	131.0
E7	T_{N-I}	55.7	58.7	58.0
K15	T_{N-I}	32.1	32.5	35.1
K21	T_{C-N}	27.6	27.0	31.0
	T_{N-I}	39.3	38.9	43.8

Table 2.5: The effect on observed transition temperatures of selected liquid crystal samples when analysis is carried out at a linear 5 °C/min or non-linear 10 °C/min heating rate.

2.6.2 Homogeneity of Heat Distribution

To measure the homogeneity of temperature distribution over the heating block an Infrared thermal imaging camera (IRRIS 256STd) was used to record the thermo-graphic image of the apparatus during a 5 °C/min heat ramp at temperatures between 50-100 °C.

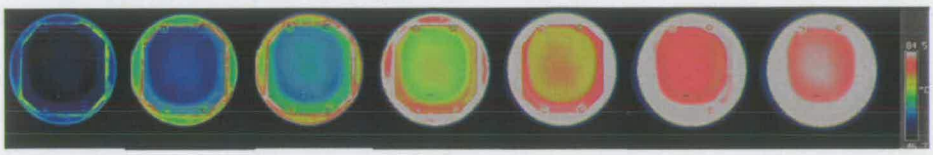

Figure 2.21: A representation of the temperature of the heating block at increasing temperatures using an IR camera.

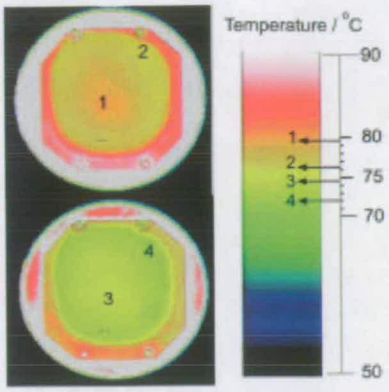

Figure 2.22: The difference between the hot spot in the centre of the heating plate and the main area of the plate is quantified by a colour-temperature calibration of the scale on the right using an external thermometer. The colour of the heating plate is then used to obtain the temperature, which can be seen to vary by approximately 3 °C over the analysis area

Figure 2.21 illustrates the change in the thermo graphic image over the temperature range 70 to 80 °C. It should be noted that the scale on the right of the image is not calibrated to the correct temperature, but does show the correct temperature range (40 °C), therefore allowing the relationship between colour and temperature to be derived. The heat distribution on heating can be seen to emanate from the hottest spot in the middle of the plate. The far corners of the plate are not under thermostatic control and hence should not be used for sample analysis due to poor uniformity. The difference between the temperature of the 'hot spot' in the centre of the plate and the surrounding area was obtained; the colour from the IR camera calibrated to the temperature measured using a flat plate thermometer. The temperature variation of approximately 2.5-3 °C from the centre of the heating block to the outer edge is significant, and explains the deviation from literature values in some measurements. An overall accuracy of ±3 °C is acceptable for a HT method and forms the main systematic error in the experiment. Where possible, to reduce the effect of this error samples should be analysed in duplicate and in randomised positions on the plate so that following averaging, the variation is reduced.

2.6.3 Sample Size

The first law of thermodynamics implies that for a larger amount of substance the energy required to instigate a phase transition is increased; therefore, the observed transition

temperature could be affected by the size of the spot deposited upon the sampling stage. As the heat flow into the sample was constant, transitions could occur at higher temperatures as the volume of the spot increased. Samples are loaded onto the apparatus either as powders or as liquids by pipette, and hence there is little control of the substance volume deposited. To ensure this large variation in sample size was not the cause of a significant error the following experiment was devised.

Spots of E7 liquid crystal with a T_{N-I} of 60.0 °C were placed on the heating stage using a micropipette. The size of the spot deposited was quantified by measurement of the spots pixel area in IPP, identifying the white pixels from the dark background. To observe the effect of the sample area on transition temperature the onset and offset temperatures were recorded, heating past the clearing point. The onset and end temperatures were taken to be the penultimate points in the data series before the change to the isotropic, and then the first data point of the isotropic phase preceding the intensity change.

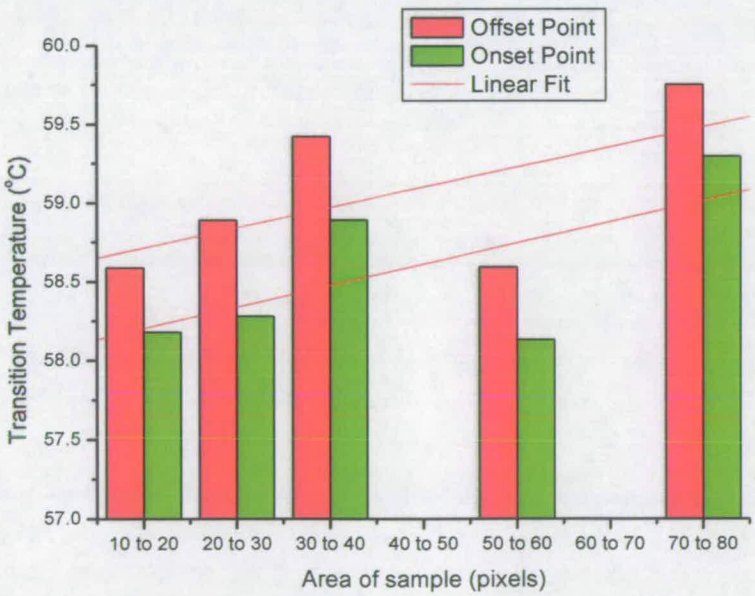

Figure 2.23: The area data, binned by sample area and onset and offset temperatures, and plotted to gain a linear correlation between area and transition temperature. It is seen that overall, the difference between the two points is constant and only a small increase in transition temperature is observed at higher spot areas.

Figure 2.23 shows, as expected, that as the spot area increased so did the temperature at which the transition occurred. However, the change in the transition is of the order of 1 °C which is smaller than the error caused by the heat distribution over the heating plate surface. It can be concluded therefore that the size of spots has a small effect on transition temperatures and would be negligible if volumes were kept approximately equal.

2.7 Comparison of the HT Method and DSC

With all optimisations in hand and using the previously described analysis methods, a range of liquid crystal samples representative of a diverse range of single components and mixtures was analysed using the HT method, enabling comparison with the data obtained in the literature[15] and by DSC. Samples used were BCH-32F, BCH-52F, MLC-6647, MLC-6884, MLC-6682, T15, K21, K27, ZLI-4792, E7 and 5CB (Merck Chemicals Ltd). The samples were spotted onto the chrome plate by pipette and the temperature ramped from 20 °C to 150 °C at 5 °C/min. The experiment was performed in duplicate. Data was analysed to obtain the temperatures at which melting, clearing and other transitions occurred, and compared with DSC data obtained using a 10 °C heat-cool-heat cycle. Previous analysis shows no variation in the results gained by DSC at rates of 5 °C/min or 10 °C/min so the data was directly comparable. Selected results are shown in Table 2.6.

LC	Transition	Literature	DSC			HT Analysis	
			Onset	Peak	Deviation	Transition	Deviation
5CB	T_{N-I}	35.1	34.4	34.6	0.7	31.9	3.2
E7	T_{N-I}	58.0	57.6	58.2	0.4	55.7	2.3
K27	T_{C-Sm}	42.0	41.5	42.1	0.5	39.5	2.5
	T_{Sm-N}	48.0	47.2	47.4	0.8	44.9	3.1
	T_{N-I}	50.0	49.3	49.4	0.7	46.9	3.1
BCH-32F	T_{C-N}	42.0	40.4	41.0	1.6	38.9	3.1
	T_{N-I}	117.3	115.6	115.8	1.7	113.4	3.9

Table 2.6: Comparison of data obtained using DSC and the HT screening apparatus and literature values. The deviation reported is that between the analysis technique and the literature value. In the case of DSC, the deviation is taken using the onset temperature.

The results show a good correlation between the DSC measurements, literature values and HT analysis data. The deviation is measured as the difference between the recorded transitions (the onset temperature in the case of DSC), from that obtained in the literature. The difference of approximately 0.7 °C by DSC is a result of differences in apparatus, analysis procedures, and the amount of substance under investigation, falling within the error expected for such a technique. The HT analysis shows a consistent error of approximately 3 °C difference between literature values, and 2 °C between DSC results. The variation in the deviation from 3.9 °C to 2.3 °C can be attributed to the error introduced in section 2.6.2, caused by the differences in heat distribution across the measurement area (±3 °C). The approximate 3 °C negative temperature shift is a result of systematic error in the apparatus, caused by a combination of lag between the heat source and analysis surface, deviation of the optimised calibration and differences between the optical measurement by the HT technique and calorimetric measurement in DSC.

2.7.1 Measurement of Transition Temperatures

The position at which the transitions were recorded was the mid point of a sharp transition or the end of a broad transition. The data obtained by HT and DSC analysis was plotted on the same axis to identify the most representative point at which to measure the phase transition (Figure 2.24)

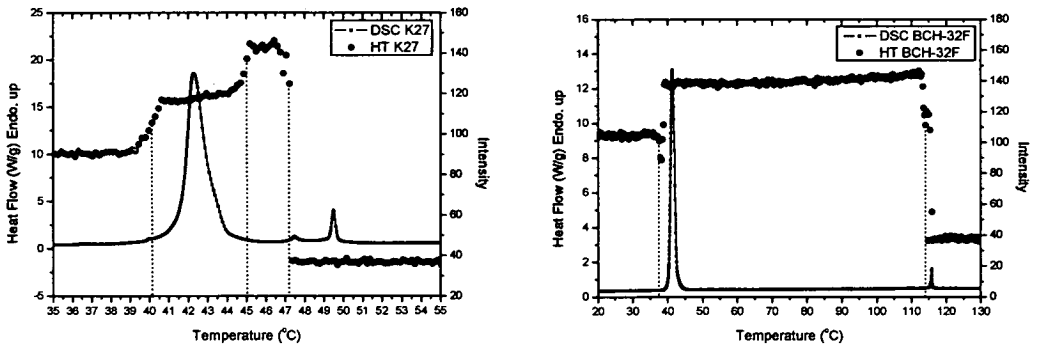

Figure 2.24: A visual comparison of the transition data as visualised by both DSC and the HT screening apparatus in both K27 (left) and BCH-32F (right). The HT data can be seen to occur at lower temperatures than DSC consistently.

The graphs clearly show that all transitions measured by the HT method appear a few degrees before the calorimetric change recorded by DSC. Currently, transitions are recorded at either the mid point of a short transition, or the offset point of a broad transition. It did not appear advantageous to alter the point at which the data was measured, as the error appeared to be a result of other factors. Therefore, no change was made in subsequent experiments. Due to the difficulty in identifying and correcting the error seen in these experiments the HT experiment was not modified. The systematic error of -3 °C present in all HT results should be taken into account in further analysis.

2.7.2 Phase Identification

In common with DSC analysis, a qualitative difference between solid, smectic, nematic and isotropic phases can be identified in the HT experiment using the relative intensity measurements of each transition. Figure 2.24 illustrates this process for both DSC and the HT results. In DSC, the different phase transitions can be identified using the size of the peaks, considering the enthalpy change as described in section 1.3.2 of Chapter 1. Using the HT technique the same three transitions can be identified, crystalline occurring at mid intensity, nematic at high intensity and isotropic at low intensity. Although this is not a foolproof method, and cannot be used in isolation for phase identification, it does allow an overview of the number and type of phases to be expected.

2.7.3 Reproducibility

Table 2.7 shows the results of an experiment where samples were heated over three successive temperature ramps and analysed in each for their phase transition temperatures using the HT apparatus.

LC	Transition	Run1 (°C)	Run2 (°C)	Run3 (°C)	Mean (°C)	Std. Deviation (°C)	Error of Mean (°C)	Literature (°C)
K27	T_{C-Sm}	39.5	40.7	40.3	40.2	0.6	1.8	42.0
	T_{Sm-N}	44.9	44.9	45.7	45.1	0.5	2.9	48.0
	T_{N-I}	47.1	47.2	48.0	47.5	0.5	2.5	50.0
BCH-32F	T_{C-N}	38.9	37.7	39.2	38.6	0.8	3.4	42.0
	T_{N-I}	116.0	114.8	116.5	115.8	0.9	1.5	117.3
T15	T_{C-N}	127.7	128.2	128.0	128.0	0.2	3.0	131.0
E7	T_{N-I}	55.6	56.2	55.6	55.8	0.3	2.2	58.0
5CB	T_{N-I}	32.0	33.2	32.4	32.5	0.6	2.6	35.1
K21	T_{C-N}	27.5	28.0	27.3	27.6	0.5	3.4	31.0
	T_{N-I}	40.0	40.6	39.7	40.1	0.4	3.7	43.8
						Average deviation	0.5 °C	
						Average error of mean	2.7 °C	

Table 2.7: Transitions of selected LC materials analysed over three consecutive runs. The deviation between the values is low and hence reproducibility is high. The data consistently shows a systematic error of -3 °C when compared with literature values.

Deviation between the successive runs was low, indicating a high reproducibility. The error of the mean from the literature value was seen to be around 3 °C confirming the previous observation that the apparatus possesses a systematic error of this magnitude. In many HT screening methods, the increase in throughput is often at the expense of accuracy. In this case, there is a reduction in the accuracy of the method when compared with DSC but overall this is small.

2.8 Addition of Sample Cooling

Without cooling the initial starting temperature at which the analysis begins is dictated by room temperature, and on completion the block can take hours to return to ambient therefore limiting analysis turnaround. Without cooling, the detection of recrystallisation[17] events and smectic phases (which can often be visualised more clearly on the cooling and reheating runs)[18] is also hindered. To extend the scope of the apparatus further a method of cooling the apparatus was developed. To provide sub-ambient cooling a stream of either liquid or gas can be passed through the heating block so that heat is transferred away from the apparatus. Because of the broad temperature-range of the heating block, the use of water-cooling was not practical due to the formation of steam above 100 °C. Therefore, the use of nitrogen was

considered. At higher temperatures, ambient nitrogen is sufficient to remove heat; in order to achieve sub-ambient temperatures the nitrogen must be cooled prior to entry into the heating block. A dip coil apparatus was constructed such that a stream of nitrogen gas was passed through a coiled tube, immersed in liquid nitrogen before entering the heating block. (Figure 2.26 and Figure 2.25)

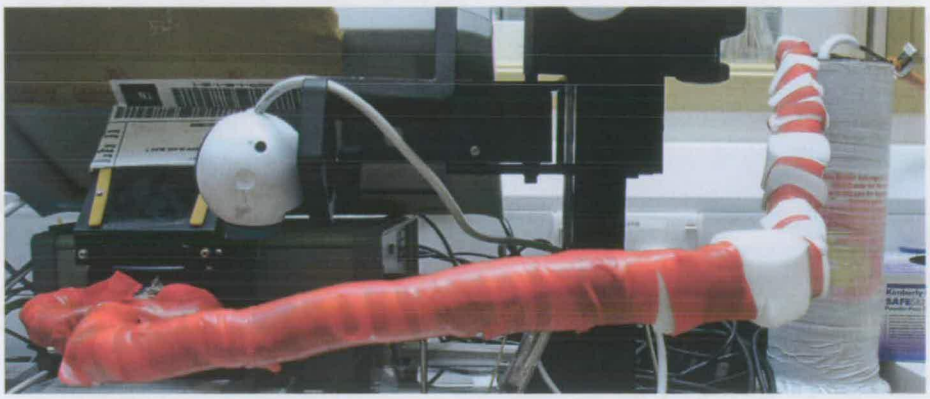

Figure 2.25: An image of the HT screening apparatus including the cooling apparatus. The red tube through which nitrogen gas was pumped, attached to channels drilled through the heating block.

To enable nitrogen to be passed through the heating block required channels to be cut through the apparatus. The heating elements lie to the bottom of the block so two channels were cut through the block, slightly offset to the heating elements. To these channels were attached a joint to ensure a gas tight seal. On exiting the heating block, one channel was vented into the enclosure on top of the heating block. This nitrogen purge prevents the formation of condensation on the heating block at sub-zero temperatures, enabling -70 °C to be achieved with minimal condensation.

The cooling rate was controlled by the flow of nitrogen through the apparatus and therefore was more effective at higher temperatures. From 150 °C rates of -15 °C/min were attainable, however at sub-zero temperatures only -4 °C/min could be achieved. (Figure 2.27)

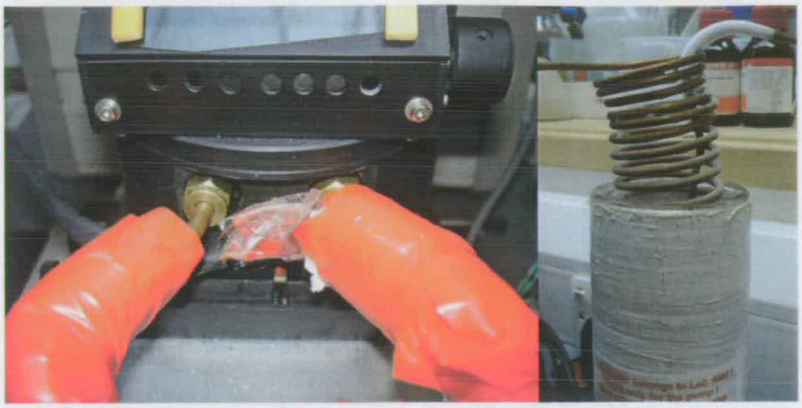

Figure 2.26: The dip coil (left) is immersed in liquid nitrogen before a flow of nitrogen gas is passed through the coil. The cooled gas passes into two channels drilled into the heating block (right) causing the temperature of the block to drop, cooling the samples.

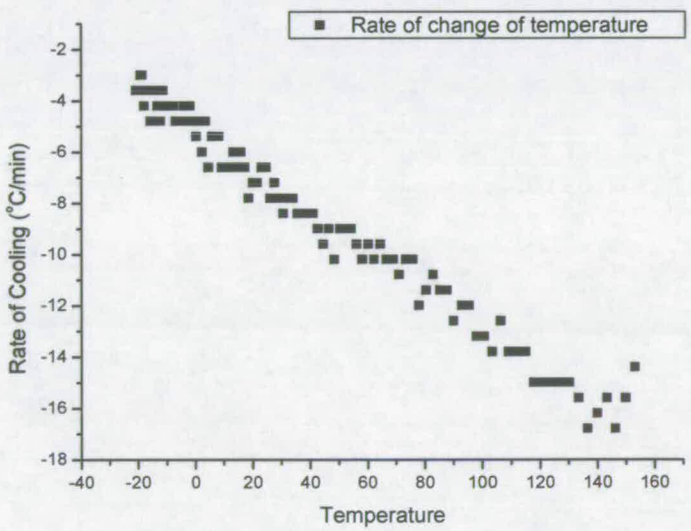

Figure 2.27: The rate at which cooling was possible when the nitrogen flow was turned to maximum. At high temperatures, fast rates were achievable however, the rate decreases with temperature.

Due to the apperatus modifications, calibration was repeated using the external thermometer in the same way as described in section 2.6.1. Repeating the analysis of a number of liquid crystal samples using this apparatus showed no significant changes in the results obtained.

2.9 Conclusion

In this section, liquid crystal characterisation was assessed with the aim of developing a method for high-throughput screening of liquid crystal materials. The characterisation of phase transitions, including the melting and clearing points, was identified as a suitable technique and an important property in initial screening experiments. Apparatus was developed initially at the prototype stage to identify liquid crystal phase transitions in parallel using an optical screening method in which the property of birefringence was used to detect change. The prototype apparatus showed the principle to be sound, identifying the temperatures of phase transitions in both single liquid crystals as well as mixtures. Optimisations to the apparatus included professional re-fabrication and optimisation of all aspects of the experiment to increase the accuracy, resolution and reproducibility. Investigation into the effects of factors such as sample size and heat distribution enabled the errors associated with the analysis to be quantified and systematic errors defined. To accompany the new apparatus methods of data analysis and data automation were developed to help prevent a bottleneck in the high-throughput process. Throughout testing, the apparatus proved to give consistent and reliable results that were comparable to techniques traditionally used for this type of analysis, such as DSC. One limitation of the technique is the wide variation in results (≈3 °C). Although this is acceptable for a screening application, it does not compare to the accuracy expected for LC characterisation of ±0.2 °C as shown by DSC.

The technique was able to distinguish qualitatively between mesophases and identify the temperature of phase transitions in both LC singles and mixtures as a first screening method to identify compounds or compositions of interest. The advantage of the HT method is the ability of parallel analysis, enabling many samples to be characterised in the time taken to analyse a single sample by a serial analysis method. In this way, the analytical dataset can be reduced so that only positive hits are taken forward for more time-consuming analysis. The use of this technique to analyse libraries of LCs produced *via* synthesis or formulation greatly can enhance the discovery process leading the way for the development of larger and more diverse combinatorial libraries of liquid crystals, which has until now been a limiting factor in the research into new HT techniques for formulation and synthesis.

2.10 References

(1) O. Deeg and P. Bauerle, *Org. Biomol. Chem.*, **2003**, *1*, 1609.
(2) E. W. McFarland and W. H. Weinberg, *Trends Biotech.*, **1999**, *17*, 107.
(3) E. Reddington, A. Sapienza, B. Gurau, R. Viswanathan, S. Sarangapani, E. S. Smotkin and T. E. Mallouk, *Science*, **1998**, *280*, 1735.
(4) E. Danielson, J. H. Golden, E. W. McFarland, C. M. Reaves, W. H. Weinberg and X. D. Wu, *Nature*, **1997**, *389*, 944.
(5) E. Danielson, M. Devenney, D. M. Giaquinta, J. H. Golden, R. C. Haushalter, E. W. McFarland, D. M. Poojary, C. M. Reaves, W. H. Weinberg and X. D. Wu, *Science*, **1998**, *279*, 837.
(6) F. C. Moates, M. Somani, J. Annamalai, J. T. Richardson, D. Luss and R. C. Willson, *Ind. Eng. Chem. Res.*, **1996**, *35*, 4801.
(7) D. Pauluth and K. Tarumi, *J. Mater. Chem.*, **2004**, *14*, 1219.
(8) M. Bradley and J. Thaburet, WO Patent, WO2005036149 (A1), **2005**.
(9) P. G. de Gennes and J. Prost, *The physics of liquid crystals*, 2nd ed. Oxford: Clarendon Press, **1993**, p 139.
(10) H. J. Coles In *The optics of thermotropic liquid crystals*, S. Elston and R. Sambles (Eds.), London: Taylor & Francis, **1998**. p 57.
(11) D. A. Dunmur In *Physical properties of liquid crystals : Nematics*, D. A. Dunmur, A. Fukuda and G. R. Luckhurst (Eds.), London: Institute of Electrical Engineers, **2001**. p 216.
(12) H. Gleeson In *Handbook of liquid crystals: Fundamentals*, H. Kelker and R. Hatz (Eds.), Weinheim: Verlag Chemie, **1998**. p 699.
(13) P. G. de Gennes, *The physics of liquid crystals*, Oxford: Clarendon Press, **1974**, p 110.
(14) G. P. Crawford and S. Zumer In *Liquid crystals in complex geometries : Formed by polymer and porous networks*, G. P. Crawford and S. Zumer (Eds.), London: Taylor & Francis, **1996**. p 1
(15) Merck KGaA, *Liqcryst datasheets,* Darmstatd, Germany, **2004.**
(16) S. J. Picken In *Physical properties of liquid crystals : Nematics*, D. Dunmur, A. Fukuda and G. R. Luckhurst (Eds.), London: Institution of Electrical Engineers, **2001**. p 89.
(17) M. Neubert In *Liquid crystals : Experimental study of physical properties and phase transitions*, S. Kumar (Ed.), Cambridge: Cambridge University Press, **2001**. p 31.
(18) M. Neubert In *Liquid crystals : Experimental study of physical properties and phase transitions*, S. Kumar (Ed.), Cambridge: Cambridge University Press, **2001**. p 36.

Chapter 3 - High Throughput Formulation

3.1 Introduction

As LCD technology evolves and applications become more complex, liquid crystals created for such uses must possess ever more stringent and demanding physical properties.[1,2] Due to the many, often contradictory requirements, single liquid crystals cannot alone provide ideal characteristics.[3] To obtain optimised materials, mixtures of liquid crystals are used to obtain properties which are related to all components.[4] One such optimisation is that of the melting point, which by the formation of a eutectic[5] mixture can be extended below that of its components therefore increasing the temperature range over which liquid crystal mesophases exist. Indeed, eutectic mixtures were used in the 1970's to increase the temperature range at which a TN display[6] could be operated,[7-10] playing an important role in successful mass commercialisation of the technology.

The preparation and screening of eutectic mixtures by experimental methods alone can involve repetitive and time-consuming formulation and characterisation of components. This procedure has been greatly simplified by the use of a theoretical calculation[11] which is considered essential for the analysis of ternary and multi-component mixtures.[12] The le Chatalier-Schroeder-van-Laar (SVL) equations [13-15] have been reported as valid descriptors for binary mixtures of liquid crystals[12,16] (Equation 3.1). They are therefore often used for the prediction of the melting temperatures of eutectic mixtures.[17-20]

$$ln\ X_A = \Delta H_A\ (1/T_A - 1/T) / R \qquad \textit{Equation 3.1}$$

The values of ΔH_A, the molar heat of fusion, together with T_A, the melting point of the pure component A, are obtained using DSC. The mole fractions of each component in the mixture X, together with the melting temperature, are obtained simultaneously for each of the mixture components A, B and C (in the case of a ternary mixture). Mixtures can then be assessed experimentally using formulation, DSC and polarising microscopy.[21,22] By solving Equation 3.1 simultaneously for N components (Equation 3.2) the values of Xi and T for the eutectic mixture can be obtained.[11]

$$\sum_{i=A}^{N} X_i = 1 \qquad \textit{Equation 3.2}$$

The SVL equation has been shown to be reasonably successful in establishing the required mole fractions necessary to give defined melting points of binary eutectic mixtures.[23] However, a number of assumptions are made in the calculation[21,22] and many components have been identified which do not show a good match to theory, resulting in the development of 'selection rules' for design of mixtures which achieve good theoretical agreement.[17-19] In the creation of ternary and multi-component mixtures the accuracy achievable through theoretical methods is poor, such that only arbitrary mol fractions can be obtained and the melting points of such mixtures tend to deviate away from the eutectic.[12] The use of experimental techniques can provide data that are far more accurate. However, the lack of a high-throughput approach to formulation and screening of mixture libraries means this process can be extremely time-consuming and requires large amounts of material.[21]

Due to the variable results obtained using SVL calculations, simple experimental methods which allow identification of eutectics using small volumes of material are required.[12,21] One such technique, described by Szulc et al,[21,22] involved the modification of existing binary eutectic compositions by incorporation of a third component in increasing concentrations to identify ternary mixture compositions exhibiting depressed melting point behaviour.

The high-throughput screening method developed in Chapter 2 for liquid crystal phase transitions,[24] was successfully applied to this area therefore removing the bottleneck that had made analysis of a large library unpractical. Use of this technique, together with a suitable method of creating a formulation library, enabled parallel identification of mixture phase behaviour and rapid identification of broad mesophase ranges so that other library members can be discarded from further analysis. In this way the library can quickly be condensed, so that only compositional areas of interest are analysed by more accurate but time-consuming characterisation[25,26] The aim of this work was to develop methods for the automated formulation of liquid crystal mixture libraries which could then be characterised using the HT screening method for phase transitions.[24] These techniques, in combination, would allow the creation and screening of a large library in which all phase space can be explored experimentally allowing the relationship between individual components and the effect they have on the bulk mixture properties to be uncovered.

3.2 Experimental Requirements for Creation of Formulation Libraries

An efficient and fast workflow requires that each step of the process (mixture formulation, sample loading, sample analysis and data processing) can be achieved at a similar rate therefore preventing a bottleneck. It is also important to consider the techniques used in the process, to ensure spatial compatibility with subsequent steps so the experimental pipeline can be continuous. The requirements of each of the processes in the creation of formulation libraries will be discussed in the following sections.

3.2.1 Mixture Formulation

Advancements in computing and robotics, together with the maturing of high-content high-throughput screening, has made available apparatus which can be used to automate the transport and reformatting of liquids[27] for creation of large libraries of unique mixtures. Such a process has many benefits over the gravimetric preparation of samples, reducing errors and increasing reproducibility, in addition to reducing the time and experimental resources required. Available for our work was one such system, a Gilson 233XL liquid handler. The platform consisted of a septum-piercing needle mounted on an XYZ arm, which could be positioned over a customisable workspace. Liquids were aspirated by means of a dual volume syringe pump (combined volume of 11 ml), pumping a system fluid that was also used to purge and clean the system. There are a number of parameters which can be changed in the aspirate / dispense cycle, related to the height of the needle, the speed of aspiration and dispensing and the time to wait between cycles.

In the creation of libraries, components may be variable viscosity liquids or crystalline solids. To dispense such a wide range of substances it is most convenient to work using solutions. Homogenisation of the physical characteristics can be achieved by addition of a suitable carrier solvent with optimised viscosity, volatility and solvation ability. Following the dispensing process this solvent must be completely removed (by heating or evaporation) to prevent destabilisation of the liquid crystal phase, resulting in irreproducible and inaccurate results. The primary requirement for automation in the creation of libraries is that dispensed volumes are reproducible and accurate. A secondary consideration is the speed of dispensing, and the amounts of substance that can be manipulated per aspiration cycle. To

ensure conformity to these requirements, the liquid handling system was used to dispense model liquids using the default instrument parameters. To assess the accuracy and reproducibility of the apparatus, three representative fluids were selected for dispensing in increasing volumes into a series of pre-weighed vials. By comparison of the volume dispensed, the density of the liquid and the weight of the liquid dispensed, the accuracy of the system can be established. To ensure reproducibility the experiment was run in triplicate. The liquids selected for this experiment were water, PGMEA (as a representative organic solvent with density = 0.97 g/ml, b.p = 146 °C), and a 20 w/w % solution of a liquid crystal (MLC-6882, Merck Chemicals Ltd.) in PGMEA (propylene glycol monomethyl ether acetate), representative of the type of solutions which require manipulation.

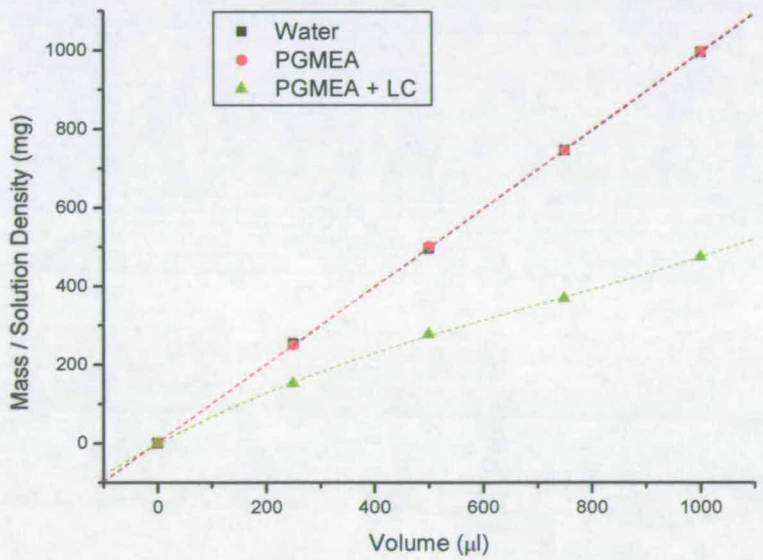

Figure 3.1: The mass divided by density of three solutions, dispensed in increasing volumes using the Gilson liquid handling robot, an aspiration rate of 1.5 ml/min.

Figure 3.1 shows the results of the experiment, with mass normalised for density so that for all solutions an ideal y = x relationship is expected. Water and PGMEA both showed an excellent linear correlation between the volume and mass of liquid dispensed; however, the PGMEA + LC mixture did not follow this linear relationship, showing a large deviation. This formulations viscosity was higher than that of the other model liquids due to its dissolved solids. On closer observation of the process, it was discovered that at high

aspiration rates a vacuum was formed ahead of the solution due to the increased viscosity and the small bore of the aspiration needle. When the needle was raised out of the solution, the vacuum was relieved by aspiration of air, therefore causing incorrect volumes of solution to be dispensed. To prevent this effect two variables were optimised. Firstly, the time taken before the needle was removed from the solution was increased (from one second to three), and the aspiration rate was optimised. To identify the fastest rate at which aspiration could take place with no detrimental effect, a series of pre-weighed vials were robotically filled with aspiration rates starting at the default setting of 1.5 ml/min and reducing from this point. Additionally, samples were prepared manually using a volumetric syringe so that the point at which correlation occurred could be identified.

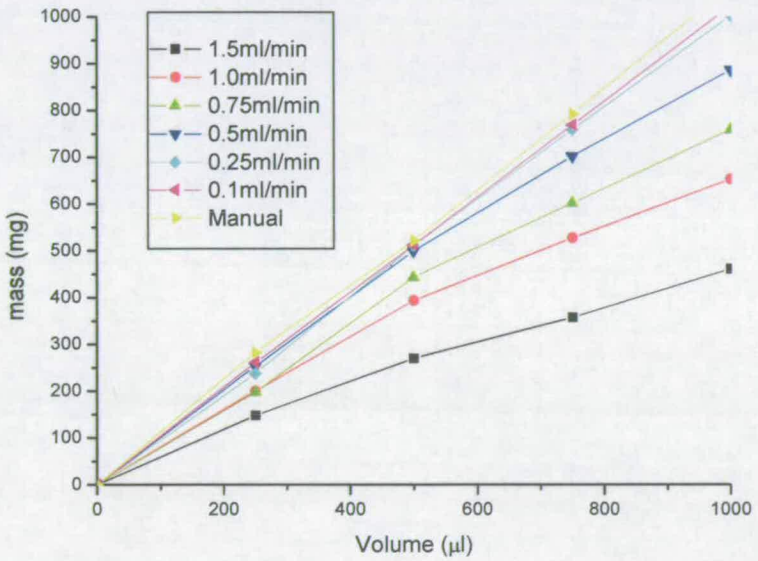

Figure 3.2: The mass of a PGMEA + LC solution dispensed both manually, and by a robotic liquid handler. The rate of aspiration was increased from 0.1 to 1.5 ml/min to identify the fastest rate achievable while maintaining a linear relationship between mass and volume.

Figure 3.2 shows that linearity was only achieved at aspiration rates lower than 0.25 ml/min, where the data was also shown to correlate with that obtained by manual preparation. Although slower rates may offer a further increased degree of accuracy, the time taken for library formulation will also increase. Already, by reducing the aspiration rate from 1.5

ml/min to 0.25 ml/min, the time to dispense 1 ml into 96 vials increases from one hour to seven hours. Over this time the liquid crystal solutions can change in concentration due to the evaporation of solvent, leading to irreproducible errors. For this reason, it was important to work on the smallest scale possible so that formulation time did not become excessive. The experiment shows that the Gilson liquid handler is suitable for HT formulation, providing that the total sample volumes and aspiration rates of more viscous solutions are kept low.

3.2.2 Sample Containment

Following creation of a library, the next stage was to load samples onto the HT apparatus for characterisation. The original method of sample spotting (using a pipette tip), leads to an irregular and variable volume pattern of sample spots which become an issue at elevated temperatures; the droplets spread and become mobile on the surface resulting in the amalgamation of adjacent samples (Figure 3.3). This amalgamation overcomplicates image analysis of the video sequence by creating false transitions as the spot moves, invalidating the experiment. For efficient screening of larger libraries a method of sample containment was required, ideally accompanied by an automated method of loading samples.

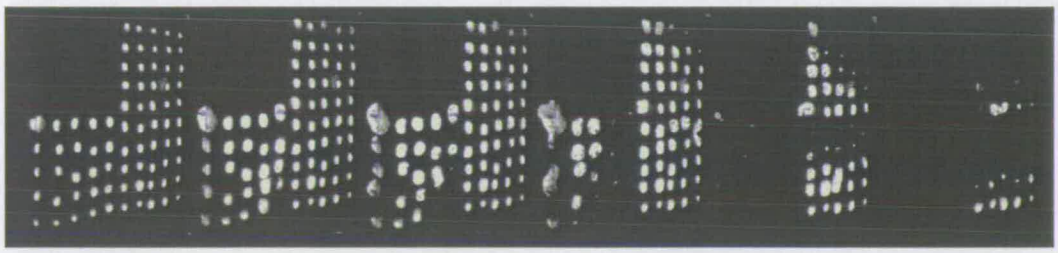

Figure 3.3: A matrix of 75 samples, spotted by pipette onto the HT screening apparatus. The sequence represents increasing temperatures at which the sample spots can be seen to become mobile and amalgamate with adjacent samples.

One method of constraining samples was by the creation of wells in the analysis substrate. To create containment wells without detrimental effect to the optical path of reflected light in the experiment, a photolithography process reported by Cabral[28] and Harrison[29] could be used. In the process ultraviolet (UV) cross-linkable multifunctional thiolene prepolymer[30-32] NOA81 (Norland optical adhesives), was used as a negative photo-resist. Coating the material onto a substrate and UV irradiating through a mask resulted in areas of exposed,

cross-linked adhesive and areas of un-exposed monomeric adhesive, which could be developed using methanol and acetone. The method is illustrated in Figure 3.4. Cured adhesive was resistant to heat and a wide range of solvents[28] and therefore is also resistant to the liquid crystals in the study.

To produce a negative photo-resist mask, Adobe Illustrator (Adobe) was used to create a scale drawing of a 10x10 matrix of 2.5x2.5 mm wells. The mask was printed onto transparency film using a 600 dpi laser printer (Figure 3.5). To produce a mask in which the dark areas were able to completely block the transmission of UV light at 254 nm, required the use of three transparencies glued together. Wells were formed on a glass coverslip (32 x 32 mm, no. 1, Fisher) substrate. The well volume was determined by the height of the cross-linked adhesive. The glue line was maintained at 500 μm using aluminium squares of the same thickness, as spacers between the substrate and release layer. The UV exposure time also influences the depth of cross-linking,[28] and therefore to cure to the full thickness longer exposures were necessary. Detrimentally, the use of a long exposure reduced the lithographic resolution of the process, making the wells slightly smaller due to the thicker walls.

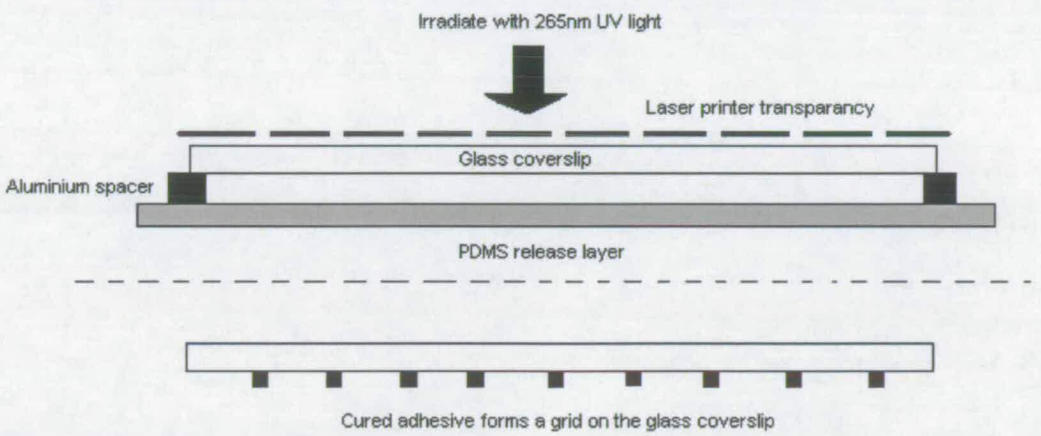

Figure 3.4: The process of negative resist contact photolithography used to create sample containment. The UV sensitive adhesive is placed between the PDMS release layer and the glass cover slip before UV exposure through the mask resulting in cross-linking.

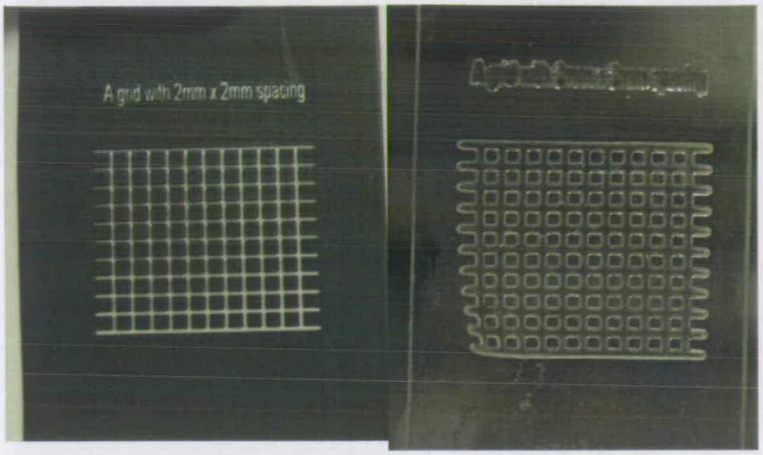

Figure 3.5: An image of the mask, printed onto a laser printer transparency using Adobe illustrator (left) and the grid created from the mask after development (right)

The use of sample containment in analysis ensures a high sample density with no amalgamation of adjacent samples. The matrix was filled as shown in Figure 3.6 with five samples. Although the filling was carried out as previously with pipette tips, the procedure was made much easier due to the wells constraining the samples and providing a crude method of volume control. Analysis of the filled microwell substrate using the HT screening apparatus showed that the reflective and birefringent properties of the liquid crystal samples were maintained. The clearing point values obtained in this experiment show no deviation from those gained using a plain glass substrate, illustrating that the cured NOA81 adhesive is stable to both heat and the liquid crystal. The only limitation is the poor resistance of the cured adhesive to chlorinated solvent. If such solvents are used in formulation care must be taken that samples are thoroughly dried prior to analysis.

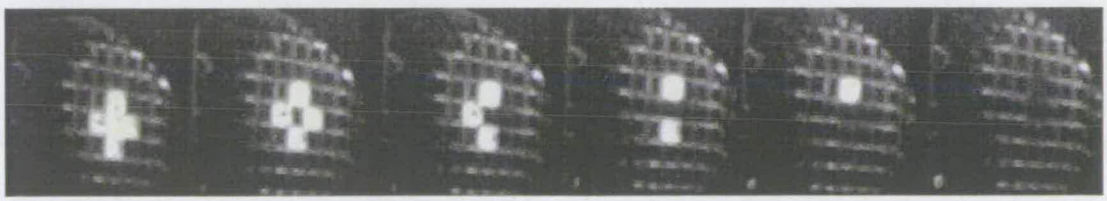

Figure 3.6: The adhesive micro well arrangement loaded with five LCs. The sequence represents low (left) to high (right) temperatures over which N-I transitions can be observed as disappearance of the white squares.

To enhance further enhance this device the use of an automated robotic technique to fill the wells would overcome a major bottleneck. Use of the Gilson liquid handler for this task was attempted, but due to its limited accuracy and minimum dispensing volume, was not suitable. At this time no other robotic device with sufficient spatial resolution or dispensing accuracy was readily available and therefore work was continued using the manual loading technique.

3.2.3 High Throughput Screening and Data Handling

Using the HT screening device developed in chapter 2 together with the sample containment micro-well device allowed 100 compounds to be simultaneously characterised. In a library of this size, the treatment of the large amount of data created must be well thought-out so a bottleneck is not created. The raw data gained from the experiment consists of a 320x320-pixel AVI video sequence of *n* samples, and a text file relating the frame number (time) of the video sequence to the temperature of the heating block. After processing the video sequence using Image Pro-plus (IPP, Media Cybernetics) a list of sample intensity for *n* samples in sequential frames was obtained. For a small number of samples, rearranging the data into columns and plotting graphs of intensity *vs.* temperature manually was not an issue. However, with the possibility of 100 or more samples being analysed over as many as 600 data collection points (total of 60000 generated data points), a method of automated data handling was required. To meet these demands a VBA (Microsoft Excel) macro sequence was written to process the data automatically. Raw, unformatted data obtained from analysis was pasted into the spreadsheet together with a number of key variables, into the highlighted yellow boxes (Figure 3.7). The variables entered included; the number of samples analysed, the equation relating the frame number to the temperature (gained through a polynomial best fit to the frame/ temperature data outputted by the Calcomms software), the sub-sample sequence used in IPP, and the upper and lower limits to be used in plots of intensity vs. temperature.

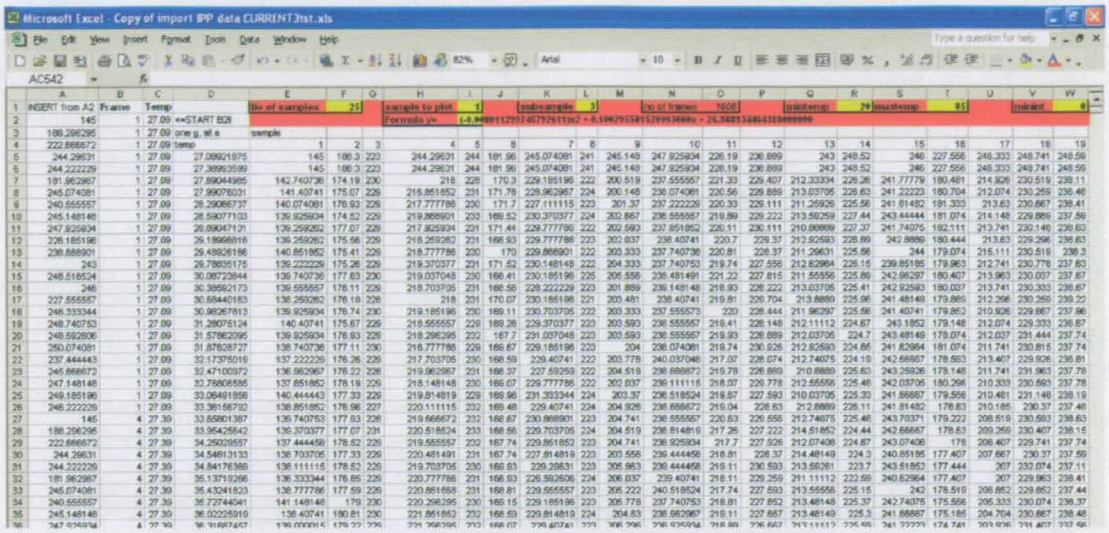

Figure 3.7: The Excel VBA macro showing processed data. The data was automatically transposed into columns and the temperature of each data point derived from the frame number.

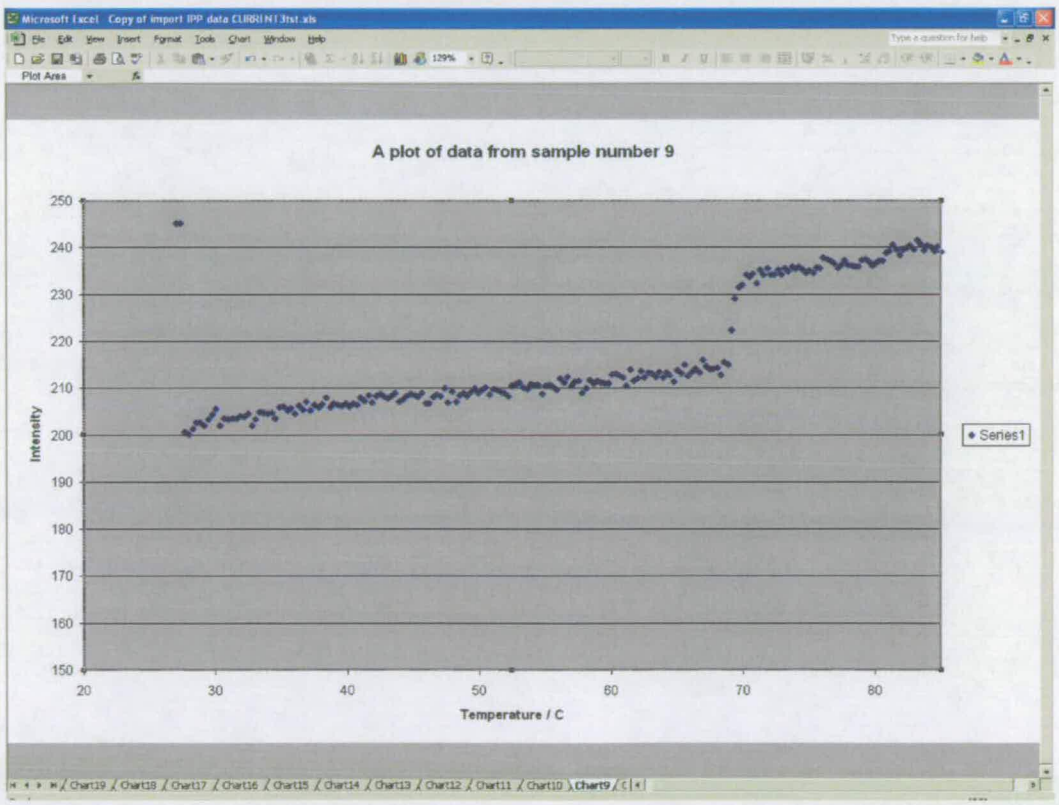

Figure 3.8: The Excel VBA macro, representing a graph obtained for all members of the library. The data can be analysed for intensity discontinuities to identify phase transitions,

On executing the macro, the temperature at which each of the data points was recorded is calculated before transposing the linear list into columns relating intensity to temperature for each sample (Figure 3.7). This table is then used to plot a graph of intensity *vs.* temperature for each of the samples (Figure 3.8). Using this macro enables the entire process, from data entry to plotting graphical data for the entire library to be achieved in less than one minute, leaving only interpretation and extraction of the phase transitions from each of the graphs to be performed. The Excel macro including the code listing is included on the supplementary data CD.

3.3 Formulation and Testing of a Liquid Crystal Mixture Library

To test the combined techniques of robotic formulation, sample containment, parallel HT screening for phase transitions[24] and analysis, a library using three commercially available liquid crystal mixtures was created. The mixture components used were MLC-6882, MLC-6684 and MLC-6647 (Merck Chemicals Ltd.) These mixtures themselves contain a number of compounds with different functionalities and volatilities, thus helping to determine if the technique was suitable for use with a wide range of compounds, and assisting in the identification of any incompatible procedures or components.

3.3.1 Library Design

To create the library three MLC liquid crystals were combined robotically into 1.5 ml brown glass vials. The maximum volume transferred to the vial was 375 µL, the small volume reducing the total formulation time and minimising solvent evaporation. Each of the liquid components was diluted to reduce viscosity by creating a 1:1 w/w % solution with DCM, chosen for its volatility, thus ensuring complete removal of solvent could be achieved post-formulation at low temperatures, preventing the evaporation of more volatile liquid crystal components.

Formulation was achieved using a strategy in which volumes of 125 µL, 94 µL, 63 µL, 31 µL or 0 µL of each component were dispensed into each target vial creating a total of 75 single, binary and ternary mixtures. The volume of the mixtures obtained using this process was variable. A number of compositions were created in duplicate using this formulation

strategy, which was used to assess reproducibility. This strategy allowed the efficient programming of the Gilson apparatus using zones. For each mixture component, all vials in which an identical volume was to be dispensed were defined graphically using the Gilson software. The process was then repeated for each identical volume to create five dispensing zones in total. The zones are illustrated graphically, as entered into the Gilson instrument, in Figure 3.9.

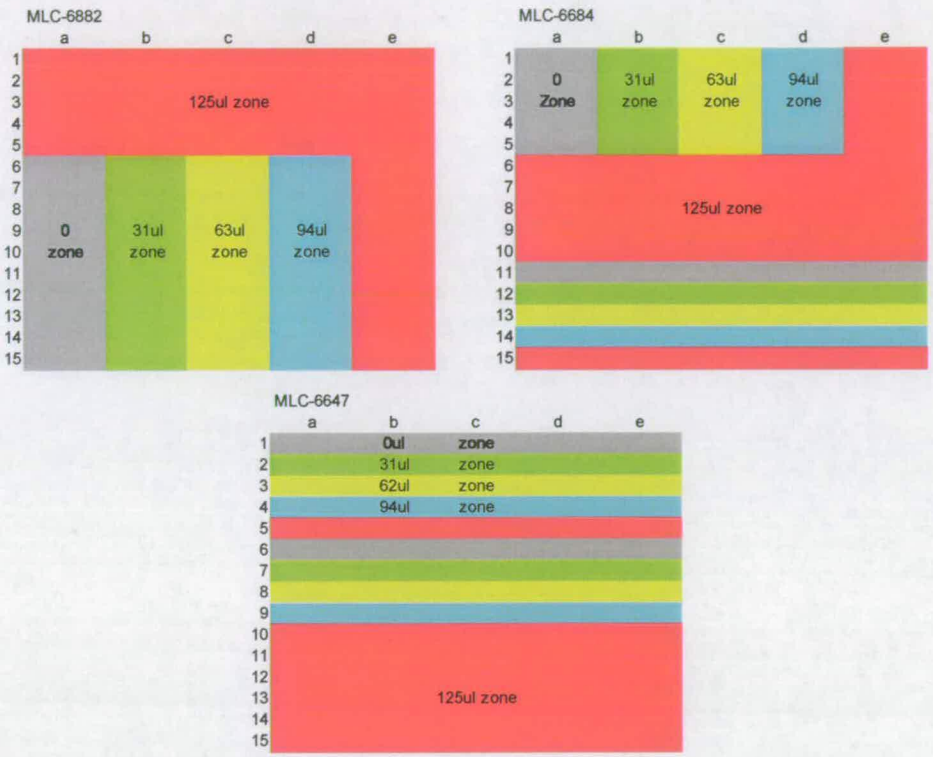

Figure 3.9: Graphical representation of the zones of different dispense volumes which were defined for the 5(a-e) x 15 array of target vials, for each of the 3 library components.

Aspirations were performed in a serial manner, collecting and dispensing each volume zone separately and completing all procedures with one component before washing and purging of the needle. On completion, the formulations were heated in an oven at 60 °C for 5 minutes to remove the carrier solvent. Each of the formulations was manually loaded onto the micro well containment (Figure 3.10), and analysed for clearing point using the HT apparatus between 25-160 °C as described in chapter 2. The resulting data were analysed and processed using the VBA macro (Section 3.2.3), producing plots of intensity vs. temperature from

which the liquid crystal to isotropic liquid transitions were derived. Full experimental results are given in Appendix 1.

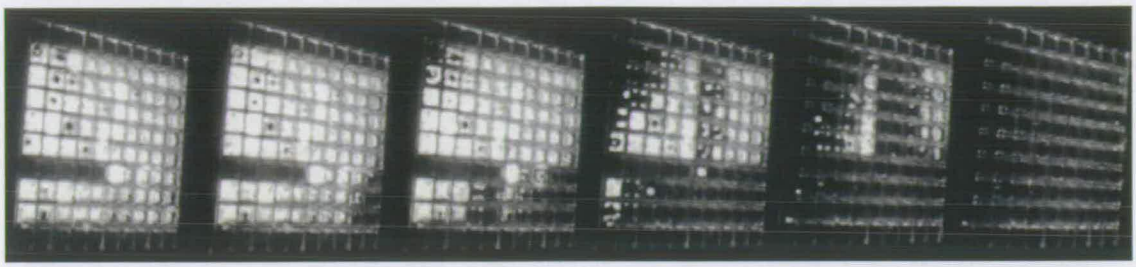

Figure 3.10: Testing the clearing point of 75 mixtures simultaneously shows the 75 compounds being analysed using the HT apparatus in the micro well device. The sequence represents low temperature (25 °C, left) to high (150 °C, right)

3.3.2 Results and Discussion

The relationship between composition and clearing point is visualised in Figure 3.11 using Spotfire DecisionSite (Spotfire, Massachusetts, US). The extremes of composition represent 'pure substances' and by comparing the clearing points gained by the HT screening with those in the literature[33] (Table 3.2) excellent agreement is seen. Comparison of results formulated with identical compositions generally shows good agreement with low standard deviation (Table 3.1), consistent with the 3 °C error between different positions on the heating plate observed using the thermographic imaging technique in chapter 2. To validate the accuracy of the formulation process a number of compositions chosen at random were produced gravimetrically and analysed by DSC. Comparison of these results, and those gained using the HT screening method (Table 3.2), also show excellent agreement proving that the accuracy of dispensing was high, solvent removal was successful and the addition of the micro well containment to the HT screening apparatus had no detrimental effect. The small error observed between the results was expected because of formulation error, but this experiment shows that the errors are small and systematic. It should be noted that in this experiment the systematic error introduced in Chapter 2 does not apply due to the use of the glass mirror in place of the chrome plated heating block. Therefore, the error in the results was expected to be approximately ±3 °C above that gained using the chrome heating plate, approximately equal to the values obtained in the literature due to the effect of heat lag.

Composition			Clearing Point			Mean T_{cp}	Standard
MLC-6882(%)	MLC-6647(%)	MLC-6684(%)	T_{cp} 1 (°C)	T_{cp} 2 (°C)	T_{cp} 3 (°C)	(°C)	Deviation (°C)
40	40	20	110.9	114.0		112.5	1.6
40	20	40	105.6	106.4	105.6	105.9	0.4
44.4	44.4	11.1	116.2	119.6		117.9	1.7
44.4	11.1	44.4	106.1	98.6		102.4	3.8
50	50	0	115.7	126.6		121.2	5.4
50	0	50	96.3	102.3		99.3	3.0
0	50	50	93.6	89.3		91.5	2.2
11.1	44.4	44.4	98.3	97.1		97.7	0.6
20	40	40	104.8	101.2		103.0	1.8
27.3	36.4	36.4	102.6	106.4		104.5	1.9
33.3	33.3	33.3	105.9	107.1	106.1	106.4	0.5
36.4	36.4	27.3	109.6	111.4		110.5	0.9

Table 3.1: Compositions that were duplicated or triplicated in the library, including the deviation of the clearing point obtained using the high-throughput apparatus

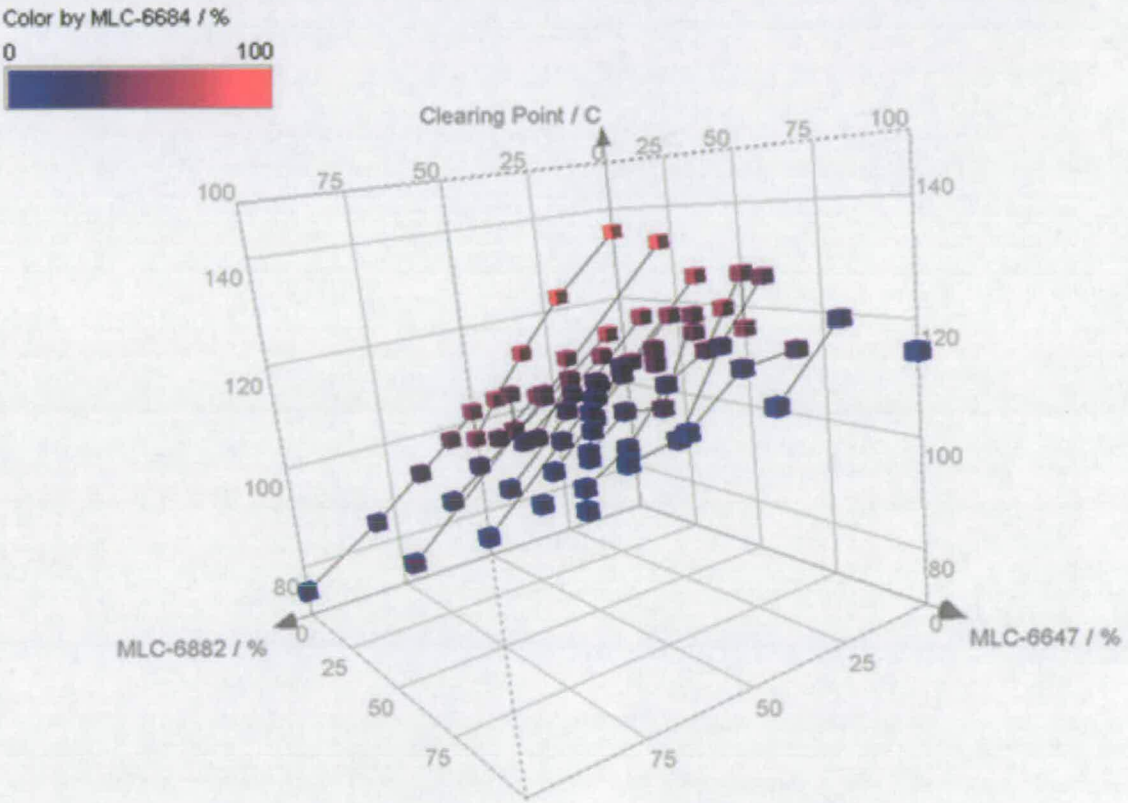

Figure 3.11: Data from the analysis of a ternary MLC library is represented as a 4 dimensional plot relating the % composition of each component to its clearing point (the 4th dimension, % of MLC-6684 is represented using colour).

Sample composition			Clearing Point using robotic formulation and HT screening	Clearing point using gravimetric formulation and DSC screening	
MLC 6647	MLC 6882	MLC 6684	Transition / °C	Onset / °C	Peak / °C
28.8%	14.2%	57.1%	93.9	93.8	99.2
50.0%	37.6%	12.4%	119.4	114.6	112.9
28.8%	57.1%	14.2%	114.7	108.6	118.4
100.0%	0.0%	0.0%	134.9	-	133.5
0.0%	100.0%	0.0%	114.7	-	111.0
0.0%	0.0%	100.0%	74.9	-	74.5

Table 3.2: Comparison between the data gained for ternary mixture of MLC liquid crystals using the HT screening apparatus and DSC

The combination of robotic formulation and HT screening using the micro well device is a powerful tool in identifying the phase transitions of mixture libraries. The entire process of formulating, screening and analysis of 75 mixtures (excluding the solvent evaporation step) takes no more than 3 hours, and produces high quality data.

3.4 Formulation and HT Characterization of a Library Exhibiting Eutectic Melting Behaviours

To evaluate the formulation method and the capability of the HT screening technique (Chapter 2) in the characterization of a large number of samples, a ternary library of three fluoro-substituted 1,1`-biphenyl [2-(4-chlorophenyl)ethyl] liquid crystals (Merck Chemicals Ltd) were created (Figure 3.12).

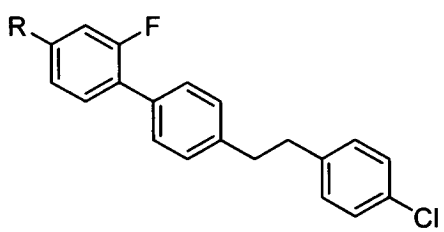

R substituent	Name	Phase transitions
Ethyl	FET-2-Cl	C 70 N (63.5) I
n-Propyl	FET-3-Cl	C 80 N 82.2 I
n-Pentyl	FET-5-Cl	C 53 SmB (19) SmA (42) N 83 I

Figure 3.12. The structures and phase transitions of the FET components

When a mixture (A+B) of miscible substances is cooled the first component (A) will begin to separate in its solid form, leaving behind a mixture of liquids which becomes more deficient in component A as the temperature decreases, until crystallisation of B occurs resulting in the formation of a solid. If the mixture possesses a eutectic point then at a defined composition the liquid phase borders directly on the solid, hence crystallisation of both components is simultaneous (Figure 3.13). The temperature at which this occurs is the eutectic temperature. Identification of the eutectic composition defines the lowest melting point of the mixture, which usually occurs without a detrimental effect on clearing point. Formulation and HT screening for phase transitions of mixtures over defined compositional space will enable the composition of the lowest melting point material to be identified. This result can be compared with that obtained through previous theoretical calculation of the eutectic, predicted to be 39.56 % FET-2-Cl, 20.11 % FET-3-Cl and 40.33 % FET-5-Cl using the le Chatelier-Schroeder-van Laar[13-15] equations.

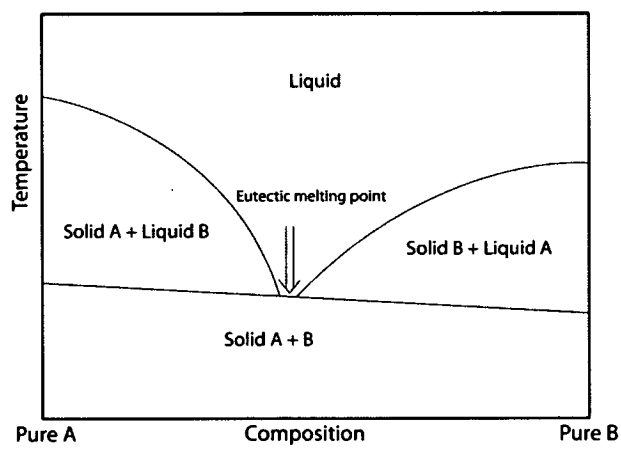

Figure 3.13: A representation of a eutectic phase diagram for a binary mixture, the point at which the liquid phase directly borders on the solid is the eutectic melting point, which can only occur at one eutectic composition.

3.4.1 Formulation of a Library using Robotic liquid Handling

The ternary composition of FET-2-CL, FET-3-Cl and FET-5-Cl was explored creating a library of mixtures in which each of the components was varied between 0 and 100 % in steps of 10 % to create 66 unique mixtures. Due to the very small amount of material that was required for HT characterisation (2-5 μL) there was no need for the production of

material on the gram scale (as required with traditional techniques). The formulation was dispensed into a 96-well plate format more conducive to smaller volumes (maximum of 240 μL per well), which beneficially reduced the time required for the dispensing of components and the volume of each component required to create the library.

Each of the formulations was manually loaded onto the micro-well containment device (Section 3.2.2). Prior to analysis, many mixtures required cooling to promote crystallisation so that the melting point could be analysed. After cooling a number of samples exhibited formation of a glassy super-cooled nematic.[34,35] Samples heated from this glassy state show no melting transition because of the preservation of liquid crystalline order (Figure 3.14). It was necessary therefore to cool the samples to temperatures as low as -40 °C to obtain fully crystalline materials. This was achieved by cooling the substrate in a freezer for upto 1 hour. The crystalline samples were analysed for clearing point transitions using the HT apparatus between 20-160 °C as described in Chapter 2. The resulting data were analysed and processed using the VBA macro (Section 3.2.3), producing plots of intensity vs. temperature from which the liquid crystal to isotropic liquid transitions were derived. Full experimental results are given in Appendix 2

3.4.1.1 Preliminary Results

Figure 3.15 illustrates the clearing point behaviour as a function of concentration. It can be seen that the data shows a similar trend to the MLC system analysed previously, indicating that the robotic dispensing is accurate and reproducible. The second graph shown in Figure 3.16 is of more interest due to the non-linear relationship between melting point and composition. The melting point at the minimum of the surface (the blue / purple area of the graph), can be seen to fall to a value lower than that of its constituent components. The eutectic composition lies in this minimum, in a similar location to that predicted by the SVL theoretical calculations. Identification of the lowest melting point transition, lying at a composition of 20,10,70 (FET-2,3,5) with melting point 32.4 °C, shows that the composition is not identical to that of the FET eutectic and is approximately 4 °C lower than the reference material. Values are shown in Table 3.3.

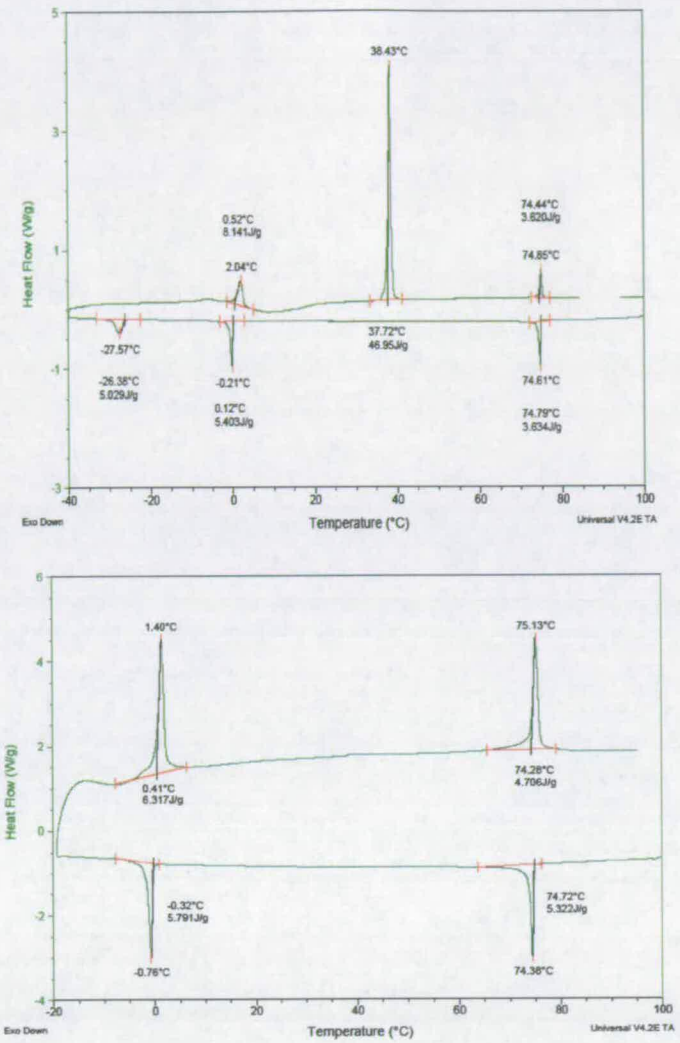

Figure 3.14: DSC traces obtained by heating FET-eutectic from room temperature to 100 °C and then cooling to -40 °C before reheating (top) and the same material heated to 100 °C but then cooled to –20 °C (bottom). In the second case crystallisation of the sample does not occur, and hence no melting transition is seen on the reheating cycle.

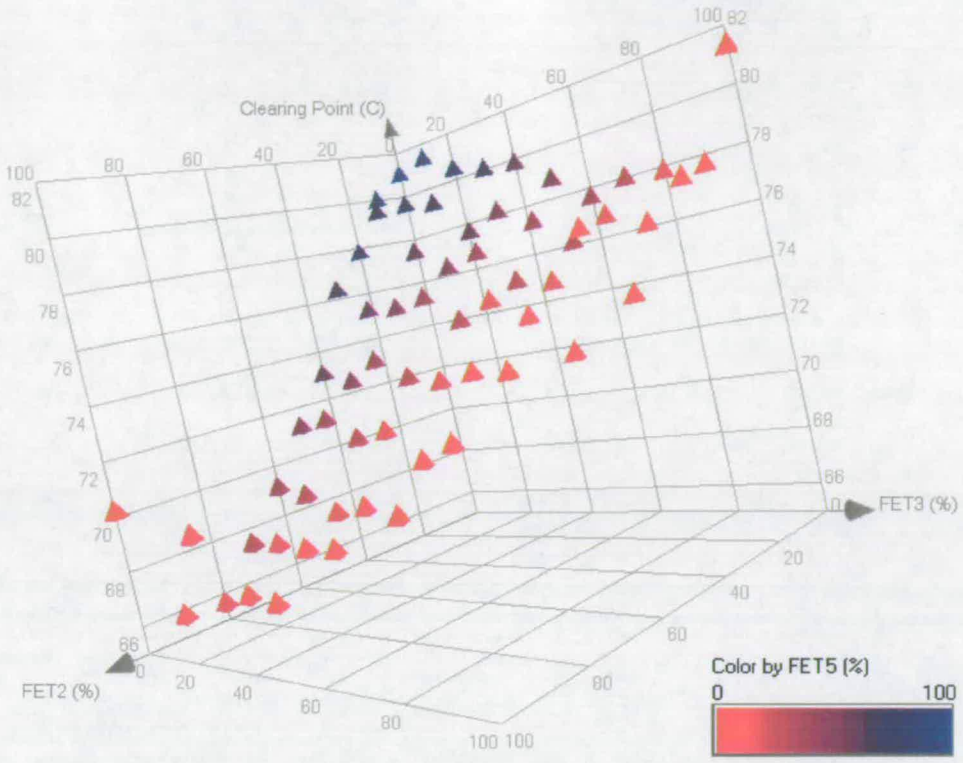

Figure 3.15: The clearing point surface of a ternary library of FET-2,3,5-Cl formulated using robotic liquid handling and characterised by the HT method. The composition of FET-5-Cl is represented using colour.

3.4.1.2 Optimisation

This experiment reveals the problems in applying a large step between subsequent formulations. The lowest melting transition cannot be easily identified due to the large voids between the data points. To reveal the detail of the curve around this area effectively requires a more in-depth analysis. In an attempt to identify this area in further detail, a focused library was produced consisting only of formulations with melting points lower than 45°C. The area defined by this melting point was from 0 to 40 % FET-2-Cl, 0 to 40 % FET-3-Cl and between 30 to 100 % FET-5-Cl. A library was reformulated, using a 5 % step size between these points, using an identical procedure. Again, it was found that some samples would remain in the liquid crystal phase even after cooling to -40 °C. To promote crystallisation in these samples a small piece of cardice was applied directly to the glass under the sample for a few seconds. This caused the sample to 'explode' into the crystalline state as excess energy was released.[260] The melting point data from the focused library are shown in Figure 3.17 and full experimental results can be found in Appendix 3.

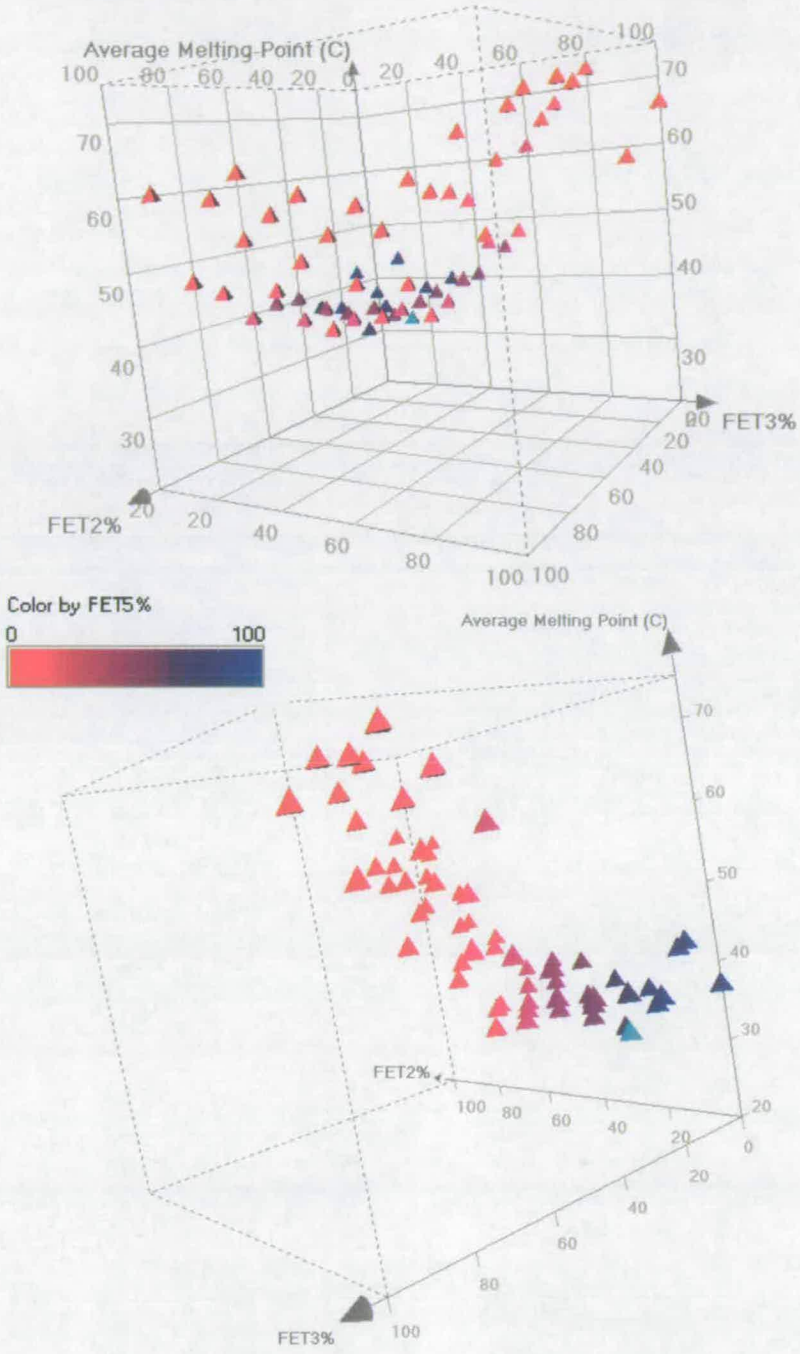

Figure 3.16: The melting transitions of a ternary FET-2,3,5-Cl formulation library, formulated using robotic liquid handling and characterised by the HT method. The composition of FET-5-Cl is represented by colour. Two data points are highlighted; the position of the 'theoretically' formulated FET Eutectic and the location of a lower melting material in a different region of the surface.

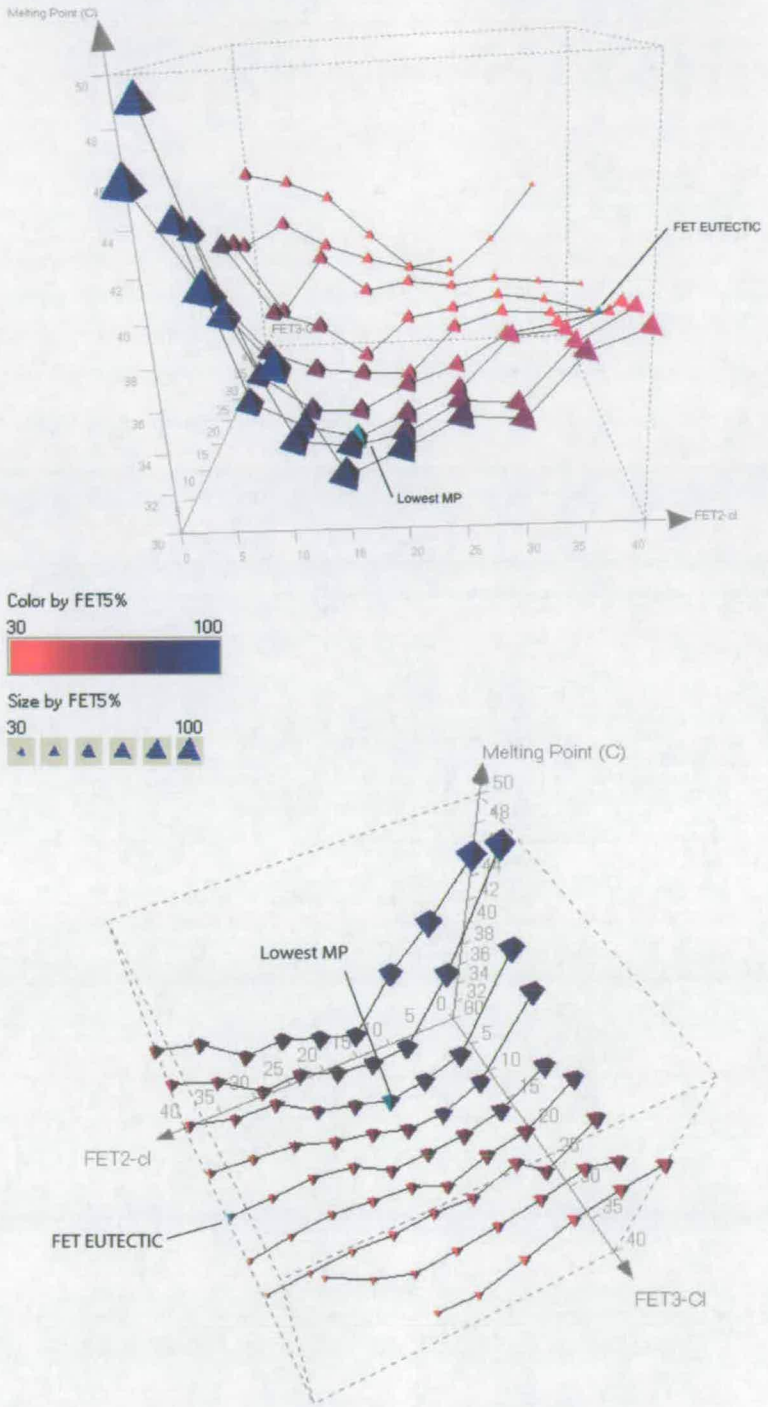

Figure 3.17: The melting point surface of a ternary FET library, formulated using robotic liquid handling and characterised by the HT method, re-formulated between focused values to reveal the lowest melting point composition.

Method	FET 2,3,5	T_{Cr-N} / °C	T_{N-I} / °C
SVL formulated Material			
Merck FET eutectic (lit)	39.56,20.11,40.33	35.0	72.0
DSC of grav sample	*39.56:20.11:40.33*	*37.4*	*74.4*
HT of grav sample	39.56:20.11:40.33	36.0	72.5
Robotic formulated material analysed using HT apparatus			
FET Eutectic composition 10%	40,20,40	36.7	73.1
Global Minimum 10% step	20,10,70	32.4	79.2
FET Eutectic composition 5%	40,20,40	35.8	-
Global Minimum 5% step	15,10,75	31.6	-
DSC of robotic min (grav.)	*15,10,75*	*33.0 (dual)*	*77.9*

Table 3.3: Comparison of the melting and clearing points of ternary formulations created using the robotic liquid handling and characterised by the HT method and values of the FET eutectic composition analysed by DSC and the HT characterisation method for phase transitions.

Using smaller steps between library members enables more intricate melting point behaviours to be identified successfully. As previously identified, FET eutectic does not lie at the global minimum of the system. Figure 3.17 and Table 3.3 revealed the FET eutectic composition at 40 % FET-2, 20 % FET-3, 40 % FET-5 to lie in a depression on the clearing point transition surface with a clearing point of 35.8 °C. The global minimum is seen in a region with higher concentration of FET-5-Cl, where the lowest melting point lays at a composition of 15 % FET-2, 10 % FET-3 and 75 % FET-5 with a melting point of 31.6 °C. Comparing the result of the 10 % and 5 % step libraries it can be seen that the clearing point obtained in both experiments is very similar, and that the minimum melting point has been reduced due to the identification of a lower melting point mixture between two large-step compositions. To validate the discovery, DSC analysis of gravimetrically formulated samples was run (Table 3.3). The DSC shows that the melting point was indeed lower than that of FET eutectic; however, the melting peak shows two distinct shoulders indicative that this is not the true eutectic composition.

3.5 Limitations for Larger Libraries

To efficiently explore phase space the compositional variation between mixtures should be minimised resulting in an exponential increase to the size of the library. A ternary library with a step size of 20 % and boundaries between 0 – 100 % results in 21 unique formulations, decreasing the step size to 10 % results in 75 unique formulations, and 5 % results in 231 unique formulations. The results achieved using the combination of robotic formulation, HT screening and sample containment, showed the potential of this screening technique in larger and more complex libraries as well as highlighting some limitations. Using the Gilson liquid handler it was possible to fill a maximum of two 96-well plates in one program cycle and therefore larger libraries require a batch formulation approach, introducing errors and more than doubling formulation time. The use of a 384 well plate format which could be spatially addressed by the Gilson was proposed as a solution to this problem; however the syringe pumps were not able to accurately transfer solutions due to their minimum reproducible dispensing volume of ~1 μL. An additional limitation for larger libraries was that analysis using the current HT screening micro well arrangement had capacity for only 100 samples. In practice, this therefore limits the library to a step size of 8 % (91 samples), sufficient for identification of the overall shape and form of the transition surface, but not to accurately determine more intricate features.

3.5.1 Alternative Technologies

Miniaturisation of the apparatus, in combination with more advanced automation offers a solution to the problems encountered with larger libraries; enabling smaller quantities of material to be handled accurately in higher density well plates.[36] The miniaturisation of technologies for HT applications is not new.[37,38] In the late 1990`s, following the establishment of combinatorial chemistry is was realised that if the format of the well plates was increased from 96 to 384 (or 1536) wells, and advanced miniaturised automation was used then the rate of screening could be increased to great commercial benefit.[36,39-42] Equipment designed for this purpose soon appeared, the capacity for 384 well plate dispensing achieved through increased accuracy and lower volume handling abilities.[41] As miniaturisation continued the demands for handling smaller volumes of liquids begin to exceed classical methods of sample delivery. The majority of early liquid handlers, including the Gilson model used in the previous experiments, utilise a system of positive displacement

in which a syringe pump is used to aspirate and dispense a system fluid, separated from the sample by air.[43] The accuracy of this method depends on the precision and size of the syringe pump and the tubing between the syringe and the needle, but generally cannot be used accurately below 1 μL.[41] To dispense volumes in the 10 to 100 ηl range required a more sensitive and controllable technique.

3.6 Inkjet Printing as a Formulation Tool

The dispensing methods which have been previously described are categorised as contact techniques, in which a substance is transferred by the contact of a dispensing needle or pin with the substrate or liquid interface. In non-contact techniques, the dispensing nozzle has no contact with the solid or liquid surface on which the drop is dispensed. Examples include peristaltic dispensing,[43] thermal inkjet printing,[44] piezo inkjet printing[45,46] and syringe solenoid dispensing[47,48] Taylor et al,[43] in the course of their work assessing liquid handler performance for application in high-throughput screening, achieved liquid dispensing in the 10 to 100 ηl range most successfully with piezo inkjet mechanisms, hence these techniques were investigated further.

Piezoelectric dispensing has been used for many years as the mechanism by which inkjet printers for home and office printing deposit ink onto the page. A piezoelectric head consists of a capillary surrounded by a piezo actuator that forms a nozzle at one end. Ink fed into the capillary is held either through negative pressure or by surface tension. Application of a voltage pulse waveform results in the contraction of the piezo actuator, creating a pressure wave that propagates through the ink. The result is that at the nozzle a small liquid column is ejected, breaking off and flying through the air with a high velocity until hitting the substrate.

Inkjet printing has been adopted for the printing of functional materials in many areas of materials research including ceramics[49-55] and polymers.[56-61] These applications have shown that ink-jet printing (IJP) can be used to formulate libraries of two or more components, which followed by HT screening can efficiently reveal optimised compositions. To create formulation libraries using IJP a method for the mixing of individual components was required. Literature illustrates three methods; The first, mixing of inks behind the inking nozzle,[52,53] was achieved using specialised apparatus consisting of pressurised reservoirs and electromagnetic valves which dispense defined volumes into a micro pump mixing chamber

prior to the dispensing nozzle. The second method, mixing of inks before inking, uses the nozzle as a micropipette to aspirate and reformat samples on high density well plates therefore creating new mixtures which are then inkjet printed onto the substrate.[47,62-65] The third method, mixing of inks on the substrate involved dispensing each separate component, in varying volume, over the top of the previously dispensed component.[59,66-71]

For our application, the method of mixing on the substrate offered the greatest benefits. Arrays could be quickly produced from small quantities of liquid crystal compounds, allowing printing directly onto the analysis substrate without the need for reformatting or mixing. The volumes of the drops are small enough to prevent the movement of samples on the surface and the large surface to volume ratio of the printed spots (90 μL) allowed for efficient evaporation of solvent. In addition, sample spotting densities of greater than 30 spots per cm^2 could be achieved, a dramatic increase over the previous manually produced arrays

3.6.1 Equipment for Inkjet Printing

Mixing on substrate has previously been reported using SOHO ink-jet printers in which the commercial printing inks have been replaced with suitable solutions or suspensions that require printing. Such equipment is inexpensive, readily available and easy to use but also has a number of major limitations.[60] As the print heads are designed to be used for inks with specific viscosities, formulated in specific solvents, they do not allow any control over the droplet-forming process and often contain plastics not compatible with the organic solvents required for dissolving liquid crystals. The majority of applications utilise a PC design package such as MS Office or MS Powerpoint to create colour patterns which determine the amount of ink that is deposited at specific locations on the substrate. Detrimentally, the complexity of PC printer drivers and the use of print optimisations such as half toning and dithering[54,66,72] to produce thousands of colours from 3 or 4 inks, result in the deposition of drops of ink not only on top of each other but in close proximity. This results in non-proportionality between the intensity of a particular element in the CMYK colour space and the volume of ink printed.[59] This can be corrected for by calibration of the amount of ink dispensed with respect to the value of the colour space by a variety of procedures[53,66,68] but this overcomplicates the method. In general, despite the limitations of SOHO printer apparatus, good results mainly attributed to the post- printing treatment of the formulation

arrays were obtained in the literature. In the case of ceramics, libraries were annealed and sintered at high temperature hence allowing for good diffusion to take place. In other applications the material were removed from the substrate once mixed.[59]

Due to the drawbacks of SOHO inkjet printers and the need to have full control over droplet formation, a commercial material printer was used. The Autodrop system (Microdrop GmbH, Norderstedt, Germany) illustrated in Figure 3.18, comprised a single AK-501 micropipette (Figure 3.19) operating in drop on demand mode *via* a piezoelectric mechanism, producing droplets at frequencies between 0 and 2 KHz monitored using a stroboscopic camera. Drop formation and aspiration duties were carried out by a MD-K-130 control unit. The system also includes a XYZ stage with integrated 96 / 384 well plate holder, substrate holder and wash / waste stations. Automation was controlled *via* a PC running Autodrop software which allowed control over the voltage, pulse width and frequency of the signal sent to the piezo nozzle, allowing liquids ranging in viscosity from zero to 20 mPas to be printed. Materials were aspirated into the printing nozzle, by applying a negative back-pressure, from 96 or 384 well plates. Application of an electronic pulse to the piezo transducer, results in the formation and expulsion of a drop from the end of the nozzle onto the substrate. Using the microdrop software the electronic pulse waveform is customisable enable the printing of a wide range of liquids; parameters which can be modified are the frequency (Hz), voltage (V) (expressed as the amplitude of the pulse) and the pulse width (ms). After printing, material was returned to the well by positive pressure flushing before aspiration of a cleaning solvent and sonication (produced by the operation of the drop generation at the nozzles eigen frequency), before flushing clean and drying the nozzle with air.

Formulation libraries were produced by the creation of a matrix of spots, each with a different composition of each of three components. To form these mixtures the number of drops deposited from the print head at each position on the XY matrix was controlled, over-printing previously deposited spots to create unique formulations. Feasibility studies have been carried out which appear to show that the kinetic energy of the droplets allows for perfect mixing.[60] To create libraries in this way the accuracy and reproducibility of the system should be high. A review by Jan de Gans et al[60] analyses a number of IJP apparatus for their suitability in such a application, concluding that the Autodrop platform conforms to expectations, with a drop volume error of 2 % and positional accuracy of 10±3 μm. The individual droplet size of 90 pl is determined mainly by the nozzle diameter (50 μm)

Figure 3.18: The Autodrop platform comprising an enclosed XYZ stage and a single AK-501 nozzle. The stage comprises of a printing area, a 96 or 384 well plate holder and wash / waste stations. Drop formation is monitored using a stroboscopic camera mounted in the right hand corner.

Figure 3.19: A microdrop AK-501 micropipette removed from the platform

3.6.2 Software Development

The Microdrop control application provides full control over all aspects of the apparatus and printing process, through either a single step manual interface or an automated macro

interface for the execution of a batch list of commands which must be created manually by typing in a list of single steps. In the formation of a ternary library consisting 231 different formulations, this requires the number of drops for dispensation at each XY position on the substrate, for each of the three LCs to be programmed equating to over 750 individual steps. Creation of this sequence by hand would be extremely time-consuming and tedious and was seen as one of the limitations of using the equipment for this application. To overcome this limitation, an application was designed and programmed in Microsoft Visual Basic 6 to be used in conjunction with the Microdrop control software. The application provides a simple interface (Figure 3.20) allowing all experimental conditions to be entered by the user. The aspiration position of each ink can be selected, as well as the flushing position, cleaning station and the associated times for filling, emptying and cleaning. The starting coordinates or spatial position of the substrate could also be selected and the spacing in the printing matrix defined. The number of drops to be printed at 0 % and 100 % could also be specified along with the step size, which defines the size of the library. Lastly, the printing parameters for each of the three inks could be entered. The application processes this data creating a series of linked text files, containing the command sequence to create the complete ternary library. A second text file was also produced relating the spatial print position of the substrate to its ternary composition for easier identification after analysis. This application reduced the time to design of a macro sequence from days to seconds, and also enabled a user with little knowledge of the Autodrop system to load samples and substrates, run the application and within minutes create large libraries. The complete application including VB source code is included on the supplementary material CD-ROM.

3.6.3 Formulation of a FET Library by Inkjet Printing

To highlight advantages and disadvantages of both the robotic and inkjet formulation methods, in combination with the HT screening, a library was prepared by both routes. This enabled a direct comparison to be drawn between the two techniques, both in terms of practicality and accuracy of results. Using the technique of IJ formulation and HT phase transition analysis, a ternary library of FET compounds was produced for compositions between 0 and 100 % of each component in 5 % steps. Before the formulation could take place a number of parameters were optimized. These consisted of the solvent to be used for

formulation, the concentration of the liquid crystal solutions printed, the driving voltage and pulse width for the solvent used, and finally the matrix parameters.

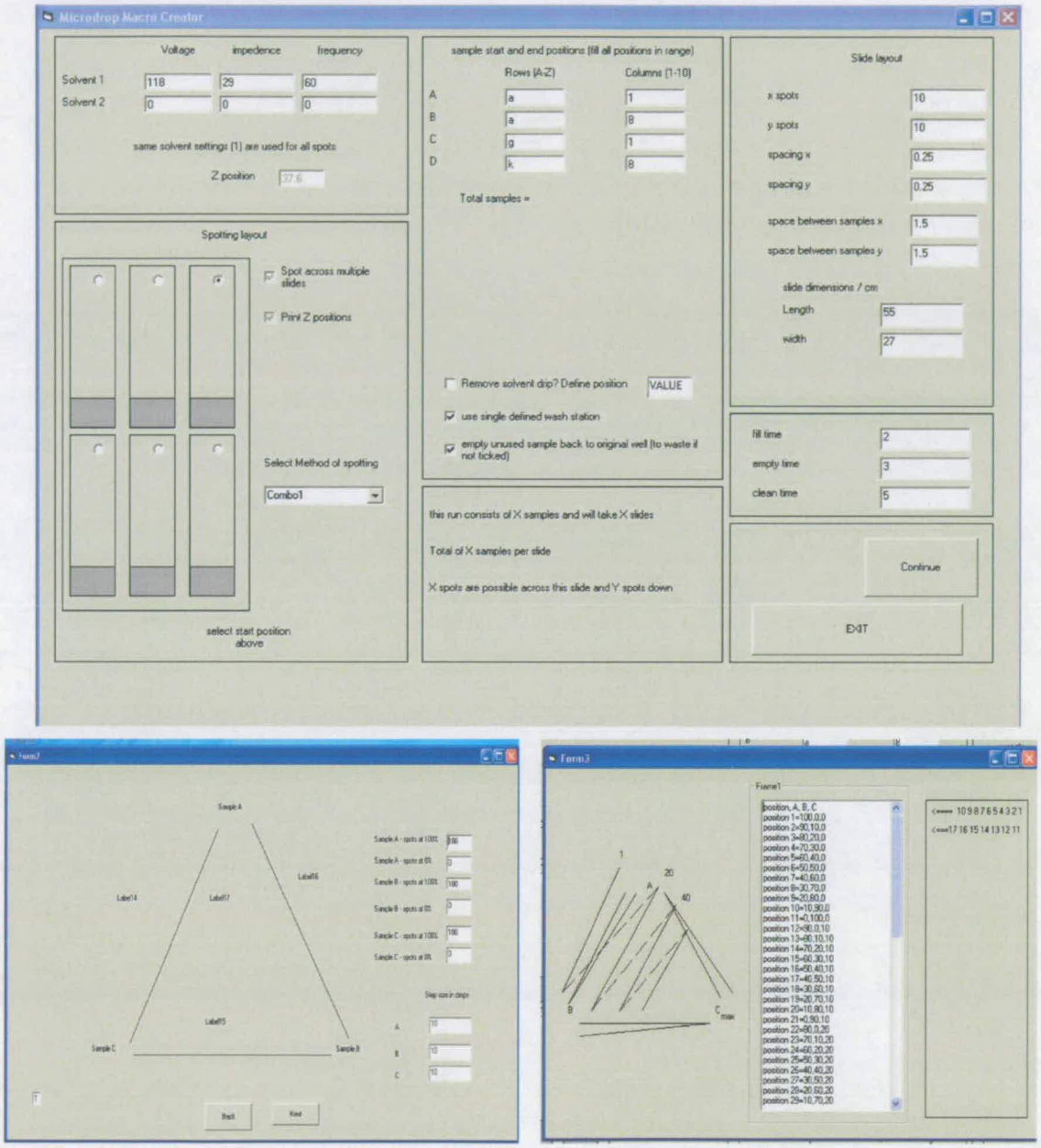

Figure 3.20: Screen shots of the VB program used for the design and execution of ternary inkjet printed libraries. The different sections allow control over the print and matrix parameters (left) the composition of the three components of the library (top right) and represent the positions and compositions of the samples deposited, both visually and in an external text file.

3.6.3.1 Solvent and Solution Concentration

In IJP the solvent performs a number of important roles and therefore must be selected carefully. As with robotic formulation, solvent was required to dissolve the liquid crystal solid/liquid, modifying the solution's viscosity so that it was amenable to the printing process. Also important was to select solvents which possessed a high enough volatility so that removal without evaporation of the liquid crystal components could be achieved, while taking into consideration that for successful mixing to occur in the IJ overprinting process once on the substrate the solvent did not fully wet the substrate, remaining as a well defined droplet, with a slow rate of evaporation. This was desirable as preliminary tests showed a liquid crystal solution printed on top of a crystalline substance did not result in adequate mixing, whereas two solutions were able to mix efficiently. Preliminary tests also revealed that the solubility limit (in a variety of solvents) of the FET materials under study was approximately 35 w/w % @ 20 °C. IJ printing of solutions at this concentration was unsuccessful which initially was thought to be due to a high viscosity. Subsequent measurements determined the viscosity of a 1:1:1 (FET-2-Cl:FET-3-Cl:FET-5-Cl) mixture in toluene to be 3.7 mPas @ 23.6 °C. As this was well within the operational limits of the Autodrop apparatus it was concluded that crystallisation was the cause of failure. A solution with a large amount of dissolved solid quickly crystallises in the end of the nozzle preventing drop formation. Reducing the concentration of solids allows for efficient printing, however much smaller quantities of substance remain on the substrate following evaporation thus hindering subsequent analysis. A solution of 17 w/w % solids was found to give reproducible, reliable printing and spots large enough for analysis.

Taking these factors into consideration a number of solvents were assessed. The first parameter to be measured was the speed at which a droplet evaporated from a glass slide at room temperature. Solvents taking longer than 180 s to evaporate were taken to the next stage in which a 5:1 w/w % solution of the solvent and a FET formulation of known clearing point were made. Solutions that showed full solubility were then printed in a 5x1 spot matrix onto a glass substrate, depositing between 1 and 100 drops per spot in 20 drop steps. To ensure successful printing of the different solvents ink jetting parameters were optimised. This was achieved by manipulation of the voltage, and pulse width of the piezo transducer so that drops formed from the nozzle tip were free of tail or satellite droplets[73] The drop formation could be monitored and assessed using a stroboscopic camera. For all solvents assessed it was found that values of 100-110 V and 30 ms pulse width at a frequency of 60

Hz gave good drop formation. Following these sequential trials the five FET solutions which printed most successfully and reproducibly were analysed using the HT screening apparatus and assessed for accuracy of the melting and clearing points.

Table 3.4 shows that of the solvents printed only two met all criteria; acetophenone and 70:30 toluene/cyclohexanone. Acetophenone was chosen over the dual solvent mixture due to its lower volatility, showing a weight loss of just 0.5 % over 20 minutes in a 96-well plate compared with 6 % loss for 70:30 toluene/cyclohexanone, and faster formation of the desirable crystal phase following solvent removal which was achieved by heating at 80 °C for 5 minutes.

Solvent	**Evaporation**	**Print quality of eutectic mixture solution on glass**	**T_{Cr-N}, T_{N-I} [°C]**
Ethyl acetate	v. fast	-	-
N-Methylpyrollidine	slow	poor reproducibility	36.0, 72.8
Dimethylformamide	slow	poor quality spots	36.0, 72.3
Propylene glycol monomethyl ether acetate(PGMEA)	slow	poor reproducibility	-
Toluene	slow	mobile on substrate	36.0, 72.3
Toluene / cyclohexanone(70:30)	slow	Excellent	Not obs. , 72.6
Ethyl Acetate / methyl benzoate	fast	-	-
Xylene	slow	Failed	-
Methyl ethyl ketone	fast	-	-
Acetophenone	slow	Excellent	36.0, 72.6
Methyl benzoate	slow	Insoluble	-
Butyl acetate	slow	Failed	-
Dioxane	slow	Failed	-
PGMEA / Ethyl acetate	fast	-	-

Table 3.4: Selection of solvents for IJP. Solvents were first tested for evaporation rate. Solvents that took longer than 180 s to evaporate were taken forward and a 5:1 w/w % solution of the FET-eutectic mixture produced. Samples that solubilised the LC were then printed in a 5x1 matrix incrementing in 20 drop steps from one to 100 drops. The matrices were assessed for quality before solvent evaporation at 80 °C, cooling and HT analysis for melting point and clearing point. The DSC derived transitions were T_m 37.4 °C and T_{N-I} 74.4 °C.

3.6.3.2 Matrix Parameters

To fit a 231 member library on a 30x30 mm substrate required a spacing of 1.9 mm between spots. To ensure that adjacent spots did not coalesce under heating the total volume of each drop required control. Tests showed that at room temperature spots begin to spread into each other when using approx 340 drops (0.03 μL) per spot with a 1.9 mm separation. 100 drops per spot were therefore used to ensure drops did not merge even if they did move slightly on heating, while still allowing sufficient material for high quality analysis.

3.6.3.3 Library Formulation

The FET library was constructed using the aforementioned solvents and parameters. A voltage of 104 V, a pulse width of 29 ms and a drop frequency of 60 Hz were used to print a total of 23100 drops of the three inks onto 231 positions. Screening of the library was carried out after solvent removal (80 °C oven, 5 min) using the HT phase transition equipment to run a heat-cool-heat temperature ramp from -50 °C to 100 °C. The optical transitions of each sample spot were then analysed to provide the temperature of the phase transitions (Figure 3.21). Full experimental results can be found in Appendix 4.

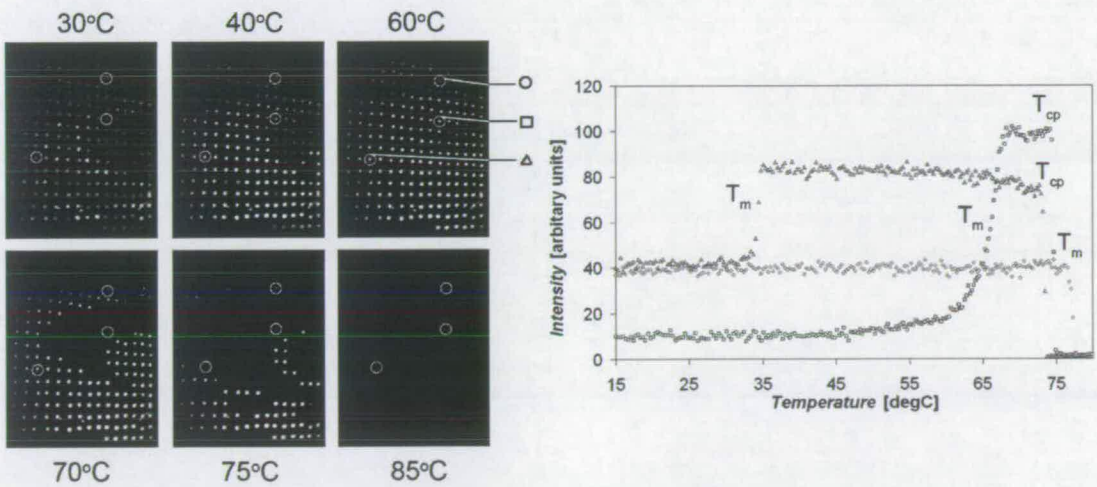

Figure 3.21: A sequence of images showing the data from IJP library screening illustrating the change in intensity of each spot on heating. Solids appear as less intense spots, LCs as bright white spots and isotropic liquids cannot be identified against the background. The graph shows the acquired data for three representative spots on the sequence, highlighted on the image to illustrate melting and clearing transitions.

3.6.3.4 Results

A number of anomalies over the Cr to I transition were observed in the data obtained using the HT method (Figure 3.22). The reason that these anomalies were not observed previously in the robotic formulated experiment is due to the smaller spot size and small adjustments to the apparatus, which have improved sensitivity and allowed results to be obtained with greater accuracy.

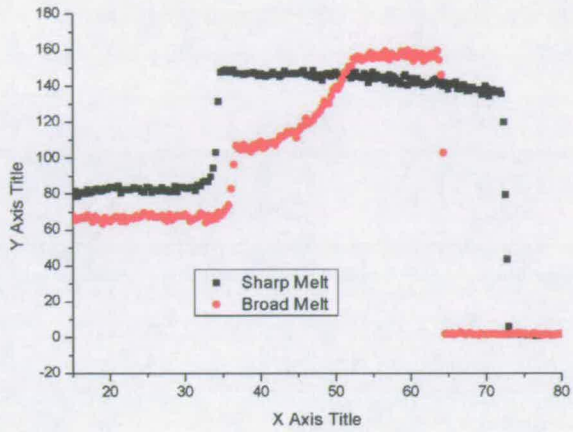

Figure 3.22: Phase transitions measured using the HT screening apparatus showing a sharp and broad Cr-N melt

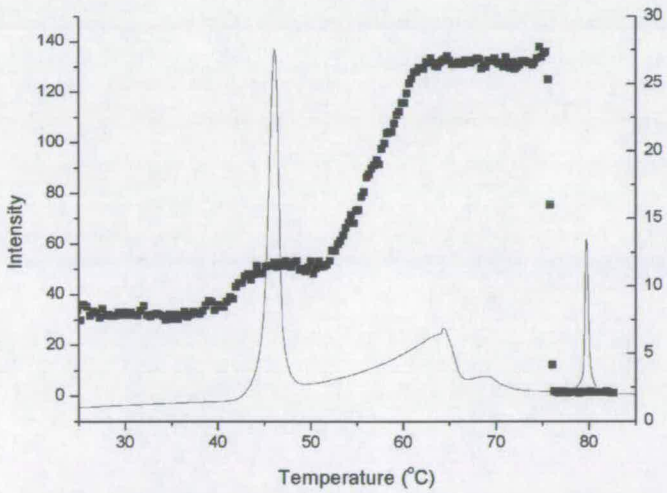

Figure 3.23: Comparison of the optical HT and DSC methods of detecting phase transitions, showing the presence of dual melting behaviour.

Initially, due to the similarity of transition intensity to that of smectic phases observed previously, it was presumed that the dual transition behaviour was attributed to the formation of such phases between the melt and the nematic phase. To confirm this assumption DSC and optical microscopy were used to analyse one such mixture. The mixture (a 70:30 mix of FET-3-Cl and FET-5-Cl) was produced gravimetrically and analysed both by DSC and using the HT apparatus. The HT result and DSC trace are reproduced in Figure 3.23.

The DSC data reveals a sharp initial transition, with enthalpy indicative of melting. The second, extremely broad transition which spans 10-15 °C and ends at approximately 75 °C has enthalpy (approximately 30 J/g) larger that that of the first melt. These observations are not indicative of a smectic transition, which is normally much sharper and of lower enthalpy (0.5 to 3 J/g). Analysis by optical polarised microscopy (Figure 3.24) shows that at the first transition the crystalline solid does indeed melt. However a liquid / solid mixture is formed in which mobile solid particles could be observed in the liquid phase. This morphology persisted until the point at which the second peak was observed, at which point a slight birefringent texture could be seen forming on the glass surface, against the solid/liquid phase. At the transition temperature, the particles were seen to melt and nematic Schlieren textures were immediately observed. The nematic phase was then seen to be replaced by the isotropic phase at the final transition. On cooling, the nematic phase remained stable until the point on the DSC trace where the broad transition occurred. At this point a number of crystallisation textures were seen, resulting in the formation of a crystalline solid. Figure 3.24 illustrates the textures observed over a range of temperatures by polarising microscopy. This phase behaviour shows clearly that a smectic phase was not formed. Instead, the material has a very broad melting range. This is consistent with a mixture formulation which does not possess a eutectic composition, and has previously been reported in the literature.[16,74] By consideration of the phase diagram (Figure 3.25) away from the eutectic point, the transition from a crystalline solid through an equilibrium phase of solid and liquid can explain the two transitions observed in the DSC and HT methods. The observation of some nematic like birefringence in the textures before the nematic phase suggests that equilibrium between liquid, nematic liquid and solid is formed. On cooling, only a single broad crystallisation is seen at a super-cooled temperature. This can be attributed to the seeding of the remaining liquid component, promoting a crystalline state.

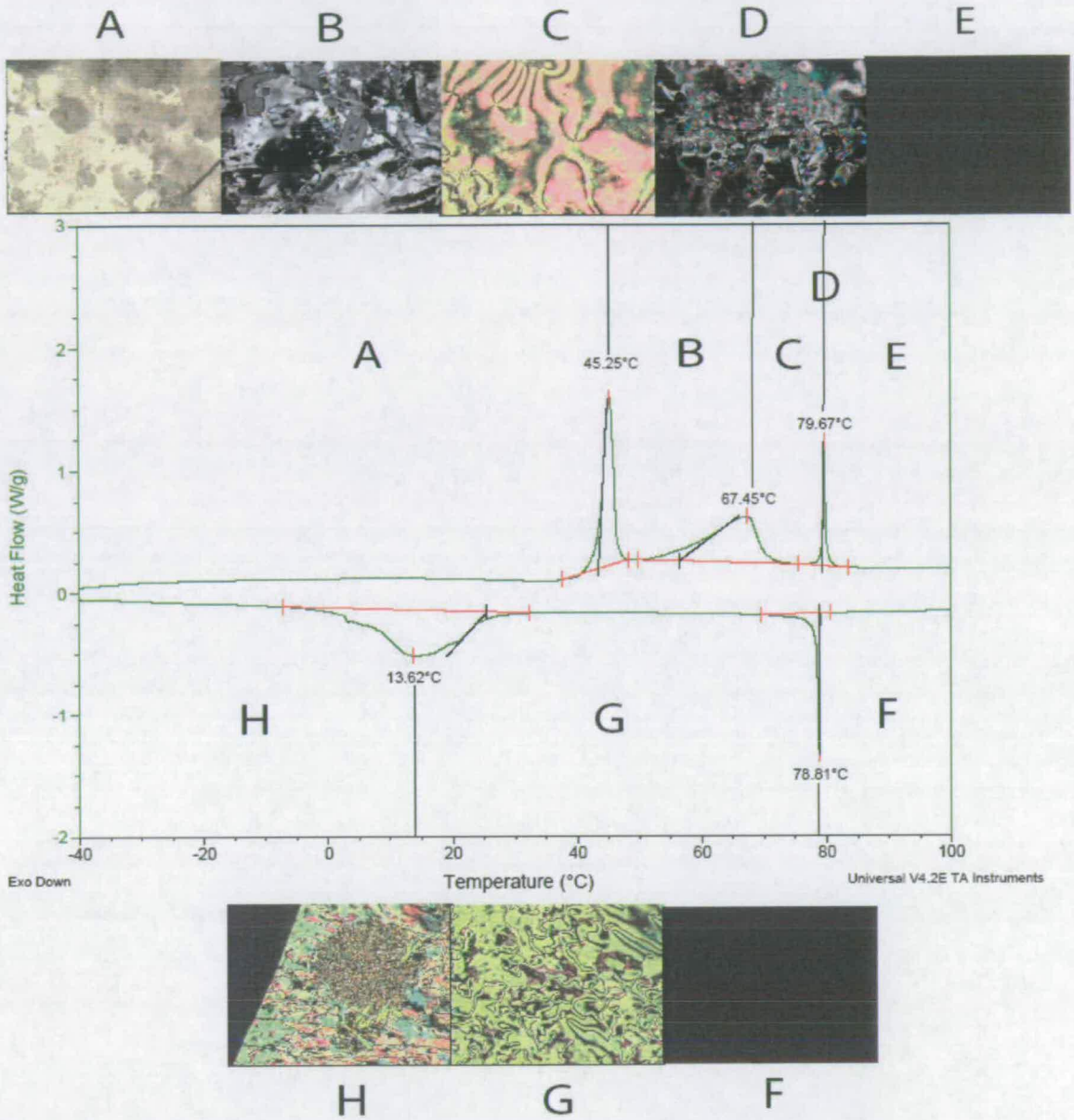

Figure 3.24: DSC of a non-eutectic formulation illustrating images obtained by polarised microscopy over the heating and cooling sequence. The nematic phase was seen to form only in region C, and the dual phase solid / nematic mixture seen in region B. On cooling, the nematic crystallises in region H. Only one transition is seen due to crystallisation of the two components simultaneously.

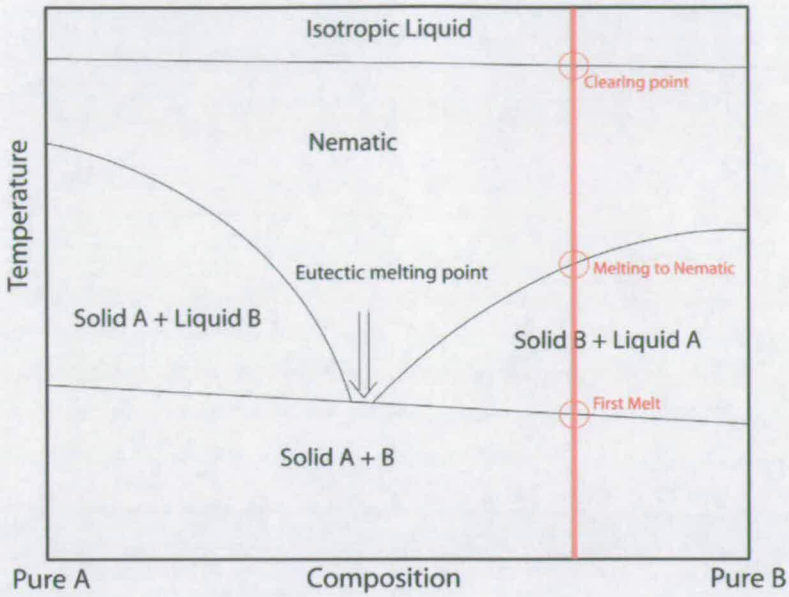

Figure 3.25: The phase diagram showing the three observed transitions between the crystalline melt and the isotropic liquid in a non-eutectic composition,

As a consequence of the presence of these dual melting points, analysing the data accurately required a modification to the way that the transition was recorded. The first, generally sharp melting point was recorded using the mid-point of the discontinuity created by the change in intensity. For materials with only one melting point this represents the crystalline to nematic (Cr-N) transition temperature, for those with dual melting behaviour this is the onset of the melting point. The broad second transition, corresponding to the Cr-N transition was recorded by identification of the penultimate data point before returning to linearity. Using the aforementioned techniques both the nematic to isotropic, crystal to nematic and crystal – crystal transitions were plotted in Figure 3.26, the green data point representing the location of the theoretical 40:20:40 FET eutectic formulations.

3.6.4 Analysis of Eutectic Regions

Using the techniques of both robotic and inkjet formulation, it can be seen (Figure 3.26) that the ternary FET mixture exhibits two minima in its melting point behaviour. The first minimum lies approximately around the SVL predicted composition; the second exists in the region of 70 % FET-5-Cl. Figure 3.27 is simplified, enabling a clearer visualisation of the lowest melting point regions, to show materials with sharp melting transitions occurring over a range of less than 2.5 °C as filled data points. This range was chosen as it represents the

temperature over which FET-eutectic melts by DSC. This treatment was required as many of the onset transition temperatures of dual melting point materials occur at low temperatures and so this prevents misinterpretation as a eutectic composition. In Figure 3.27 three points are highlighted; the FET eutectic composition, the lowest melting point of the local minimum in which FET eutectic lies, and finally the melting point in the global minimum.

The data revealed that the FET eutectic composition lies on the edge of a minimum and therefore was not the optimal, lowest melting formulation in this region. The lowest melting point FET material was found to have a 45:25:30 % composition. The DSC trace for both the FET-eutectic and the lower melting point material are shown for comparison in Figure 3.28. Due to the sharp transitions it can be concluded that this material is a true eutectic composition with lower melting point to that of FET eutectic.

A gravimetrically produced FET-eutectic 39.56:20.11:40.33 % composition produced transitions $T_{Cr\text{-}N}$ 37.4 °C and $T_{N\text{-}I}$ 74.4 °C as measured by DSC, and $T_{Cr\text{-}N}$ 36.0 °C as measured by the HT method. The IJP technique both produced a 40:20:40 % formulation with transitions $T_{Cr\text{-}N}$ 34.0 °C and $T_{N\text{-}I}$ 71.1°C by the HT method. A summary of the minimum melting behaviour is shown in Table 3.5. The observed difference between DSC and HT techniques of ≈3 °C is attributed to systematic error in the HT analysis, as discussed in Chapter 2. There also exist contributions to the error from the IJP formulation method, although these are small in comparison. It should also be taken into consideration that the IJP compositions are all rounded to whole numbers due to dispensing limitations, and hence marginally different from the gravimetric FET-eutectic sample.

Figure 3.27 highlights that the eutectic 'bowl' that lies around the local minimum covers a wide compositional range, while in contrast the global minimum around 70 % FET-5-Cl shows relatively few data points with sharp melting transitions which are more compositionally specific. The minimum melting point in this region lies at approximately 15:15:70 % composition. However, due to the errors associated with the method DSC was used to analyse gravimetrically produced samples of the two lowest melting transitions and the interim compositions between them (Figure 3.29) to confirm this result.

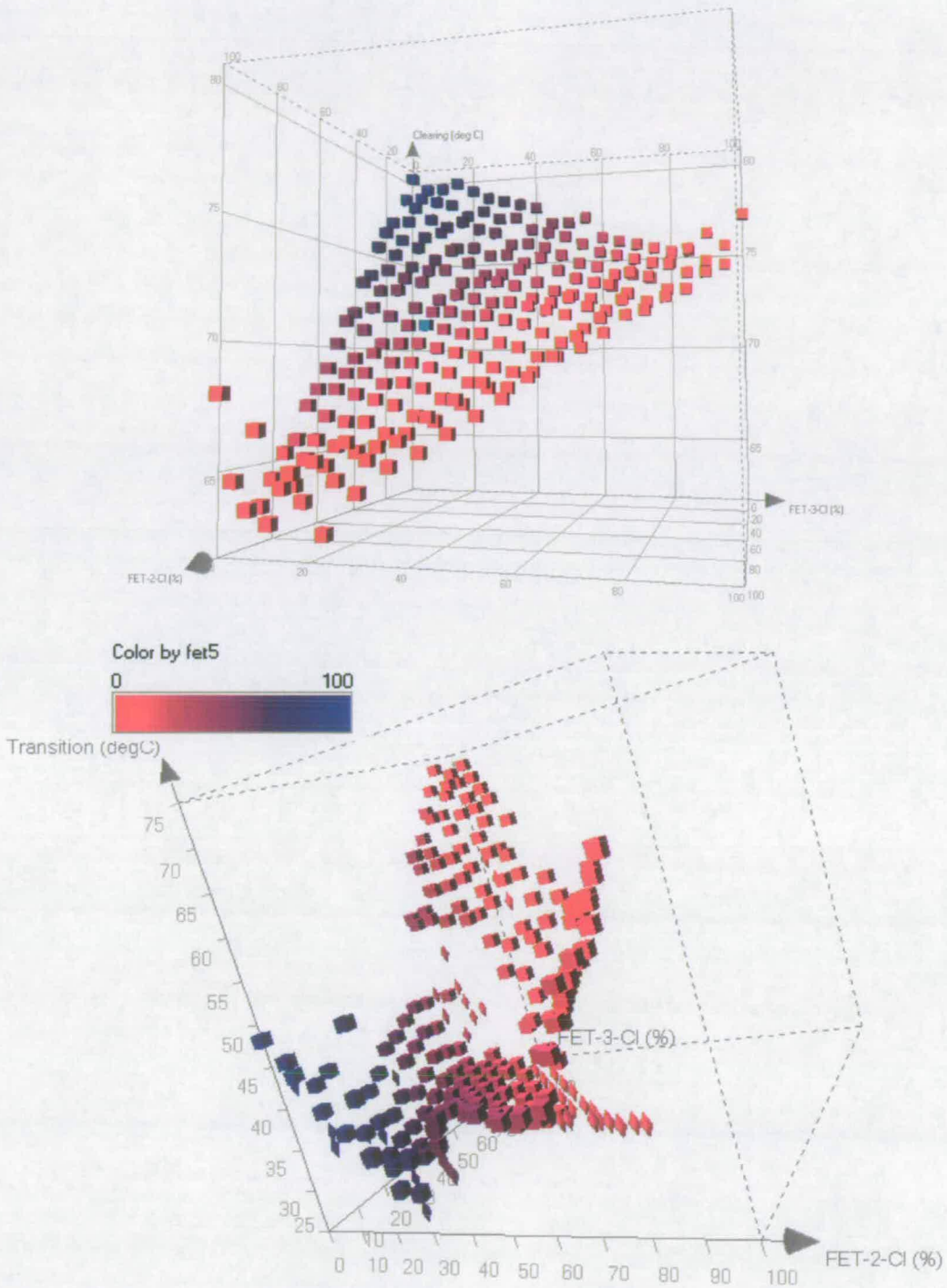

Figure 3.26: Data from the HT analysis plotting the percentage of FET-2-Cl, 3-Cl and 5-Cl in each formulation against the melting point (left) and clearing point (right). FET-5-Cl is visualised by a gradient (red at 0 % blue at 100 %) in both graphs. The melting point surface also shows intermediate transitions, visualised by the diamond data points. The highlighted point on each plot shows the location of the theoretically calculated eutectic composition.

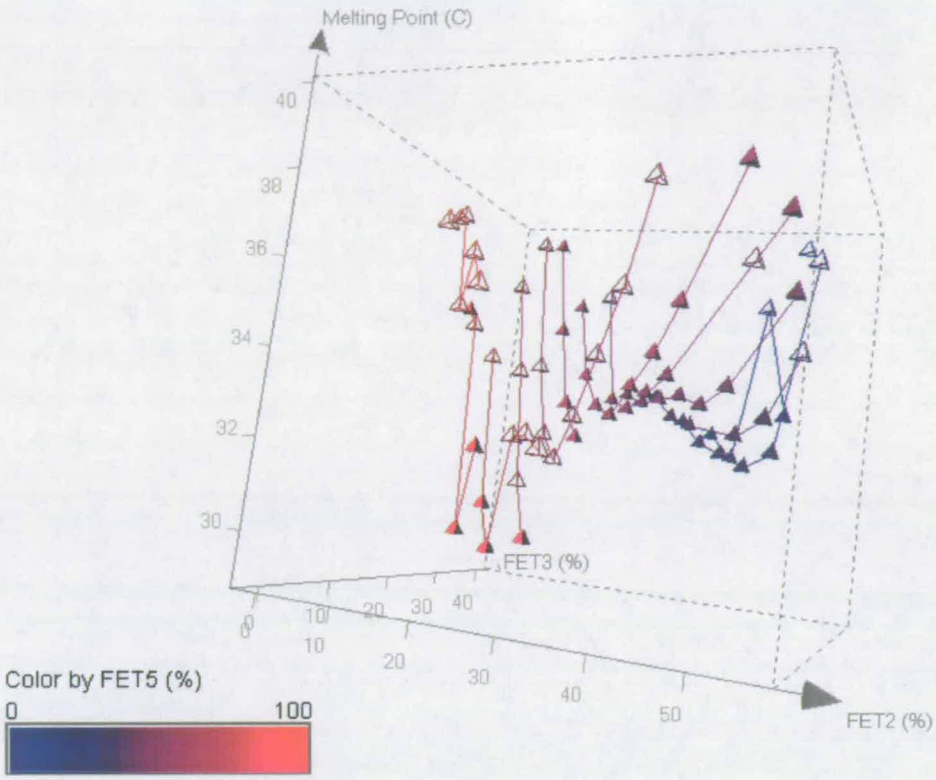

Figure 3.27: A plot showing transitions with melting transitions occurring over less than 2.5 °C (filled triangles) and other transitions showing broad non-eutectic phase behaviour (empty triangles)

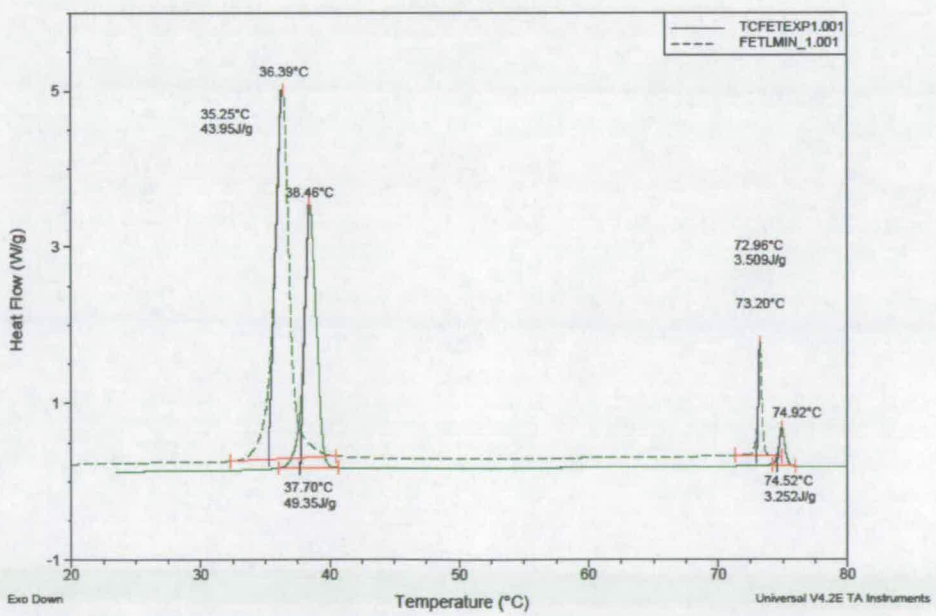

Figure 3.28: DSC of the FET-Eutectic and experimentally calculated lowest melting point material, located in the systems local minimum.

Method	%FET 2,3,5	T_{Cr-N} / °C	T_{N-I} / °C
SVL formulated Material			
Merck FET eutectic (lit)	39.56,20.11,40.33	35.0	72.0
DSC of grav sample	*39.56:20.11:40.33*	*37.4*	*74.4*
HT of grav sample	39.56:20.11:40.33	36.0	72.5
Inkjet formulated material tested using the HT apparatus			
FET eutectic composition	40.20.40	34.0	71.1
Local minimum	45,25,30	32.7	70.0
Global minimum	15,15,70	30.0	76.6
DSC of local minimum (grav)	*45,25,30*	*35.2*	*73.0*
DSC of global minimum (grav)	*15,15,70*	*34.6*	*78.6*

Table 3.5: Results of the Inkjet formulation and high-throughput screening of phase transitions.

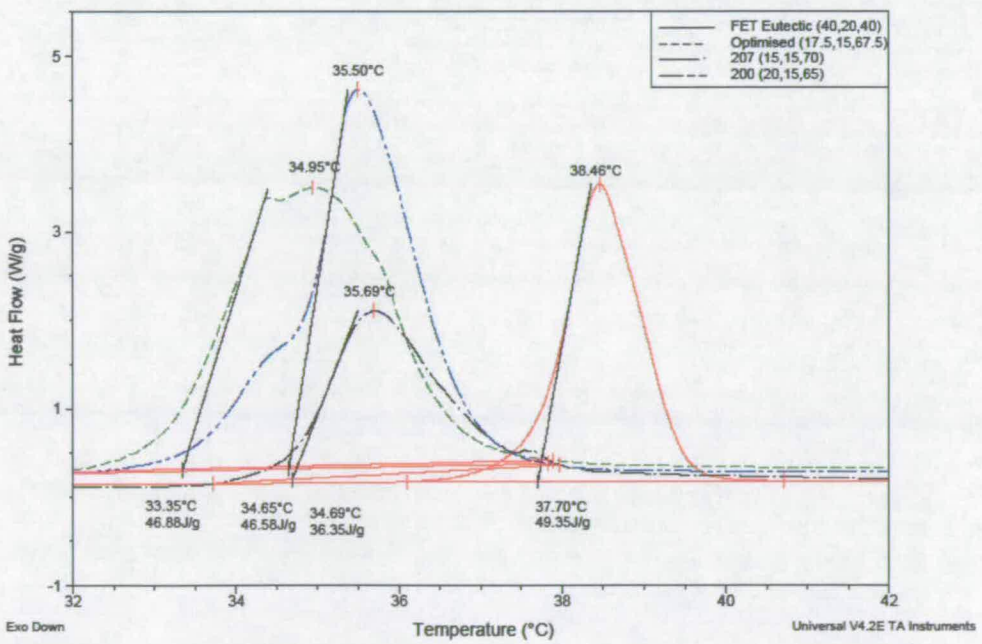

Figure 3.29: DSC traces of the eutectic composition lying in the local minimum (red) and three compositions in the systems global minimum (green, blue, black) illustrating the broadening and non-symmetry of the peaks obtained in the global minimum, indicative of deviation from the eutectic composition.

The DSC data in Figure 3.29 compares three transitions identified in the global minimum, to that of FET eutectic. The transitions are seen to exhibit broader melts to that of FET eutectic, due to the presence of shoulders accompanying the melting peak, indicative of a non-eutectic mixture with dual melting-point behaviour. The most symmetric peak is that of the 15,15,70 % composition; however this still shows some broadening at the tail, and the peak width is substantially greater than that of the FET Eutectic composition showing a deviation from the eutectic. It is possible that the global eutectic lies at a very precise composition near the 15,15,70 % composition and hence it has been missed in this crude experiment. Alternatively it is feasible that the eutectic does not form at all this point. To clarify this situation requires further analysis by creation of an ultra-focused library. Although it was entirely possible to achieve such analysis using the apparatus already developed, by formulating a similar sized library with a step size of 1 or 0.5 % in the required region, this was not completed due to time constraints.

Even in the case where the eutectic composition can be identified in this global minimum, there are a number of advantages to using the eutectic found in the local minimum. The local minimum in which FET eutectic lies is extremely broad, with a number of eutectics forming with subtly different composition. If a eutectic in this region is used in an application there is greater tolerance to compositional errors. If deviation occurs then the eutectic can still form, albeit with a marginally higher melting point. In the global minimum this tolerance would be reduced due to the steep sides of the minimum. Deviation in formulation can result in the eutectic not forming, instead producing a mixture with broad melting behaviour or containing solid particles. The phase diagrams of the 40 % and 70 % FET compositions illustrate this point further in Figure 3.30.

3.7 Comparison of Results; Robotic, Inkjet HT Screening and DSC

Comparison both visually (Figure 3.31), and numerically (Table 3.6) of the robotic and inkjet formulation methods showed remarkable consistency between both methods. This not only illustrates the reproducibility and accuracy of this apparatus, but also of the HT screening technique. The identification of the minimum melting points in the IJP experiment in the first iteration clearly illustrates that from the onset libraries produced in this way should be designed to exploit the largest number of mixtures possible to reveal clear trends.

Although this was possible using the robotic handling method in two iterations, this doubles the time for formulation and analysis. Overall using this process it took in excess of 4 days requiring approximately 6ml of each FET component to achieve such results. The robotic formulation also requires a greater amount of human involvement in preparing solutions, programming the robotic sequence and finally manually spotting each mixture into the analysis micro wells. In contrast using the IJP formulation method[75] eliminates these steps. The process of library creation, formulation and loading onto the analysis substrate was fully automated. As a result, the IJP method used only 200 µL of a 5:1 solution of each component, equating to 33 µL of each pure FET component. The creation of a 231-member library from conception to completion including all programming steps was achieved in 30 minutes, a fraction of the time required for a robotically produced library formulation. The total time for full analysis of such a library was achieved in less than 3 hours. DSC analysis of the results obtained by inkjet formulation and robotic formulation prove that there are no issues with the reliability or reproducibility of either method (Table 3.6)

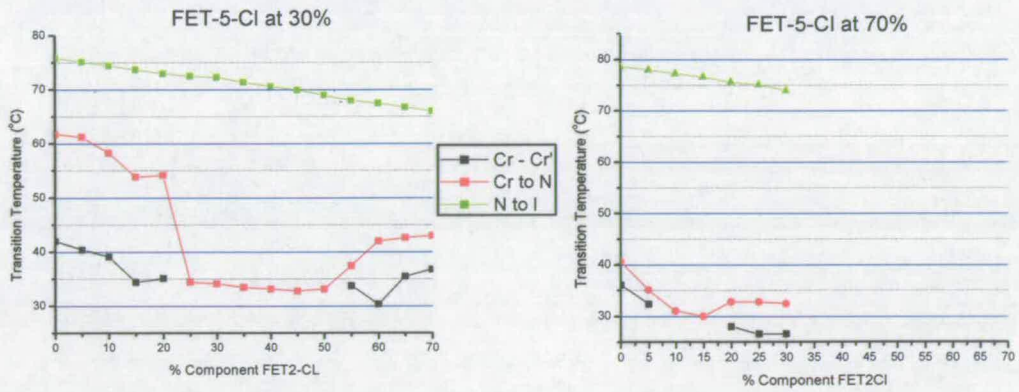

Figure 3.30: Phase diagrams for compositions of FET-5-Cl at 30 % (left) and 70 % (right). Using 30 % FET-5-Cl gives a larger compositional eutectic region (the point at which the red line meets the black)

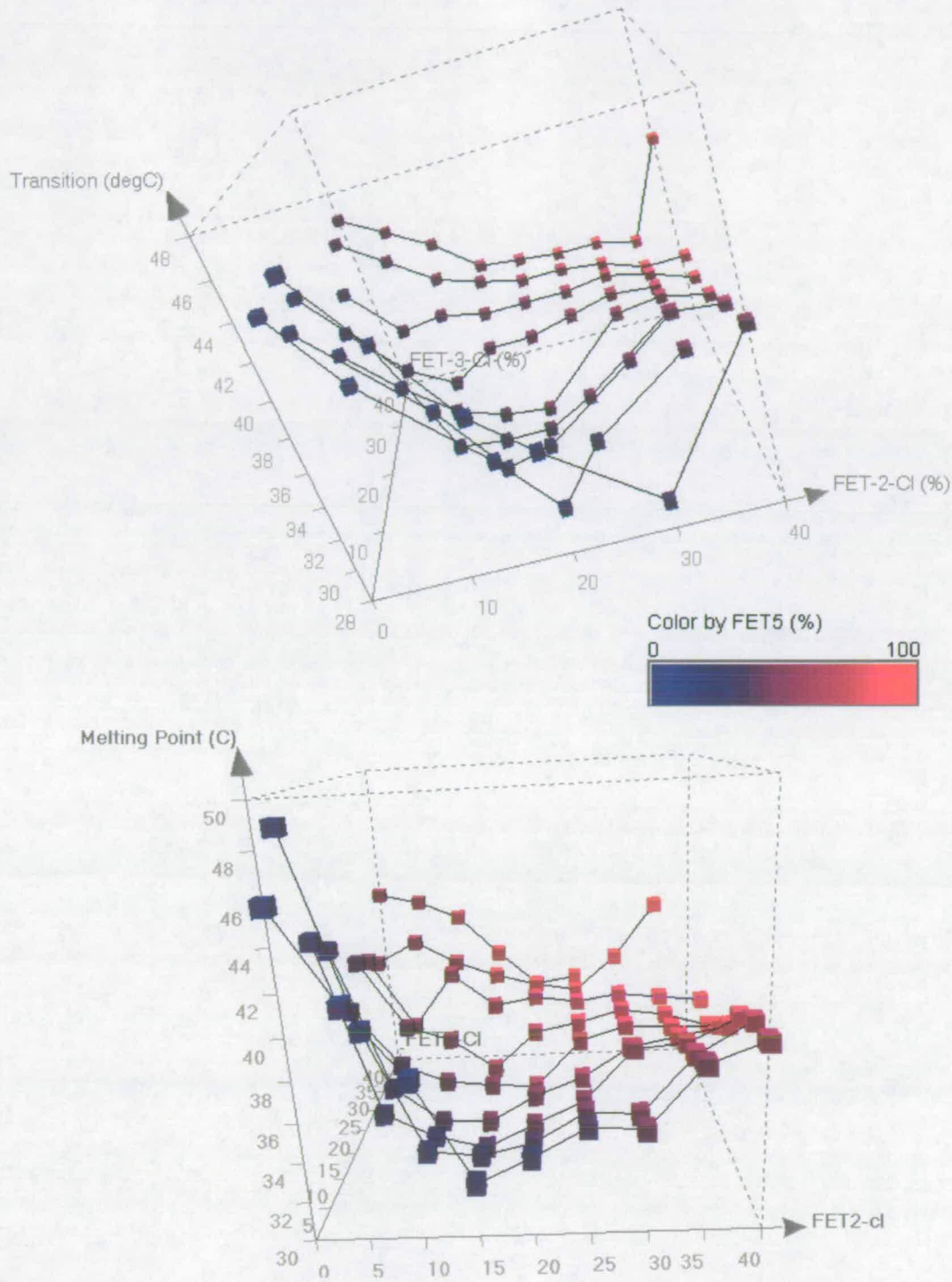

Figure 3.31: Data from an identical library produced by robotic formulation (top) and inkjet printing formulation (bottom). Both libraries were analysed for melting point using the HT screening apparatus.

Method	FET 2,3,5	T_{Cr-N} / °C	T_{N-I} / °C
SVL formulated Material			
Merck FET eutectic (lit)	39.56,20.11,40.33	35.0	72.0
DSC of grav sample	*39.56:20.11:40.33*	*37.4*	*74.4*
HT of grav sample	39.56:20.11:40.33	36.0	72.5
Robotic formulated material analysed using HT apparatus			
FET Eutectic composition 10%	40,20,40	36.7	73.1
Global Minimum 10% step	20,10,70	32.4	79.2
FET Eutectic composition 5%	40,20,40	35.8	-
Global Minimum 5% step	15,10,75	31.6	-
DSC of robotic min (grav.)	*15,10,75*	*33.0 (dual)*	*77.9*
Inkjet formulated material tested using the HT apparatus			
FET eutectic composition	40.20.40	34.0	71.1
Local minimum	45,25,30	32.7	70.0
Global minimum	15,15,70	30.0	76.6
DSC of local minimum (grav)	*45,25,30*	*35.2*	*73.0*
DSC of global minimum (grav)	*15,15,70*	*34.6*	*78.6*

Table 3.6: Results comparing the FET-eutectic to the robotic and IJP formulation methods.

3.8 Conclusion

In this chapter, the creation of multi-component liquid crystal libraries was investigated. Robotic liquid handling was found to be an accurate and reproducible method, providing that the aspiration rate was optimised for more viscous solutions. A ternary library of liquid crystal mixtures was formulated then analysed using the technique of high-throughput screening for phase transitions. The data showed a linear relationship between clearing point and composition and the absence of substantial deviations over the surface in combination with literature correlation of pure components at each of the three corners proves the accuracy and reproducibility of the two techniques in parallel. A second, much larger ternary

library was produced using the same technique of robotic formulation, illustrating limitations in the speed of formulation and the need for time-consuming manual reformatting onto the HT apparatus. Due to the much greater sample densities required to analyse hundreds of samples, containment was required to prevent the amalgamation of samples at elevated temperatures. To achieve this, a lithography technique was successfully used to create a micro-well device.

Inkjet printing was also evaluated as a method of formulation and the technique of overprinting components was identified as the most beneficial. Creation of an identical ternary library to that produced by robotic liquid handling showed remarkable similarity in the relationship between clearing / melting point and the composition of the three components. Comparison of the HT Inkjet formulation method with DSC results also showed excellent correlation, proving that the technique of overprinting drops to create mixtures was extremely accurate, reproducible and efficient. The method had many advantages: It was extremely fast, only required microlitres of each component and was used to create an array of unique formulations onto substrate that could be directly used for HT analysis, eliminating the reformatting procedure required in robotic formulation. The reduced scale and increased accuracy enabled a three-fold increase in sample density, whilst the size of drops eliminated the issue of sample amalgamation.

Analysis of the melting and clearing points of the tertiary library, formulated using both methods revealed areas of eutectic behaviour, which correlated well with those predicted by the SVL equations, although further improvement in the reduction of melting temperatures was achieved. Additionally a second region with lower melting point was identified, where the eutectic composition appeared within a very confined range. Analysis by DSC of this region showed the melting peaks to possess shoulders therefore showing a deviation from the eutectic composition. To identify the exact point at which the eutectic lies requires reformulation of the library over a small area.

The combination of high-throughput formulation together with parallel screening techniques has been shown to be a valuable tool for the exploration of ternary eutectic formulation. Inkjet printing is the preferred technique for its ability to simultaneously dispense, mix and reformat mixtures in a HT manner. Both methods show excellent reproducibility, accuracy and correlation with analogous mixture analysed by DSC. Using these methods makes experimental exploration of ternary and higher compositions feasible, therefore overcoming

the limitations of theoretical eutectic prediction in multi-component mixtures, which cannot reveal the true and subtle full picture of phase space.

3.9 References

(1) J. A. Castellano In *The physics and chemistry of liquid crystal devices*, G. J. Sprokel (Ed.), New York ; London: Plenum Press, **1980**.
(2) P. J. Collings and M. Hird, *Introduction to liquid crystals : Chemistry and physics*, London: Taylor & Francis, **1997**, p 278.
(3) D. Pauluth and K. Tarumi, *J. Mater. Chem.*, **2004**, *14*, 1219.
(4) G. W. Gray and S. M. Kelly, *J. Mater. Chem.*, **1999**, *9*, 2037.
(5) P. G. de Gennes and J. Prost, *The physics of liquid crystals*, 2nd ed. Oxford: Clarendon Press, **1993**, p 91.
(6) M. Schadt and W. Helfrich, *Appl. Phys. Lett.*, **1971**, *18*, 127.
(7) E. P. Raynes, *J. Chem. Soc., Chem. Commun.*, **1974**, 98.
(8) R. Eidenschink, D. Erdmann, J. Krause and L. Pohl, *Angew. Chem., Int. Ed. Engl.*, **1978**, *17*, 133.
(9) R. Eidenschink, G. Haas, M. Romer and B. S. Scheuble, *Angew. Chem., Int. Ed. Engl.*, **1984**, *23*, 147.
(10) P. Kirsch, V. Reiffenrath and M. Bremer, *Synlett*, **1999**, 389.
(11) D. S. Hulme and E. P. Raynes, *J. Chem. Soc., Chem. Commun.*, **1974**, 98.
(12) D. Demus, C. Fietkau, R. Schubert and H. Kehlen, *Mol. Cryst. Liq. Cryst.*, **1974**, *25*, 215.
(13) H. L. Le Chatalier, *C. R. Acad. Sci.*, **1885**, *100*, 50.
(14) I. Z. Schroeder, *Z. Phys. Chem.*, **1893**, *11*, 449.
(15) J. J. van Laar, *Z. Phys. Chem.*, **1908**, *63*, 216.
(16) E. C. H. Hsu and J. F. Johnson, *Mol. Cryst. Liq. Cryst.*, **1973**, *20*, 177.
(17) J. D. Margerum, J. E. Jensen and A. M. Lackner, *Mol. Cryst. Liq. Cryst.*, **1981**, *68*, 1085.
(18) J. D. Margerum, S. M. Wong, A. M. Lackner and J. E. Jensen, *Mol. Cryst. Liq. Cryst.*, **1981**, *68*, 1105.
(19) J. D. Margerum, A. M. Lackner, J. E. Jensen, L. J. Miller, W. H. Smith, S. M. Wong and C. I. Vanast, *Mol. Cryst. Liq. Cryst.*, **1984**, *111*, 103.
(20) E. C. H. Hsu and J. F. Johnson, *Mol. Cryst. Liq. Cryst.*, **1974**, *27*, 95.
(21) J. Szulc, Z. Witkiewicz and R. Dabrowski, *Mol. Cryst. Liq. Cryst.*, **1984**, *109*, 125.
(22) J. D. Margerum, C. I. Van Ast, G. D. Myer and W. H. Smith, Jr., *Mol. Cryst. Liq. Cryst.*, **1991**, *198*, 29.
(23) R. I. Nessim, *Thermochim. Acta*, **2000**, *343*, 1.
(24) T. Cull, M. Goulding and M. Bradley, *Rev. Sci. Instrum.*, **2005**, *76*, 062216.
(25) D. Dunmur, A. Fukuda and G. R. Luckhurst In *Physical properties of liquid crystals : Nematics*, D. Dunmur, A. Fukuda and G. R. Luckhurst (Eds.), London: Institution of Electrical Engineers, **2001**.
(26) S. Singh, *Liquid crystal fundamentals*, New Jersey ; London: World Scientific, **2002**, p 57.
(27) J. Major, *J. Biomol. Screen.* , **1998**, *3*, 13.
(28) J. T. Cabral, S. D. Hudson, C. Harrison and J. F. Douglas, *Langmuir*, **2004**, *20*, 10020.
(29) C. Harrison, J. Cabral, C. M. Stafford, A. Karim and E. J. Amis, *J. Micromech. Microeng.*, **2004**, *14*, 153.
(30) N. B. Cramer, J. P. Scott and C. N. Bowman, *Macromolecules*, **2002**, *35*, 5361.

(31) N. B. Cramer, T. Davies, A. K. O'Brien and C. N. Bowman, *Macromolecules*, **2003**, *36*, 4631.
(32) N. B. Cramer, S. K. Reddy, A. K. O'Brien and C. N. Bowman, *Macromolecules*, **2003**, *36*, 7964.
(33) Merck KGaA, *Liqcryst datasheets,* Darmstatd, Germany, **2004.**
(34) J. Cognard and C. Ganguillet, *Mol. Cryst. Liq. Cryst.*, **1978**, *49*, 33.
(35) M. Sorai and S. Seki, *Bull. Chem. Soc. Jpn.*, **1971**, *44*, 2887.
(36) R. Kapur, K. A. Giuliano, M. Campana, T. Adams, K. Olson, D. Jung, M. Mrksich, C. Vasudevan and D. L. Taylor, *Biomed. Microdev.*, **1999**, *2*, 99.
(37) W. Stahl, *J. Biomol. Screen.* , **1999**, *4*, 117.
(38) M. J. Felton, *Anal. Chem.*, **2003**, *75*, 397A.
(39) S. Fox, S. Farr-Jones and M. A. Yund, *J. Biomol. Screen.* , **1999**, *4*, 183.
(40) M. Divers, *J. Biomol. Screen.* , **1999**, *4*, 177.
(41) C. Haber, M. Boillat and B. van der Schoot, *Assay Drug Dev. Technol.*, **2005**, *3*, 203.
(42) J. G. Houston and M. Banks, *Curr. Opin. Biotechnol.*, **1997**, *8*, 734.
(43) P. B. Taylor, S. Ashman, S. M. Baddeley, S. L. Bartram, C. D. Battle, B. C. Bond, Y. M. Clements, N. J. Gaul, W. E. McAllister, J. A. Mostacero, F. Ramon, J. M. Wilson, R. P. Hertzberg, A. J. Pope and R. Macarron, *J. Biomol. Screen.* , **2002**, *7*, 554.
(44) D. I. Stimpson, P. W. Cooley, S. M. Knepper and D. B. Wallace, *BioTechniques*, **1998**, *25*, 886.
(45) P. James and R. Papen, *Drug Discovery Today*, **1998**, *3*, 429.
(46) A. Schober, R. Gunther, A. Schwienhorst, M. Doring and B. F. Lindemann, *BioTechniques*, **1993**, *15*, 324.
(47) A. V. Lemmo, J. T. Fisher, H. M. Geysen and D. J. Rose, *Anal. Chem.*, **1997**, *69*, 543.
(48) D. Rose, *Drug Discovery Today*, **1999**, *4*, 411.
(49) A. R. Bhatti, M. Mott, J. R. G. Evans and M. J. Edirisinghe, *J. Mater. Sci. Lett.*, **2001**, *20*, 1245.
(50) X. Zhao, J. R. G. Evans, M. J. Edirisinghe and J. H. Song, *J. Mater. Sci.*, **2002**, *37*, 1987.
(51) M. Mott and J. R. G. Evans, *Mater. Sci. Eng., A*, **1999**, *271*, 344.
(52) M. M. Mohebi and J. R. G. Evans, *J. Comb. Chem.*, **2002**, *4*, 267.
(53) M. M. Mohebi and J. R. G. Evans, *J. Am. Ceram. Soc.*, **2003**, *86*, 1654.
(54) J. Wang and J. R. G. Evans, *J. Comb. Chem.*, **2005**, *7*, 665.
(55) X. D. Sun, K. A. Wang, Y. Yoo, W. G. Wallace-Freedman, C. Gao, X. D. Xiang and P. G. Schultz, *Adv. Mat.*, **1997**, *9*, 1046.
(56) T. Kawase, H. Sirringhaus, R. H. Friend and T. Shimoda, *Adv. Mat.*, **2001**, *13*, 1601.
(57) H. Sirringhaus, T. Kawase, R. H. Friend, T. Shimoda, M. Inbasekaran, W. Wu and E. P. Woo, *Science*, **2000**, *290*, 2123.
(58) B. Chen, T. H. Cui, Y. Liu and K. Varahramyan, *Solid-State Electron.*, **2003**, *47*, 841.
(59) S. K. Hwang, K. D. Lee and K. H. Lee, *Jpn J Appl Phys 2*, **2001**, *40*, L580.
(60) B. J. de Gans and U. S. Schubert, *Macromol. Rapid Commun.*, **2003**, *24*, 659.
(61) H. Q. Zhang, R. Hoogenboom, M. A. R. Meier and U. S. Schubert, *Meas. Sci. Technol.*, **2005**, *16*, 203.
(62) H. M. Reichenbach and P. J. McGinn, *Appl. Catal., A*, **2003**, *244*, 101.
(63) Z. L. Luo, B. Geng, J. Bao and C. Gao, *J. Comb. Chem.*, **2005**, *7*, 942.
(64) A. V. Lemmo, D. J. Rose and T. C. Tisone, *Curr. Opin. Biotechnol.*, **1998**, *9*, 615.
(65) L. Chen, J. Bao and C. Gao, *J. Comb. Chem.*, **2004**, *6*, 699.
(66) Y. Yoshioka and G. E. Jabbour, *Adv. Mat.*, **2006**, *18*, 1307.
(67) Y. Yoshioka, P. D. Calvert and G. E. Jabbour, *Macromol. Rapid Commun.*, **2005**, *26*, 238.
(68) E. Reddington, A. Sapienza, B. Gurau, R. Viswanathan, S. Sarangapani, E. S. Smotkin and T. E. Mallouk, *Science*, **1998**, *280*, 1735.
(69) S. Okamura, R. Takeuchi and T. Shiosaki, *Jpn J Appl Phys 1*, **2002**, *41*, 6714.

(70) B. Jandeleit, D. J. Schaefer, T. S. Powers, H. W. Turner and W. H. Weinberg, *Angew. Chem., Int. Ed. Engl.*, **1999**, *38*, 2495.
(71) G. M. Nishioka, US Patent, US5449754, **1995**.
(72) J. Wang, M. M. Mohebi and J. R. G. Evans, *Macromol. Rapid Commun.*, **2005**, *26*, 304.
(73) W. T. Pimbley and H. C. Lee, *IBM J. Res. Dev.*, **1977**, *21*, 21.
(74) H. Onusseit and H. Stegemeyer, *Mol. Cryst. Liq. Cryst.*, **1984**, *111*, 31.
(75) T. Cull, M. Goulding and M. Bradley, *Adv. Mat.*, **2007**, *19*, 2355.

Chapter 4 - Application of HT Formulation and Screening Methods to Other Areas; Chiral Reactive Mesogen Libraries

4.1 Introduction

Calamitic thermotropic liquid crystals used in displays are able to undergo structural reorientation on application of an electric field, and are therefore in a dynamic form.[1] For other applications, a major limitation of this arrangement is that the material must be maintained within a defined temperature range to ensure stability of the LC mesophase. Additionally, the liquid crystal must be confined and hermetically sealed into a uniform thin cell arrangement which limits its practicality. In more recent applications, these issues have been overcome in the creation of optical filters using thermotropic reactive mesogens. Mesogens possessing direactive functional groups such as acrylate or vinyl,[2-8] are able to be polymerised *via* in-situ photoinitiation.[9,10] In the polymerised state, the anisotropic optical properties of the monomeric LC phase are preserved and the structure no longer exhibits mesophase transitions[11-16] so creating a durable, temperature-independent, anisotropic polymeric film.[3,17-21] Films produced in this way have found use in the compensation of LC displays, to overcome undesirable effects of LCs used in the dynamic form and to increase contrast, brightness and viewing angles.[22,23] Reactive mesogens have also been used in the creation of a variety of optical effects.[24-29]

The aims of this chapter were to assess requirements for the HT formulation and screening of chiral nematic reactive mesogen mixtures, suitable for photo-polymerised preparation of visible-wavelength selectively reflecting films. A general proof of concept for high-throughput processing of thin films will be established by evaluation of both new and previously developed techniques, many of which have been developed for the formulation and characterisation of liquid crystal mixtures described in chapters 2 and 3. One key outcome is to assess the application of inkjet printing and robotic liquid handling[30,31] to reactive mesogens films as a HT deposition technique.

4.2 Formulation, Processing and Characterisation of Chiral Nematic Reactive Mesogens

Selectively reflecting films, introduced in chapter 1, consist of a number of components in addition to a chiral dopant. Many of these components are added to enable photo polymerisation,[10,32] and hence do not have a major effect on mesophase formation. In the following sections a brief overview of the main components of a chiral nematic reactive mesogen, including the components used throughout this work will be discussed.

4.2.1 Components of Selectively Reflecting Reactive Mesogen Films

The reactive mesogen host forms the basis of a selectively reflecting film, from which the bulk properties (refractive index, melting point, clearing point and solubility) are derived. For free radical initiation and propagation, acrylate functionality is included in the structure. The formation of an anisotropic polymer network which possesses both high flexibility and durability, necessitates an elastomer network in which both mono and diacrylate functionalised mesogens are used. A key requirement of the host is for it to possess a broad nematic range, which if ambient processing is desired, should span ambient temperatures.[7] To achieve this aim involves formation of multi-component mixtures, and the identification of eutectic compositions. This has previously been shown in Chapters 1 and 2 to be possible using high-throughput techniques. In this work, a quaternary mixture was created using components synthesised by Merck Chemicals (Figure 4.1).

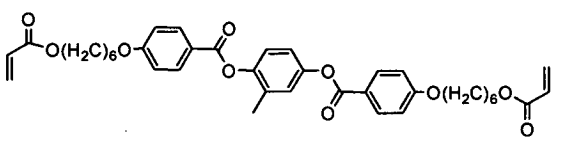

RM82 Cr 88 N 118 I

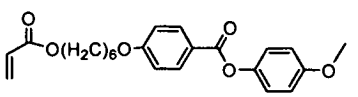

RM105 Cr 64 I

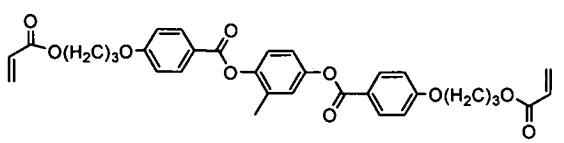

RM257 Cr 66 N 127 I

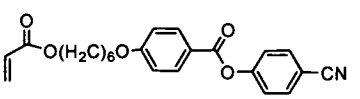

RM23 Cr 75 N (53) I

Figure 4.1: Merck reactive mesogens and their phase transitions (°C)

The components RM23, RM105, RM 82 and RM105 (Merck Chemicals Ltd.) are reactive mesogens possessing both diacrylate functionality to allow in-situ photo polymerisation, and monoacrylate functionality, which acts as a plasticiser in the elastomer for control over the durability and flexibility of the polymer (Figure 4.2).[33] When combined in a 25:25:10:40 % composition, a eutectic phase is formed which exhibits a room temperature nematic phase.

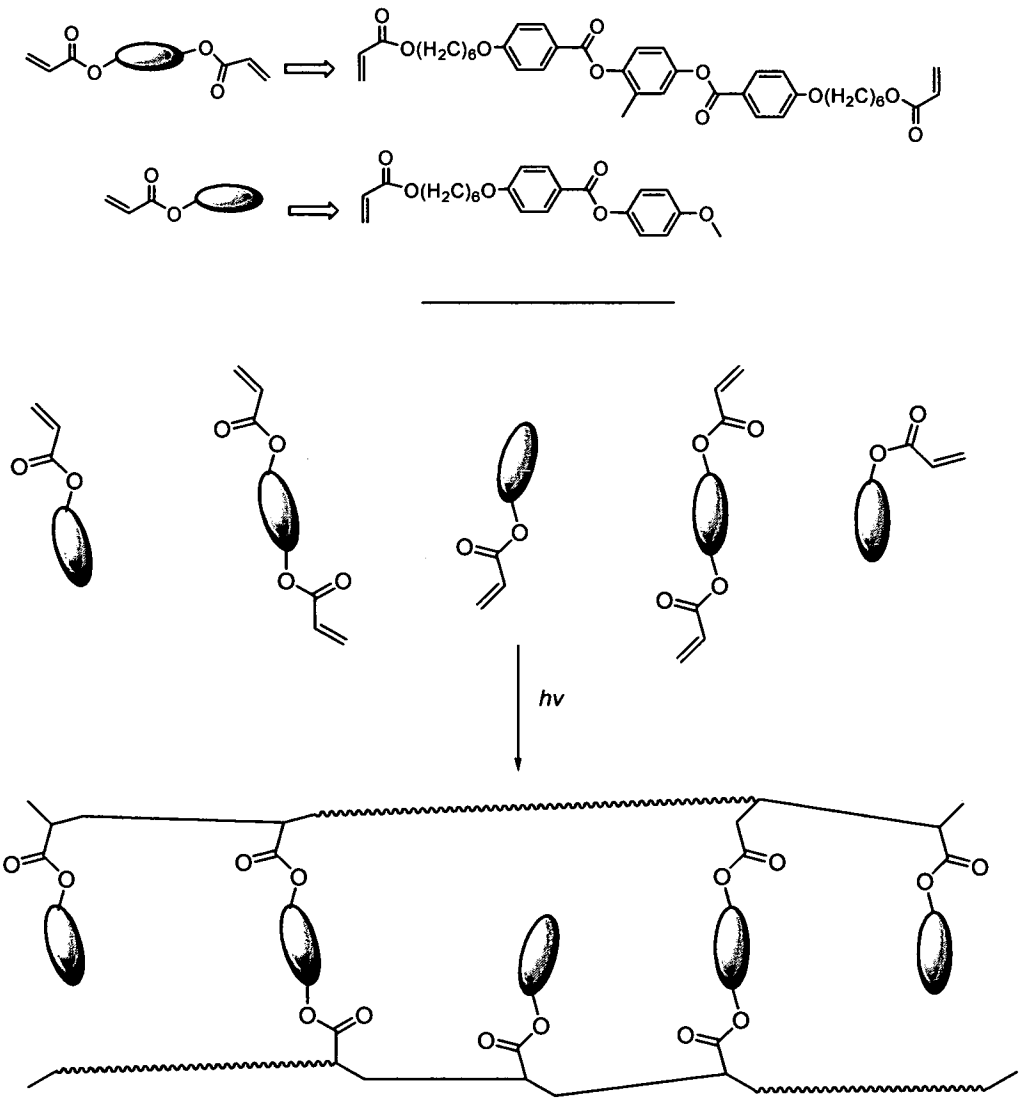

Figure 4.2: A simplified representation of the chemical structure of a diacrylate and monoacrylate mixture of mesogens before, and after photo initiated cross-linking

The photo-polymerisation reaction requires initiation using a photo-initiator. In this work initiation was achieved using Irganox 651 (Ciba, 2,2-dimethoxy-2-phenylacetophenone), a free radical initiator with absorption at 250 nm and 340 nm, which allows both UVA and UVB photo initiation. The initiator was incorporated at low concentration (1 w/w %), preventing modification of the pre-polymerisation mesophase transition temperature,[34] and additionally reducing the formation of short polymer chains which can create brittle films. In addition to the photoinitiator, a sterically hindered phenolic oxidative stabilizer (Ciba, Irgacure 1076; octadecyl 3,5-di-tert-butyl-4-hydroxyhydrocinnamate) which inhibits thermal degradation by reaction with free radicals, was incorporated at 0.08 w/w %. A non-ionic fluorinated surfactant (3M, Fluorad FC-171) providing wetting and levelling properties of the film, particularly at the air interface,[24] was incorporated at 0.6 w/w %. The type, and quantity of these components was representative of a typical reactive mesogen formulation produced by Merck.

For optical properties such as selective reflection to be observed in reactive mesogens requires that they are processed into thin films. Addition of a solvent to the mixtures provides such processability. Choice of the solvent used, and variation of mixture parameters such as solute concentration, solvent volatility and solvent wetting, requires optimisation to ensure reproducible film thickness and homogenous films. Common solvents used in Merck reactive mesogen solution (RMS) formulations include PGMEA, toluene and xylene.

4.2.2 Processing of Thin Films

Two techniques, bar coating and spin coating are commonly used to process solutions into thin films. The choice of method is dependent on the properties of the substrate, the thickness of film required and the amount of material available for coating.

Bar coating involves drawing a solution down a substrate using a wire-wound 'K-Bar' to produce a thin film. K-bars are produced by winding a steel wire around a steel rod so that a pattern of identical grooves is produced on the bar. It is these grooves that control the thickness of solution deposited, and bars providing thicknesses from 4 to 500 μm are available. After coating, the substrate is usually heated to remove the solvent in which the solution was coated. The k-bar can either be drawn down the substrate by hand, or using an automated system. One advantage of this process is that two or more coatings can be applied in a single operation, which is of particular interest in a high-throughput system.

Spin coating is a technique in which a solution is distributed over the substrate by centrifugal forces. An excess of material to be coated is deposited in the centre of the substrate, before the substrate is rotated at high speed. The solvent used in the coating is selected to be volatile, so that during spinning it evaporates leaving only the solute as a homogeneous film on the substrate. The thickness of the film depends not only on the time and speed of rotation, but also on the concentration of solution and the solvent used. The disadvantage of this technique is that the substrates should be rigid, of a small size (for a typical laboratory spin coater) and have a regular shape, to ensure a homogeneous coating. Additionally, it is only possible to coat one solution simultaneously so the coating of many substrates can be a tedious, and time consuming task.

To obtain films exhibiting homogeneous and sharp selective reflectance characteristics, planar alignment should be induced to create a chiral nematic monodomain such that incoming light, normal to the film surface, is transmitted parallel to the chiral helix.[35] Due to the dependence of λ_{max} on the angle of incident light with respect to the chiral helix, a film coated in the absence of alignment will show variations in the wavelength of reflected light, and poor transmittance / reflectance efficiency. In these studies, planar surface alignment was achieved by the mechanical rubbing of polymer films such as triacetylcellulose (TAC) or polyethylene terephthalate (PET). The long molecular axis of the reactive mesogen liquid crystal preferentially aligns, as a result of strong molecular interactions with the polymer chains on the surface.[36] Following coating of the reactive mesogen solutions (RMS) using the desired technique, the solvent must be removed and the film annealed to obtain good surface alignment. To ensure formation of the chiral nematic phase, annealing was carried out at a temperature not exceeding that of the materials N-I transition. Following annealing, the film was cooled and then photo-polymerised using 254 nm UV irradiation to obtain a tack-free polymer. It is important when using a free radical initiator, to cure the sample in an inert (N_2) atmosphere to prevent inhibition of chain propagation by oxygen.[34] Additional flood UV irradiation, or a thermal post cure can be used to enhance the durability of the films, causing any residual monomeric units to become polymerised.

4.2.3 Characterisation of Thin Films

Characterisation of selectively-reflecting films involves the determination of the wavelengths, λ_{max}, which are either transmitted,[37] or reflected[38-40] by the film. The value of

λ_{max} reported for each sample is the wavelength which lies at the centre of the reflected wavelength band, the bandwidth being dependent on the average refractive index of the nematic host.[24] In this study, ultraviolet-visible (UV/vis) spectroscopy was used to measure the transmittance or absorbance of incident radiation passing through a film. The technique required that substrate films were mounted for analysis (such as in a slide mount) to ensure orthogonal irradiation. Radiation incident on the circularly dichroic film was split into its two circularly polarised components and over the wavelengths of reflection 50 % of the light was reflected, the other 50 % being transmitted. The intensity of transmitted light could be enhanced using circularly polarising filters of identical handedness.

4.3 High-Throughput Methods for Chiral Reactive Mesogen Libraries

The preparation and screening of chiral nematic reactive mesogen films can become time-consuming and require large amounts of materials when larger libraries of mixtures are to be produced. Using previously explored HT techniques, there is potential to increase the throughput of the reactive mesogen formulation process. One such technique, robotic formulation, could be used to quickly and efficiently formulate libraries of reactive mesogens with variable concentration or type of chiral dopant. Considering this method, a workflow for formulation and analysis of the library was designed, and individual elements examined prior to combination. These elements are discussed in more detail in the following sections.

4.3.1 Robotic Formulation

To achieve libraries of reactive mesogens by robotic formulation, a Gilson 233XL liquid handler was used to vary the concentration of chiral dopant in discrete mixtures which exhibit selective reflection properties when coated as thin films. Reactive mesogens are particularly suited to liquid handling as their formulations all contain a large percentage of solvent, allowing solid components to be dispensed as solutions. The low concentrations of chiral dopant (between 0.5 and 5 w/w % of the total mixture) required to produce selective reflectance in the visible region, can be easily achieved through the dispensing of dilute solutions. Accurate dispensing of low concentrations is important due to the sensitive

relationship between chiral dopant concentration and the helical pitch. Small fluctuations in concentration can produce a large variation in pitch of the chiral nematic (Equation 4.1). One drawback of using dilute solutions is that over the range of mixtures, the volume of chiral dopant solution dispensed is dramatically varied as the concentration of chiral dopant is increased, resulting in an increased overall solution volume. To maintain the overall weight / weight percentage (w/w %) between solid and solute throughout the library, necessitates a three-component strategy incorporating a make-up solution (a diluted reactive mesogen solution at a concentration identical to that of the chiral dopant solution). (Figure 4.3)

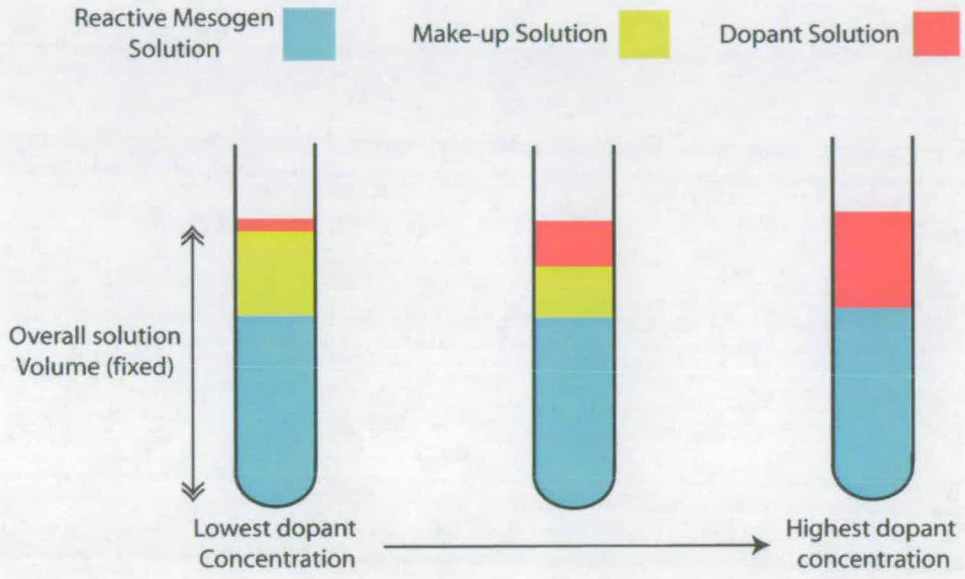

Figure 4.3: Three-component strategy for constant volume dispensing of components for a chiral nematic reactive mesogen library

One consideration in the design of a library using this strategy was to ensure that the concentration of solution was neither too low, nor too high such that the components did not dissolve. A balance exists in which the reactive mesogen solution should contain enough solvent to allow solubility, while at the same time the concentration of the chiral dopant solution should be minimised to increase the accuracy of small-weight-percent dispensing. To achieve this balance, the minimum amount of solvent able to dissolve the reactive mesogen solids component was investigated. The solvent used in these experiments was PGMEA, a component of the Merck commercial formulations, and a representative solvent for the production of films. To test the maximum solid-content that PGMEA could support a

series of solutions with concentration 90 to 30 w/w % solid reactive mesogen were produced, using sonication to aid complete dissolution. Of the concentrations where dissolution was observed, the samples were left at room temperature for 12 hours to observe any crystallisation of solid components. The result of this experiment reveals the limit of solubility to be approximately 50 w/w %, and therefore the relative concentrations of RM and chiral dopant solutions were designed with this limit in mind.

4.3.2 Processing of Films – Parallel Bar Coating

After formulation dispensing the technique of bar coating was used to process the formulations as thin films. To assess the dry thickness of films created by K-bars constructed of increasing gauge windings, three reactive mesogen solutions (Merck Chemicals) containing 33 w/w % solids in PGMEA were coated onto TAC film. Three k-bar grades were used to give approximate wet-coat thicknesses of 2, 6, and 12 μm (size 0, 1 and 2). The films were then annealed at 60 °C for 30 seconds, and UV cured at 365 nm for 60 seconds before each was analyzed for thickness. Figure 4.4 shows that to create films with dry thickness of 1.2 μm or 2.5 μm, bar sizes of 1 or 2 can be used respectively. The deviation from linearity observed in this graph is attributed to experimental error. When dry coated, reactive mesogen films are preferred to have a thickness of between 1 and 3 μm, Figure 4.5 illustrates the decrease in transmitted UV-vis intensity when thinner films are created (K-bars of smaller sizes), due to the incomplete transmittance and reflectance of each circularly polarized component. Only when using K-bar No.2 do side bands in the selective reflection spectra emerge, characteristic of high-quality film formation. The coating of films thicker than 3 μm can be detrimental, the surface alignment unable to fully influence the LC alignment in the bulk, resulting in poorly defined chiral nematic domains which tend to scatter light.

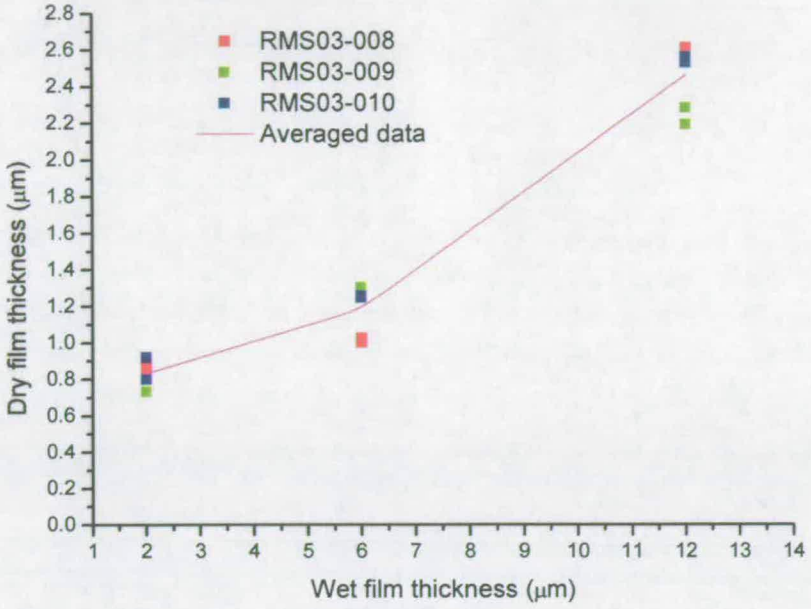

Figure 4.4: Relationship between the wet thickness of films determined by the size of bar used for coating, and the dry film thickness for three commercial reactive mesogen solutions.

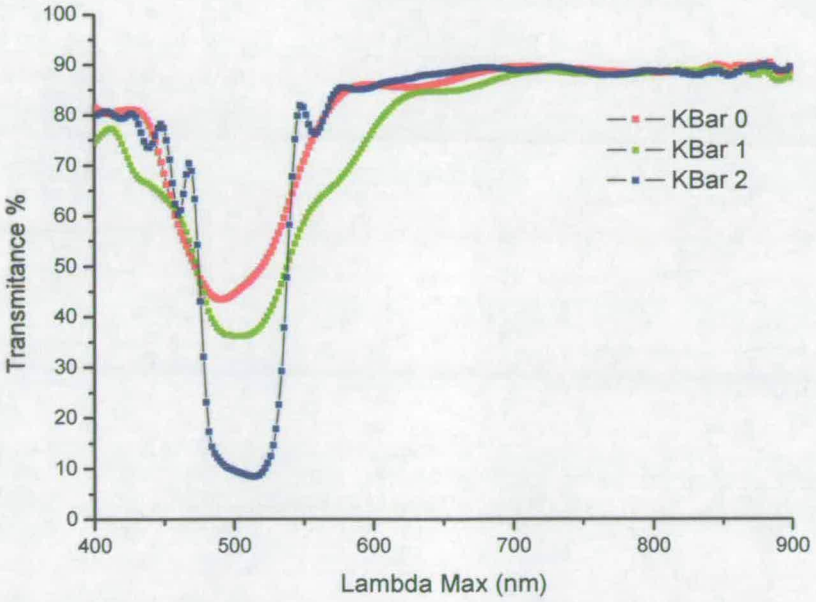

Figure 4.5: The effect of increasing dry film thickness using increasing grades of k-bars, on the transmittance spectra measured using a diode array UV-vis spectrometer.

One of the drawbacks of using a technique such as bar coating is that the process is low throughput. The creation and analysis of films is time-consuming, involving a great deal of manual work in a long sequence of steps, *e.g.* manual formulation and mixing of the solution components, coating, annealing and curing of thin films and UV-vis characterisation of λ_{max}. Using robotic formulation many mixtures can be created in a short time, so therefore the rate-limiting step is the bar coating process. Traditionally, when creating substrates by bar coating a single material is coated onto a single substrate. Using a method developed in our group the triacetylcellulose substrate was cut into a comb structure, resulting in strips of substrate separated by a channel, which allows multiple depositions of thin films in one coating operation (Figure 4.6). Depending on the film width required for analysis (dependent on the UV-vis instrumentation used), as few or as many substrates were made as required. Characterisation of these substrates using the diode array spectrometer could be achieved only if film widths greater than 1.5 cm were maintained (diameter of the spectrometer radiation source). This method, although simple, increases the efficiency of bar coating, with no detrimental effect on the film quality. In addition, because less material is required to produce each film, the formulation scale can be reduced making the 96-well format feasible.

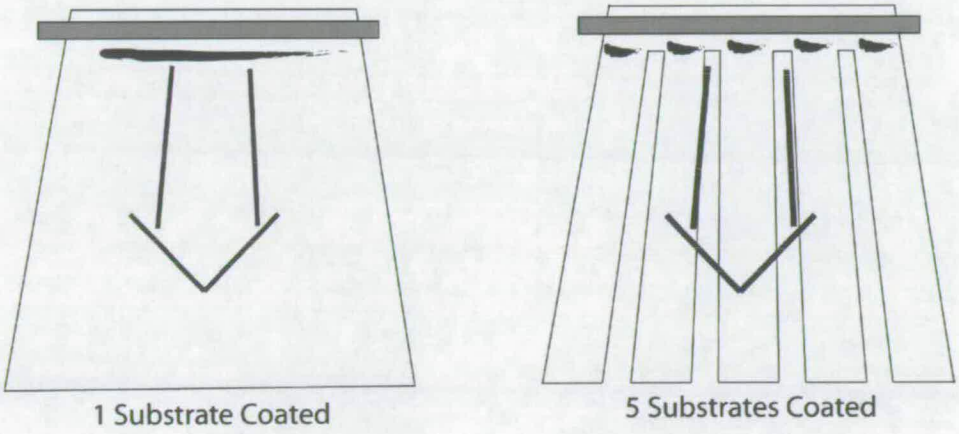

Figure 4.6: Illustration of the technique for parallel bar coating

4.4 Validation of the High Throughput Process

To validate both the robotic liquid handling method and the parallel bar coating technique, two discrete libraries of selectively reflecting reactive mesogen solutions were created in which the concentration of two non-reactive non-mesogenic chiral dopants, BDH-1281 and

IS-9193 (Merck Chemicals Ltd) were varied. BDH-1281 is a cyclic, sugar-based dopant possessing a chiral centre, and IS-9193 is a rotameric chiral dopant. Both dopants invoke a left-handed chiral nematic pitch when introduced to a nematic host. Where the dopants differ is in their helical twisting power, BDH-1281 has a HTP, β, of 76 μm^{-1} and IS-9193 has β of 100 μm^{-1} so a lower concentration of the higher HTP dopant is required to produce an identical λ_{max} reflection wavelength. Analysis of λ_{max} for each library enables the relationship between chiral dopant concentration and reflected wavelength to be obtained. The library was compared to three reference reactive mesogen solutions, formulated using known amounts of BDH-1281 dopant to create red, green and blue reflective films. (Figure 4.7).

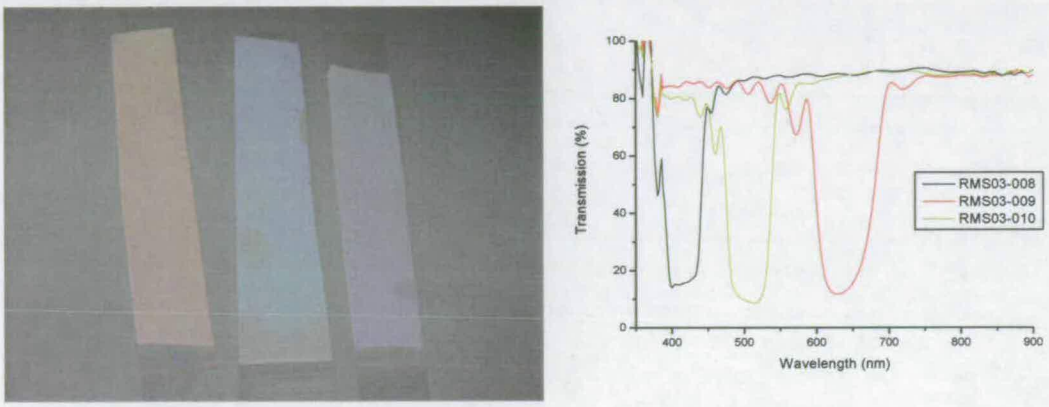

Figure 4.7: Image (left) of three films incorporating BDH-1281 chiral dopant in increasing concentration. The films of RMS-008, 009 and 010 (right) reflect a band of RH polarised light with wavelength dependent on the pitch of the helix.

4.4.1 Library Formulation

The two chiral dopant libraries share common components as described in section 4.2.1, differing only in the dopant composition (Table 4.1).

Solid Component	Percentage
RM23	24.6
RM105	24.6
RM82	9.72
RM257	39.4
FC171	0.6
Irganox 651	1
Irgacure 1076	0.08

Table 4.1: The constituents of the reactive mesogen solution (RMS), formulated at 53.3 w/w % solid content in PGMEA

Libraries were produced in parallel, applying the strategy introduced in section 4.3.1 with common reactive mesogen and makeup solutions. Mixtures were produced on a 1.45 ml scale in 1.5 ml brown glass vials. To achieve dopant concentrations between 1.8 w/w % and 5.8 w/w % in individual formulations (The reference solutions contain dopant between 3 and 4.5 w/w % for reflection of visible wavelengths), dopant solutions of 4.8 w/w % in PGMEA were required, matched to a reactive mesogen solution of 53.3 w/w % in PGMEA. These concentrations enabled the entire concentration range to be formulated, whilst maintaining a ratio of 34 w/w % solids in each individual solution. The makeup solution was produced from an aliquot of the reactive mesogen solution, diluted to a concentration of 4.8 w/w % in PGMEA. Due to the highly viscous nature of the reactive mesogen solution, it was necessary to aspirate and dispense at a rate of 250 µL min^{-1} to ensure accuracy and reproducibility. For each of the two dopants, the concentration was increased in 0.2 w/w % steps to create two 20 member libraries.

Vial	1 / 21	2 / 22	3 / 23	4 / 24	5 / 25	6 / 26	7 / 27	8 / 28	9 / 29	10 / 30
Volume of Dopant solution (µl)	180	200	220	240	260	280	300	320	340	360
Volume of Make-up solution (µl)	380	360	340	320	300	280	260	240	220	200
Volume of RM solution (µl)	890	890	890	890	890	890	890	890	890	890
Concentration of dopant (w/w)%	1.8	2.0	2.2	2.4	2.6	2.8	3.0	3.2	3.4	3.6
Vial	**11 / 31**	**12 / 32**	**13 / 33**	**14 / 34**	**15 / 35**	**16 / 36**	**17 / 37**	**18 / 38**	**19 / 39**	**20 / 40**
Volume of Dopant solution (µl)	380	400	420	440	460	480	500	520	540	560
Volume of Make-up solution (µl)	180	160	140	120	100	80	60	40	20	0
Volume of RM solution (µl)	890	890	890	890	890	890	890	890	890	890
Concentration of dopant (w/w)%	3.8	4	4.2	4.4	4.6	4.8	5	5.2	5.4	5.6

Vials 1 to 20 comprise BDH-1281 dopant, Vials 21 to 40 comprise IS-9193 dopant

Table 4.2: Formulation of a library of reactive mesogens with increasing concentration of chiral dopant

The volumes of each component transferred, as entered into the Gilson liquid handling software, are shown in Table 4.2. The sequence was duplicated for the second library, selecting the IS-9193 source vial in place of the BDH-1281. As the volume of dopant solution was increased, the volume of makeup solution was decreased by an equivalent amount. At the highest concentration of chiral dopant no makeup solution was dispensed.

4.4.2 Film Analysis

Using the parallel bar coating technique described previously, each mixture was coated onto triacetyl cellulose using a size 2 k-bar which resulted in a film of 2.5 µm thickness. After obtaining UV-vis spectra, the λ_{max} values were obtained by manually identifying the wavelength located at the apex of the reflection band (Figure 4.8), and were plotted against the w/w % of chiral dopant. In an additional experiment, the clearing point of each of the two libraries was measured using the HT apparatus and techniques described in Chapter 3.

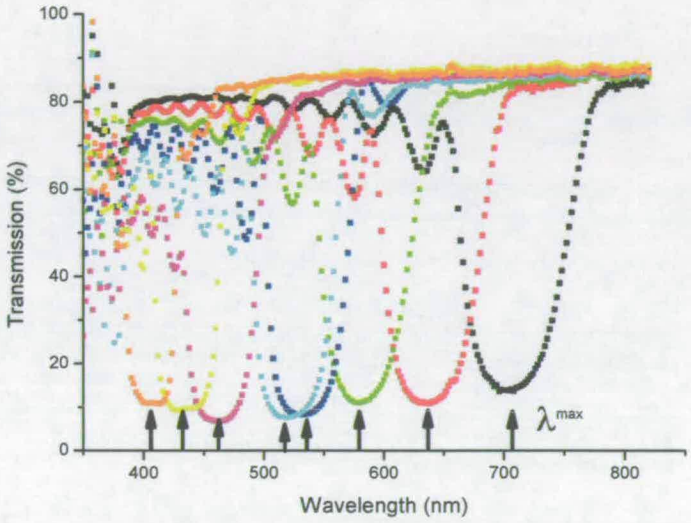

Figure 4.8: UV-Vis spectra of parallel bar coated reactive mesogen solutions, formulated by liquid handling with increasing concentration of chiral dopant. Marked is the position at which λ_{max} was read for each dopant concentration.

4.4.3 Results

Figure 4.10 shows the relationship between the w/w % of chiral dopant and the λ_{max} of reflected light for each dopant. The BDH-1281 dopant shows excellent correlation with the three gravimetrically produced Merck reference samples. This not only illustrates that the robotic formulation has the required accuracy and reproducibility, but also that the technique of parallel bar coating can be used to increase throughput with no detriment on quality. The data for the IS-9193 dopant library was shifted due to its increased HTP, to lower concentrations of chiral dopant with respect to the BDH-1281 data. Both libraries exhibit a near-linear relationship of λ_{max} with chiral dopant concentration, although values at extreme

wavelengths become compressed. This deviation at the extremes is due to the spectral limitation of the UV-Vis spectrometer at around 900 nm, where only the onset of reflection bands occuring higher that this wavelength could be seen. At the lower end of the spectrum, a similar effect is seen caused by absorption of the film below 400 nm (Figure 4.9).

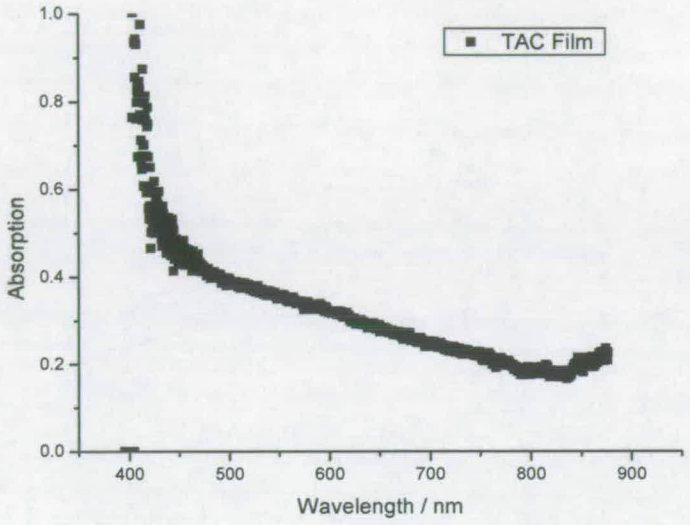

Figure 4.9: The spectra of TAC film showing the absorption below 400 nm, and the limit of the UV apparatus at 900 nm

Using the HT clearing point apparatus, the uncured formulations were analysed for phase transitions. The results in Figure 4.11 show that the clearing point of the mixtures decreases on addition of higher chiral dopant concentration, due to the low extrapolated clearing point of the chiral dopants. Linear extrapolation to 100 w/w % concentration of chiral dopant shows a theoretical clearing point of -76.5 °C for BDH-1281 and -214.0 °C for IS-9193, which has a marked effect on the clearing point of the mixture. Linear extrapolation of each of the libraries to zero concentration, the point representing the theoretical clearing point of the nematic reactive mesogen mixture, shows interception with the X-axis at 73.3 °C for BDH-1281 and 71.5 °C for IS-9193. The clearing point for this mixture obtained by DSC is approximately 70 °C, the deviation in the HT measurement attributed to experimental error and the approximate fitting of the two lines.

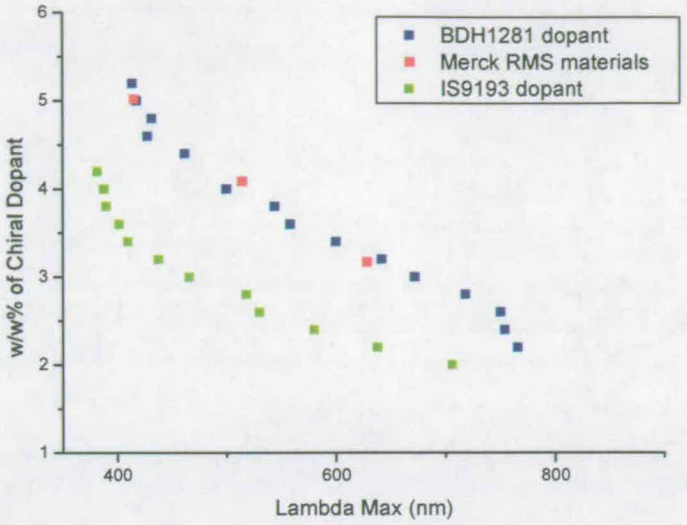

Figure 4.10: The dependence of λ_{max} of reflected light on the concentration, and type of chiral dopant incorporated into a nematic reactive mesogen formulation.

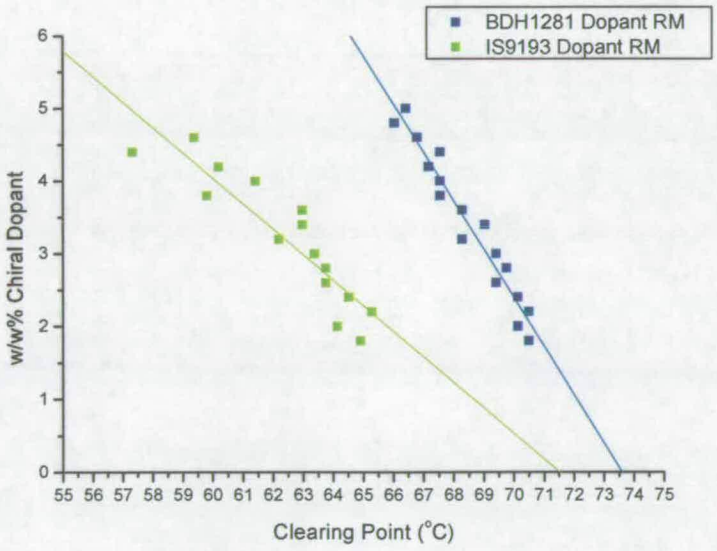

Figure 4.11: Clearing points of the two chiral nematic reactive mesogen formulation libraries containing increasing concentrations of chiral dopant

4.4.4 Theoretical Results

The calculation for the λ_{max} value introduced in Section 1.2.2 can be used to compare the HT results, and the Merck reference materials, with theoretical prediction.

$$\lambda_o = \tilde{n}.(c.\beta)^{-1} \qquad \textit{Equation 4.5}$$

The HTP of both chiral dopants are known (BDH-1281 β= 76 μm^{-1}, IS-9193 β = 100 μm^{-1}), and the mean refractive index of the nematic host, $\tilde{n}$, is approximately 1.55. Using these values, calculations to gain the λ_{max} at varying concentrations of dopant were performed and plotted together with the experimental results.

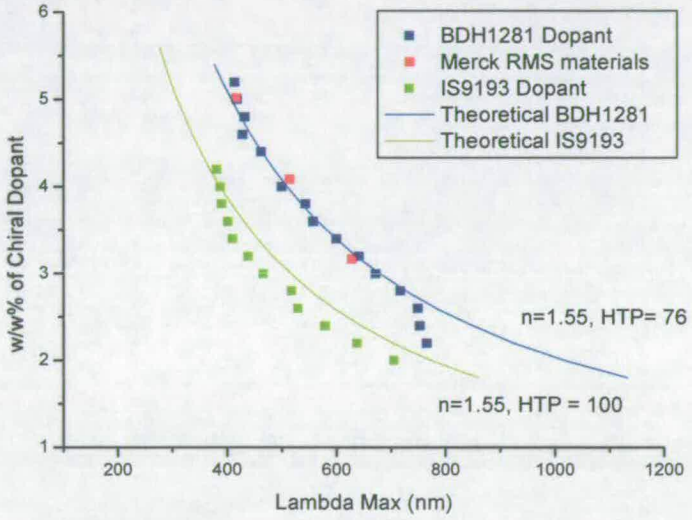

Figure 4.12: Comparison of theoretical and experimental values obtained both classically and by a HT process to reveal the relationship between the λ_{max} of reflected light on the concentration, and type of chiral dopant incorporated into a nematic reactive mesogen formulation

Figure 4.12 shows the HT formulated BDH-1281 and IS-9193 libraries, together with the three Merck RMS materials and the theoretical prediction for each library. An excellent correlation is seen for all of the BDH-1281 data points. The IS-9193 data points show a slight shift from the theoretical values to lower wavelengths. However, the shape of the data matches the theory well, suggesting that deviations are not a result of experimental error but instead due to variation in either the refractive index of the mixture or the HTP, from the

approximations used in the calculations. The refractive index is expected to deviate slightly due to the addition of increasing concentrations of chiral dopant into the nematic host. The literature value for HTP of the IS-9193 dopant is derived from measurements in a host of higher refractive index than that used in this experiment, and so this may also contribute to the discrepancy. Overall, it can be concluded that the theoretical and experimental results are in good agreement, both in the case of classically formulated reference materials, and in HT robotically formulated libraries.

4.5 Inkjet Printing for Film Formation

The use of liquid handling robotics for formulation allows for a rapid increase in the rate at which RM solutions can be produced. The liquid handling process can create a large number (>100) of formulations in a short space of time, and so in order to match this rate, a process is required in which many formulations can be coated in a fully automated manner. Unfortunately, thin film processing of the resulting solutions becomes the limiting step. Bar coating, even when using a parallel technique was difficult to adapt to a true HT methodology. At this time there did not exist a commercially available method for high-throughput coating, with most apparatus being designed for larger volume/area, single substrate work.

Previous studies have identified inkjet printing techniques to be invaluable for HT formulation,[41-43] including the use of such a technique for the thin film type deposition of polymer solutions onto a substrate.[44] Reactive mesogen solutions are inherently suitable for the process of IJP due to their solvent component. To date this type of HT film formation has only been applied to dilute (1 w/w %) polymer solutions,[44] through deposition of multiple drops in close proximity so that on contact with the substrate they join to form a larger film. In the current application, solutions used are generally of much higher concentrations, up to 33 w/w % solid content. However, the development of this technique for reactive mesogen films offers potential in enabling robotically formulated libraries to be printed onto substrates in a fully automated manner, greatly reducing the time required and therefore enabling the creation of larger datasets.

The migration of coating from a mechanical contact technique to a non-contact technique brings with it many problems, most importantly the issue of alignment and film quality. The mechanical forces and stresses exerted on the LC during coating play a part in the alignment

and structuring of the LC on the substrate surface. Spin coating or bar coating both involve directional shear forces, which orientate the bulk direction of the monomers on the substrate in the direction of shear. If these stresses are removed then the monomers experience no force by which surface alignment can take place. The study by Tekin et al[44] shows that gaining homogeneous films by IJP to be difficult, but progress has been made by the optimisation of solvents and solvent blends, and by variation of the pattern and distance in which adjacent spots are printed. However, the polymer systems which have been studied, due to their low concentration and different physical characteristics, will have little bearing on a high solids reactive mesogen system, leading to different behaviours on drying and hence different surface morphologies.

The work on HT formulation using inkjet printing techniques has shown that mixture formulation could be efficiently achieved by the overprinting of individual mixture components in single spots.[43] Therefore, it was proposed that a similar technique could be adapted in producing reactive mesogen film mixtures, overprinting in a grid to produce films with variable composition. Attempts at library formation in this way were unsuccessful, not only because of the inhomogeneous distribution of the chiral dopant but also because of the lack of significant alignment forces. The nematic mesophase, already aligned on the surface was not affected by the presence of the chiral moiety, instead forming a dual layer structure with the nematic film lying under the layer of solid chiral dopant. Due to the poor results and difficulty in optimisation of this formulation approach, the method was abandoned, instead relying on the robotic liquid handling method which had been previously shown to produce excellent results using IJP for film formation after the formulation process.

4.6 Design and Optimisation of the IJP Process

In describing the IJ process it is convenient to define 'spot' as the substance that has been deposited onto the substrate, and 'drop' as the number of drops dispensed in forming this spot. To create a film, a matrix of spots can be printed and optimised so that amalgamation of the matrix occurs on the substrate. In all experiments, the substrate used was unidirectional rubbed triacetylcellulose (TAC) film, which is widely used in the optoelectronics industries and chosen because of its optically transparent properties, which enable UV-vis transmission data to be obtained. The process of creating a film[44] is illustrated in Figure 4.13. A number of parameters must be considered to produce a film which is of

good homogeneity. The variables are the spacing between the spots in the XY directions, and the number of drops deposited on each spot position. The number of spots printed in each of the XY directions defines the dimensions of the film. For successful homogeneous film formation, the choice of solvent is crucial to prevent effects such as 'coffee rings'[45-47] discussed in section 4.6.2.

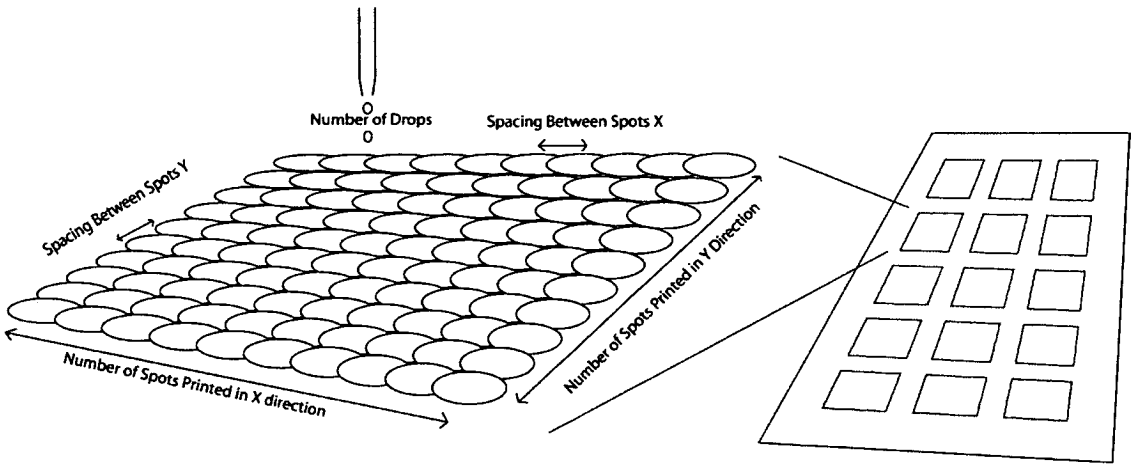

Figure 4.13: Schematic showing how films are created by printing of a matrix of overlapping spots. For optimal film quality, a number of parameters require optimisation.

4.6.1 Software

To achieve the printing of a matrix of spots, a software tool was required to provide control over each of the aforementioned parameters so that multiple films could be created and parameters optimised. The Microdrop software used for control of the IJ deposition is limited in its ability to create complex, repeatable patterns, but has capability for the creation of macro sequences for the execution of a batch list of commands. Due to the complexity of manually creating a sequence for the printing of a 100 spot matrix (spotting a single drop in a defined position requires typing seven lines into the macro consisting of 15 variables), an application was designed and coded from first principles in Microsoft Visual Basic 6 to be used in conjunction with the Microdrop control software. The application provides a simple, user-friendly interface in which instrument parameters and experimental conditions can be entered by the user. The aspiration position of each ink can be selected, as well as the flushing position, cleaning station and the associated times for filling, emptying and cleaning. The starting coordinates or spatial position of the substrate to be printed could also be selected. There are a number of parameters which define the film matrix. The software

allows the number of spots to be printed in the X and Y directions, the number of drops deposited per spot, and the spacing between each spot in the matrix to be defined. Additionally the number of times the film is reproduced can be defined, and an option is provided for the randomisation of matrix positions. In this mode the spatial position of samples is recorded and output as a text file for library devolution. For use in optimisation studies, the software has the ability to create sequences in which the spacing between the drops, or the number of drops deposited, can be varied so that the effect of these parameters on the film quality can be quickly determined.

This software provides a tool to perform many different experiments and has now found widespread use in our group, not only in the work on reactive mesogen coatings but also in biological, polymer and pigment applications. This application reduced the time to design and produce a macro sequence from days to seconds, and enabled a user with little knowledge of the Autodrop system to load samples and substrates, run the application, and within minutes create large libraries. The application and the source code are included on the supplementary material CD ROM (Appendix E3).

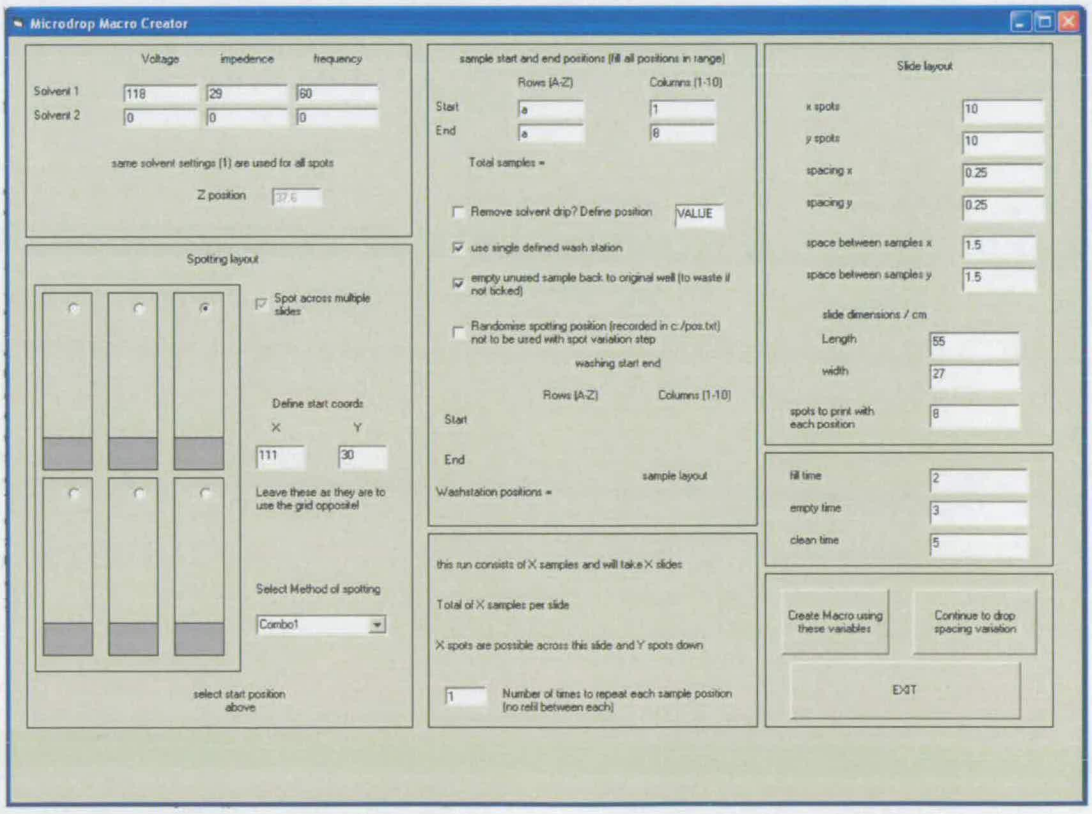

Figure 4.14: Software for the creation of reactive mesogen films by inkjet printing

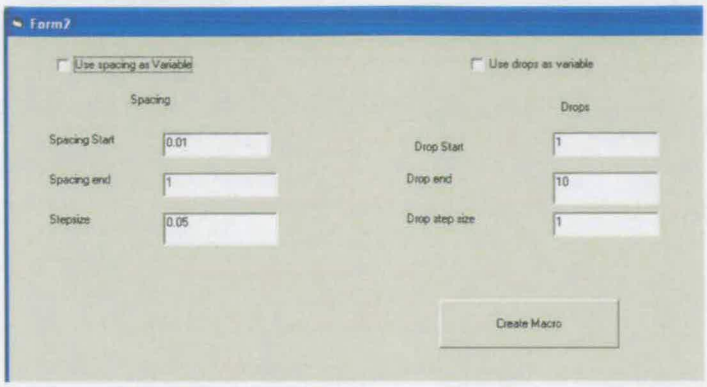

Figure 4.15: Software enabling the number of drops and spacing to be modified between subsequent printed films for efficient optimisation

4.6.2 Solvent Selection

Selecting a printing solvent is crucial in obtaining well-defined and homogeneous films. There are a number of properties which must be taken into consideration and optimised to achieve this aim, and to ensure acceptable and reproducible printability.[48,49] One of the major issues identified in the printing of polymer films is the appearance of a 'coffee ring' where the solid components are deposited around the edges of a dried printed drop.[44] (Figure 4.16)

Figure 4.16: An image illustrating homogeneous film formation (middle) and a coffee ring (left). The picture on the right is a drop of coffee allowed to dry, and shows the name origin for this effect.

The 'coffee ring' effect has been studied in great detail by Deegan *et al*[45-47] and Hu *et al*,[50] who concluded that the cause was due to the contact line of the deposited drop becoming 'pinned' to irregularities on the surface, and therefore unable to move. As evaporation removes solvent from the contact line around the circumference of the pinned drop,[45,47] a replenishing flow of solvent from the centre to the edges is established, which maintains the

contact line. The overall result is to decrease the drop volume without a reduction in its diameter. This process of solvent replenishment toward the edges continues, transporting solute towards the contact line and therefore creating a ring like deposit on complete evaporation of the solvent.[47,48]

To prevent the 'coffee ring' effect a low-vapour-pressure solvent can be used to reduce the rate of evaporation, therefore increasing homogeneity. A explanation for this process is that at slower evaporation rates the time for the de-pinning of the contact line matches the rate of evaporation.[44,48] An alternative approach is the use of two-component solvent mixtures.[44,48] Evaporation of the higher boiling point solvent creates a higher concentration of the lower boiling point solvent, thus reducing the rate of evaporation at the contact line[44,48] (Figure 4.17). Another application of dual solvent systems is in the use of solvents with high and low boiling points, the high boiling solvent having low solubility for the solute. As evaporation occurs the solvent composition becomes richer in the solvent with poorer solubility, and therefore the solute precipitates before ring formation can occur.[48,50] This approach is not so desirable as rapid crystallisation may be detrimental to the morphology of the film.[48]

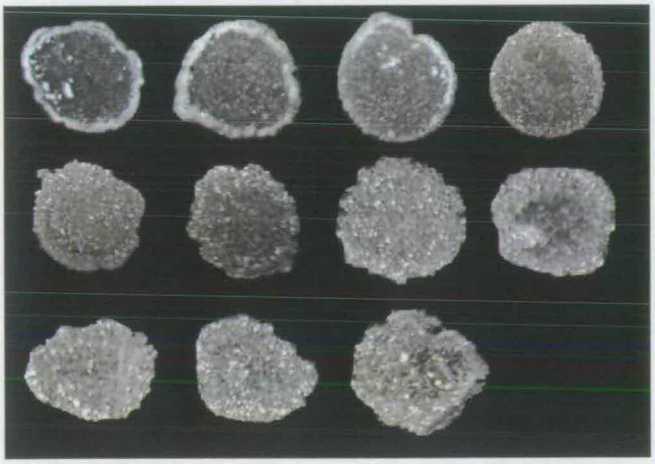

Figure 4.17: Drop cast solutions of a liquid crystal (RM257) in ethyl acetate with drops of methyl benzoate added to the solution. As the concentration of methyl benzoate is increased (left to right) the coffee ring around the circumference of the drop is suppressed.

Another important parameter to optimise is the interaction of solvent with the substrate. Firstly, this process ensures that the solvent is compatible with the material and does not cloud or dissolve the substrate. Secondly, the wetting of the solvent on the substrate surface

needs careful consideration. In the construction of a film, a solvent with good wetting of the substrate will spread too efficiently, therefore creating a broad, unconfined layer with poor homogeneity, which in a dense library may run into adjacent films. In contrast, a solvent with poor wetting will not adhere to the substrate in the place it was deposited, forming an irregular shaped and irreproducible film (Figure 4.18).[44]

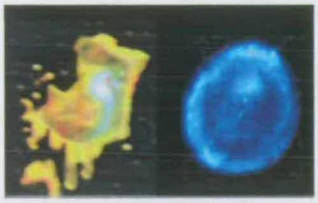

Figure 4.18: A film created using solvent with poor wetting characteristics on the substrate (left) and another showing excessive substrate wetting (right)

Literature on the IJP of polymer films describes a range of solvents which can be successfully printed using on demand piezo-actuated printing.[44,48,49] A selection of these solvents, covering a range of boiling points and vapour pressures were assessed, together with two-component mixtures comprising a high-boiling and low-boiling component. To assess suitability each solvent was analysed by a number of criteria. Solvents which did not pass criteria were excluded from the study (Table 4.3).

Table 4.3 shows the results of the experiment. Substrate compatibility was tested by drop casting each of the solvents onto TAC film, removing any residual solvent after five minutes under a flow of nitrogen. Solvents that clouded or reacted with the film were deemed unsuitable and seven solvents were excluded at this point. The remaining solvents were tested for their inkjet performance, judging the formation and reproducibility of films, created by printing a formulation consisting of the majority components Merck RMS (50:50 RM257/ RM82), representative of the types of compound to be printed. An ideal film should show a homogeneous and well-defined film, with no imperfections, voids, or ring effects.

Commercial RM solutions (Merck Chemicals Ltd.) consisted of a 33 w/w % solid composition in PGMEA. Attempted printing of one such solution following the optimisation of jetting parameters to ensure adequate drop formation and reliable printing, revealed that the latency (the minimum time before nozzle blocking after standing idle) of this formulation was poor. The time over which the solution was aspirated into the print head, and the print

head moved into position for printing, was sufficient to cause blocking of the nozzle through the crystallisation of solids as a result of solvent evaporation.[49] The speed of crystallisation is thought to be due to the high solid content of such solutions and therefore can be avoided using less concentrated solutions. In previous work (Chapter 3) on the printing of liquid crystal materials, 17 w/w % solids had been used to good effect. To begin the evaluation of conditions this ratio was used to screen for solvents able to reproducibly print solutions at this concentration.

Solvent	Vapor Pressure (mmHg @ °C)	Boiling Point (°C)	Compatable with TAC	Print quality of 20% solution	Film reproducability
Ethyl acetate	76 @ 20	77	No	-	-
N-Methylpyrollidine	0.5 @ 25	202	Yes	Deforms TAC	-
Dimethylformamide	2.7 @ 20	153	yes	Deforms TAC	-
Propylene glycol monomethyl ether acetate(PGMEA)	3.7 @ 20	146	Yes	Spots spread	Poor
Toluene	22 @ 20	110	Yes	Good films	Good
Toluene / cyclohexanone(70:30)	22 @ 20 / 5 @ 26	110 / 155.4	Yes	Good films	Good
Ethyl acetate / methyl benzoate(70:30)	76 @ 20 / 1 @ 40	77 / 199	No	-	-
Xylene	51 @ 20	141	Yes	Good films	Fair
Methyl ethyl ketone	78 @ 20	79	No	-	-
Acetophenone	0.4 @ 25	103	Yes	Good films	Good
Methyl benzoate	1 @ 40	199	No	-	-
Butyl acetate	15 @ 25	121	yes	Poor	Poor
Dioxane	37 @ 25	102	No	-	-
Ethylene glycol dimethyl ether	48 @ 20	85	No	-	-
PGMEA / Ethyl acetate (70:30)	3 @ 20/76 @ 20	146 / 77	no	-	-

Table 4.3: Grid for solvent selection experiments. Only solvents that passed the set criteria were carried forward.

Prior to printing each solvent was assessed to determine optimised jetting parameters, ensuring the formation of single drops without observable tails or satellites. Using identical parameters for each solvent of 105 V and a 30 μs pulse width at 60 Hz, gave good drop formation. Films of each solution were printed in duplicate, using 0.25 mm spacing and 10 drops per spot over a 10 x 10 matrix. These parameters were chosen based on the observation that a spot of 17 w/w % solids solution consisting of 10 drops has a diameter of approx. 0.5 mm. A spacing of 0.25 mm should therefore ensure sufficient amalgamation of

adjacent spots. Once printing was complete, each film was assessed for its reproducibility and quality of film formation to eliminate solvents that were not amenable to this process. Three solvents were identified from this process, of which the two with the most homogeneous film formation were toluene / cyclohexanone (70:30) and acetophenone. Of these acetophenone was the most desirable, due to its low vapour pressure and low volatility, showing a weight loss of just 0.5 % over 20 minutes in a 96-well plate compared with 6 % loss for toluene / cyclohexanone. When printing a large library of films this becomes important so that the first solution aspirated and deposited in the library has a negligible concentration difference to the solution aspirated and deposited last.

4.6.3 Solute Concentration and Drop Morphology

The production of films using an IJP matrix requires that three parameters are optimised. These are the amount of solvent to be used in the solutions, the number of drops to be deposited per spot and the spacing between the spots. This task is made more difficult due to the interaction of all three parameters on the film quality. If the concentration of reactive mesogen in solution is too high then this can result in crystallisation in the nozzle tip and hence prevent or deflect the drop's formation. If the concentration is too low, there will not be a sufficient amount of reactive mesogen printed, resulting in selective reflection of the light not being observed. In order to assess the morphology of IJ printed spots and films, a method of visualisation was required. Into the reactive mesogen formulation a fluorescent dye was incorporated, which allowed the morphology of the dried spots to be easily visualised. The first experiment for matrix optimisation was to determine the relationship between the solid content of the reactive mesogen solution, the morphology of spots formed using this solution, and the number of drops deposited.

A fluorescent dye was added to the reactive mesogen formulation containing 1% chiral dopant BDH-1281, and solutions of 17, 20, 23 and 26 w/w % solid were produced using the previously identified solvent system of acetophenone. Using IJP in conjunction with the software described previously, sequences of drops were printed from each solution over the range 1 to 13 drops per spot in a 1x4 matrix, onto a rubbed TAC substrate. On completion the spots were annealed at 60 °C for 5 minutes before fluorescence analysis. Using the FIPS-2 software the spots could be clearly seen and the diameter of each of the spots could be measured. The colour gradient is used to visualise the fluorescence intensity, and hence gives

an indication of the distribution of solids in the dried drop. The fluorescence gradient can also be used to represent height, therefore enabling a 3D representation of each drop (Figure 4.21)

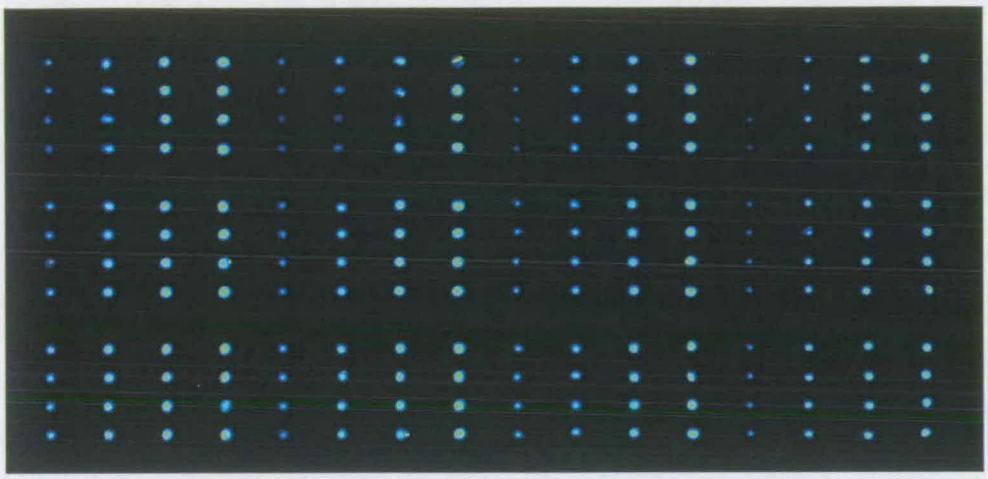

Figure 4.19: Fluorescence analysis of spots created using increasing number of drops (1 to 12), and with increasing of solid content (17 w/w % to 27 w/w %)

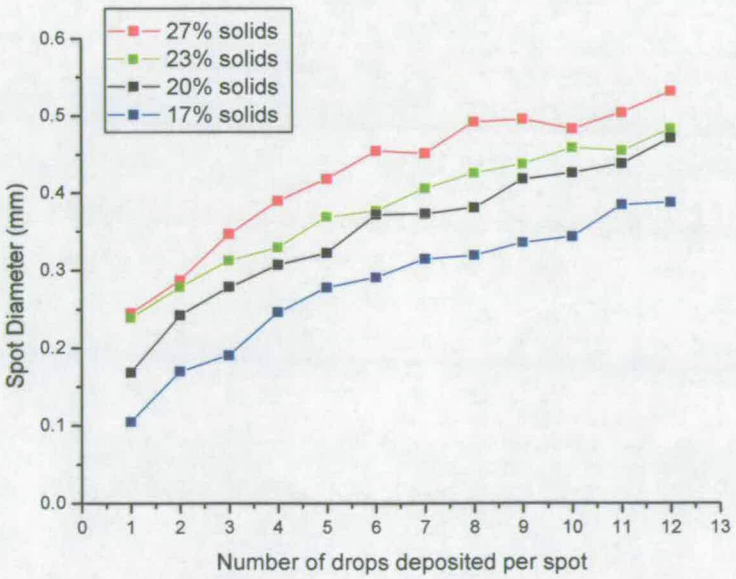

Figure 4.20: Relationship between the diameter of a spot to the solid content and number of drops deposited in the spot.

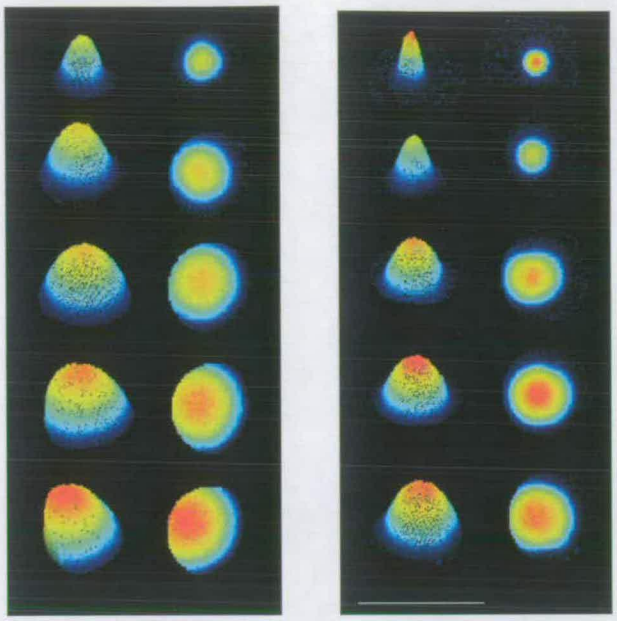

Figure 4.21: The increase in size and intensity of a 27 w/w % reactive mesogen solids solution from at 1, 3, 6, 9, 12 drops (Left) and the same images using the 17% reactive mesogen solids solution (Right)

The results show that as the solids content of the reactive mesogen solution becomes greater, the spots become larger in diameter due to the increase amount of substance in the mixture. As the number of drops increase, it is seen that the morphology of the spot remains well defined and symmetrical. However, at nine drops the spot begins to deform, having a greater concentration of reactive mesogen on one side than the other. This is an undesirable effect when trying to produce homogeneous films. When using a 17 w/w % solution the spot did not show this deterioration, instead remaining well defined throughout the range of drops. Low solvent concentrations were therefore used to ensure reliability, and prevent crystallisation in printing runs where 100's of films would be produced.

The diameter of the spots formed can be used as a guide to the range of spot spacing that should be used. For efficient amalgamation the spots should be overlapped a distance greater than their radius, but less than their diameter. Considering a spot with eight drops this equates to a minimum spacing at 17 w/w % reactive mesogen solids of 0.15 mm, and a maximum spacing of 0.3 mm. For the 27 w/w % solution this increases to a minimum of 0.25 mm and a maximum of 0.5 mm. Therefore, if adopting a low solids content of 17 w/w %, then for matrix optimisation values between 0.15 and 0.3 mm should be used to probe for the most efficient film formation spacing.

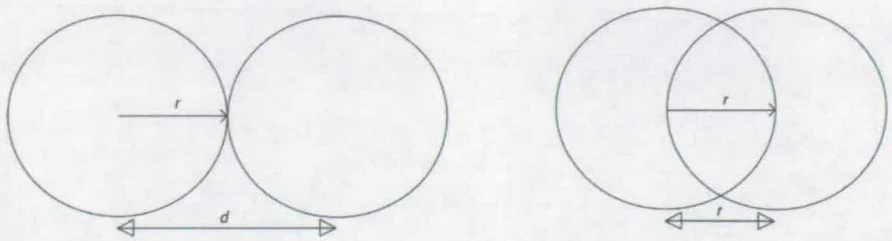

Figure 4.22: The range over which efficient amalgamation of adjacently printed spots should be printed to form films. Distances greater than the spots diameter will result in no overlap, while distances less than the spots radius may result in films of poor morphology.

4.6.4 Film Quality and Matrix Optimisation

To optimise the film formation process a 10x10 array of spots was printed, using a 17 w/w % reactive mesogen solids solution in acetophenone, and containing a fluorescent dye. Using the visual basic software described previously the parameters were entered to vary the number of drops per spot and the spacing between spots, to form a matrix in which the two parameters were both varied. Using the results of the previous experiments the drops per spot was varied between 6 and 12 drops to ensure homogeneous drop formation, and the spacing between adjacent spots was varied between 0.16 mm and 0.32 mm in 0.04 mm steps. After printing and UV curing of the films, they were profiled using fluorescence analysis. The films in Figure 4.23 show a small section of the library where ideal film formation was observed

Figure 4.23 illustrates a number of features. The top row in which the spacing is 0.16 mm the spots coalesce. However, more of a large drop is formed rather than a film due to excessive amounts of solid being deposited in a small area. It can be seen that by drawing apart the adjacent spots (moving down the images in columns), a film is formed until the spacing becomes too large (0.28 mm) and voids in the film begin to form where the diameter is not sufficient for coalescence. This can be overcome by increasing the number of drops deposited, as seen in the bottom right plot, although in this case inconsistencies still appear. As the spots are pulled apart, the formation of a coffee stain effect can be seen as material collects around the edges of the spot and evaporation occurs from the centre. This can be reduced by further separation of the spots, and the middle film surface shows a reasonably good morphology, exhibiting a flat top, defined square shape and only a small degree of

coffee staining, At approximately 0.24 mm the film shows a good morphology, at eight drops per spot the surface is homogeneous, and no voids are seen. It should be noted that a small amount of the coffee ring can be seen in this sample, visualised by the yellow/orange ring around the perimeter of the sample. This could be removed by increasing the spacing slightly to 0.25 mm. Using the results of this experiment, films could be produced using a spacing of 0.25 mm and 8 drops per spot.

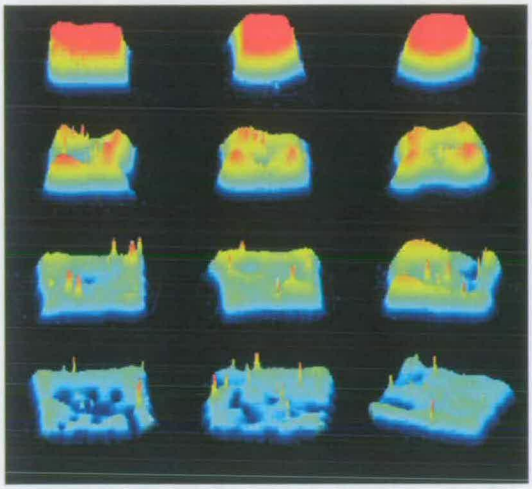

Figure 4.23: Fluorescence analysis of IJ printed films. Matrix created using drops per spot of 7, 8, 9 from left to right and spacing of 0.16 mm, 0.20 mm, 0.24 mm, 0.28 mm from top to bottom,

4.6.5 Film Characterisation and Data Handling

Using IJP, the reactive mesogen films which are formed have a surface area of only 2.5 mm^2 and therefore they are unsuitable for UV-Vis analysis using a traditional instrument. For characterisation of samples of this size, a fibre optic UV-vis (FO UV-vis) source and analyser (Ocean Optics) were used (Figure 4.24). The UV-vis spectrum of each film was obtained by passing the film through the spectrometer in the order films were printed, saving the data with a numerical prefix from *1* to *x* where *x* is the total number of films printed, so that the number of the spectra corresponds to the film position. This enables films printed using position randomisation to be identified by comparison with the file produced by the printing application relating the position of the sample on the substrate to the well from which the solution was aspirated.

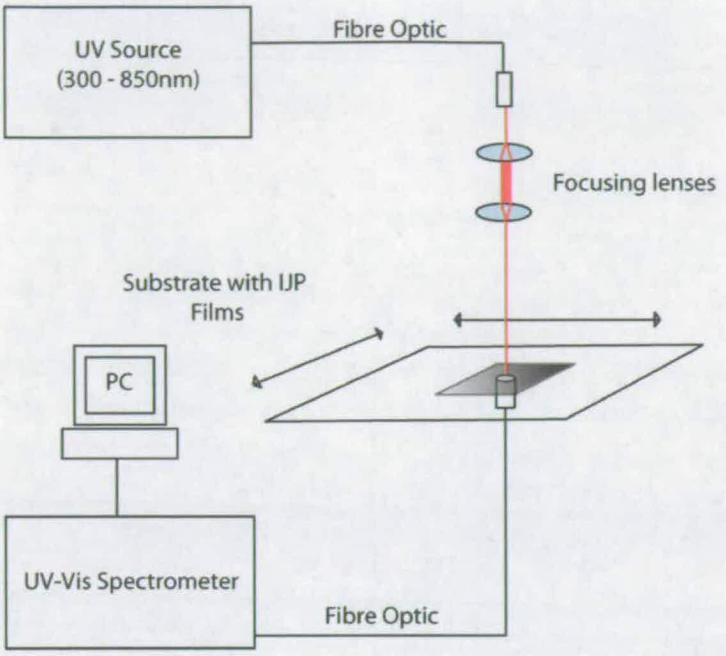

Figure 4.24: Schematic of the fibre optic UV-Vis spectrometer. The light source emerging from a fibre optic cable is passed through two height adjustable lenses, which broaden the beam and allow it to be focussed onto the end of the second fibre optic cable whilst passing through the IJP substrate. The fibre optic cable is connected to a spectrometer, interfaced to a PC via a USB.

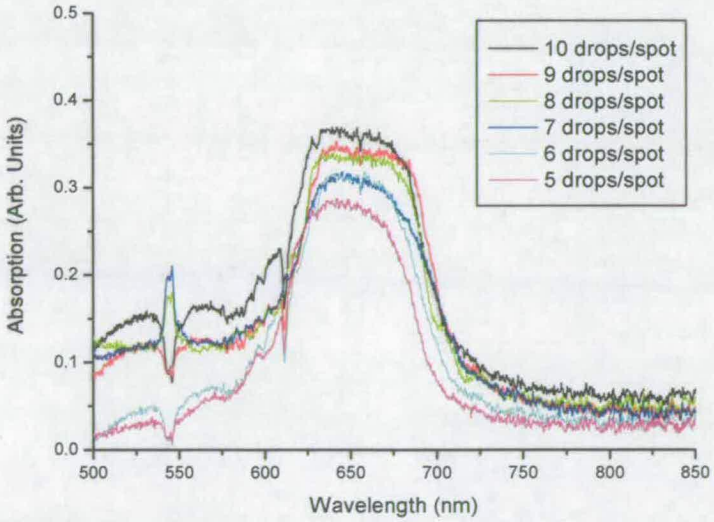

Figure 4.25: The fibre optic UV-Vis absorption spectra of a doped chiral nematic reactive mesogen film printed by inkjet with between 5 and 10 drops forming each spot in a 10x10 matrix, deposited to form a film.

Figure 4.25 shows the absorption spectra of films created using between 5 and 10 drops per spot, showing that the intensity of the absorption is not significantly affected by changing the morphology and amount of reactive mesogen solid in the film.

In the analysis of multiple films, a number of individual spectra are gained from the ocean optics software and outputted as ASCII files. Each of these files requires processing into Microsoft Excel, and data plotting such that λ_{max} can be obtained. For large libraries, to prevent an analysis bottleneck automation is required, and therefore an Excel VBA macro was written (Appendix E4). The macro imports each library spectra and automatically produces plots of wavelength vs. absorption, prompting the user to enter λ_{max} value for each plot before exporting the data into a text file. Combination of the text file containing the well plate reference to the film position and the file containing the film position to the λ_{max}, allowed the concentration of dopant and the λ_{max} values to be plotted.

4.6.6 Reproducibility

To check the analysis reproducibility of films produced by IJP, a range of samples with varying λ_{max} values were printed in duplicate and analysed using the fibre optic UV-vis apparatus. The data illustrated in Figure 4.26 shows the λ_{max} (duplicate analysis) plotted against one another. The deviation between the two analyses was determined to be a maximum of ±36 nm.

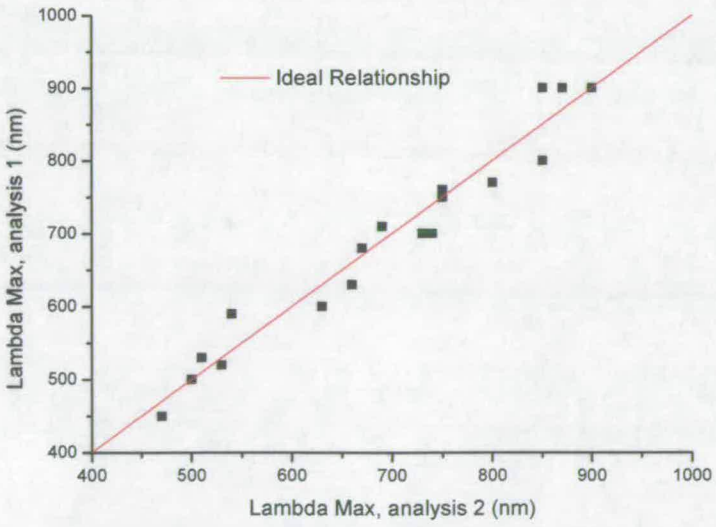

Figure 4.26: Duplicate analysis of inkjet printed films using the fibre optic UV-Vis spectrometer. The first and second analyses were plotted against each other. The line shows an ideal linear relationship.

4.7 The Influence of Enatiomeric Excess on Selective Reflection Wavelength

In previous experiments only the pure left-handed enantiomer of the chiral dopant IS-9193 was used to investigate the relationship between concentration of chiral dopant and λ_{max}. It is also possible to create reflective films using the opposite enantiomer. Visually the films will show identical selective reflection. However the sense of chirality of the helical pitch is reversed and so the LH dopant will reflect only RH polarised light whereas the RH dopant will reflect only LH polarised light.[51] It is also possible to create films using a mix of both LH and RH components, equivalent to using an enantiomeric mix of a chiral dopant.[52] The concept of enantiomeric excess, *ee*, can be used to describe this mixture of the *R* (right handed sense) and *S* (left handed sense) enatiomers.[53]

$$ee(\%) = ((R-S) / (R+S)) * 100 \qquad \textit{Equation 4.1}$$

Therefore, a dopant in exclusive *R* form has an *ee* of 100% while a 50/50 mix of *R* and *S* enantiomers has an *ee* of 0% (*i.e.* racemic). In the study of selectively reflective films the theoretical equation can be modified to incorporate the *ee* of the chiral dopant, the pitch and hence the wavelength of λ_{max} sensitive to chiral perturbation .[54]

$$\lambda_o = \tilde{n}.(c.\beta.ee)^{-1} \qquad \textit{Equation 4.2}$$

$$\textit{therefore;}\quad \lambda_o = \tilde{n}.(c.\beta.[(R-S)/(R+S)])^{-1} \qquad \textit{Equation 4.3}$$

The *ee* is expressed as an number between 1 and 0 (100 % to 0 %) and therefore at 100 % *ee* there is no modification to the selective reflection characteristics, whereas at 50 % *ee* the pitch and hence the selective reflection properties tend to infinity, becoming essentially nematic.[52] These properties are due to one enantiomer compensating the HTP of the other, giving an effect similar to reducing the concentration of the enatiomerically pure component in the formulation. These relationships can be explored experimentally, using a similar strategy to that adopted previously. In this case, the size of the library is increased by the inclusion of a second variable. To formulate such a library manually is neither practical nor effective, and therefore the adaptation of the process to high-throughput technology is desirable. By the development of automated and high-throughput techniques a concentration

/ wavelength dependence can be determined by the rapid formulation, coating and screening of a large number of individual components. Such a library was created to test the techniques of formulation, inkjet printing, characterisation and data handling, and the validity of the theoretical calculation. This was achieved using two chiral dopants synthesised within Merck. IS-9193 (LH) and IS-9326 (RH) are structurally identical, rotameric chiral dopants of opposite absolute configuration. These components can be incorporated individually to produce films exhibiting either RH or LH selectively reflective films. In this study, the two materials were combined to accuracy influence the enatomeric purity *ee,* so that the relationship between *ee* and reflected λ_{max} could be investigated. Figure 4.27 is a theoretical plot of the expected dependence.

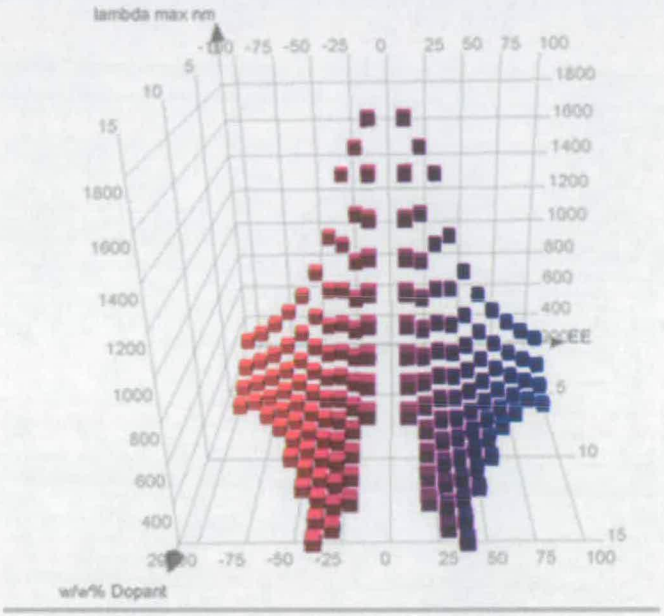

Figure 4.27: Theoretical results of the relationship between dopant concentration, ee and λ_{max}, plotted in three dimensions.

4.7.1 Formulation

Libraries were created by varying the total concentration of chiral dopant solution incorporated in the nematic host, then varying the ratio of the LH and RH chiral rotamers (IS-9193 and IS-9326) used to formulate each of these concentrations. The nematic host consists of reactive mesogen and photo-initiation components identical to those described in section 4.2.1 and Table 4.1. The concentrations investigated were selected over a wide range

(4 to 14.5 %), and the *ee* of each formulation was varied from 100% to -100% in steps of 10%, equating to concentrations of between 0 and 100 % of each dopant.

To incorporate such large concentrations of dopant, and additionally to enable to direct IJP of the solutions without the need for additional dilution, the concentration of solids was lowered compared to previous experiments, to a 20 w/w % solution. For all formulations acetophenone was used due to its slow evaporation at room temperature and its superior film formation. The three component strategy (section 4.3.1) was employed, creating dopant and makeup solutions at 5 w/w %, and reactive mesogen solution at 35 w/w %.

The large number of mixtures created in this experiment necessitated the use of a 96-well plate format, which was beneficial for a number of reasons. Previously, using the bar coating technique the volume of material required was greater than the capacity of a 96-well plate. The use of the IJP technique only requires μL of each mixture and therefore the formulation can be achieved on a smaller scale, dispensing 200 μL into each well. Additionally, the use of this format for formulation eliminates the need for time-consuming reformatting. The volumes of each component transferred, as entered into the Gilson liquid handling software, are shown in Table 4.4 and Table 4.5. The volume of reactive mesogen solution was constant, and volumes of dopant solution were increased whilst volumes of makeup solution were reduced by an equivalent amount. At the highest concentration of chiral dopant no makeup solution was dispensed. To achieve 168 formulations two 96-well plates were required. The solutions used in the formulation were of lower viscosity than previously dispensed compositions due to the lower solid contents, and therefore the dispensing rate was increased to a rate of 500 μL min^{-1}. This rate halves the time taken for formulation, preventing unwanted solvent evaporation.

Vials	1 to 21	22 to 42	43 to 63	64 to 84	85 to 105	106 to 126	127 to 147	148 to 168
ee	100 to -100	100 to -100	100 to -100	100 to -100	100 to -100	100 to -100	100 to -100	100 to -100
dopant concentration (% w/w)	3.96	5.35	6.78	8.25	9.75	11.30	12.89	14.53
Total volume of dopant solution (μl)	30	40	50	60	70	80	90	100
Volume of Make-up solution (μl)	70	60	50	40	30	20	10	0
Volume of RM solution (μl)	100	100	100	100	100	100	100	100

Table 4.4: The variation in overall dopant concentration in the library. Each concentration of dopant is then divided into 21 (Table 4.5) to incorporate values of ee between 100 and -100.

Vial	1	2	3	4	5	6	7
Volume of IS-9193 solution (µl)	30	29	27	26	24	23	21
Volume of IS-9326 solution (µl)	0	1	3	4	6	7	9
Enantomeric Excess	100.0	90.0	80.0	70.0	60.0	50.0	40.0
Vial	**8**	**9**	**10**	**11**	**12**	**13**	**14**
Volume of IS-9193 solution (µl)	20	18	17	15	14	12	11
Volume of IS-9326 solution (µl)	10	12	13	15	16	18	19
Enantomeric Excess	30.0	20.0	10.0	0.0	-10	-20	-30
Vial	**15**	**16**	**17**	**18**	**19**	**20**	**21**
Volume of IS-9193 solution (µl)	9	8	6	5	3	2	0
Volume of IS-9326 solution (µl)	21	22	24	25	27	28	30
Enantomeric Excess	-40	-50	-60	-70	-80	-90	-100

Table 4.5: Representative formulations for vials 1 to 21 comprising 30 µL of dopant solution split between dopants IS-9193 and IS-9326 to create variable values of ee.

4.7.2 Printing and Characterisation

Following the formulation process, the well plate was immediately loaded into the Microdrop apparatus and programmed to print in randomised duplicated positions, matrices of 10 x 10 spots consisting of 8 drops per spot, to form thin films of reactive mesogens on TAC substrate. The positions of printed samples were output as a text file relating the coordinates of the 96-well-plate to the print position, numbered sequentially across the substrate from right to left and starting at the top right hand print position. The completed library is shown in Figure 4.28. The large substrate was cut into strips of 12 x 3 samples and each strip analysed using the fibre optic UV-vis spectrometer and associated data handling macro (Appendix E4), to obtain the average λ_{max} value for each of the 168 formulations.

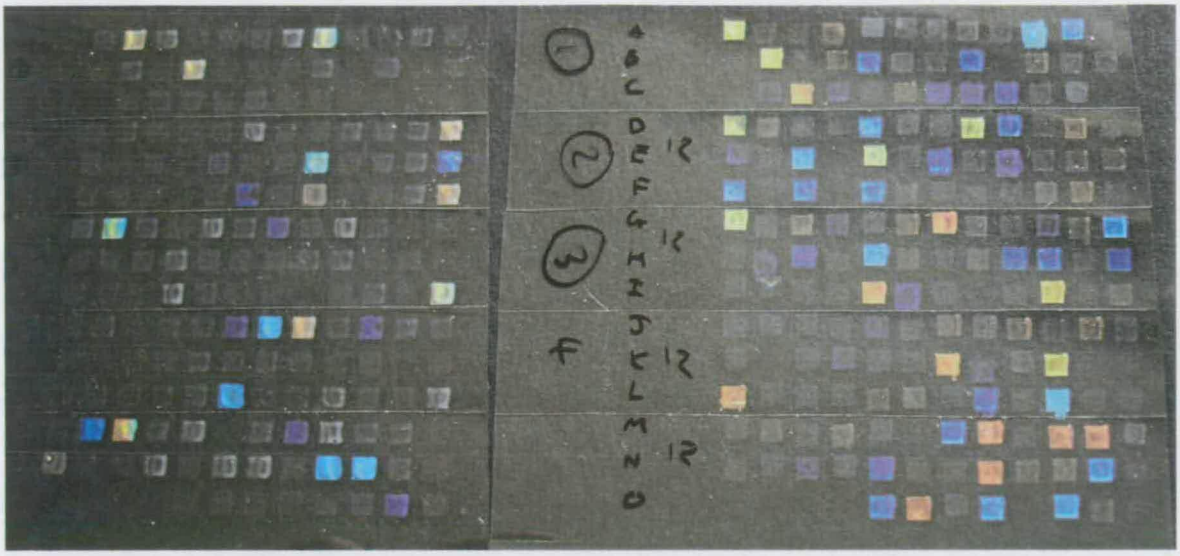

Figure 4.28: Robotically formulated inkjet printed library showing films, printed in duplicate exhibiting selective reflection properties

4.7.3 Results

Figure 4.29 shows the experimental data plotted in two dimensions, the dashed lines representing the theoretical λ_{max} values for changes in concentration, *c*, calculated using Equation 4.9 (values of 1.55 for the refractive index, and 100 μm^{-1} for the HTP were used). The experimental data can be seen to show good correlation to theory, with exponentially increasing values of λ_{max} as the *ee* is reduced to zero. It can also be seen that as the concentration of the dopant is reduced the curve broadens. Figure 4.30 represents the same results in a 3D plot. Figure 4.31 illustrates the theoretical results, which again exhibits good correlation to experimental results, recreating the same envelope.

Slight deviation of the experimental results, showing an error of greater magnitude than the standard derivation in addition to a number of absent data points, indicates a limitation of the robotic formulation method. During formulation, in order to dispense into a 96-well format the robot was operated on the limit of dispensing accuracy (1 µL), and therefore the reproducibility and accuracy may have been sacrificed.

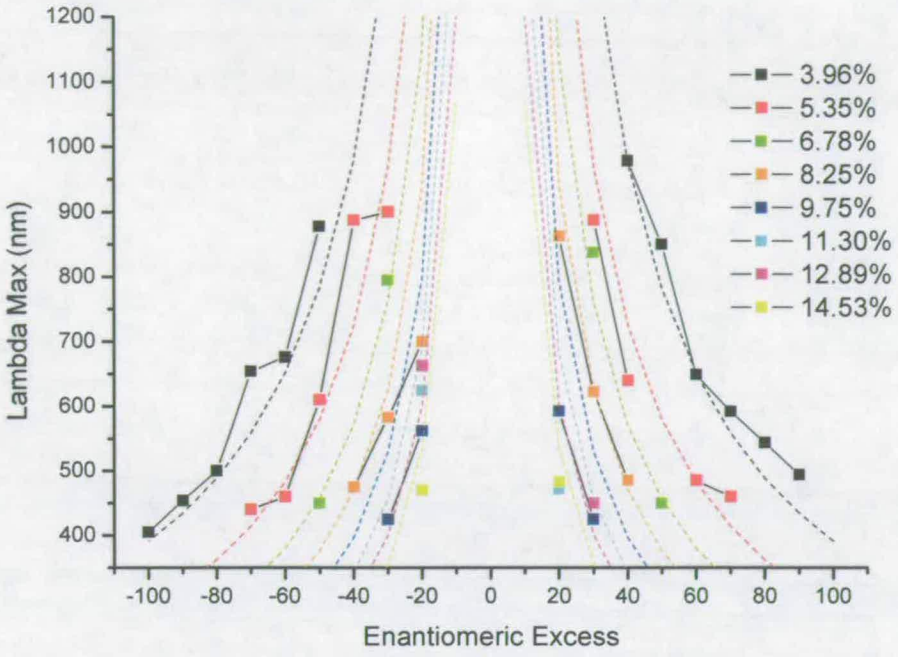

Figure 4.29: Robotically formulated inkjet printed library revealing the relationship between dopant concentration, ee and λ_{max}

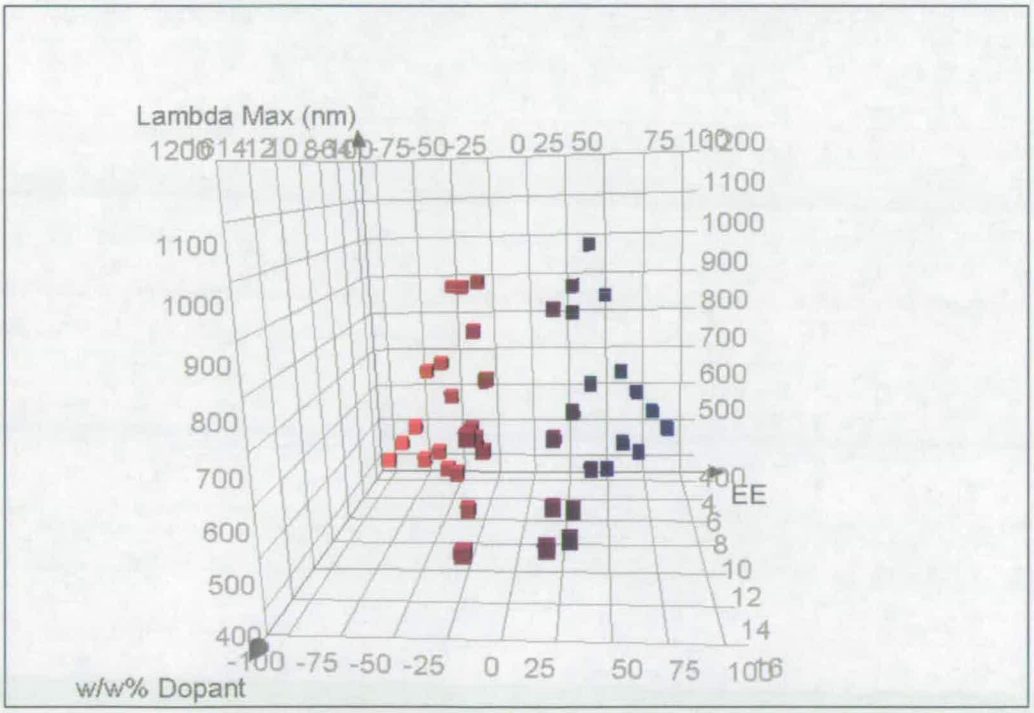

Figure 4.30: Robotically formulated inkjet printed library revealing the relationship between dopant concentration, ee and λ_{max} plotted in three dimensions.

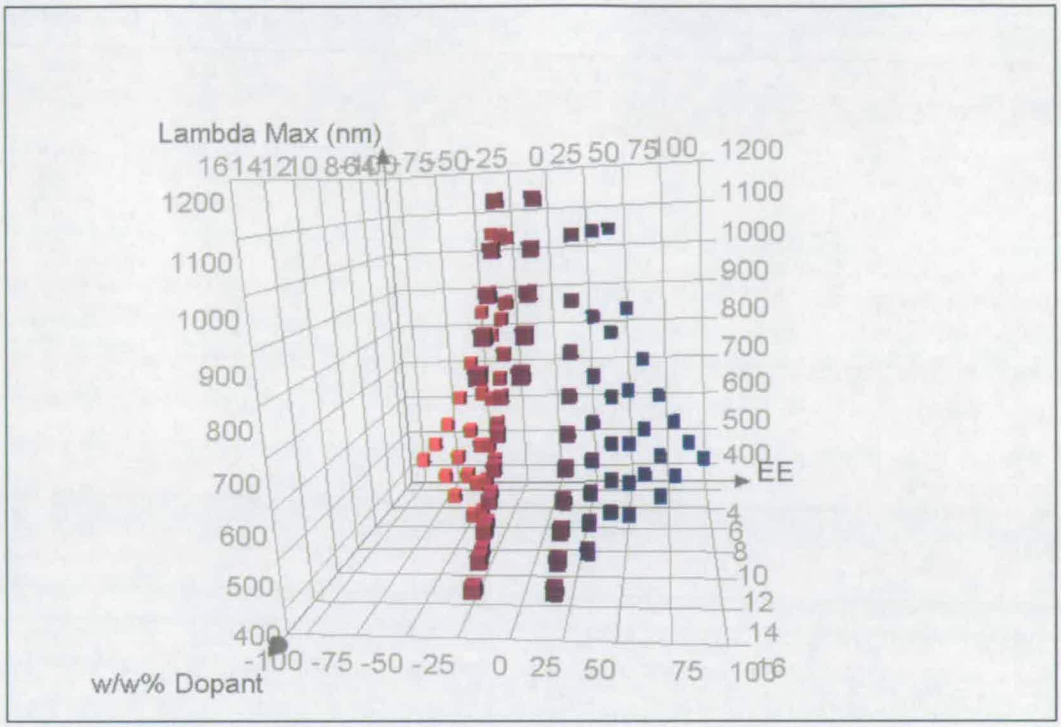

Figure 4.31: The theoretical results of the relationship between dopant concentration, ee, and λ_{max}.

Another problem, inherent to the experiment is the small number of data points collected at each concentration. At higher concentrations, only one film was obtained which exhibited a measurable λ_{max} reflection within the UV-vis spectrum. At lower concentration the curve is broader and hence the rate of change smaller, therefore changing the *ee* in steps of 10% produces many data points. At higher dopant concentrations, the rate of change is much greater (tending to infinity) hence a small increase in the *ee* of the dopant results in a massive change to the pitch of the chiral nematic. The result is that the range over which a UV-Vis reflection can be observed is miniscule. More data points would show a more conclusive fit, but the outline could be visualised adequately using the current data.

At higher concentrations, the experimental data are seen to shift more towards zero *ee* values than the theoretical data. This can be explained by the relatively large concentration of the dopant in the nematic host which modifies the refractive index of the material, and hence the theory does not correlate well for these compositions. This is a known limitation of the theoretical approach, which is only valid at low concentrations.

4.7.4 Discussion

The technique of IJP and UV analysis of thin films has been found to be successful in obtaining reproducible results, but the experiment has shown that the process requires improvements in some areas, such as in the quality of the printed films. In the experiment films were of variable quality, some exhibiting coffee drop effects while others were inhomogeneous producing cloudy, poorly aligned films. These effects can be eliminated by a more comprehensive investigation into printing solvents, dual solvent systems and printing conditions which due to time constraints was not feasible in this work.

The major limitation in the experiment was using the robotic liquid handling technique for formulation. Although this technique is useful in formulation of small libraries on 1.5ml scale, the problem occurs when larger libraries are produced in the 96-well format. The small quantities of chiral dopants, in combination with the solvent volume limitation, can compromise the accuracy of the experiment. Due to the strong dependence of the pitch on chiral dopant concentration, small deviations in the volume dispensed can cause large changes in λ_{max}. The minimum dispense volume also limits the number of data points which can be obtained. In order to produce more data points requires a smaller increase of chiral dopant, unobtainable using the Gilson apparatus.

Due to time restraints, a comprehensive optimisation of this technique was not possible. However, three adaptations can be made to the technique to overcome many of the more important problems, improving the reliability of the method. The first improvement is to extend the characterisation analysis range into the IR, to investigate the behaviour of higher concentrations of chiral dopant and low concentrations near values of 0% *ee*. This can be achieved by using a UV/vis/NIR spectrometer to extent the analysis range to values of 2500 nm. Below 400 nm expansion is difficult due to absorption of the triacetylcellulose substrate.

The second improvement would be to replace the Gilson liquid handling apparatus with a system able to accurately dispense smaller quantities of liquid. One approach to this is to use the Microdrop system as a micro-liquid handler, programming the reformatting of source reactive mesogen and dopant solutions into a 96-well plate format by varying the number of drops deposited into each well to control the concentration of components. On completion, each of the formulations can then be printed directly from the 96-well plate onto the substrate. Not only would such a method give much greater control and reproducibility in formulation, but it can also streamline the process, making it truly high-throughput and requiring no user intervention. To achieve this would require the development of the

software application in section 4.6.1 to include the ability to formulate libraries into a 96-well plate. Finally to increase the throughput and increase the accuracy of fibre optic spectroscopy an automated X-Y stage could be incorporated. This would speed up the data collection process and additionally allow many more measurements to be taken at defined areas on the film. Averaging of these data points will reduce the effects of small deviation in the λ_{max}, reducing the errors discussed previously.

4.8 Conclusions

In this chapter, the application of high-throughput technologies to the field of liquid crystal reactive mesogens was investigated. Robotic formulation was shown to be a feasible and highly-adaptable approach to the creation of chiral nematic reactive mesogen libraries, although questions over reliability at low-dispense volumes were highlighted. A library, comprising an increasing concentration of two chiral dopants with different helical twisting power was formulated, in order to investigate the effect of dopant concentration on the wavelength of selective reflection. The library was deposited as a thin film using a parallel bar coating technique and was found to show excellent correlation with the results obtained using commercial reference materials and theoretical calculations.

Inkjet printing was identified as a possible technique to overcome the limited throughput of bar coating in the creation of thin films. Printing a matrix of spots in close proximity such that amalgamation occurred resulted in a film for which selective reflection properties were observed. Printing of films was made possible by the creation of a versatile software tool. The method was optimised by variation in the spacing of drops, solvent concentration and solvent type and the effect on film homogeneity studied. Fluorescence analysis was used to aid visualisation in order to identify conditions where coffee staining was eliminated.

A larger library involving changing the concentration and enantiomeric excess of the chiral dopant was formulated, and processed as thin films using inkjet printing before analysis for lambda max using a fibre optic UV-Vis spectrometer. The library showed a good fit with theoretical calculations, although the reliability of the method was compromised by irreproducible robotic solution transfers at the low volumes required on the 96-well format. The improvements required to eliminate such a problem have been discussed.

The inkjet process was overall extremely successful and was shown to be feasible and a valuable tool in HT research in the field of reactive mesogens. The technique has particular

application in cases where formulations such chiral nematics with very small or large dopant concentrations, modified dopant structures or novel dopant mixtures are not able to be predicted theoretically, therefore requiring a practical approach. Outside the LC research area, the inkjet technique has applications in the method described by van Delden *et al* [55,56] for the determination of *ee*, removing the bottleneck of spin coating and therefore allowing many more samples to be prepared and analysed in an automated HT fashion.

4.9 References

(1) R. Williams, *J. Chem. Phys.*, **1963**, *39*, 384.
(2) D. J. Broer, J. Boven, G. N. Mol and G. Challa, *Makromol. Chem.*, **1989**, *190*, 2255.
(3) D. J. Broer, G. N. Mol and G. Challa, *Makromol. Chem.*, **1991**, *192*, 59.
(4) H. Jonsson, H. Andersson, P. E. Sundell, U. W. Gedde and A. Hult, *Polym. Bull.*, **1991**, *25*, 641.
(5) H. Andersson, U. W. Gedde and A. Hult, *Polymer*, **1992**, *33*, 4014.
(6) R. A. M. Hikmet and R. Howard, *Phys. Rev. E*, **1993**, *48*, 2752.
(7) D. J. Broer, J. Lub and G. N. Mol, *Macromolecules*, **1993**, *26*, 1244.
(8) S. Jahromi, J. Lub and G. N. Mol, *Polymer*, **1994**, *35*, 622.
(9) D. J. Broer, H. Finkelmann and K. Kondo, *Makromol. Chem.*, **1988**, *189*, 185.
(10) P. J. Shannon, *Macromolecules*, **1984**, *17*, 1873.
(11) D. J. Broer In *Liquid crystals in complex geometries : Formed by polymer and porous networks*, G. P. Crawford and S. Zumer (Eds.), London: Taylor & Francis, **1996**. p 240.
(12) R. A. M. Hikmet and B. H. Zwerver, *Mol. Cryst. Liq. Cryst.*, **1991**, *200*, 197.
(13) R. A. M. Hikmet and B. H. Zwerver, *Liq. Cryst.*, **1992**, *12*, 319.
(14) R. A. M. Hikmet and B. H. Zwerver, *Liq. Cryst.*, **1993**, *13*, 561.
(15) D. K. Yang, J. L. West, L. C. Chien and J. W. Doane, *J. Appl. Phys.*, **1994**, *76*, 1331.
(16) L. Liebert and L. Strzelecki, *Bull. Soc. Chim. Fr.*, **1973**, 603.
(17) D. J. Broer, *Mol. Cryst. Liq. Cryst.*, **1995**, *261*, 513.
(18) L. Lestel, G. Galli, M. Laus and E. Chiellini, *Polym. Bull.*, **1994**, *32*, 669.
(19) Y. Bouligand, P. E. Cladis, L. Liebert and L. Strzelecki, *Mol. Cryst. Liq. Cryst.*, **1974**, *25*, 233.
(20) S. B. Clough, A. Blumstein and E. C. Hsu, *Macromolecules*, **1976**, *9*, 123.
(21) L. Liebert, L. Strzelecki and D. Vacogne, *Bull. Soc. Chim. Fr, B*, **1975**, 2073.
(22) D. J. Broer, J. Lub and G. N. Mol, *Nature*, **1995**, *378*, 467.
(23) A. Mori, *J. Display Technol.*, **2005**, *1*, 179.
(24) D. Coates, O. Parri, M. Verrall, K. Slaney and S. Marden, *Macromol. Symp.*, **2000**, *154*, 59.
(25) J. L. Fergason, *Sci. Am.*, **1964**, *211*, 76.
(26) J. L. Fergason, N. N. Goldberg and R. J. Nadalin, *Mol. Cryst.*, **1966**, *1*, 309.
(27) R. D. Ennulat and J. L. Fergason, *Mol. Cryst. Liq. Cryst.*, **1971**, *13*, 149.
(28) D. J. Broer and I. Heynderickx, *Macromolecules*, **1990**, *23*, 2474.
(29) I. Heynderickx and D. J. Broer, *Mol. Cryst. Liq. Cryst.*, **1991**, *202*, 113.
(30) C. Harrison, J. Cabral, C. M. Stafford, A. Karim and E. J. Amis, *J. Micromech. Microeng.*, **2004**, *14*, 153.
(31) J. T. Cabral, S. D. Hudson, C. Harrison and J. F. Douglas, *Langmuir*, **2004**, *20*, 10020.
(32) J. Lub, D. J. Broer, R. A. M. Hikmet and K. G. J. Nierop, *Liq. Cryst.*, **1995**, *18*, 319.

(33) S. M. Kelly, *J. Mater. Chem.*, **1995**, *5*, 2047.
(34) D. J. Broer In *Liquid crystals in complex geometries : Formed by polymer and porous networks*, G. P. Crawford and S. Zumer (Eds.), London: Taylor & Francis, **1996**. p 242.
(35) D. A. Dunmur and K. Toriyama In *Handbook of liquid crystals: Fundamentals*, D. Demus, J. W. Goodby, G. W. Gray, H.-W. Spiess and V. Vill (Eds.), Weinheim ; Chichester: Wiley-VCH, **1998**, Vol. 1. p 215
(36) J. Stohr, M. G. Samant, A. Cossy-Favre, J. Diaz, Y. Momoi, S. Odahara and T. Nagata, *Macromolecules*, **1998**, *31*, 1942.
(37) L. C. Scala and G. D. Dixon, *Mol. Cryst. Liq. Cryst.*, **1970**, *10*, 411.
(38) L. B. Leder, *J. Chem. Phys.*, **1971**, *55*, 2649.
(39) L. B. Leder, *J. Chem. Phys.*, **1971**, *54*, 4671.
(40) J. E. Adams and W. E. L. Haas, *Mol. Cryst. Liq. Cryst.*, **1971**, *15*, 27.
(41) H. Q. Zhang, R. Hoogenboom, M. A. R. Meier and U. S. Schubert, *Meas. Sci. Technol.*, **2005**, *16*, 203.
(42) B. J. de Gans and U. S. Schubert, *Macromol. Rapid Commun.*, **2003**, *24*, 659.
(43) T. Cull, M. Goulding and M. Bradley, *Adv. Mat.*, **2007**, *19*, 2355.
(44) E. Tekin, B. J. de Gans and U. S. Schubert, *J. Mater. Chem.*, **2004**, *14*, 2627.
(45) R. D. Deegan, O. Bakajin, T. F. Dupont, G. Huber, S. R. Nagel and T. A. Witten, *Nature*, **1997**, *389*, 827.
(46) R. D. Deegan, O. Bakajin, T. F. Dupont, G. Huber, S. R. Nagel and T. A. Witten, *Phys. Rev. E*, **2000**, *62*, 756.
(47) R. D. Deegan, *Phys. Rev. E*, **2000**, *61*, 475.
(48) B. J. de Gans and U. S. Schubert, *Langmuir*, **2004**, *20*, 7789.
(49) B. J. de Gans, E. Kazancioglu, W. Meyer and U. S. Schubert, *Macromol. Rapid Commun.*, **2004**, *25*, 292.
(50) H. Hu and R. G. Larson, *J. Phys. Chem.*, **2002**, *106*, 1334.
(51) T. R. Welter, WO Patent, WO2005061425, **2005**.
(52) P. J. Collings and M. Hird, *Introduction to liquid crystals : Chemistry and physics*, London: Taylor & Francis, **1997**, p 10.
(53) J. W. Goodby In *Handbook of liquid crystals: Fundamentals*, D. Demus, J. W. Goodby, G. W. Gray, H. W. Spiess and V. Vill (Eds.), Weinheim ; Chichester: Wiley-VCH, **1998**, Vol. 1. p 115.
(54) G. Solladie and R. G. Zimmermann, *Angew. Chem., Int. Ed. Engl.*, **1984**, *23*, 348.
(55) R. A. van Delden and B. L. Feringa, *Angew. Chem., Int. Ed. Engl.*, **2001**, *40*, 3198.
(56) R. A. van Delden and B. L. Feringa, *Chem. Commun.*, **2002**, 174.

Chapter 5 - Overall Conclusion

In this thesis a method for the high-throughput formulation and screening of liquid crystal phase transitions has been developed. The screening apparatus allows analysis of birefringent properties observed only in crystalline solids and liquid crystal mesophases to alidentify in parallel, the temperature of phase transitions occurring in both LC singles and mixtures. The technique can also give a qualitative indication of the type of mesophase transition. The apparatus underwent extensive testing and optimisation to give consistent and reliable results comparable to traditional DSC techniques. Systematic errors associated with the technique have been quantified. The technique is of particular value in initial screening, where a large dataset can be reduced through identification of compounds or compositions which possess the desired mesophase range of interest. The use of this technique to analyse libraries of LCs produced *via* synthesis or formulation greatly enhances the discovery process and leads the way for the development of larger, and more diverse combinatorial libraries of liquid crystals. Such development is of great importance to the sustained growth of the liquid crystal industry, and may enable the realisation of further synergistic relationships between technology and application, both in display and non-display fields.

To produce libraries of a size conducive to HT screening requires methods of HT formulation. The use of established techniques such as robotic liquid handling has enabled large liquid crystal mixture libraries to be produced. Robotic liquid handling has been shown to be a valuable technique, but possess some limitations. Datasets could only be accurately produced in relatively large volumes and reformatting of large libraries was a tedious and time-consuming process, which additionally required the creation of a micro-well slide to provide a physical barrier between samples. Other cutting-edge techniques, such as inkjet printing were investigated, establishing the method of inkjet overprinting as a highly efficient and reliable method for the creation of large libraries from <50μL of each material. In contrast to traditional liquid handling, inkjet printing could be used to simultaneously dispense, mix and reformat mixtures for analysis in one automated step. Ternary libraries formulated using both methods and then analysed using the HT clearing point apparatus showed excellent correlation, both with one another and with analogous materials measured using DSC. The study identified the limitations of theoretical eutectic prediction in multi-

component mixtures, which cannot reveal the true and subtle picture of experimental phase space. The combination of high-throughput formulation and a parallel screening technique has been shown as a valuable tool for the exploration of ternary eutectic formulation libraries.

The use of high-throughput methods in other areas of liquid crystal science has been illustrated by the application of techniques to the formulation and characterisation of chiral nematic reactive mesogens in a HT workflow. Robotic formulation was again used to provide a highly-adaptable approach to library mixture creation, producing chiral nematic reactive mesogen libraries with selective reflection properties. Subsequent analysis of such libraries showed excellent correlation not only to commercial reference materials, but also to theoretical calculation. Extension of the technique to larger libraries of chiral nematic reactive mesogens, incorporating a second variable in the form of an enantiometic excess in the dopant composition, highlighted the major bottleneck in the process to be thin film processing using bar coating. To overcome this bottleneck, the use of inkjet printing to deposit a thin film was developed. Optimisation of matrix parameters and solvents, in combination with bespoke purpose-written software enabled films with good homogeneity to be produced. Fibre optic UV-Vis analysis of a robotically formulated, inkjet-printed binary library showed good correlation to theory, proving the method accurate. Further optimisations improved the reliability of the method and the quality of the IJP films. The method of IJP for thin film formation has many applications, not only in reactive mesogen research but also outside of the area, where the benefits of the high-throughput / formulation processing method can be applied to any process in which bar or spin coating is used, allowing throughput to be increased dramatically.

This processes developed in this thesis are of importance for the continued advancement of display technologies. Although the work has barely scratched the surface of the potential for HT methods in this area, it has demonstrated that HT technologies allow a great many more materials to be screened, using smaller quantities of material and in a reduced time-frame. Speculativly, the development of additional methods for HT screening of LC properties, together with further advancement in combinatorial and high-throughput synthesis can make the HT process more attractive, consequently enabling a greatly improved discovery process. The generation of enhanced and refined materials can be considered for application in future

technologies. Many emerging technologies such as low-power displays, ultra-large displays, paper-like displays and head-mounted displays are likely to offer oppertunities for liquid crystal materials. Also of importance is the possibility of using LC materials in non-display applications, where a great many materials have application potential but are yet to be established as commercially viable. In the discovery of materials with enhanced physical proprties, the same synergistic relationship between technology and application which drove the development of LCD technology over 30 years ago, may result in further new and exciting applications.

Chapter 6 - Experimental Procedures

6.1 General Experimental

6.1.1 Procedure and Apparatus for the High Throughput Analysis of Phase Transitions

Phase transitions were analysed using the equipment described in Chapter 1.[1] The apparatus comprised a steel block containing two 24 V heaters, a thermocouple and drilled channels for nitrogen purging. Heating was achieved *via* a Ventacon instrument containing a Calcomms 3300 temperature control unit operating on a thermostatic feedback loop, interfaced to a PC provided data logging. To the face of the steel block was mounted a reflective 100 x 100 x 5 mm chromed brass plate. Around this was attached a removable enclosure, the roof of which was constructed of linear polarising film. The device was operated in the normally black mode where the films were aligned with their planes of polarisation at 90°. Above one polarising film was mounted a display backlight, and above the other a webcam, interfaced to a PC providing video capture capability. The webcam was adjusted and focused to give an image of the chromed plate through the polarisers. Parameters in the webcam software were adjusted from the default (Brightness 4357, Contrast 5143, Hue 8000, Saturation 4357, Sharpness 5071, White Balance 1143, Gamma 5429, Backlight 6214, Exposure 1/120s, Low light boost OFF, Colour boost OFF, 1 FPS, 320x240 resolution) to provide a good contrast between birefringent samples and the black background (Figure 6.1).

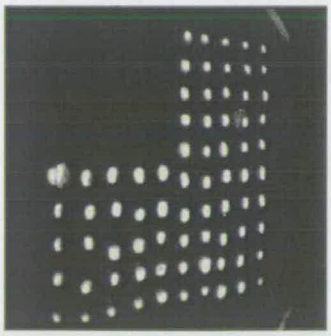

Figure 6.1: Spots of liquid crystal visualised through the webcam in which optimum parameters have been entered

6.1.1.1 Sample Loading

Samples were loaded onto the chromed plate in one of two ways. For smaller sample numbers (<50) samples were spotted using a Pasteur pipette, directly onto the plate. For larger libraries the micro-well confinement device was used, the samples spotted into wells using the same pipetting technique, and the device placed onto the chromed plate for analysis. For libraries created using inkjet printing the glass substrate was loaded directly onto the chromed plate.

6.1.1.2 Data Acquisition

Data was collected by acquisition of the temperature (T) of the heating block at time (t) and at the same time recording a video sequence from the webcam, showing the samples spotted onto the plate viewed through the linear polarizer aligned at 90° to the plane of incoming polarised light, with frames / images acquired every second (t). The Calcomms software was used to monitor the temperature and Creative webcam software was used to collect the video sequences. Data collection was initiated by simultaneously providing power to the heating element and commencing temperature and video sequence collection. Temperature was recorded every 4 seconds and a movie frame was recorded every second (1fps). The temperature was ramped at 5 °C/min from room temperature (~20 °C) to 150 °C.

To cool the apparatus a purge of nitrogen gas, cooled by means of a liquid nitrogen dip coil was run through the steel block. To maintain the cooling rate the flow of nitrogen was increased as the temperature decreased, until approximately -30 °C was obtained. Optionally the temperature ramp was then repeated. When heating from sub ambient temperatures the nitrogen purge was reduced but not stopped entirely to ensure the chamber was continually purged with nitrogen which avoiding frosting of the chromed plate. Temperature data was exported in a text file.

6.1.1.3 Data Analysis

Video data was exported into Image Pro-Plus software (Media Cybernetics). The sequence was sub-sampled by 4 to reduce the number of data points. The manual tag function was used to define spatial tags with a size of 3 pixels, at each point on the image where a sample was spotted. Using the data collector function the white intensity of each of the tagged points

(between 0 and 255) was calculated and exported out of IPP to Microsoft Excel as a list of macro sequence to obtain the intensity (I) of every sample in every sequence frame.

6.1.1.4 Data Processing for Visualisation

The text file containing temperature data was imported into Microsoft Excel. Time data in the file was represented in an hh:mm:ss clock format and therefore to obtain the time increment between each frame, adjacent times were subtracted and multiplied by a conversion factor (86400) to obtain values in seconds. This data was used to plot a graph of time vs. temperature and a linear line of best fit applied. Transposition of the intensity values imported from IPP into Microsoft Excel was achieved using an Excel VBA macro (Appendix E1). The linear list of intensities together with the value of the sequence sub-sample applied, the equation relating the time (equal to the frame number) to temperature and the desired graphing limits were entered and the macro executed, resulting in plots of intensity vs. temperature for every member of the library.

6.1.1.5 Data Interpretation

Transitions either crystal to liquid transitions, crystal to liquid crystal transitions, liquid crystal to liquid crystal transitions or liquid crystal mesophase to isotropic liquid transitions, were identified by discontinuities in the graphs of intensity vs. temperature. The majority of data plots showed sharp transition discontinuities and in these cases the temperature of the central data point in the transition was recorded. In the case of broader transitions the temperature reading from the penultimate data point prior to stabilisation of intensity was used as a measure of temperature change. In cases where transitions were not clear the data was processed further by dividing the intensity value of each point by the average of the previous three values. Producing a scatter plot of this data identified transitions as points which occurred significantly over the standard deviation of the dataset. Generally where a heat cool cycle was performed only data for the heating run was presented, unless features not seen in the heating cycle were observed in the cooling run. The transitions observed in the cooling run were generally observed at lower temperatures than on the heating cycle.

6.1.1.6 Modification using a Mirror for Analysis

For experiments in which the glass mirror was used in place of the chromed plate, camera settings were modified (brightness 5714, contrast 3286, hue 9429, saturation 3188, sharpness 5071, wb 0 not auto, gamma 3857, , backlight 5000, exposure 1/100, gain 1985, low light boost on, colour boost on, 1 FPS, 320x240 resolution).

6.1.2 Differential Scanning Calorimetry

Transition temperatures and enthalpies of transition (ΔH Jg^{-1}) were determined using a TA Instruments Q1000 differential scanning calorimeter fitted with an integrated cooling system allowing analysis down to -70 °C under a nitrogen atmosphere. The calorimeter was calibrated with indium (ΔH = 28.45 J/g, T_{mp} = 156.60 °C) and zinc (ΔH = 106.7 J/g, T_{mp} = 419.47 °C) reference samples. Samples of 1-2 mg were analysed in sealed-lid aluminium pans at 10°C/min between -50 °C and 100 °C. For samples requiring higher temperatures, analysis was continued to a point approximately 20 °C above the clearing point transition. Samples were initially heated from room temperature to the maximum and then cooled at 10 °C/min to -50 oC. Once this temperature was achieved the sample was reheated at 10 °C/min once more to the maximum. Data processing was performed using TA Instruments Universal Analysis software. The temperatures reported are transition onset values unless otherwise stated.

6.1.3 Robotic Liquid Handling

A Gilson 233XL was used for liquid handling tasks. The system comprised a robotic XYZ arm onto which was mounted a septum piercing needle. The needle was attached to a Gilson 402 Dual syringe pump (combined maximum stroke of 11 mL) through tubing with a 1100 µL internal volume, which defined the maximum transfer volume. The system fluid, used to purge and clean the needle. was changed depending on the solvent used for dispensing.

The system was controlled using the Gilson 735 sampler software in which the workspace, method, racks and trays were defined and the transfer of liquids between vessels programmed. The workspace and target vessel format was adapted depending on the volume and number of solutions to be handled. Either pre-set racks and vial arrangements were used or customized racks were created. The software enabled parameters relating to the aspirate /

dispense procedure and the position and height of the needle to be modified. Sequences were designed using a graphical interface. Liquid handling tasks were chosen from a list and dragged and dropped to create a sequence. Each task could be edited to define parameters and the volumes for transfer.

6.1.4 Inkjet Printing Apparatus

The Microdrop Autodrop system used for inkjet printing comprised a single AK-501 piezoelectric micropipette operating in drop on demand mode. Drop formation and aspiration were carried out by a MD-K-130 control unit. The system included a XYZ platform with 96 / 384 well plate holder, substrate holder and wash / waste stations. The movement of the platform, position of drops and the drop dispensing process was controlled *via* a PC interface using the Autodrop software. Materials were aspirated and held in the printing nozzle from a 96 or 384 well plate by application of a back pressure. On completion of printing the material was returned to the well by flushing, before aspiration of a cleaning solvent and sonication, produced by the operation of the drop generation at the nozzles eigenfrequency, before flushing clean the nozzle with air.

Drops were produced by the application of an electronic pulse to the piezo nozzle. The waveform of the pulse was customisable in the Autodrop software enabling the voltage (amplitude) pulse width (wavelength) and frequency of the pulse to be modified. Prior to printing each solvent was assessed to determine optimised waveform parameters; ensuring the formation of single drops without tails or ligaments. Drop formation was monitored using an inbuilt stroboscopic camera. Generally voltages of between 90 – 110 V with a 30 μs pulse width and at a frequency of 60 Hz were used.

6.2 Chapter 2 Experimental

6.2.1 Analysis Using the Multiple Melting Point Apparatus

The reported procedure[2] was used without modification.

6.2.2 Calibration of Calcomms Temperature Controller

The Calcomms instrument was calibrated using three integral calibration routines, documented in the user manual. The first calibration was the 'Autotune' sequence, requiring the heating range (-30 °C to 150 °C), and the heating rate (5 °C/min) to be entered. The second calibration was the 'cycle time auto tune' which optimised the sampling and response time in the thermostat feedback loop. Finally the Calcomms device was calibrated to an external instrument by attaching a digital thermometer with a 1 cm diameter surface probe (Fisher Scientific) to the centre of the heating block using silver thermal paste. The apparatus was ramped at 5 °C/min to 150 °C. At every 10 °C the temperature shown by the external thermometer was recorded. The two data points were then processed using the formula documented in the Calcomms user guide to obtain a correction factor which was entered into the instrument.

6.2.3 Infrared Imaging

To measure the homogeneity of temperature distribution over the heating block an Infrared thermal imaging camera (IRRIS 256STd) was used to record the thermo graphical images over a 5 °C/min heat ramp at temperatures between 50 and 100 °C. Images were captured using a PC containing a TV input card (PCTV2000) with composite video capture capability. As images were captured the temperature of the heating block in various positions was obtained using the digital thermometer and used to calibrate the pseudo-colour IR scale to temperature.

6.2.4 Determination of Drop Area

The liquid crystal E7 was loaded onto the chromed plate using a micropipette to create a range of drops with different sizes. Analysis was then carried out as described in Section 6.1.1, between the temperatures of 20 and 80 °C. During transition analysis the procedure was modified to obtain the onset and offset values of all transitions, the onset determined by the penultimate point in the data series before the change to the isotropic, and then the first data point of the isotropic phase preceding the intensity change.

To determine the effect of sample area on the transition temperature the first frame of the video sequence obtained from the analysis was extracted as an image using Image Pro-Plus

(Media Cybernetics) Using the auto-tag function all white areas of the frame were selected, and the sensitivity of the selection decreased until only the areas corresponding to the birefringent liquid crystal samples were highlighted. The size of each sample was then calculated by the number of pixels contained in the selected area, and exported to an Excel spreadsheet. The values were used together with the onset and end values of the clearing point to draw relationships between area of spots and the clearing point. To obtain transition data from samples the standard analysis procedure was used.

6.3 Chapter 3 Experimental

6.3.1 Fabrication of a Micro-well Containment Device

To create a micro-well device a negative lithography procedure was used.[3] Adobe Illustrator was used to create a negative image of the grid design of a 10x10 square each square having dimensions of 2.5 mm. The mask was printed three times onto transparent film using a HP LaserJet 4050 printer with a 600 dpi resolution. Each of the masks were cut out and adhered together to create a UV impermeable film.

A release surface was produced using Sylgard 184 silicon elastomer kit (Dow Corning) in a 1:10 ratio of base curative to elastomer. The mixed silicon was poured into a mould so as to create a flat slab, and thermally cured at 60 °C for 90 minutes before turning out the silicon slab. Onto the release surface two 500 μm aluminium spacers (5 mm x 10 mm) were placed, and the area between the spacers was filled with NOA81 (Norland) optical adhesive. A thin glass cover slip (32 x 32 mm no. 1, Fisher), onto which the grid was formed was carefully placed on top of the spacers so that the glue line spread, ensuring that no air bubbles were created. A second glass slide on which the mask was attached was then laid onto the smaller cover slip. With the mask in place the construction was irradiated with UV light at 256 nm for 10 s at an intensity of 7 mW/cm^2. The silicon elastomer, spacers and the mask were then carefully removed so that the glass cover slip was revealed. The substrate was washed with acetone/ethanol and blasted with a stream of nitrogen to remove all uncured adhesive. On completion the glass slide was post cured for 60 seconds using 254 nm UV light and then baked at 60 °C for 10 min.

6.3.2 Formulation of a Ternary Library of MLC Components

Three liquid crystal mixtures MLC-6882, MLC-6684 and MLC-6647 (Merck Chemicals Ltd.) were formulated into 75 new mixtures using the robotic liquid handling apparatus (Gilson). The Gilson apparatus was configured to hold 3 racks, a 3x9 array of 10 ml glass tubes, a 3x1 array of 200 ml plastic bottles and a 5x16 array of 1.5 ml glass vials. Each of the MLC components was diluted 1:1 w/w with DCM and loaded onto the instrument in a 10 ml glass tube, sealed with a septum. For the creation of mixtures a total of 8 ml of each component solution was produced. To create mixtures a strategy of mainjtaining the volume of one component whilst modifying the other two was used, repeating for each component. Zones were defined on the target vials of the 5x16 array in which one of three volumes (125, 94, 63, 31 or 0 μL) of each component were dispensed. A serial dispense task was defined to aspirate solution from the source tube and dispense volumes into all target vials in the zone. The sequence was repeated with each of the three source tubes and for each of the 5 solution volumes to complete the library. The procedure is illustrated graphically in Figure 6.2.

An aspiration rate of 0.25 ml/min was used, the needle dropped to a depth just short (3 mm) of the tube base. On dispensing the needle was lowered into the vial below the liquid level, such that accurate transfer resulted. The 125 μL volumes were dispensed first in all cases. To prevent cross contamination dispensing into each vial in the zone was carried out individually, washing and purging the needle between aspiration and dispensing. After completion of one zone the needle was purged using the system fluid and acetone. The system fluid used in this experiment was acetone.

After dispensing the vials were sealed and shaken before uncapping and oven heating at 60 °C for 5 min to remove the carrier solvent, before cooling at room temperature for 30 min. The library was then analysed for phase transitions using the high-throughput apparatus by the standard procedure, including the use of the micro-well device. The concentration and volumes of each of the MLC components in the library are shown in Table 6.1

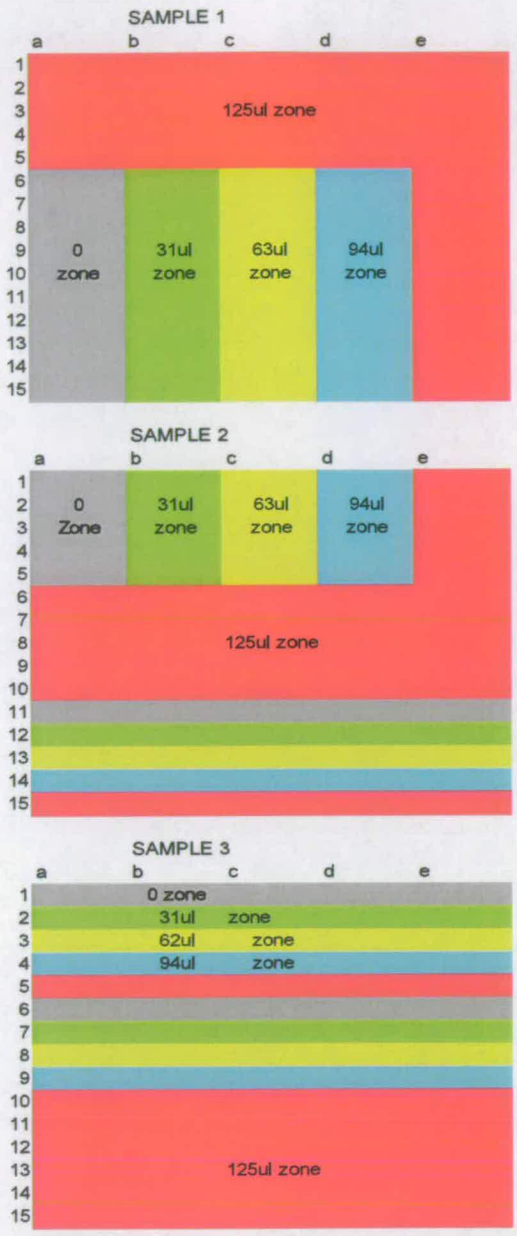

Figure 6.2: Graphical representation of the zones of different dispense volumes which were defined for the 5x15 array of target vials, for each of the 3 library components.

Number	MLC-6684(ul)	MLC-6647(ul)	MLC-6882(ul)	%MLC-6684	%MLC-6647	%MLC-6882	Number	MLC-6684(ul)	MLC-6647(ul)	MLC-6882(ul)	%MLC-6684	%MLC-6647	%MLC-6882
a1	125	0	0	100.0	0.0	0.0	d8	94	125	63	33.3	44.3	22.3
b1	125	31	0	80.1	19.9	0.0	e8	125	125	63	39.9	39.9	20.1
c1	125	63	0	66.5	33.5	0.0	a9	0	125	94	0.0	57.1	42.9
d1	125	94	0	57.1	42.9	0.0	b9	31	125	94	12.4	50.0	37.6
e1	125	125	0	50.0	50.0	0.0	c9	63	125	94	22.3	44.3	33.3
a2	125	0	31	80.1	0.0	19.9	d9	94	125	94	30.0	39.9	30.0
b2	125	31	31	66.8	16.6	16.6	e9	125	125	94	36.3	36.3	27.3
c2	125	63	31	57.1	28.8	14.2	a10	0	125	125	0.0	50.0	50.0
d2	125	94	31	50.0	37.6	12.4	b10	31	125	125	11.0	44.5	44.5
e2	125	125	31	44.5	44.5	11.0	c10	63	125	125	20.1	39.9	39.9
a3	125	0	63	66.5	0.0	33.5	d10	94	125	125	27.3	36.3	36.3
b3	125	31	63	57.1	14.2	28.8	e10	125	125	125	33.3	33.3	33.3
c3	125	63	63	49.8	25.1	25.1	a11	0	0	125	0.0	0.0	100.0
d3	125	94	63	44.3	33.3	22.3	b11	31	0	125	19.9	0.0	80.1
e3	125	125	63	39.9	39.9	20.1	c11	63	0	125	33.5	0.0	66.5
a4	125	0	94	57.1	0.0	42.9	d11	94	0	125	42.9	0.0	57.1
b4	125	31	94	50.0	12.4	37.6	e11	125	0	125	50.0	0.0	50.0
c4	125	63	94	44.3	22.3	33.3	a12	0	31	125	0.0	19.9	80.1
d4	125	94	94	39.9	30.0	30.0	b12	31	31	125	16.6	16.6	66.8
e4	125	125	94	36.3	36.3	27.3	c12	63	31	125	28.8	14.2	57.1
a5	125	0	125	50.0	0.0	50.0	d12	94	31	125	37.6	12.4	50.0
b5	125	31	125	44.5	11.0	44.5	e12	125	31	125	44.5	11.0	44.5
c5	125	63	125	39.9	20.1	39.9	a13	0	63	125	0.0	33.5	66.5
d5	125	94	125	36.3	27.3	36.3	b13	31	63	125	14.2	28.8	57.1
e5	125	125	125	33.3	33.3	33.3	c13	63	63	125	25.1	25.1	49.8
a6	0	125	0	0.0	100.0	0.0	d13	94	63	125	33.3	22.3	44.3
b6	31	125	0	19.9	80.1	0.0	e13	125	63	125	39.9	20.1	39.9
c6	63	125	0	33.5	66.5	0.0	a14	0	94	125	0.0	42.9	57.1
d6	94	125	0	42.9	57.1	0.0	b14	31	94	125	12.4	37.6	50.0
e6	125	125	0	50.0	50.0	0.0	c14	63	94	125	22.3	33.3	44.3
a7	0	125	31	0.0	80.1	19.9	d14	94	94	125	30.0	30.0	39.9
b7	31	125	31	16.6	66.8	16.6	e14	125	94	125	36.3	27.3	36.3
c7	63	125	31	28.8	57.1	14.2	a15	0	125	125	0.0	50.0	50.0
d7	94	125	31	37.6	50.0	12.4	b15	31	125	125	11.0	44.5	44.5
e7	125	125	31	44.5	44.5	11.0	c15	63	125	125	20.1	39.9	39.9
a8	0	125	63	0.0	66.5	33.5	d15	94	125	125	27.3	36.3	36.3
b8	31	125	63	14.2	57.1	28.8	e15	125	125	125	33.3	33.3	33.3

Table 6.1: Volumes of each MLC component dispensed using the Robotic liquid handler.

6.3.3 Formulation of a Ternary Eutectic Library Using Robotic Liquid Handling

Three liquid crystals FET-2-Cl, FET-3-Cl and FET-5-Cl were formulated into a 66 member library using the robotic liquid handling apparatus. A ternary library was created by varying the concentration of each component between 0 % and 100 % of the total, with incremental steps of 10 %. The overall volume of each solution was kept constant at 150 μL and formulated into a 96-well plate. The Gilson apparatus was configured to hold 3 racks, a 3x9 array of 10 ml glass tubes, a 3x1 array of 200 ml plastic bottles and a customised rack holding a standard 96-well plate with volume of 240 μL per well. FET components were diluted with DCM in a 3:1 w/w % ratio, and loaded onto the instrument in a 10 cm glass tube, sealed with a septum. For the creation of all mixtures a total of 4 ml of each solution was produced.

The library was created by aspiration of variable amounts of each solution from the glass vial and into the target well of the 96-well plate. The dispensing was carried out serially, re-aspirating solution after each well, and then repeating the procedure for the remaining components. The amount of each solution dispensed into each well, as programmed into the liquid handling apparatus is detailed in Table 6.2. After the complete dispensing of each component the needle was rinsed and purged with the system solvent to prevent contamination. An aspiration rate of 0.500 ml min^{-1} was used and the needle dropped to a depth just short (3 mm) of the tube base. On dispensing, the needle was lowered to just above the level of solution. After dispensing completely one component zone the needle was purged using the system fluid and acetone from the 200 ml plastic bottle. The system fluid used in this experiment was acetone.

	FET-2-Cl	FET-3-Cl	FET-5-Cl		FET-2-Cl	FET-3-Cl	FET-5-Cl
1	0	0	150	34	75	30	45
2	0	15	135	35	90	15	45
3	15	0	135	36	105	0	45
4	0	30	120	37	0	120	30
5	15	15	120	38	15	105	30
6	30	0	120	39	30	90	30
7	0	45	105	40	45	75	30
8	15	30	105	41	60	60	30
9	30	15	105	42	75	45	30
10	45	0	105	43	90	30	30
11	0	60	90	44	105	15	30
12	15	45	90	45	120	0	30
13	30	30	90	46	0	135	15
14	45	15	90	47	15	120	15
15	60	0	90	48	30	105	15
16	0	75	75	49	45	90	15
17	15	60	75	50	60	75	15
18	30	45	75	51	75	60	15
19	45	30	75	52	90	45	15
20	60	15	75	53	105	30	15
21	75	0	75	54	120	15	15
22	0	90	60	55	135	0	15
23	15	75	60	56	0	150	0
24	30	60	60	57	15	135	0
25	45	45	60	58	30	120	0
26	60	30	60	59	45	105	0
27	75	15	60	60	60	90	0
28	90	0	60	61	75	75	0
29	0	105	45	62	90	60	0
30	15	90	45	63	105	45	0
31	30	75	45	64	120	30	0
32	45	60	45	65	135	15	0
33	60	45	45	66	150	0	0

Table 6.2: Volumes of each FET component dispensed using the robotic liquid handler

After dispensing, the 96-well plate was oven heated at 60 °C for 5 minutes to remove the carrier solvent, before cooling at room temperature for 30 minutes. The library was then

analysed for phase transitions using the high-throughput apparatus by the standard procedure, including the use of the micro-well device. Many mixtures required cooling to promote crystallisation so that the melting point could be analysed. It was necessary therefore to cool the samples to temperatures as low as -40 °C to obtain crystalline materials. The crystalline samples were then loaded onto the HT apparatus and analysed for a clearing point between 20-160 °C.

6.3.4 Formulation of a Focused Ternary Eutectic Library Using Robotic Liquid Handling

To produce a more focused library the above procedure was repeated using concentrations of 0 to 40 % FET-2-Cl, 0 to 40 % FET-3-Cl and 30 to 100 % FET-5-Cl. A 5 % step size between concentrations was used to achieve a library of 78 mixtures. The amounts entered into the Gilson software for dispensing are detailed in Table 6.3.

FET-2-Cl(ul)	FET-3-Cl(ul)	FET-5-Cl(ul)	FET-2(%)	FET-3(%)	FET-5(%)	FET-2-Cl(ul)	FET-3-Cl(ul)	FET-5-Cl(ul)	FET-2(%)	FET-3(%)	FET-5(%)
0	0	150	0	0	100	30	23	98	20	15	65
0	8	143	0	5	95	30	30	90	20	20	60
0	15	135	0	10	90	30	38	83	20	25	55
0	23	128	0	15	85	30	45	75	20	30	50
0	30	120	0	20	80	30	53	68	20	35	45
0	38	113	0	25	75	30	60	60	20	40	40
0	45	105	0	30	70	38	0	113	25	0	75
0	53	98	0	35	65	38	8	105	25	5	70
0	60	90	0	40	60	38	15	98	25	10	65
8	0	143	5	0	95	38	23	90	25	15	60
8	8	135	5	5	90	38	30	83	25	20	55
8	15	128	5	10	85	38	38	75	25	25	50
8	23	120	5	15	80	38	45	68	25	30	45
8	30	113	5	20	75	38	53	60	25	35	40
8	38	105	5	25	70	38	60	53	25	40	35
8	45	98	5	30	65	45	0	105	30	0	70
8	53	90	5	35	60	45	8	98	30	5	65
8	60	83	5	40	55	45	15	90	30	10	60
15	0	135	10	0	90	45	23	83	30	15	55
15	8	128	10	5	85	45	30	75	30	20	50
15	15	120	10	10	80	45	38	68	30	25	45
15	23	113	10	15	75	45	45	60	30	30	40
15	30	105	10	20	70	45	53	53	30	35	35
15	38	98	10	25	65	45	60	45	30	40	30
15	45	90	10	30	60	53	0	98	35	0	65
15	53	83	10	35	55	53	8	90	35	5	60
15	60	75	10	40	50	53	15	83	35	10	55
23	0	128	15	0	85	53	23	75	35	15	50
23	8	120	15	5	80	53	30	68	35	20	45
23	15	113	15	10	75	53	38	60	35	25	40
23	23	105	15	15	70	53	45	53	35	30	35
23	30	98	15	20	65	53	53	45	35	35	30
23	38	90	15	25	60	60	0	90	40	0	60
23	45	83	15	30	55	60	8	83	40	5	55
23	53	75	15	35	50	60	15	75	40	10	50
23	60	68	15	40	45	60	23	68	40	15	45
30	0	120	20	0	80	60	30	60	40	20	40
30	8	113	20	5	75	60	38	53	40	25	35
30	15	105	20	10	70	60	45	45	40	30	30

Table 6.3: Volumes of FET components dispensed to create a focused library by robotic liquid handling.

6.3.5 Formulation of a Ternary Eutectic Library Using Inkjet Printing

Using the inkjet printing apparatus in parallel with software for the creation of macro sequences, overprinting was used to formulate ternary libraries of FET-2-Cl, FET-3-Cl and FET-5-Cl.[4] Each solid component was diluted in a 5:1 ratio of acetophenone, a 96-well plate filled with 200 µL of each solution and loaded into the Autodrop printer. Prior to formulation solvent jetting parameters of 104 V pulse voltage, 29 ms pulse width and a 60 Hz drop frequency were used. The Microdrop Triangular Formulation Library Macro Creator (Appendix E2) was populated with printing variables for creation of a sequence of macro commands. Formulations were created with a total of 100 drops, the number of drops of each of the components varied between 0 and 100 in 5 drop steps to create 231 unique mixtures

onto a glass cover slip (32x32 mm, no.1 Fisher Scientific). Each mixture was deposited 1.9 mm apart with 1.9 mm between rows. A fill time of 2 s, an empty time of 5 s (returning into the source well) followed by a 5 s ultrasonic cleaning cycle was used. The solvent used for cleaning was identical to the solvent used to dissolve the components of the library.

The Macro sequence was loaded into the Autodrop software and the program executed. Dispensing was carried out serially, using one aspiration for all 231 positions of one component. On completion, solvent was removed by oven heating the substrate at 80 °C for 5 min and cooled to room temperature. Mixtures were then analysed for phase transitions using the HT screening apparatus, using the text file produced by the Microdrop Triangular library macro creator to correlate the composition of spots to their spatial position on the glass substrate. The composition of all components is illustrated in Table 6.4.

A = FET-2-Cl, B = FET-3-Cl, C = FET-5-Cl															
position	A	B	C	position	A	B	C	position	A	B	C	position	A	B	C
1	100	0	0	59	5	85	10	117	45	25	30	175	5	45	50
2	95	5	0	60	0	90	10	118	40	30	30	176	0	50	50
3	90	10	0	61	85	0	15	119	35	35	30	177	45	0	55
4	85	15	0	62	80	5	15	120	30	40	30	178	40	5	55
5	80	20	0	63	75	10	15	121	25	45	30	179	35	10	55
6	75	25	0	64	70	15	15	122	20	50	30	180	30	15	55
7	70	30	0	65	65	20	15	123	15	55	30	181	25	20	55
8	65	35	0	66	60	25	15	124	10	60	30	182	20	25	55
9	60	40	0	67	55	30	15	125	5	65	30	183	15	30	55
10	55	45	0	68	50	35	15	126	0	70	30	184	10	35	55
11	50	50	0	69	45	40	15	127	65	0	35	185	5	40	55
12	45	55	0	70	40	45	15	128	60	5	35	186	0	45	55
13	40	60	0	71	35	50	15	129	55	10	35	187	40	0	60
14	35	65	0	72	30	55	15	130	50	15	35	188	35	5	60
15	30	70	0	73	25	60	15	131	45	20	35	189	30	10	60
16	25	75	0	74	20	65	15	132	40	25	35	190	25	15	60
17	20	80	0	75	15	70	15	133	35	30	35	191	20	20	60
18	15	85	0	76	10	75	15	134	30	35	35	192	15	25	60
19	10	90	0	77	5	80	15	135	25	40	35	193	10	30	60
20	5	95	0	78	0	85	15	136	20	45	35	194	5	35	60
21	0	100	0	79	80	0	20	137	15	50	35	195	0	40	60
22	95	0	5	80	75	5	20	138	10	55	35	196	35	0	65
23	90	5	5	81	70	10	20	139	5	60	35	197	30	5	65
24	85	10	5	82	65	15	20	140	0	65	35	198	25	10	65
25	80	15	5	83	60	20	20	141	60	0	40	199	20	15	65
26	75	20	5	84	55	25	20	142	55	5	40	200	15	20	65
27	70	25	5	85	50	30	20	143	50	10	40	201	10	25	65
28	65	30	5	86	45	35	20	144	45	15	40	202	5	30	65
29	60	35	5	87	40	40	20	145	40	20	40	203	0	35	65
30	55	40	5	88	35	45	20	146	35	25	40	204	30	0	70
31	50	45	5	89	30	50	20	147	30	30	40	205	25	5	70
32	45	50	5	90	25	55	20	148	25	35	40	206	20	10	70
33	40	55	5	91	20	60	20	149	20	40	40	207	15	15	70
34	35	60	5	92	15	65	20	150	15	45	40	208	10	20	70
35	30	65	5	93	10	70	20	151	10	50	40	209	5	25	70
36	25	70	5	94	5	75	20	152	5	55	40	210	0	30	70
37	20	75	5	95	0	80	20	153	0	60	40	211	25	0	75
38	15	80	5	96	75	0	25	154	55	0	45	212	20	5	75
39	10	85	5	97	70	5	25	155	50	5	45	213	15	10	75
40	5	90	5	98	65	10	25	156	45	10	45	214	10	15	75
41	0	95	5	99	60	15	25	157	40	15	45	215	5	20	75
42	90	0	10	100	55	20	25	158	35	20	45	216	0	25	75
43	85	5	10	101	50	25	25	159	30	25	45	217	20	0	80
44	80	10	10	102	45	30	25	160	25	30	45	218	15	5	80
45	75	15	10	103	40	35	25	161	20	35	45	219	10	10	80
46	70	20	10	104	35	40	25	162	15	40	45	220	5	15	80
47	65	25	10	105	30	45	25	163	10	45	45	221	0	20	80
48	60	30	10	106	25	50	25	164	5	50	45	222	15	0	85
49	55	35	10	107	20	55	25	165	0	55	45	223	10	5	85
50	50	40	10	108	15	60	25	166	50	0	50	224	5	10	85
51	45	45	10	109	10	65	25	167	45	5	50	225	0	15	85
52	40	50	10	110	5	70	25	168	40	10	50	226	10	0	90
53	35	55	10	111	0	75	25	169	35	15	50	227	5	5	90
54	30	60	10	112	70	0	30	170	30	20	50	228	0	10	90
55	25	65	10	113	65	5	30	171	25	25	50	229	5	0	95
56	20	70	10	114	60	10	30	172	20	30	50	230	0	5	95
57	15	75	10	115	55	15	30	173	15	35	50	231	0	0	100
58	10	80	10	116	50	20	30	174	10	40	50				

Table 6.4: The number of drops of each FET component inkjet printed to create mixtures.

6.3.6 Polarised Light Optical Microscopy

Polarised light optical microscopy was performed using an Olympus BH2 polarising Microscope fitted with linear polarisers set at 90° to one another. The sample temperature was controlled using a Mettler FP82HT hot stage, controlled by a Mettler FP90 central processor. The hot stage was fitted with a nitrogen cooling purge to permit sub-ambient measurements. The temperature range of compounds analysed was from ambient temperatures to at least 10 °C above the point at which the isotropic liquid was observed. For those samples in which cooling was required, temperatures down to -10 °C were obtained. Samples were examined between glass microscope slides, the surfaces of which were optionally treated with various aligning agents. Photomicrographs of optical textures of mesophases were obtained using the same microscope fitted with a JVC TK1085-E colour video camera linked to a PC providing image capture capability.

6.4 Chapter 4 Experimental

6.4.1 Alignment on Polymer Substrates

Polymer films (TAC or PET) were aligned by repeated unidirectional rubbing using a steel bar wrapped in a velvet cloth. The rubbing was achieved manually, pulling the bar from the top of the material to the bottom, repeating the process 10 times.

6.4.2 Bar Coating

Creation of thin films was achieved using a K Control Coater Model 101 (RK Print coat instruments). A yellow No.1 K-bar (0.08 mm wire diameter) was used to give films of approximately 1.5 μm, or a red no.2 K-Bar (0.12mm wire diameter) used to give approximately 2.5 μm film thickness onto the TAC or PET substrate. The bar was drawn at a speed of 8 m/min. The substrate was then removed and annealed in an oven at 60 °C for 1 minute before UV curing.

6.4.3 Parallel Bar Coating

An identical procedure to bar coating was used for parallel bar coating except for the following modifications. The substrate was cut into strips of 2 cm width with a 1 cm channel between strips. The combed substrate was loaded onto the K control coater and a line of material placed on the film below the level of the K-Bar, a different material above each strip.

6.4.4 UV Curing of Reactive Mesogen Films

Reactive mesogen films were cured by UV irradiation. Following heat annealing the film was allowed to cool to room temperature. A 100W B-100A (Blak-ray) UV light with a 365 nm emission wavelength was used. The samples were positioned 10 cm from the lamp. An enclosure was created with an inlet for nitrogen gas and with a transparent window made of PET on the top face. Prior to the cure the enclosure was purged with nitrogen for 1 min. The samples were placed into the chamber, ensuring that no areas were obscured from the UV light. The lid was replaced and the enclosure purged before placing the whole apparatus under the UV light source. Samples were irradiated for 60 seconds, receiving approximately 7 mW/cm^2 of irradiation. The films were then checked for tack, by applying pressure to a corner of the film using a second piece of TAC film, and if found to be incompletly cured UV irradiated under nitrogen for a further 30 s.

6.4.5 UV/Vis Spectroscopy

UV/Vis spectra were obtained using a Hewlett-Packard 8452A diode array spectrometer. Films were mounted over the analyser aperture and spectra were obtained between 250 and 900 nm in the transmittance mode. This technique was only used with films greater than 1.5 cm width. Optionally, to analyse light of only one polarisation a circularly polarising filter of one handedness was attached to the source aperture of the spectrometer. The software was used to obtain the value of λ_{max} the wavelength at which the lowest transmission (maximum reflection) was observed.

6.4.6 Determination of Film Thickness

The thickness of reactive mesogen films was determined using a KLA Tencor Alphastep 500 surface profiler instrument. The stylus was set at 2.2 mg weight and analysis performed at 10 μm/s over a 1000 μm length. Films were prepared by tearing the surface using adhesive tape producing a step in the coating over which the analysis was carried out in duplicate, repeating at different points along the tear.

6.4.7 Formulation of Reactive Mesogen Libraries Containing BDH-1281 and IS-9193 Chiral Dopants

The two libraries were made using the robotic liquid handling apparatus, creating two libraries, identical except for the chiral dopant. The Gilson apparatus was configured to hold 4 racks, a 3x9 array of 2 cm diameter, 12 cm depth glass tubes, a 2x8 array of 4 cm diameter, 12 cm depth glass tubes, a 3x1 array of square plastic bottles and a 5x16 array of 1.5 ml glass vials. Formulations consisted of three components, a reactive mesogen solution, a chiral dopant solution and a make up solution. The reactive mesogen solution was a multi-component mixture containing the components listed in Table 6.5.

Solid Component	Percentage
RM23	24.6
RM105	24.6
RM82	9.72
RM257	39.4
FC171	0.6
Irganox 651	1
Irgacure 1076	0.08

Table 6.5: The components of the reactive mesogen solution used for library formulation

Mixtures were produced on a 1.45 ml scale in 1.5 ml brown glass vials. The concentration of chiral dopant in the solution was incremented between 1.8 and 5.6 w/w % in 0.2 w/w % steps resulting in two libraries of 20 mixtures each. The concentration of solids in dopant solutions was 4.8 w/w % and in the RM solution 53.3 w/w %. PGMEA was used as both the formulation solvent and the system fluid. The makeup solution was produced using an aliquot of the RM solution diluted to 4.8 w/w %. For the full formulation 10ml of each of the

dopant solutions, 10 ml of the makeup solution and 45ml of the reactive mesogen solution were required. The smaller volume solutions were loaded onto the instrument in a glass tube, sealed with a septum, the RM mixture into a larger volume tube and also sealed.

Using these concentrations the volumes required for transfer were calculated and programmed into the Gilson liquid handling software. To achieve two libraries the sequence was entered in duplicate, the first time selecting the BDH1281 source vial and the second the IS9193 vial. The library was created by aspiration first of the reactive mesogen solution which was added in equal amounts to each target vial. The dispensing was carried out serially, the aspirate step used to draw up the full volume and dispense to a single target vial. This was repeated until all the target wells had been filled with the first component. Then the same procedure of dispensing was used for the chiral dopant solutions, except the volumes were variable and between dispensing to each well, due to immersion of the needle below the level of the fluid, the needle was purged and refilled. After the complete dispensing of each component the needle was rinsed and purged to prevent contamination. This was achieved by flushing with the system fluid before immersing in acetone. Aspiration of solution was carried out at 0.250 ml / min and the needle depth set to reach the bottom of the tube. On completion of the library the vials were capped and shaken.

Vial	1 / 21	2 / 22	3 / 23	4 / 24	5 / 25	6 / 26	7 / 27	8 / 28	9 / 29	10 / 30
Volume of Dopant solution (µl)	180	200	220	240	260	280	300	320	340	360
Volume of Make-up solution (µl)	380	360	340	320	300	280	260	240	220	200
Volume of RM solution (µl)	890	890	890	890	890	890	890	890	890	890
Concentration of dopant (w/w)%	1.8	2.0	2.2	2.4	2.6	2.8	3.0	3.2	3.4	3.6
Vial	**11 / 31**	**12 / 32**	**13 / 33**	**14 / 34**	**15 / 35**	**16 / 36**	**17 / 37**	**18 / 38**	**19 / 39**	**20 / 40**
Volume of Dopant solution (µl)	380	400	420	440	460	480	500	520	540	560
Volume of Make-up solution (µl)	180	160	140	120	100	80	60	40	20	0
Volume of RM solution (µl)	890	890	890	890	890	890	890	890	890	890
Concentration of dopant (w/w)%	3.8	4	4.2	4.4	4.6	4.8	5	5.2	5.4	5.6

Vials 1 to 20 comprise BDH-1281 dopant, Vials 21 to 40 comprise IS-9193 dopant

Table 6.6: The construction of mixtures dispensed by robotic liquid handling to create chiral nematic reactive mesogen formulations with varying concentration of chiral dopant

6.4.8 Formulation of a Reactive Mesogen Library Containing IS-9193 to investigate the Effect of Enatiomeric Excess by IJP

The Robotic liquid handling apparatus was used to create a two variable libraries of concentration and enantiomeric excess of chiral dopant in a reactive mesogen mixture. The Gilson apparatus was configured to hold 4 racks, a 3x9 array of 10 ml glass tubes, a 2x8 array of 60 ml glass tubes, and two customised racks holding standard 96-well plates with a volume per well of 240 μL. Formulations consisted of three components, a reactive mesogen solution, a chiral dopant solution and a make up solution. The reactive mesogen solution is a multi-component mixture containing the components in Table 6.5

Mixtures were produced in a 96-well plate format using 200 μL of solution per vial. Chiral dopant concentrations of between 4 and 14.5 % were selected incrementing in ~1.4 % steps (Table 6.7). For each concentration an enantiomeric excess of chiral dopant was created between 100 and -100 in steps of 10, by the addition of an enatiomerically opposite isomer, to produce 168 unique formulations. The solid content of the chiral dopant solutions and the makeup solution was 5 w/w % and the reactive mesogen solution was 35 w/w %. The solvent used in this system for both the formulation solvent and the system fluid was acetophenone. For the full formulation 7 ml of each of the dopant solutions, 7 ml of the makeup solution and 20 ml of the reactive mesogen solution were required. The smaller volume solutions were loaded onto the instrument in a glass tube, sealed with a septum, the RM mixture into a larger volume tube and also sealed. Using these concentrations the volumes required for transfer were calculated and programmed into the Gilson liquid handling software. To achieve 168 formulations two 96-well plates were used.

Vial	1	2	3	4	5	6	7	8	9	10	11	12	13	14
IS-9193 (µl)	30	29	27	26	24	23	21	20	18	17	15	14	12	11
IS-9326 (µl)	0	2	3	5	6	8	9	11	12	14	15	17	18	20
Makeup solution (µl	70	70	70	70	70	70	70	70	70	70	70	70	70	70
RM solution (µl)	100	100	100	100	100	100	100	100	100	100	100	100	100	100
ee	100	90	80	70	60	50	40	30	20	10	0	-10	-20	-30
Chiral dopant (w/w%	3.96	3.96	3.96	3.96	3.96	3.96	3.96	3.96	3.96	3.96	3.96	3.96	3.96	3.96
Vial	15	16	17	18	19	20	21	22	23	24	25	26	27	28
IS-9193 (µl)	9	8	6	5	3	2	0	40	38	36	34	32	30	28
IS-9326 (µl)	21	23	24	26	27	29	30	0	2	4	6	8	10	12
Makeup solution (µl	70	70	70	70	70	70	70	60	60	60	60	60	60	60
RM solution (µl)	100	100	100	100	100	100	100	100	100	100	100	100	100	100
ee	-40	-50	-60	-70	-80	-90	-100	100	90	80	70	60	50	40
Chiral dopant (w/w%	3.96	3.96	3.96	3.96	3.96	3.96	3.96	5.35	5.35	5.35	5.35	5.35	5.35	5.35
Vial	29	30	31	32	33	34	35	36	37	38	39	40	41	42
IS-9193 (µl)	26	24	22	20	18	16	14	12	10	8	6	4	2	0
IS-9326 (µl)	14	16	18	20	22	24	26	28	30	32	34	36	38	40
Makeup solution (µl	60	60	60	60	60	60	60	60	60	60	60	60	60	60
RM solution (µl)	100	100	100	100	100	100	100	100	100	100	100	100	100	100
ee	30	20	10	0	-10	-20	-30	-40	-50	-60	-70	-80	-90	-100
Chiral dopant (w/w%	5.35	5.35	5.35	5.35	5.35	5.35	5.35	5.35	5.35	5.35	5.35	5.35	5.35	5.35
Vial	43	44	45	46	47	48	49	50	51	52	53	54	55	56
IS-9193 (µl)	50	48	45	43	40	38	35	33	30	28	25	23	20	18
IS-9326 (µl)	0	3	5	8	10	13	15	18	20	23	25	28	30	33
Makeup solution (µl	50	50	50	50	50	50	50	50	50	50	50	50	50	50
RM solution (µl)	100	100	100	100	100	100	100	100	100	100	100	100	100	100
ee	100	90	80	70	60	50	40	30	20	10	0	-10	-20	-30
Chiral dopant (w/w%	6.78	6.78	6.78	6.78	6.78	6.78	6.78	6.78	6.78	6.78	6.78	6.78	6.78	6.78
Vial	57	58	59	60	61	62	63	64	65	66	67	68	69	70
IS-9193 (µl)	15	13	10	8	5	3	0	60	57	54	51	48	45	42
IS-9326 (µl)	35	38	40	43	45	48	50	0	3	6	9	12	15	18
Makeup solution (µl	50	50	50	50	50	50	50	40	40	40	40	40	40	40
RM solution (µl)	100	100	100	100	100	100	100	100	100	100	100	100	100	100
ee	-40	-50	-60	-70	-80	-90	-100	100	90	80	70	60	50	40
Chiral dopant (w/w%	6.78	6.78	6.78	6.78	6.78	6.78	6.78	8.25	8.25	8.25	8.25	8.25	8.25	8.25
Vial	71	72	73	74	75	76	77	78	79	80	81	82	83	84
IS-9193 (µl)	39	36	33	30	27	24	21	18	15	12	9	6	3	0
IS-9326 (µl)	21	24	27	30	33	36	39	42	45	48	51	54	57	60
Makeup solution (µl	40	40	40	40	40	40	40	40	40	40	40	40	40	40
RM solution (µl)	100	100	100	100	100	100	100	100	100	100	100	100	100	100
ee	30	20	10	0	-10	-20	-30	-40	-50	-60	-70	-80	-90	-100
Chiral dopant (w/w%	8.25	8.25	8.25	8.25	8.25	8.25	8.25	8.25	8.25	8.25	8.25	8.25	8.25	8.25
Vial	85	86	87	88	89	90	91	92	93	94	95	96	97	98
IS-9193 (µl)	70	67	63	60	56	53	49	46	42	39	35	32	28	25
IS-9326 (µl)	0	4	7	11	14	18	21	25	28	32	35	39	42	46
Makeup solution (µl	30	30	30	30	30	30	30	30	30	30	30	30	30	30
RM solution (µl)	100	100	100	100	100	100	100	100	100	100	100	100	100	100
ee	100	90	80	70	60	50	40	30	20	10	0	-10	-20	-30
Chiral dopant (w/w%	9.75	9.75	9.75	9.75	9.75	9.75	9.75	9.75	9.75	9.75	9.75	9.75	9.75	9.75
Vial	99	100	101	102	103	104	105	106	107	108	109	110	111	112
IS-9193 (µl)	21	18	14	11	7	4	0	80	76	72	68	64	60	56
IS-9326 (µl)	49	53	56	60	63	67	70	0	4	8	12	16	20	24
Makeup solution (µl	30	30	30	30	30	30	30	20	20	20	20	20	20	20
RM solution (µl)	100	100	100	100	100	100	100	100	100	100	100	100	100	100
ee	-40	-50	-60	-70	-80	-90	-100	100	90	80	70	60	50	40
Chiral dopant (w/w%	9.75	9.75	9.75	9.75	9.75	9.75	9.75	11.30	11.30	11.30	11.30	11.30	11.30	11.30
Vial	113	114	115	116	117	118	119	120	121	122	123	124	125	126
IS-9193 (µl)	52	48	44	40	36	32	28	24	20	16	12	8	4	0
IS-9326 (µl)	28	32	36	40	44	48	52	56	60	64	68	72	76	80
Makeup solution (µl	20	20	20	20	20	20	20	20	20	20	20	20	20	20
RM solution (µl)	100	100	100	100	100	100	100	100	100	100	100	100	100	100
ee	30	20	10	0	-10	-20	-30	-40	-50	-60	-70	-80	-90	-100
Chiral dopant (w/w%	11.30	11.30	11.30	11.30	11.30	11.30	11.30	11.30	11.30	11.30	11.30	11.30	11.30	11.30
Vial	127	128	129	130	131	132	133	134	135	136	137	138	139	140
IS-9193 (µl)	90	86	81	77	72	68	63	59	54	50	45	41	36	32
IS-9326 (µl)	0	5	9	14	18	23	27	32	36	41	45	50	54	59
Makeup solution (µl	10	10	10	10	10	10	10	10	10	10	10	10	10	10
RM solution (µl)	100	100	100	100	100	100	100	100	100	100	100	100	100	100
ee	100	90	80	70	60	50	40	30	20	10	0	-10	-20	-30
Chiral dopant (w/w%	12.89	12.89	12.89	12.89	12.89	12.89	12.89	12.89	12.89	12.89	12.89	12.89	12.89	12.89
Vial	141	142	143	144	145	146	147	148	149	150	151	152	153	154
IS-9193 (µl)	27	23	18	14	9	5	0	100	95	90	85	80	75	70
IS-9326 (µl)	63	68	72	77	81	86	90	0	5	10	15	20	25	30
Makeup solution (µl	10	10	10	10	10	10	10	0	0	0	0	0	0	0
RM solution (µl)	100	100	100	100	100	100	100	100	100	100	100	100	100	100
ee	-40	-50	-60	-70	-80	-90	-100	100	90	80	70	60	50	40
Chiral dopant (w/w%	12.89	12.89	12.89	12.89	12.89	12.89	12.89	14.53	14.53	14.53	14.53	14.53	14.53	14.53
Vial	155	156	157	158	159	160	161	162	163	164	165	166	167	168
IS-9193 (µl)	65	60	55	50	45	40	35	30	25	20	15	10	5	0
IS-9326 (µl)	35	40	45	50	55	60	65	70	75	80	85	90	95	100
Makeup solution (µl	0	0	0	0	0	0	0	0	0	0	0	0	0	0
RM solution (µl)	100	100	100	100	100	100	100	100	100	100	100	100	100	100
ee	30	20	10	0	-10	-20	-30	-40	-50	-60	-70	-80	-90	-100
Chiral dopant (w/w%	14.53	14.53	14.53	14.53	14.53	14.53	14.53	14.53	14.53	14.53	14.53	14.53	14.53	14.53

Table 6.7: The construction of mixtures dispensed by robotic liquid handling to create chiral nematic reactive mesogen formulations with varying concentration of chiral dopant and enantioners IS9193 and IS-9326.

The library was created by aspiration of the reactive mesogen solution which was added in equal amounts to each target vial. The dispensing was carried out serially, the aspirate step used to draw up the full volume and dispense to a single target vial. This was repeated until all the target wells had been filled with the first component. Then the same procedure of dispensing was used for the chiral dopant solutions, except the volumes were variable and between dispensing to each well, due to immersion of the needle below the level of the fluid, the needle was purged and refilled. After the complete dispensing of each component the needle was rinsed and purged to prevent contamination. This was achieved by flushing with the system fluid before immersing in the square plastic bottle containing acetone.
The solutions used in the formulation were less viscous due to the higher solvent content, and therefore to prevent unwanted solvent evaporation the aspiration and dispensing rate was increased from that used previously to a at a rate of 0.500 μL / min, halving the time taken for formulation and the needle depth set to reach the bottom of the tube. On completion of the library the well plates were sealed using a Titer-top (Diversified-Biotech) seal

6.4.9 Analysis of Morphology by Fluorescence Visualisation

Fluorescence visualisation was achieved using a LaVision Bio Analyzer 4F running FIPS-2 software. Images of reactive mesogens containing small quantities of dye from a red Staedtler Lumocolour permanent marker pen were obtained. Inkjet printed substrates were loaded into the analyzer and images obtained with a Cy3 filter. Areas of interest were defined using a grid lattice from which two or three dimensional height-intensity images were obtained.

6.4.10 Drop Morphology

Using the technique of inkjet printing in combination with the Microdrop Macro Creator software (appendix E3) rows of a reactive mesogen solution of increasing concentration (17, 20, 23 and 26 w/w %) in acetophenone solvent, and containing a fluorescent dye (Staedler Lumocolour) were printed from a 96-well plate. Printing variables were entered into the software to create a sequence of macro commands. A pre-determined optimum voltage of 104 V, a pulse width of 29 ms and a drop frequency of 60 Hz were used. Using the 'spots as variables function' of the software each concentration was printed incrementing from 1 drop,

in steps of 1, to 12. For each drop count a 1x4 matrix was defined with a 1.5 mm separation between drops and adjacent rows onto an aligned TAC film substrate. A solution fill time of 2 seconds and an empty time of 5 seconds was used (returning into the source well), followed by a 5 second ultrasonic cleaning cycle. The solvent used for cleaning was identical to the solvent used for formulation. The Macro sequence was loaded into the Autodrop software and executed. On completion the substrate was annealed in an oven at 60 °C for 5 minutes and cooled at room temperature prior to fluorescence analysis.

6.4.11 Film Morphology

Using the technique of inkjet printing in combination with the Microdrop Macro Creator software (appendix E3) 10x10 array of spots was printed from a 96-well plate, using a 17 w/w % RM solids solution in acetophenone containing a fluorescent dye (Staedler Lumocolour).

Using the Microdrop Macro Creator software variables for printing were entered and a sequence of macro commands created. A pre-determined optimum voltage of 104 V, a pulse width of 29 ms and a drop frequency of 60 Hz were used. Using the 'spots as variables' in combination with the 'spacing as variables' function of the software the drops deposited in each spot position in the matrix were varied between 6 and 12 drops whilst simultaneously the spacing between the adjacent spots creating the film was varied between 0.16 mm and 0.32 mm in 0.04 mm steps. A library of 35 films was therefore produced onto aligned TAC film substrate. A solution fill time of 2 seconds and an empty time of 5 seconds was used (returning into the source well), followed by a 5 second ultrasonic cleaning cycle. The solvent used for cleaning was identical to the solvent used for formulation. The Macro sequence was then loaded into the Autodrop software and executed. After printing the films were annealed and cured using standard procedures and then the films profiled using fluorescence analysis.

6.4.12 Inkjet Printing of Reactive Mesogen Thin Films

Using the Inkjet printing apperatus together with software for the creation of macro sequences matricies of closely printed drops were printed to create thin film libraries. Samples of chiral nematic reactive mesogens formulated in a 96-well plate format and

containng a 20 w/w % solids content were loaded directly onto the microdrop apperatus. Prior to formulation the solvent jetting parameters were obtained. A voltage of 105 V, a pulse width of 30 ms and a drop frequency of 60 Hz were used.

The printing substrate, an aligned TAC film was placed flat onto the printing platform. Films were created from each position of the 96-well plate, and due to the number of samples had to be performed in two runs. Using the Microspot Macro Creator program (Appendix E3) variables for printing were entered to create a sequence of macro commands. A 10x10 matrix of spots, consisting of eight drops per spot and with a spacing of 0.25 mm between each spot on the matrix was printed onto the substrate in duplicate and in randomised positions for each of the formulations. Films were separated by 1.5 mm on each side. A fill time of 2 seconds and a empty time of 5 seconds was used (returning into the source well), followed by a 5 second ultrasonic cleaning cycle. The solvent used for cleaning was identical to the solvent used dissolving the components of the library. The Macro sequence was then loaded into the Autodrop software and executed. The positions of printed samples were output as a text file relating the coordinates of the 96-well plate to the print position, numbered sequentially across the substrate from right to left. On completion the library was processed acording to the standard UV curing procedures before analysis for λ_{max} by the fibre optic technique.

6.4.13 Fibre Optic UV-Vis Spectroscopy

Inkjet printed films were analysed using an Ocean optics USB2000 UV-Vis spectrometer together with a DT-MINI Deuterium / Tungsten-halogen source with spectral output 200 nm – 2000 nm. The apparatus was connected *via* two Ocean optics fibre-optic patch cables of 100 μm diameter with peak transmission between 300-800 nm. The output of the UV source was directed onto the end of the optical fibre connected to the spectrometer using two UV transmitting fused silica lenses to achieve sharp focus. The substrate onto which the films were printed was placed in the beam between the source and analyser fibre optics and the spectra collected between 300 and 900nm, visualised in the absorbance mode producing positive peaks where selective reflection was observed. The spectra files were then imported into Microsoft Excel by means of a VBA macro to produce plots of absorption vs. wavelength for each film from which values of λ_{max} were collected.

6.5 References

(1) T. Cull, M. Goulding and M. Bradley, *Rev. Sci. Instrum.*, **2005**, *76*, 062216.
(2) M. Bradley and J. Thaburet, WO Patent, WO2005036149 (A1), **2005**.
(3) J. T. Cabral, S. D. Hudson, C. Harrison and J. F. Douglas, *Langmuir*, **2004**, *20*, 10020.
(4) T. Cull, M. Goulding and M. Bradley, *Adv. Mat.*, **2007**, *19*, 2355.

Appendix 1

MLC-6684 / %	MLC-6647 / %	MLC-6882 / %	Clearing Point / °C	MLC-6684 / %	MLC-6647 / %	MLC-6882 / %	Clearing Point / °C
100.0	0.0	0.0	134.9	33.3	33.3	33.3	106.1
80.0	20.0	0.0	132.7	27.3	36.4	36.4	102.6
66.7	33.3	0.0	125.7	27.3	36.4	36.4	106.4
57.1	42.9	0.0	119.4	36.6	27.7	36.6	106.4
50.0	50.0	0.0	115.7	50.0	12.5	37.5	104.8
0.0	100.0	0.0	114.7	12.5	50.0	37.5	98.6
20.0	80.0	0.0	119.2	20.0	40.0	40.0	104.8
33.3	66.7	0.0	112.7	20.0	40.0	40.0	101.2
42.9	57.1	0.0	126.1	40.0	20.0	40.0	105.6
50.0	50.0	0.0	126.6	30.0	30.0	40.0	103.9
44.4	44.4	11.1	116.2	40.0	20.0	40.0	106.4
44.4	44.4	11.1	119.6	40.0	20.0	40.0	105.6
50.0	37.5	12.5	119.4	57.1	0.0	42.9	103.7
37.5	50.0	12.5	113.2	0.0	57.1	42.9	97.7
57.1	28.6	14.3	118.9	44.4	11.1	44.4	106.1
28.6	57.1	14.3	114.7	33.3	22.2	44.4	98.3
66.7	16.7	16.7	115.0	11.1	44.4	44.4	98.3
16.7	66.7	16.7	111.7	44.4	11.1	44.4	98.6
80.0	0.0	20.0	122.7	11.1	44.4	44.4	97.1
40.0	40.0	20.0	110.9	22.2	33.3	44.4	99.2
0.0	80.0	20.0	106.7	37.5	12.5	50.0	98.0
40.0	40.0	20.0	114.0	25.0	25.0	50.0	98.9
44.4	33.3	22.2	111.2	12.5	37.5	50.0	94.8
33.3	44.4	22.2	102.8	0.0	50.0	50.0	93.6
50.0	25.0	25.0	112.2	50.0	0.0	50.0	96.3
25.0	50.0	25.0	108.5	50.0	0.0	50.0	102.3
36.4	36.4	27.3	109.6	0.0	50.0	50.0	89.3
36.4	36.4	27.3	111.4	42.9	0.0	57.1	97.4
57.1	14.3	28.6	111.4	28.6	14.3	57.1	93.9
14.3	57.1	28.6	99.4	14.3	28.6	57.1	91.5
40.0	30.0	30.0	107.7	0.0	42.9	57.1	90.8
30.0	40.0	30.0	111.7	0.0	33.3	66.7	84.8
22.2	44.4	33.3	104.2	33.3	0.0	66.7	92.1
44.4	22.2	33.3	108.5	16.7	16.7	66.7	89.0
66.7	0.0	33.3	112.2	20.0	0.0	80.0	84.5
33.3	33.3	33.3	105.9	0.0	20.0	80.0	80.2
0.0	66.7	33.3	102.8	0.0	0.0	100.0	74.9
33.3	33.3	33.3	107.1				

Clearing point transition data obtained by the high-throughput robotic formulation and analysis of a ternary Merck Liquid Crystal (MLC) library.

Appendix 2

FET2%	FET3%	FET5%	Average Melting Transition /°C	Average Clearing Transition /°C	FET2%	FET3%	FET5%	Average Melting Transition /°C	Average Clearing Transition /°C
0	0	100	36.9	81.0	40	60	0	64.1	72.0
20	10	70	32.4	79.2	10	10	80	35.5	79.3
10	40	50	40.2	77.9	20	20	60	35.0	77.1
30	30	40	37.1	75.1	50	0	50	40.2	71.1
40	30	30	37.1	72.3	0	70	30	67.5	77.9
40	40	20	42.3	72.0	0	80	20	72.3	77.8
30	60	10	48.7	73.6	80	0	20	46.6	65.5
10	90	0		77.2	70	20	10	55.2	67.1
90	10	0		68.7	50	50	0	58.2	69.9
0	10	90	43.3	81.3	20	0	80	36.2	77.7
30	0	70	37.4	76.3	30	10	60	36.4	75.1
20	30	50	37.4	76.1	0	60	40	61.3	77.6
40	20	40	36.7	73.1	10	60	30	48.0	76.0
50	20	30	36.2	70.4	10	70	20	65.1	76.6
50	30	20	43.3	70.6	0	90	10	58.1	77.6
40	50	10	55.9	72.1	80	10	10	58.2	65.9
20	80	0	70.8	73.6	60	40	0	55.4	67.8
100	0	0		70.1	0	30	70	39.5	79.9
10	0	90	41.5	79.9	40	0	60	39.9	73.0
0	40	60	40.3	79.8	10	50	40	46.2	77.1
30	20	50	37.4	75.0	20	50	30	53.6	75.0
50	10	40	37.6	71.3	20	60	20	59.5	74.6
60	10	30	43.3	68.7	10	80	10	70.1	76.0
60	20	20	47.7	68.0	90	0	10	59.7	65.7
50	40	10	51.2	69.4	70	30	0	57.7	67.1
30	70	0	67.3	72.1	10	20	70	33.3	79.0
0	20	80	37.8	80.4	0	50	50	44.8	78.7
10	30	60	38.1	77.4	20	40	40	37.4	76.4
40	10	50	38.3	72.5	30	40	30	36.2	74.0
60	0	40	39.0	69.1	30	50	20	55.4	74.5
70	0	30	43.9	67.3	20	70	10	69.8	76.3
70	10	20	51.8	67.3	0	100	0	65.9	81.2
60	30	10	51.4	68.2	80	20	0	61.6	65.7

Clearing point and melting point transition data obtained by the high-throughput robotic formulation and analysis of a ternary FET library

Appendix 3

FET2-Cl(%)	FET3-Cl(%)	FET5-Cl(%)	Average Clearing Point	FET2-Cl(%)	FET3-Cl(%)	FET5-Cl(%)	Average Clearing Point
0	0	100	45.7	20	15	65	33.1
0	5	95	48.6	20	20	60	32.5
0	10	90	42.9	20	25	55	34.8
0	15	85	41.7	20	30	50	36.1
0	20	80	37.4	20	35	45	36.1
0	25	75	39.5	20	40	40	35.3
0	30	70	38.8	25	0	75	35.4
0	35	65	37.9	25	5	70	34.8
0	40	60	41.9	25	10	65	34.1
5	0	95	41.3	25	15	60	34.1
5	5	90	39.2	25	20	55	35.2
5	10	85	33.6	25	25	50	35.3
5	15	80	33.9	25	30	45	35.7
5	20	75	34.1	25	35	40	35.6
5	25	70	35.4	25	40	35	35.7
5	30	65	34.5	30	0	70	35.2
5	35	60	39.2	30	5	65	34.6
5	40	55	41.3	30	10	60	36.8
10	0	90	37.9	30	15	55	35.8
10	5	85	32.9	30	20	50	36.0
10	10	80	32.3	30	25	45	36.0
10	15	75	31.8	30	30	40	36.1
10	20	70	32.9	30	35	35	37.7
10	25	65	34.5	30	40	30	
10	30	60	37.7	35	0	65	38.1
10	35	55	37.7	35	5	60	37.4
10	40	50	40.2	35	10	55	37.0
15	0	85	32.7	35	15	50	36.3
15	5	80	32.6	35	20	45	35.8
15	10	75	31.6	35	25	40	35.6
15	15	70	31.7	35	30	35	35.8
15	20	65	32.6	35	35	30	41.0
15	25	60	32.5	40	0	60	39.1
15	30	55	35.6	40	5	55	39.0
15	35	50	36.8	40	10	50	38.2
15	40	45	37.5	40	15	45	36.8
20	0	80	34.0	40	20	40	35.8
20	5	75	33.2	40	25	35	34.8
20	10	70	32.8	40	30	30	35.5

Clearing point transition data obtained by the high-throughput robotic formulation and analysis of a ternary FET library, formulated over a focused region

Appendix 4

FET2-Cl(%)	FET3-Cl(%)	FET5-Cl(%)	Transition C_1 - C_2	C_2 - N	N - I	C - I
100	0	0				68.0
95	5	0				68.5
90	10	0		63.5	64.8	
85	15	0		62.2	63.3	
80	20	0		59.3	63.8	
75	25	0	56.1	58.5	64.8	
70	30	0		54.9	65.3	
65	35	0	54.1	60.7	68.0	
60	40	0		53.2	66.8	
55	45	0		54.1	67.5	
50	50	0	54.4	56.9	68.5	
45	55	0				69.4
40	60	0				70.4
35	65	0				71.4
30	70	0				72.3
25	75	0		67.0	71.8	
20	80	0		68.7	72.5	
15	85	0		70.6	73.0	
10	90	0		72.8	74.0	
5	95	0				74.7
0	100	0				77.3
95	0	5	61.2	63.3	64.5	
90	5	5	59.1	60.7	62.5	
85	10	5	58.8	60.9	63.5	
80	15	5	56.9	59.6	64.3	
75	20	5		55.2	65.0	
70	25	5		54.1	65.8	
65	30	5	52.1	53.8	66.8	
60	35	5				67.5
55	40	5				68.2
50	45	5		51.5	68.0	
45	50	5		54.1	68.7	
40	55	5	57.2	59.1	69.4	
35	60	5	57.2	61.2	70.2	
30	65	5	60.1	63.0	70.6	
25	70	5		64.0	71.6	
20	75	5		67.0	72.3	
15	80	5	65.5	68.2	73.0	
10	85	5		70.4	74.0	
5	90	5		72.1	74.7	
0	95	5				75.6
90	0	10		60.7	63.3	
85	5	10		58.0	64.0	
80	10	10				66.0
75	15	10		52.7	65.8	
70	20	10	39.1	53.0	65.5	
65	25	10	45.8	53.5	66.0	
60	30	10	45.1	48.2	66.5	
55	35	10	42.9	47.3	67.3	
50	40	10	43.6	50.0	68.0	
45	45	10	43.2	51.8	68.7	
40	50	10	46.1	51.8	69.4	
35	55	10	49.4	56.9	70.2	
30	60	10	54.1	60.7	70.9	
25	65	10	57.2	62.5	71.8	
20	70	10	59.1	64.5	72.8	
15	75	10		65.8	73.7	
10	80	10		70.4	74.4	
5	85	10		69.2	75.4	
0	90	10		73.2	76.1	
85	0	15	36.1	57.7	63.3	
80	5	15	35.1	55.5	64.0	
75	10	15	32.4	52.1	64.8	
70	15	15	42.9	50.6	65.3	
65	20	15	43.6	47.9	66.0	
60	25	15	32.0	46.7	66.8	
55	30	15	32.0	44.8	67.5	
50	35	15	32.4	44.8	68.2	
45	40	15	32.7	46.4	69.0	
40	45	15	33.1	51.2	69.7	
35	50	15	45.8	52.1	70.6	
30	55	15	53.2	56.3	71.6	
25	60	15	53.8	59.6	72.1	
20	65	15	56.6	60.7	73.3	
15	70	15	59.6	63.6	74.0	
10	75	15	58.3	66.0	73.7	
5	80	15	63.0	67.5	74.7	

FET2-Cl(%)	FET3-Cl(%)	FET5-Cl(%)	Transition C_1 - C_2	C_2 - N	N - I	C - I
0	85	15	49.4	70.9	75.4	
80	0	20	36.4	52.1	64.0	
75	5	20	35.4	49.7	65.0	
70	10	20	34.4	47.0	65.5	
65	15	20	41.3	45.1	66.5	
60	20	20		41.0	67.3	
55	25	20	32.4	43.6	68.0	
50	30	20	32.7	38.7	68.7	
45	35	20	32.7	43.6	69.2	
40	40	20	33.1	47.0	70.2	
35	45	20	33.4	47.6	71.1	
30	50	20	49.7	54.4	71.8	
25	55	20		53.2	72.5	
20	60	20	39.0	59.1	72.8	
15	65	20	37.4	60.7	73.3	
10	70	20	57.5	63.8	74.0	
5	75	20		67.0	74.7	
0	80	20		67.5	75.4	
75	0	25	36.7	49.4	65.3	
70	5	25	40.4	46.4	65.8	
65	10	25	36.4	45.4	66.5	
60	15	25		39.4	67.5	
55	20	25	33.1	40.7	68.0	
50	25	25		34.1	69.0	
45	30	25	32.7	37.1	69.4	
40	35	25		33.1	70.6	
35	40	25		33.7	71.4	
30	45	25		34.4	72.1	
25	50	25	45.8	54.1	72.3	
20	55	25	49.7	55.5	72.8	
15	60	25	34.7	58.3	73.5	
10	65	25	39.4	61.2	74.2	
5	70	25	55.2	62.0	74.9	
0	75	25	42.6	64.3	75.6	
70	0	30	36.7	42.9	66.0	
65	5	30	35.4	42.6	66.8	
60	10	30	30.3	42.0	67.5	
55	15	30	33.7	37.4	68.0	
50	20	30		33.1	69.0	
45	25	30		32.7	69.9	
40	30	30		33.1	70.6	
35	35	30		33.4	71.3	
30	40	30		34.1	72.3	
25	45	30		34.4	72.5	
20	50	30	35.1	54.1	73.0	
15	55	30	34.4	53.8	73.7	
10	60	30	39.0	58.3	74.4	
5	65	30	40.4	61.2	75.1	
0	70	30	42.0	61.7	75.9	
65	0	35		37.4	67.3	
60	5	35		38.1	68.0	
55	10	35	28.6	35.1	68.2	
50	15	35		33.7	69.2	
45	20	35		33.4	69.9	
40	25	35	30.3		70.9	
35	30	35		33.8	71.6	
30	35	35		34.1	72.3	
25	40	35		34.7	73.3	
20	45	35		34.4	73.5	
15	50	35	35.4	62.7	74.0	
10	55	35	37.4	53.8	74.7	
5	60	35	40.0	55.8	75.4	
0	65	35	42.0	61.5	76.1	
60	0	40		37.7	68.0	
55	5	40		36.1	68.7	
50	10	40	28.6		69.4	
45	15	40		34.4	70.2	
40	20	40		34.1	71.1	
35	25	40		34.4	71.8	
30	30	40		34.4	72.5	
25	35	40		34.4	73.3	
20	40	40		34.7	74.2	
15	45	40		35.1	74.9	
10	50	40		36.7	75.1	
5	55	40	40.4	54.7	75.9	
0	60	40	42.9	55.5	76.3	
55	0	45		37.4	69.0	

FET2-Cl(%)	FET3-Cl(%)	FET5-Cl(%)	Transition C_1 - C_2	C_2 - N	N - I	C - I
50	5	45	34.1	36.7	69.4	
45	10	45			70.2	
40	15	45				
35	20	45		34.7	71.6	
30	25	45		34.4	72.8	
25	30	45		34.1	73.5	
20	35	45		34.4	74.0	
15	40	45	34.7	37.7	74.7	
10	45	45		37.4	75.6	
5	50	45		40.0	76.3	
0	55	45		42.6	77.5	
50	0	50		38.4	70.4	
45	5	50				70.9
40	10	50		36.1	71.6	
35	15	50		35.1	72.1	
30	20	50		34.4	72.5	
25	25	50		33.7	73.5	
20	30	50		34.1	74.0	
15	35	50		35.1	75.1	
10	40	50		37.4	75.9	
5	45	50		40.0	76.6	
0	50	50		42.9	77.3	
45	0	55				71.3
40	5	55				72.1
35	10	55				73.0
30	15	55				73.7
25	20	55				74.2
20	25	55		33.1	74.7	
15	30	55		34.1	75.1	
10	35	55		36.4	75.9	
5	40	55		39.4	76.3	
0	45	55		42.0	77.3	
40	0	60	31.0	38.1	71.8	
35	5	60	30.7	36.1	73.0	
30	10	60	29.7	34.7	73.7	
25	15	60	29.3	33.4	74.2	
20	20	60	28.3	32.4	74.9	
15	25	60	28.6	33.1	75.6	
10	30	60	31.4	35.1	76.3	
5	35	60	36.4	39.1	77.3	
0	40	60	36.7	42.3	78.2	
35	0	65				73.5
30	5	65				74.2
25	10	65				74.4
20	15	65		30.3	74.9	
15	20	65	28.6	31.7	75.6	
10	25	65	29.3	34.7	76.3	
5	30	65	31.7	37.4	77.3	
0	35	65	33.4	40.4	78.0	
30	0	70	28.6	32.4	74.0	
25	5	70	28.6	32.7	75.1	
20	10	70	27.9	32.7	75.6	
15	15	70		30.0	76.6	
10	20	70		31.0	77.3	
5	25	70	32.4	35.1	78.0	
0	30	70	36.1	40.7	78.7	
25	0	75	36.1	70.2	75.6	
20	5	75				76.1
15	10	75	30.0	32.4	76.3	
10	15	75		30.3	77.0	
5	20	75	31.7	35.7	77.8	
0	25	75		36.4	79.2	
20	0	80	30.3	35.7	76.6	
15	5	80	29.0	36.7	77.3	
10	10	80	27.3	35.7	77.5	
5	15	80	31.7	38.4	78.5	
0	20	80	35.7	38.7	78.4	
15	0	85	31.0	37.1	77.3	
10	5	85				78.2
5	10	85				78.7
0	15	85	35.7	42.3	79.9	
10	0	90	29.7	44.2	79.0	
5	5	90	33.7	42.9	79.4	
0	10	90	38.1	45.8	79.0	
5	0	95	40.7	43.9	79.7	
0	5	95		48.2	80.4	

Clearing point and melting point transition data obtained by the high-throughput inkjet formulation and analysis of a ternary FET library

Appendix 5 – Oral Presentations

- Bradley group presentation, March 2003, Edinburgh (UK)
- Merck CASE conference, April 2003, Southampton (UK)
- Bradley group presentation, November 2003, Southampton (UK)
- Bradley group presentation, March 2004, Edinburgh (UK)
- Merck CASE conference, April 2004, Southampton (UK)
- Bradley group presentation, December 2004, Edinburgh (UK)
- Final year presentation, April 2005, Firbush (UK)
- Leanne Green memorial prize talk, May 2005, Edinburgh (UK)
- Bradley group presentation, November 2005, Edinburgh (UK)

Development of Combinatorial Parallel Synthesis and High Throughput Screening Methods for Liquid Crystalline Materials

Toby Cull [a], Mark Bradley [a], Mark Goulding [b], George Attard [a]

a. University of Southampton, Highfield, Southampton, SO14 1BJ b. Merck NB-SC, Chilworth Science Park, Southampton, SO16 7QD

Why Combinatorial Synthesis?

• The use of liquid crystals (LC's) in display devices is a rapidly growing area which is finding a multitude of new applications. This dictates the need for ongoing research into LC's to discover new and desirable properties and keep ahead of the competition. Achieving novel properties often involves manipulation of one specific section of the molecule, for example the polar end group. To assess the influence of the segment under investigation on the bulk properties of the molecule a number of homologues can be made with varying structures incorporating the aforementioned section. Traditional methods of synthesis involve individual multiple reactions, to gain a number of different compounds to be tested. This method is reliable and is amenable to large scale synthesis but has a major drawback in that it is extremely inefficient and time consuming.

Figure 1. Typical applications of liquid crystals in display devices

• Combinatorial chemistry can solve this problem. By the practice of efficient, parallel synthesis many more chemical compounds can be generated than the number of steps used. Traditional combinatorial synthesis pioneered by Merrifield[1] on functionalised resin beads is not appropriate to LC synthesis due to the large amounts (grams) of material that are required for testing. A parallel solution based approach can be adopted instead.

How is synthesis achieved?

• A synthesis of 4-propyl-4'-cyanobiphenyl is illustrated in figure 2. If a range of five alkyl analogues of this LC were required traditional chemistry states 5 separate reactions are needed to gain the 5 products. If combinatorial chemistry is used only one reaction is required to gain the 5 products. By introducing all 5 acid chlorides to the Friedel crafts reaction in the first step a mixture of five 4-alkonylbiphenyls will form[2].

1. R. Merrifield, *J. Am. Chem. Soc.*, **1963**, 2149-54

2. M. Goulding, R. Tanner, K. Adlem, *Mol. Cryst. Liq. Cryst.* In Press

3. O. Deeg, P. Kirsch, D. Panluth, P. Bauerle, *Chem. Commun*, **2002**, 2762 – 2763

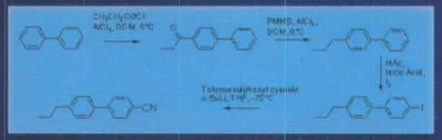

Figure 2. A traditional liquid crystal synthesis

The components in the mixture are not isolated until the final step of the reaction scheme. Separation can be achieved by chromatography or if the homologues are difficult to separate preparative HPLC may be required.

• By applying combinatorial chemistry to LC research it has been shown both by previous work by M.Goulding[2] and O.Deeg[3] and also by current research into the synthesis of 4-alkyl-4'-cyanobiphenyl libraries, that parallel reactions can be used to great gain, offering a benefit over traditional synthesis. The work has also highlighted an important issue which must be addressed for combinatorial parallel synthesis to become successful.

Post-synthetic screening issues

• On completion of a LC synthesis the product must be characterised. The characterisation measures the bulk properties of the LC and these can then be used to consider how the material will perform in a display device. Properties that are tested for include, clearing point, phase behaviour, dielectric anisotropy, optical anisotropy and elastic constants. Tests can be run either on the pure compound or in a host mixture.

• Many of these tests are time consuming and require large amounts of liquid crystal in order to obtain good results. A full characterisation can take up to a day to characterise. For traditional synthesis this is not an issue as the testing rate is still faster than the rate of production. However as the synthetic throughput is increased the screening becomes the rate limiting step in the process.

• As current methods are not suitable for the screening of large libraries there is a need for the development of high throughput (HT) screening methods to accompany the parallel synthesis. To achieve this current methods can be adapted or changed. An example is the use of an automated differential scanning calorimeter (DSC) to measure the phase transitions of O.Deeg's libraries[3].

Developing High Throughput Screening

• Work on high throughput adaptation has to date focused on the determination of clearing point – the temperature at which the LC undergoes the transition to an isotropic liquid. Traditionally the test is conducted using a photodiode and a light source to measure the opacity of the sample as the temperature is increased. This method is reliable, but a sample can take 40 minutes to run. An alternative approach was used in the development of a HT test. The experimental setup can be seen in figures 3 and 4.

Figures 3 and 4. The schematic of the experiment and a picture of the setup.

• A box is constructed on a heating stage in such a way that light is only able to enter the experiment through the top of the box which is covered by two sheets of linear polarizing film placed next to each other, one on each side. The polarizer's are arranged so that their plane of polarization lies parallel. Above one polarizer is placed a web cam, and above the other a light source. On the heating stage is placed a mirror, on to which samples of the liquid crystal to be tested are spotted. When the liquid crystal is mesogenic the plane polarised light entering the box is rotated by the optical properties of the liquid crystal and therefore is unable to pass the second polarizer, creating a dark spot visible to the camera. The temperature is increased and as the clearing point is reached the LC becomes isotropic and spot disappears. This technique at present can be used to identify up to 6 clearing points simultaneously in under an hour.

Where next?

The success of combinatorial parallel synthesis of LC's means the method can now be applied to producing libraries of novel liquid crystals. Work is in progress on the production of a library of high dielectric anisotropy LC's using a new end group. Once library synthesis is complete it can be tested quickly for clearing point using the new apparatus. To test the dielectric anisotropy a new HT screen will need to be developed. Using this equipment the rapid discovery of new liquid crystals with desirable properties should be possible.

High Throughput Liquid Crystal Synthesis and Screening

Toby Cull[a], Prof. Mark Bradley[a], Dr. Mark Goulding[b]
a. University of Southampton, Highfield, Southampton, SO17 1BJ b. Merck Chemicals Ltd., Chilworth Science Park, Southampton, SO16 7QD

Introduction

Current methods of liquid crystal (LC) development are based on traditional synthetic approaches followed by time consuming screening of individual compounds by DSC or polarized optical microscopy. With the development of parallel and combinatorial strategies, large numbers of compounds can be synthesised at an increased rate[1,2]. However it is important that analysis can perform at a similar rate to prevent creation of a bottleneck in the discovery process.

High Throughput Synthesis

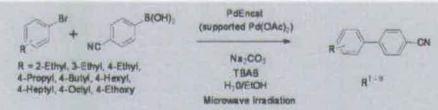

Scheme 1; Synthesis of a 9 member LC library

The synthesis shown in *Scheme 1* was carried out in parallel using Pdencat (*ex* Avecia), an immobilised $Pd(OAc)_2$ catalyst. Water was used as the solvent. The Pdencat was used at 0.05 mol%, preventing side reactions and Pd leaching. Under these conditions the reaction took only 5 minutes. To further increase throughput, reaction preparation was carried out by liquid handling robot and purification using parallel chromatography.

Using these methods allows liquid crystals to be produced quickly in good yield (40-100%) and high purity.

Development of a Test Method

The clearing point (CP) of a liquid crystal has been identified as an important initial screen. The CP is the temperature at which the transition from a LC mesophase to an isotropic liquid occurs. Discovery of the CP reveals the temperature below which the LC's novel properties can be exploited.

High Throughput Screening

A device was designed to simultaneously identify the clearing point of a large number of materials using an optical method. A LC sample below its clearing point and placed between two crossed polarising films will appear as a white spot. As the material is heated and passes its clearing point, the birefringent properties are lost and hence can no longer be visualised between the films. This change was monitored in the high throughput analysis device

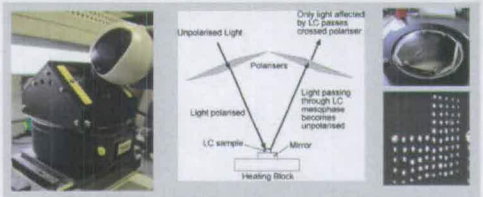

Figure 1; Schematic and photos of the HT clearing apparatus

The apparatus, shown in *Figure 1* consists of a heating block with a chrome plated brass surface, onto which the samples were spotted. Two perpendicularly aligned polarisers were attached above the heating block. Behind one polariser was placed an intense and homogenous cold cathode light, and behind the other a webcam. The webcam and heating block were interfaced to a PC. The liquid crystal library was spotted onto the chrome surface and heated at 5°C/min from 25°C to 150°C.

Data Collection and Analysis

The video data collected from the experiment was processed to give the white intensity of each sample spot w.r.t temperature. Plotting this data shows a drop in intensity when a clearing point occurs. The melting point can also be seen as the point when the intensity increases (*Figure 2*).

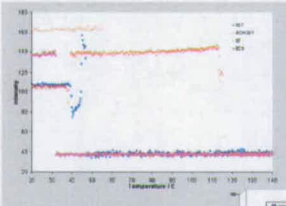

Figure 2; High throughput clearing point determination of 4 LC samples

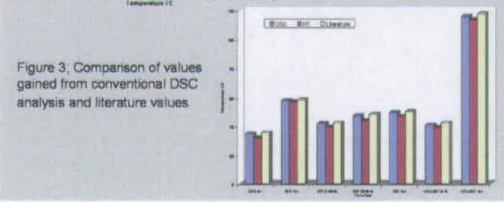

Figure 3; Comparison of values gained from conventional DSC analysis and literature values

A series of compounds with known clearing points were analysed using the High Throughput method and compared to results gained by traditional DSC to validate the method. The results in *Figure 3* show the HT method to give results comparable to those gained by DSC and close to the literature values[3].

Liquid Crystal Mixture Screening

In addition to the screening of synthesis libraries the apparatus can be used to analyse mixtures of liquid crystals. One such example is the analysis of a 75 compound library which was created by robotic combination of 3 LC formulations in varying quantities. The samples were then evaluated in parallel for their clearing point (*Figure 4*). This method was successful in allowing structure property relationships to be investigated quickly and easily.

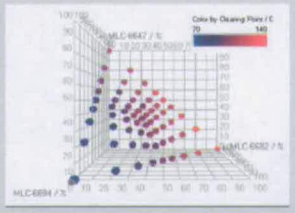

Figure 4; The relationship between the amounts of three liquid crystals in a mixture and the clearing point

Conclusion

Parallel synthesis of liquid crystal libraries have highlighted a need for a fast parallel screening method for clearing point. Apparatus to obtain melting and clearing point data of 100's of compounds simultaneously has been designed, giving accurate and reproducible results

The apparatus is of great advantage both in the screening of liquid crystal libraries, and in the screening of complex mixture libraries created by robotic automation. The technique is crucial in providing a fast and reliable technique and preventing a rate limiting step in the discovery process and allowing efficient exploration of phase space.

References

1. M. Goulding, R. Tanner, K. Adlem, *Mol. Cryst. Liq. Cryst.*, **2004**, *411*, 1-16
2. O. Deeg, P. Kirsch, D. Pauluth, P. Bauerle, *Chem. Comm.*, **2002**, 2762-2763
3. Merck Licristal© datasheets, *Merck KGaA, Darmstadt.*

A Parallel, High Throughput Approach to Liquid Crystal Screening

Tobias Cull[1], Mark Goulding[2], Mark Bradley[1]
[1]School of Chemistry, University of Edinburgh, West Mains Road, Edinburgh, EH9 3JJ
[2]Merck Chemicals Ltd., Chilworth Science Park, Southampton, SO16 7QD
T.R.Cull@sms.ed.ac.uk

Introduction

The demand for synthesis of large numbers of liquid crystals (LCs) in an attempt to explore structure property relationships and to develop specific properties for applications such as liquid crystal displays (LCDs) has recently lead to the application of a variety of high-throughput (HT) methods in LC library formulation. The subsequent screening of these libraries for LC phase transitions has to date been achieved by a range of traditional methods such as Differential scanning calorimetry (DSC) followed by optical polarising microscopy, both well established but time consuming techniques. For analysing a large library a range of rapid screening process are necessary. Therefore a new method for HT screening of such libraries is required

Principle of the HT Method

An optical HT method was developed[1] to measure phase transitions, revealing the range over which materials were liquid crystalline from measurement of the melting and clearing point.
The apparatus designed utilised the phenomena of optical anisotropy, observed only when a material is in its LC state. A sample, in a LC mesophase when observed through two crossed polarising films will appear as a white spot, due to the circular polarisation of the linearly polarised light by the anisotropic sample. As the material is heated and passes its clearing point, the anisotropic properties are lost and hence can no longer be visualised between the films. It was this optical change that was monitored in the high throughput analysis device.

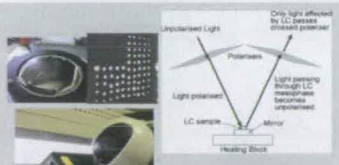

Figure 1; *Schematic and photos of the HT clearing apparatus and LC samples spotted onto the plate*

High Throughput LC Screening Apparatus

The apparatus, shown in *Figure 1* consists of a heating block with a chrome plated brass mirror surface, onto which the samples were spotted. Two perpendicularly aligned polarisers were attached above the heating block. Behind one polariser was placed an intense and homogenous cold cathode light, and behind the other a web cam. The web cam was used to record the image of the heating block onto which the liquid crystal library was spotted and heated at 5°C/min from 25°C to 150°C monitoring for changes in the intensity of the white spots

Data Collection and Analysis

The video sequence collected from the experiment was processed to give the white intensity of each sample spot w.r.t temperature. Plotting this data shows a drop in intensity when a clearing point occurs. The melting point can also be seen as the point when the intensity increases (*Figure 2*).
To validate the experiment a series of compounds with known clearing points were analysed using the HT method and compared to results gained by DSC and their literature values. The results in *Figure 3* show the HT method gave results comparable to those gained by DSC and close to the literature values[2], proving the viability of the experiment.

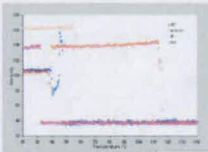

Figure 2; *High throughput clearing point determination of 4 LC samples*

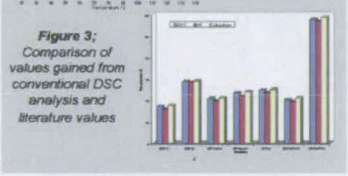

Figure 3; *Comparison of values gained from conventional DSC analysis and literature values*

Liquid Crystal Mixture Screening

To illustrate the power of the HT technique it was used to determine the composition of a three component mixture necessary to give a minimum eutectic melting point. The components were each combined at between 0% and 100% to cover 75 possible permutations. Robotic liquid handlers were used in the mixing and preparation enabling the library to be quickly and efficiently produced. Subsequent analysis of the samples for their melting points was carried out by the HT apparatus. The results of the experiment are shown in *Figure 4*

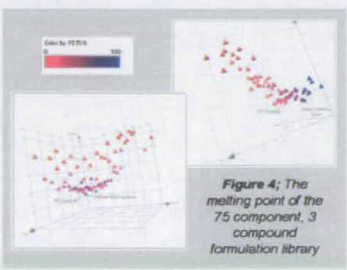

Figure 4; *The melting point of the 75 component, 3 compound formulation library*

Merck provided a sample of material believed to have the minimum eutectic melting point, derived via theoretical calculations. This is labelled as FET Eutectic in *Figure 4*. The melting point of this material was found to be higher, and lie at a different composition ratio than the lowest formulated melting point from the library.

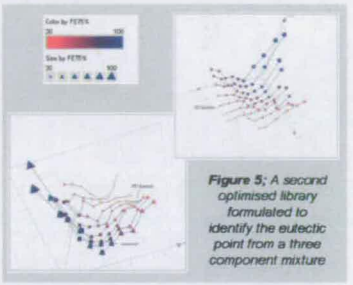

Figure 5; *A second optimised library formulated to identify the eutectic point from a three component mixture*

In-Depth Analysis of the Minimum

The area around the lowest melting point was analysed further by reformulation of the library at compositions giving a MP of less than 40°C. The second library was then tested and the results are shown in *Figure 5*. It appears that the FET eutectic material, shown on the graph lies in a minimum, but this lies on the rim of a much larger, well defined global minimum. Subsequent testing of the lowest melting point material by DSC confirms this result and suggests that the theory used to calculate eutectic points may require modification in such LC systems. The relationship between theoretical and experimental phase space is to be explored in future work to establish if this is indeed the case.

Conclusion

Parallel synthesis of liquid crystal libraries have highlighted a need for a fast parallel screening method for clearing point. Apparatus to obtain melting and clearing point data of 100's of compounds simultaneously has been designed, giving accurate and reproducible results.
The apparatus is of great advantage both in the screening of liquid crystal libraries, and in the screening of complex mixture libraries created by automation. The technique is crucial in providing a fast and reliable technique and preventing a rate limiting step in the discovery process and allowing efficient exploration of phase space

References

1. T.Cull, M. Goulding, M. Bradley, *Rev. Sci. Instr.*, 2005, *76*, 062216
2. Merck Licristal© datasheets, *Merck KGaA, Darmstadt.*

Appendix 7 – Publications

Cull, T., Goulding, M., Bradley, M., *Review of Scientific Instruments*, **2005**, *76*, 062216
http://link.aip.org/link/?RSINAK/76/062216/1

Cull, T.; Goulding, M.; Bradley, M., *Advanced Materials*, **2007**, *19*, 2355
http://www3.interscience.wiley.com/cgi-bin/fulltext/114299872/PDFSTART

PDF versions of publications are included on the supplimentary data CD-ROM